UNIVERSIDAD DE GRANADA
FACULTAD DE CIENCIAS

Departamento de Física Aplicada
Grupo de Coloides y Fluidos

Efectos Hofmeister en Sistemas Coloidales

Teresa López León

TESIS DOCTORAL

Editor: Editorial de la Universidad de Granada
Autor: Teresa López León
D.L.: Gr. 2059 - 2006
ISBN: 978-84-338-4123-0

Efectos Hofmeister en Sistemas Coloidales

por

TERESA LÓPEZ LEÓN

Licenciada en Ciencias Físicas

DIRECTORES:

Dr. D: Juan Luis Ortega Vinuesa
Prof. Titular de Física Aplicada

Dr. Dña. Delfina Bastos González
Prof. Titular de Física Aplicada

Este trabajo de investigación se presenta
Para alcanzar el grado de
DOCTOR ENCIENCIAS FÍSICAS
DOCTOR EUROPEUS

Hofmeister effects are truly universal. They are we believe as important in the scheme of things as Mendel's work was to genetics.
Except that Mendel's work was understood, Hofmeister's not.

Werner Kunz
Pierandrea Lo Nostro
Barry W. Ninham

COCIS, Agosto 2004

Prólogo

Los fenómenos Hofmeister se refieren a la especificidad iónica manifiesta en sistemas y propiedades de muy diversa índole. Éstas van desde solubilidad de la sal hasta coeficientes de actividad, entropía de dilución, tensión superficial, viscosidad, conductividad, pH, potencial zeta, concentración micelar crítica, estructura de microemulsiones, solubilidad de proteínas, transporte a través de membranas, transiciones de fase en microgeles, estabilidad coloidal, y la lista continúa. Las más de novecientas referencias citadas en el extenso review de Collins & Washabaugh publicado en 1985 en "Quarterly Review of Biophysics" dan una idea del alcance de los efectos Hofmeister. Se trata de fenómenos universales presentes en biología, bioquímica y ciencia de coloides y superficies. Sin embargo, y a pesar de que fueron observados por primera vez hace más de un siglo, su origen es aún incierto. Tradicionalmente las aportaciones a este tema se han limitado a la mera recopilación de observaciones experimentales. Los fenómenos Hofmeister no se han abordado desde un punto de vista fundamental hasta hace unos años, entre otras cosas porque no se disponía del marco teórico adecuado para ello. El poder incluir estos efectos "específicos" de los iones dentro una teoría capaz de predecir las evidencias experimentales es uno de los grandes retos de la físico-química hoy en día. El número de publicaciones concernientes a este tema se ha disparado recientemente. Grandes progresos en el dominio teórico y de las simulaciones numéricas han abierto nuevos horizontes, y aunque una teoría completa que dé cuenta de la totalidad de estos fenómenos se vislumbra aún lejos, se intuye que se va por buen camino. El avance de las mismas está sujeto al contraste con la experiencia. Sin embargo, a pesar de la gran cantidad de publicaciones que ponen de manifiesto la existencia de efectos Hofmeister, apenas existen estudios experimentales exhaustivos orientados a comprobar la validez de las predicciones teóricas. En este marco se encuadra el contenido de esta tesis doctoral.

ÍNDICE

INTRODUCCIÓN

Si se añade algún surfactante (por ejemplo DHDA) a una disolución salina se observa lo siguiente. Si la sal es un acetato o un hidróxido el surfactante se disuelve, dando lugar a un medio transparente. Si por el contrario lo que se le añade es yodo o bromo el surfactante precipita y la suspensión se vuelve turbia.[1] La pregunta es obvia ¿cuál es el mecanismo que hace que estos iones, de idéntica valencia, tengan efectos tan diferentes? Esta pregunta, que por su formulación pudiera parecer de fácil respuesta, fue planteada hace más de un siglo y, hoy por hoy, sigue sin tener una respuesta plenamente satisfactoria. En 1888 Hofmeister observó, al estudiar la solubilidad de proteínas, que la cantidad de sal necesaria para hacer precipitar la proteína dependía de la naturaleza de los electrolitos utilizados.[2,3] La idea de ordenar los iones según su efecto estabilizante (*salting-in*) o desestabilizante (*salting-out*) fue clave en este estudio.

$$\underset{\text{(kosmotropic anions)}}{\text{Citrate}^{3-} > SO_4^{2-} > PO_4H^{2-} > F^- > CH_3COO^- > Cl^- > Br^- > I^-} > \underset{\text{(chaotropic anions)}}{NO_3^- > ClO_4^- > SCN^-}$$

$$\underset{\text{(kosmotropic cations)}}{N(CH_3)_4^+ > NH_4^+ > Cs^+ > Rb^+ > K^+ > Na^+} > \underset{\text{(chaotropic cations)}}{H^+ > Ca^{2+} > Mg^{2+}}$$

El mismo orden, hoy en día conocido como *series de Hofmeister* o *series liotrópicas*, apareció común a todas las proteínas. Lejos de ser una propiedad específica a las proteínas, las series de Hofmeister han resultado ser universales. Para muchos autores, el entendimiento de estas series supone un paso clave en el avance de la ciencia de coloides y superficies.[4] Y es que las bases teóricas en las que se apoyan la físico-química y ciencia de coloides actuales no son capaces de resolver el complejo puzzle Hofmeister en el que distintas contribuciones debidas a interacciones superficie-superficie, superficie-electrolito, electrolito-agua, electrolito-electrolito, superficie-agua y agua-agua se ponen en juego. Por tanto, indagar en el origen de los fenómenos Hofmeister supone un análisis en profundidad de las interacciones intermoleculares presentes en cualquier sistema coloidal o interfase en agua. A pesar de la inherente complejidad del problema, la comprensión de los efectos Hofmeister se ha convertido en uno de los retos actuales de esta ciencia. Se han desarrollado dos marcos conceptuales distintos con el fin de explicar estos fenómenos. El primero, ya sugerido por Hofmeister bajo el concepto de *"the*

water withdrawing power of salt", hace referencia a los cambios en la estructura del agua causados por los electrolitos. El segundo, desarrollado hace apenas unos años, se basa en una adsorción específica de iones en interfases debido a fuerzas de dispersión (o de origen cuántico).

Estructura del agua

Los fenómenos Hofmeister han sido explicados tradicionalmente mediante mecanismos basados en la capacidad de los electrolitos para alterar la estructura del agua que los rodea.[5-10] De acuerdo con esto, los iones se han clasificado en dos tipos. Aquellos en los que la interacción ión-agua es más fuerte que la interacción agua-agua se denominan iones *kosmotrópicos* o *structure-maker*. Se trata por tanto de iones que refuerzan la red de enlaces de hidrógeno del solvente. Por otra parte, aquellos que interaccionan con el agua más débilmente que el agua consigo misma se denominan *caotrópicos* o *structure-breaker*. Estos iones, o cosolutos en general, debilitan la estructura del agua entorno a ellos. Por supuesto, entre las dos naturalezas extremas existe toda una gama de comportamientos intermedios. Las importantes modificaciones estructurales que los electrolitos inducen en el agua se han puesto de manifiesto experimentalmente mediante técnicas de electroquímica,[11,12] medidas difracción de neutrones,[13] dispersión cuasielástica de neutrones,[14] espectroscopia vibracional[15,16] o resonancia magnética nuclear[17]. Diferencias fundamentales se han observado con iones de distinta naturaleza. Éstas van desde entropías positivas/negativas de dilución hasta cambios configuracionales reflejados en la función de distribución radial g(r) del agua. En concreto, iones muy caotrópicos pueden generar un desorden en la estructura del agua equivalente a someter la disolución a algunos kilobares de presión. Gran número de evidencias experimentales han puesto de manifiesto la correlación entre carácter kosmotrópico/caotrópico del ión y su posición en la series de Hofmeister,[5] lo que sugiere el papel crucial de la estructura del agua en este tipo de fenómenos. Por otra parte, y de manera análoga, la presencia de cualquier soluto, partícula coloidal o superficie en disolución también perturba la estructura del solvente en las proximidades de la interfase.[18] Desde esta perspectiva, los fenómenos Hofmeister se interpretan incluyendo en las interacciones ión-superficie las modificaciones estructurales que ambas especies inducen en el agua que les rodea. Los avances realizados

bajo este enfoque han supuesto un estudio pormenorizado a nivel molecular de las interacciones superficie-agua y agua-agua. [19,20]

Fuerzas de dispersion ion − superficie

Un enfoque completamente distinto ha surgido en los últimos años a raíz de las aportaciones teóricas de Ninham y colaboradores.[21-24] Este nuevo enfoque ha supuesto una revisión de la base teórica sobre la que se sustenta la ciencia de coloides, en especial de la teoría de estabilidad coloidal conocida como DLVO (Deryaguin, Landau, Verwey, Overbeek).[26,27] El punto de partida ha sido el siguiente. Como ya se ha visto, gran número de fenómenos en los que intervienen electrolitos se escapan a las predicciones teóricas. Los fallos de la teoría suelen atribuirse a "efectos específicos" de los iones. Este hecho resulta un tanto inquietante. Por una parte, cuesta creer que la mayor parte de la físico-química sea específica. Desde otro punto de vista, la situación se vuelve todavía más insatisfactoria: cuando una teoría tiene que apelar tan a menudo a especificidades que varían de caso a caso, quizás es porque ésta es inadecuada y necesita ser revisada. La teoría DLVO, que ha sido una pieza clave en la ciencia de coloides durante más de 50 años, constituye el punto por el cual se comenzó a diseccionar el problema.[22] Esta teoría se construye bajo la consideración de que el agua en que están inmersas las partículas coloidales es un medio continuo desde el seno de la disolución hasta la superficie de las mismas. Esta suposición es importante ya que permite separar las fuerzas de tipo electrostático de todas aquellas fuerzas atractivas que predice la electrodinámica cuántica debido a fluctuaciones electrónicas. De este modo, la teoría DLVO establece dos tipos de fuerzas de largo alcance que determinan la interacción entre partículas coloidales: fuerzas repulsivas de origen electrostático y fuerzas atractivas de dispersión. Desde un punto de vista fundamental, el problema electrostático se aborda de manera no lineal. Bien mediante el uso de la ecuación de Poisson-Boltzmann, en una aproximación de campo medio; o bien, si se incluyen correlaciones iónicas de tamaño y carga, mediante ecuaciones integrales del tipo cadena hiper-reticulada (*hypenetted chain*).[27] En cualquier caso, los electrolitos en disolución son considerados como entidades discretas desde un punto de vista eléctrico. El perfil de distribución iónica establecido por una superficie cargada resulta ser no uniforme, dando lugar a lo que se conoce como doble capa eléctrica. Es justamente el solapamiento de esta doble capa eléctrica entorno a las partículas lo que causa

la fuerza repulsiva entre las mismas. Por el contrario, las fuerzas atractivas de origen mecánico-cuántico son tratadas haciendo uso de la teoría lineal de Lifshitz.[28] En esta línea los iones se consideran parte del medio continuo de dispersión, es decir, sus posibles efectos se engloban en las propiedades del *"bulk"*. Ninham y colaboradores han demostrado que el tratamiento asimétrico de las fuerzas eléctricas y fuerzas de origen cuántico o fuerzas de dispersión tiene la consecuencia no trivial de ser termodinámicamente inconsistente.[21,23] Estos autores argumentan así la necesidad de extender la teoría de Lifshitz de manera que se tengan en cuentan las fuerzas de dispersión entre superficies e iones. Cuando éstas se consideran, la especificidad iónica surge de manera natural a través de la polarizabilidad de los iones. Este parámetro refleja el desplazamiento dinámico del núcleo positivo con respecto a la nube electrónica negativa de los átomos, iones y moléculas en respuesta a un autoconsistente campo externo. Depende esencialmente de la configuración electrónica de la entidad química y, por tanto, es específico de cada especie.

A partir de los avances teóricos llevados a cabo por Ninham y colaboradores se concluye que las fuerzas de dispersión entre iones y superficies, de carácter universal, deben ser contempladas en cualquier teoría que pretenda explicar las propiedades físico-químicas de sistemas en presencia de iones. Sin embargo, no podemos pensar que con ello el problema está resuelto. En la teoría de Ninham, al igual que en la DLVO, el solvente sigue considerándose como un medio continuo, de manera que todas las particularidades relacionadas con la estructura del agua quedan descartadas. Es necesario, por tanto, considerar ambos mecanismos (fuerzas de dispersión ion-superficie y alteraciones de la estructura del agua entrono a iones y superficies) para poder explicar satisfactoriamente los efectos Hofmeister.

OBJETIVOS Y ESQUEMA

Esta tesis doctoral tiene como objetivo estudiar el doble mecanismo subyacente a los efectos Hofmeister. Como ya se ha comentado en la introducción, actualmente existen dos corrientes que intentan dar cuenta de este tipo de fenómenos. La más tradicional se basa en las modificaciones que iones y superficies producen en la estructura del agua. Sin embargo, recientes desarrollos teóricos y simulaciones ponen de manifiesto la existencia de procesos de acumulación/exclusión iónica cuyo origen reside en las universales fuerzas de dispersión. En esta tesis doctoral se pretende demostrar, mediante evidencias macroscópicas, la existencia simultánea de ambos mecanismos. Además, se han utilizado las teorías más recientes en este dominio para interpretar los resultados experimentales.

Con este fin se emplearon gran número de técnicas experimentales y sistemas coloidales diferentes. Se utilizaron prácticamente todas las técnicas de dispersión de luz de las que dispone el Grupo de Biocoloides y Fluidos de la Universidad de Granada: PCS (*Photocorrelation Spectroscopy*), SLS (*Static Light Scattering*), SCLS (*Single Cluster Light Scattering*), técnicas de electroforesis, nefelometría, turbidimetría, etc. En cuanto a sistemas experimentales se emplearon desde partículas de poliestireno o sílice, hasta microgeles termosensibles basados en PNIPAM o partículas de quitosano. En este sentido creo importante destacar que en este trabajo no se pretende investigar propiedades relacionadas con un sistema experimental o técnica concreta, sino servirse de todas las herramientas a nuestro alcance para ahondar en el origen de estos fenómenos de carácter universal. Citando a B. W. Ninham,[4] en este momento son necesarios datos experimentales diseñados para poder ser contrastados con la teoría y que den pistas para el avance en el entendimiento de estos fenómenos.

La mayor parte de este estudio se refleja en los once artículos que conforman esta memoria. Algunos de ellos se encuentran publicados en revistas de investigación, otros ya han sido enviados para su publicación y los más recientes están en fase de revisión y serán enviados a publicar en breve. En muchos casos se trata de colaboraciones con otros investigadores cuyas aportaciones han resultado ser clave para el desarrollo de esta tesis. Nuevos sistemas experimentales, técnicas de medida, modelos teóricos, y sobre todo, nuevos puntos de vista han permitido tratar el problema que nos planteamos

en esta tesis con mayor profundidad y perspectiva. El orden de los artículos que se presenta no es cronológico, sino que éstos han sido ordenados por bloques temáticos. Aunque cada uno de ellos hace referencia a propiedades o sistemas concretos, en todos ellos se estudia el efecto específico de seis electrolitos con distintas posiciones en las series de Hofmeister: sulfato, cloro, nitrato, sulfocianuro, amonio, sodio y calcio.

$$\underset{\text{(kosmotropic anions)}}{\text{Citrate}^{3-} > \mathbf{SO_4^{2-}} > PO_4H^{2-} > F^- > CH_3COO^-} > \underset{\text{(chaotropic anions)}}{\mathbf{Cl^-} > Br^- > I^- > \mathbf{NO_3^-} > ClO_4^- > \mathbf{SCN^-}}$$

$$\underset{\text{(kosmotropic cations)}}{N(CH_3)_4^+ > \mathbf{NH_4^+} > Cs^+ > Rb^+ > K^+} > \underset{\text{(chaotropic cations)}}{\mathbf{Na^+} > H^+ > \mathbf{Ca^{2+}} > Mg^{2+}}$$

En el primer bloque se investiga la estabilidad coloidal y propiedades electrocinéticas de sistemas coloidales tipo "hard sphere". Está constituido por los siguientes trabajos:

- Paper I: *Hofmeister Effects on the Stability and Electrophoretic Mobility of Polystyrene Latex Particles* (*J. Phys. Chem. B* **2003**, 107, 5696-5708)

- Paper II: *Hofmeister Effects on the Colloidal Stability of an IgG-coated Polystyrene Latex* (*J. Colloid Interface Sci.* **2005**, 284, 139–148).

- Paper III: *Hofmeister Effects on the Restabilization of IgG-Latex Particles: Testing Ruckenstein's Theory* (*Langmuir* **2005**, *21*, 87-93).

- Paper IV: *Inversions in the Hofmeister Sequences observed in Colloidal Systems* (Borrador para ser enviado a *J. Colloid Interface Sci.*).

En el segundo bloque se analiza en detalle la cinética de los procesos de agregación mediante: el análisis de las constantes cinéticas de agregación, la dimensión fractal de los agregados y la evolución temporal de la distribución en tamaño de dichos agregados. Esta investigación se llevó a cabo exclusivamente con partículas de poliestireno. Los resultados obtenidos se detallan en los trabajos:

-Paper V: *Specific Ionic Effects on Aggregation Kinetics and Fractal Dimensions of Polystyrene Nanoparticles* (Borrador para ser enviado a *Langmuir*).

-Paper VI: *Hofmeister Effects in Colloidal Suspensions: Experimental Evidences in Aggregation Kinetics* (Borrador para ser enviado a *J. Phys. Chem. B*).

En el tercer y más extenso bloque se estudia la estabilidad, propiedades electrocinéticas y transiciones de fase de "soft particles", concretamente partículas termosensibles basadas en PNIPAM. Cinco trabajos constituyen este último boque:

-Paper VII: *Cationic and Anionic Poly(N-isopropylacrylamide) Based Submicron Gel Particles: Electrokinetic Properties and Colloidal Stability* (*J. Phys. Chem. B* **2006,** *110,* 4629-4636).

-Paper VIII: *Hofmeister Effects on PNIPAM Microgel Particles: Macroscopic Evidences of Ion Adsorption and Changes in Water Structure* (Aceptado en *ChemPhysChem*, septiembre 2006).

-Paper IX: *Probing the Entropic Influence of Ions Macroscopically: De-Swelling Neutral Microgels with Salt* (Enviado a *Physical Review E*).

-Paper X: *Salt Interference in Co-nonsolvency of Poly(N-sopropylacrylamide) Microgel Particles in Mixed Ethanol-Water Solutions* (Enviado a *Langmuir*).

-Paper XI: *Thermosensitive Reversible Nanoparticles Formed by Self-Assembly of Poly(N-Isopropylacrylamide) Charged Chains: Testing Hofmeister Effects* (Borrador para ser enviado a *Macromolecules*).

Tal y como se requiere en esta modalidad de tesis doctoral orientada a optar a la mención de "Doctorado Europeo", a continuación se presenta un breve resumen y discusión de los resultados presentados en formato artículo de investigación, además de conclusiones y perspectivas.

BREVE RESUMEN Y DISCUSIÓN DE RESULTADOS

Paper I: "*Hofmeister Effects in the Stability and Electrophoretic Mobility of Polystyrene Latex Particle*".

En este trabajo se aborda el tema de la especificidad iónica haciendo uso de un sistema coloidal modelo: las partículas de poliestireno. El contenido del mismo se puede estructurar en tres bloques: propuesta de modelos microscópicos, estudios de estabilidad y movilidad electroforética, y consideraciones teóricas.

En primer lugar se presenta el estado del arte a esa fecha entorno a los fenómenos Hofmeister. Ello supone el análisis de las interacciones ion-agua, agua-agua, superficie-agua, superficie-ion y superficie-superficie. En base a esta discusión se proponen dos modelos microscópicos para explicar la especificidad iónica en una interfase del tipo sistema-hidrófobo/agua. El primer modelo predice una acumulación/exclusión iónica específica entorno a la superficie hidrófoba de origen entrópico. El segundo mecanismo, sin embargo, se basa en una orientación cooperativa de las moléculas de agua adyacentes a la superficie inducida por la presencia de iones. Esto generaría un gradiente de polarización que se traduce en un cambio en el potencial superficial de la interfase. Ambos modelos se han utilizado para explicar los resultados obtenidos con las partículas de poliestireno.

Los resultados experimentales que se presentan forman parte de un extenso estudio en el que, por primera vez, se analizan de manera sistemática tres aspectos fundamentales relacionados con los efectos Hofmeister en nanopartículas: i) carácter hidrófilo/hidrófobo de las partículas, ii) signo y iii) densidad de carga de la superficie coloidal. Concretamente, aquí se tratan los puntos ii) y iii). Para ello se utilizaron tres superficies con propiedades de carga distintas. Concretamente dos látexes aniónicos (sulfonato y carboxilo) y uno catiónico (amidina). Debido al carácter ácido/base débil de los látexes carboxilo/amidina respectivamente, el control del pH permitió trabajar con superficies de muy diversa carga (σ = -20.5, -9.6, -6.1, 4.0, 18.3 $\mu C/cm^2$) a la vez que se mantenía aproximadamente constante el carácter hidrófobo de las mismas. En la publicación se presenta una completa caracterización de la superficie de las partículas. El efecto desestabilizante de los aniones y cationes

Hofmeister fue analizado en cada una de estas superficies. Diferencias importantes en la concentración crítica de coagulación (ccc) de las partículas se encontraron con iones de igual valencia cuestionando la validez de la teoría clásica de estabilidad coloidal DLVO. En cuanto al efecto comparativo de los iones, se obtuvo el orden Hofmeister al clasificar las distintas especies de acuerdo con los correspondientes valores de ccc en todos los casos. El valor de la densidad de carga de la superficie no mostró ser determinante. Sin embargo, se observaron series inversas con partículas positivas y negativas. Los iones con efecto más desestabilizador en un caso, resultaron ser que más estabilizaban en superficies de signo contrario. Estas observaciones fueron confirmadas con medidas de movilidad electroforética. En base a estos resultados y trabajos realizados por otros autores, se concluyó que los aniones caotrópicos tienden a hacer más negativo el potencial eléctrico asociado a interfases hidrófobas, mientras que los kosmotrópicos tienen un efecto contrario (en comparación con el efecto del Cl^-). Los cationes, sin embargo, se comportan de manera contraria. Estas tendencias pusieron de manifiesto procesos de acumulación iónica que, como se comprueba en trabajos posteriores, están relacionados con la distinta polarizabilidad de los iones.

Finalmente, con el fin de extender la teoría DLVO a este tipo de fenómenos, se propuso incluir una dependencia lineal entre la concentración local de electrolito en la interfase (c_0) y el incremento del potencial superficial de la misma debido al efecto específico del electrolito ($\Delta\psi = \psi_{0_{sal}} - \psi_{0_{NaCl}}$). De esta manera, el potencial superficial que aparece en el termino eléctrico de la teoría DLVO, quedaría: $\psi_0 = \psi_{0_{NaCl}} + S\,I\,c_0$, donde S e I son factores que dan cuenta del carácter hidrófilo/hidrófobo de la superficie y de la naturaleza del electrolito respectivamente. A pesar de ser un tratamiento un tanto burdo, ciertas tendencias lineales se observaron con nuestros resultados experimentales.

Paper II: "Hofmeister Effects in the Colloidal Stability of an IgG-coated Polystyrene Latex".

Dentro del estudio sistemático de los factores que rigen el orden Hofmeister en nanoparticulas, este trabajo trata el aspecto del carácter hidrófilo/hidrófobo de la superficie. Para ello se emplearon partículas de poliestireno recubiertas con la proteína IgG (inmunogammaglobulina-G), de carácter más hidrófilo que el poliestireno. Concretamente el recubrimiento se

realizó sobre las partículas catiónicas empleadas en el artículo anterior. El estudio se llevó a cabo a través del análisis de: la estabilidad coloidal, movilidad electroforética y reestabilización de las partículas observada a altas concentraciones de sal.

Las medidas de estabilidad coloidal se hicieron a pH 4 y pH 10. Dado el carácter anfótero de la proteína, esto permitió trabajar con superficies tanto positivas como negativas. Además, el recubrimiento proteico de las partículas redispersadas a pH 10 resultó ser superior al que se tiene a pH 4, variando así también el carácter hidrófilo de las mismas. Solo en el primer caso el cambio en hidrofilicidad de la superficie fue lo suficientemente importante para observar modificaciones en el orden de los iones. Concretamente, un cambio sustancial se observó con el ion más caotrópico, el sulfocianuro, que vimos tiende a adsorberse en las superficies hidrófobas. En este caso, el aumento del carácter hidrófilo de la superficie supuso una inversión en el comportamiento de este ion, dando lugar a la excusión del mismo (adsorción negativa) en las proximidades de la interfase.

La tendencia observada con la muestra a pH 4, característica de superficies hidrófobas, fue confirmada con medidas de movilidad electroforética. Para ello se analizó el efecto del la sal tanto en el punto isoelectrico del complejo latex-IgG como en el potencial-ζ de las partículas. Todos los resultados apuntaron en la misma dirección: la acumulación de iones caotrópicos y exclusión de iones kosmotrópicos en las proximidades de la superficie. La teoría de Ohshima para *soft-particles* fue utilizada para cuantificar esta acumulación relativa de iones en la interfase. Los resultados más llamativos se obtuvieron con el ion más caotrópico, el SCN^-. A pH 4 el fenómeno de acumulación fue tan intenso que dio lugar a la inversión del potencial-ζ de las partículas (de positivo a negativo) a concentraciones de sal entorno a 100 mM. Un efecto contrario pero igualmente intenso se observó a pH 10 donde, a pesar de que el SCN^- actúa como coión, el aumento en la concentración de sal supuso de nuevo la inversión del potencial-ζ de las partículas, esta vez de potenciales negativos a positivos. Este último resultado confirma la exclusión del SCN^- de las proximidades de la interfase cuando la superficie es más hidrófila.

Resultados muy interesantes se obtuvieron al estudiar la reestabilización de las partículas a altas concentraciones de sal. Mientras que a pH 4 solo provocaron reestabilización los iones de naturaleza más extrema,

NaSCN y $Ca(NO_3)_2$, a pH 10 este fenómeno también se observó con el $NaNO_3$ y NH_4NO_3. Dado que los procesos de re-estabilización tienen su origen en las fuerzas repulsivas que surgen cuando dos superficies altamente hidratadas se acercan, la mayor reestabilización observada a pH 10 confirmó el carácter más hidrófilo de la superficie. Generalmente la aparición de estas fuerzas en partículas coloidales se ha atribuido a la presencia de cationes muy hidratados (en general multivalentes y actuando como contraiones) adsorbidos en la superficie hidrófila de las partículas. Los resultados presentados suponen la primera evidencia experimental de fenómenos de reestabilización gobernados por aniones débilmente hidratados (monovalentes) incluso cuando estos actúan como coiones. Estos resultados fueron atribuidos a la capacidad de los iones de modificar la estructura del agua. En el *paper IV* se comprueba que, tanto la exclusión de iones caotrópicos de interfases hidrófilas, como la reestabilización observada en estos sistemas a altas concentraciones de sal, tienen un origen común: la distinta manera en que iones y superficie estructuran el agua que les rodea.

Paper III: "Hofmeister Effects in the Restabilization of IgG-Latex Particles: Testing Ruckenstein's Theory"

Los novedosos resultados obtenidos al estudiar la re-estabilización de complejos latex-IgG en presencia de sales Hofmeister, se utilizan en este tercer trabajo para comprobar la validez de la teoría de Ruckenstein, ampliamente utilizada para explicar la re-estabilización de sistemas coloidales hidrófilos.

Según esta teoría las fuerzas de hidratación surgen de las correlaciones locales entre dipolos presentes en la superficie de las partículas y los dipolos del agua. A diferencia de otros modelos teóricos que tratan de dar cuenta de los fenómenos de re-estabilización añadiendo un *término repulsivo de hidratación* a la teoría DLVO, el modelo de Ruckenstein incluye esta interacción repulsiva en la formación de la doble capa eléctrica. En concreto, el campo creado por el momento dipolar y la carga eléctrica de la superficie se acoplan en un sistema de ecuaciones diferenciales no lineales de segundo orden constituido por: i) la ecuación de Poisson-Boltmann para medios dieléctricos en general y ii) una ecuación constitutiva que da cuenta de la polarización del medio en función del campo eléctrico aplicado. El desarrollo matemático de esta teoría se detalla en este *paper III*. La expresión del factor de estabilidad obtenida en base al modelo de Ruckenstein, se utiliza en este artículo para

ajustar nuestros resultados experimentales. La predicción teórica es solo satisfactoria en algunos casos concretos. En particular aquellos en los que la reestabilización se debe al efecto de contraiones. Sin embargo, el modelo de Ruckenstein falla al explicar, por ejemplo, la reestabilización del NaSCN ó $NaNO_3$ a pH 10.

Las divergencias encontradas entre teoría y medidas experimentales cobran sentido si se analiza con detalle las consideraciones del modelo de Ruckenstein. Los autores proponen que, debido a la presencia de grupos cargados en la superficie de las partículas, se establece un equilibrio de asociación (formación de pares iónicos) entre éstos y los electrolitos de signo contrario en disolución, dando lugar a la aparición de un momento dipolar no nulo perpendicular a la interfase. Según las teorías macroscópicas del continuo, que consideran al agua como un dieléctrico homogéneo, el campo creado por una superficie de este tipo (sin carga y con una distribución uniforme de dipolos) es cero más allá de la interfase. Esto es así ya que el efecto de unos dipolos se ve contrarrestado de manera simétrica por el de otros. Sin embargo, a nivel microscópico el agua no puede considerarse homogénea, y es lógico pensar que las interacciones entre moléculas vecinas están mucho menos apantalladas que las interacciones entre moléculas lejanas. Esto hace que se genere un gradiente de polarización en las proximidades de la superficie que se atenúa con la distancia. Cuando dos partículas se acercan, el solapamiento de estas capas de agua orientada da lugar a un aumento de la energía libre del sistema, lo que se traduce en una interacción repulsiva entre las partículas. De acuerdo con esta discusión, no cabría esperar fuerzas de reestabilización causadas por coiones, pues estos no pueden formar pares iónicos con las cargas de la superficie.

Paper IV: "Inversions in the Hofmeister Sequences Observed in Colloidal Systems"

Este trabajo supone un estudio a modo de corolario en el que las tendencias observadas con partículas de poliestireno (*paper I*) y complejos latex-IgG (*paper II*) se comparan con las obtenidas en otro tipo de superficies, llegando así a conclusiones más generales. En la primera parte de este artículo se analizan las nuevas superficies. Éstas fueron elegidas de tal modo que, incluyendo los sistemas anteriormente investigados, se cubriera la gama de hidrófobo a hidrófilo de manera gradual, tanto para sistemas positivos como

negativos. Las partículas que se eligieron con estos requisitos fueron: un latex anfótero muy cargado, un latex de poliestireno aniónico (sulfonato) recubierto de IgG, partículas sílice y partículas de quitosano. El estudio se centró en el efecto de los electrolitos en la estabilidad coloidal de los distintos sistemas. Las conclusiones desprendidas tras comparar las secuencias obtenidas con las distintas superficies se destacan a continuación.

En el caso de sistemas claramente hidrófobos como el poliestireno, se obtuvieron series opuestas con superficies positivas y negativas. Esta inversión debido al signo de carga de las partículas, se explica mediante la teoría de Ninham y Yaminski que considera las fuerzas de dispersión que existen entre iones y superficies. En base a esto, los iones más polarizables presentan una mayor tendencia a acercarse a las proximidades de la interfase que iones menos polarizables, independientemente de la carga de la superficie. Esta acumulación iónica conlleva la modificación del potencial de interacción entre partículas y da lugar a las especificidades iónicas observadas experimentalmente. Así un ión altamente polarizable que actúe como coion intensifica el potencial eléctrico en las proximidades de la superficie, dando lugar a partículas más estables. Sin embargo, cuando éste actúa como contraion la acumulación del mismo supone la disminución del potencial eléctrico y, por tanto, la menor estabilidad del sistema.

Por otra parte, también se observaron alteraciones en el orden de las series con superficies de igual signo pero distinto grado de hidrofilicidad. Este tipo de alteraciones, mucho más sutiles, sólo se manifestaron en las situaciones más extremas. Es decir, en el caso de aniones (cuyo efecto específico es más acusado) y principalmente en superficies negativas (en las que los aniones actúan como coiones y las fuerzas atractivas culombianas son menos significativas). Además, las inversiones se hacen patentes con mayor facilidad (son necesarias superficies menos hidrófilas) cuanto más caotrópico es el ion. Concretamente se observa que aquellos iones con mayor tendencia a acumularse en superficies hidrófobas, tienden a alejarse de superficies hidrófilas. Este proceso de exclusión iónica no puede explicarse mediante la teoría de Ninham, que predice acumulación siempre que el índice de refracción de la superficie sea mayor que el del agua. La correlación encontrada entre procesos de exclusión iónica y reestabilización a altas concentraciones de sal (comúnmente asociados a fuerzas de hidratación) puso de manifiesto el origen estructural de este tipo de inversiones.

Las inversiones inducidas por cambios en la hidrofilicidad de la superficie se interpretaron en base al concepto *"like seeks like"* particularizado al caso de superficies e iones. Cuando una superficie se introduce en agua modifica la estructura del solvente en torno a la interfase. Aquellos iones que originan estructuras de agua análogas a la inducida por la superficie tienden a acumularse en la interfase. Por el contrario cuando la superficie y los iones generan estructuras de agua antagónicas, los iones tienden a alejarse de la interfase. Ambos son procesos entrópicamente favorables. Esto explicaría la acumulación de iones caotrópicos (débilmente hidratados) en superficies hidrófobas y la exclusión de los mismos en las proximidades de superficies hidrófilas. Este mismo argumento permite generalizar el concepto de reestabilización coloidal en superficies hidrófilas, generalmente atribuido a la presencia de iones muy hidratados, al caso de especies caotrópicas. A concentraciones elevadas de sal, la doble capa eléctrica está totalmente comprimida, de manera que los electrolitos están confinados en las proximidades de la interfase. En esta situación los reajustes que tanto el agua como el ion inducen en el solvente están acoplados. En el caso de superficies hidrófilas e iones kosmotrópicos, ambos con fuerte tendencia a hidratarse, esto supone la formación de estructuras de agua densas en torno a la interfase. Sin embargo, el acoplamiento de estructuras antagónicas como la originada por una superficie hidrófila y un ion caotrópico, da lugar a capas de agua muy rígidas tipo hielo. En ambos casos, se conforma una estructura en torno a la interfase que supone una barrera estérica cuando dos partículas se acercan, dando lugar a la restabilización del sistema.

Paper V: "*Specific Ionic Effects on Aggregation Kinetics and Fractal Dimensions of Polystyrene Nanoparticles*"

Las alteraciones que los distintos electrolitos provocan en la estructura del agua, además de ser responsables de los fenómenos de reestabilización a altas concentraciones de sal, modifican las cinéticas de los procesos de agregación tal y como se concluye en este *paper V*. Este estudio comprende el análisis de: *i)* concentraciones críticas de coagulación (ccc), *ii)* constantes cinéticas asociadas a los primeros instantes de procesos de agregación (k_R) y *iii)* dimensión fractal de los agregados formados en dichos procesos (d_f). Tanto los valores de ccc como las k_R, fueron obtenidas mediante nefelometría o dispersión de luz a bajo ángulo. Las dimensiones fractales, por el contrario, se obtuvieron a partir del factor de estructura de sistema, es decir, mediante la

detección angular de la luz dispersada por la muestra. En este estudio se utilizaron partículas de poliestireno (sulfonato) de tamaño pequeño apropiadas para las técnicas de dispersión de luz empleadas.

Las diferencias en ccc obtenidas con los distintos iones confirmaron la secuencia observada con otras partículas aniónicas de poliestireno. En este artículo se presenta una descripción semicuantitativa de los mecanismos de acumulación iónica propuestos en trabajos anteriores para explicar dichas series. Según la teoría de Ninham y Yaminski, la energía potencial de un ion con respecto a una superficie cargada presenta, además de una contribución eléctrica, un término imagen y otro de dispersión. En este trabajo se resuelve numéricamente la ecuación de Poisson-Bolzmann incluyendo estos términos adicionales con el fin de obtener el potencial eléctrico autoconsistente y, a partir de él, la distribución de iones en las proximidades de la superficie de la partícula. Se concluye que aquellos aniones más polarizables tienden a acumularse más intensamente sobre la superficie de las partículas tal y como se observa experimentalmente.

El análisis de las constantes cinéticas de agregación k_R permitió obtener información adicional a cerca del potencial de interacción entre las partículas. Se observó que el aumento de la concentración de sal conlleva cinéticas de agregación más rápidas independientemente de la sal empleada. Sin embargo, a concentración de sal fija, las cinéticas asociadas a los distintos electrolitos resultan ser muy diferentes. Estas diferencias perduran incluso después de haberse alcanzado el régimen de agregación rápido, es decir, a concentraciones de sal superiores a la ccc. Las secuencias obtenidas al ordenar los iones de acuerdo con los valores de $k_{R\text{-}r}$ (k_R en régimen de agregación rápido) coinciden con las obtenidas a partir de valores de ccc. En el caso de los aniones, se observa de manera clara como el carácter más caotrópico del ion lleva asociado cinéticas de agregación más lentas. Los valores de d_f confirmaron estas conclusiones: aquellos iones que inducen cinéticas de agregación más lentas dan lugar a agregados con mayor dimensión fractal. Estos resultados se justificaron en base la estructura del agua en torno a los distintos iones. Dicha estructura, aún considerando que no altera el potencial de interacción entre las partículas, supone una barrera estérica que impide que las partículas se acerquen totalmente. Por tanto, la mayor dimensión fractal de los agregados obtenidos con los electrolitos más caotrópicos puede ser consecuencia, o bien de la necesidad de múltiples choques debido a la existencia de una barrera de potencial repulsiva no nula, o bien debido a la fragmentación de los agregados

debido a pozos de potencial de poca profundidad. Esta cuestión se resuelve en el artículo siguiente.

Paper VI: "Hofmeister Effects in Colloidal Suspensions: Experimental Evidences in Aggregation Kinetics"

Información mucho más detallada sobre la cinética de los procesos agregación inducidos por los distintos electrolitos se obtuvo mediante la técnica SCLS (Single Cluster Light Scattering). Dicha técnica permite determinar distribuciones en tamaño de agregados pequeños sin hacer ninguna suposición sobre la estructura del agregado. Este estudio, también realizado con partículas de poliestireno, se llevó a cabo exclusivamente con tres sales: NaCl, $NaNO_3$ y NaCl. El trabajo se estructura en cuatro partes: *i)* determinación de las concentraciones críticas de coagulación (ccc) asociadas a las distintas especies iónicas, *ii)* utilización de la teoría de Ninham y Yaminski para justificar los valores de ccc obtenidos *iii)* seguimiento de la evolución temporal de la distribución en tamaño de agregados a una concentración de sal superior a la ccc y *iv)* interpretación de las curvas de distribución de tamaño mediante la introducción de un kernel de fragmentación en la ecuación maestra del método estocástico.

La determinación de concentraciones críticas de coagulación supuso la obtención de series de Hofmeister (directas e inversas con partículas positivas y negativas respectivamente) confirmando los resultados obtenidos con otros látexes de poliestireno. A partir de la teoría de Ninham y Yamiski se calculó la distribución de iones en torno a la superficie de las partículas, teniendo en cuenta fuerzas de dispersión ion-superficie. Estas curvas muestran como los aniones más polarizables tienden a acumularse más intensamente sobre la superficie de las partículas, estabilizando los sistemas aniónicos y desestabilizando los catiónicos. Esta distinción entre partículas positivas y negativas desaparece al analizar las cinéticas de los procesos de agregación que se alcanzan por encima de la ccc.

Los resultados obtenidos al analizar las cinéticas de agregación fueron sorprendentes. En el caso del ion indiferente (Cl^-) se obtuvo una evolución de la distribución en tamaño de agregados típica de un régimen rápido de agregación DLCA (*Diffusion Limited Cluster Aggregation*). En este caso los agregados de tamaño pequeño tienden a desaparecer a tiempos largos debido a que se asocian para formar agregados de mayor tamaño. Sin embargo, la

tendencia observada con el ion más caotrópico (SCN^-) a tiempos largos resultó ser completamente distinta. En este caso, el proceso de agregación evoluciona hasta llegar a un punto en el que aparentemente la reacción se congela, de manera que el número de cada tipo de agregado permanece constante en el tiempo. Estas curvas representan la primera medida directa de un proceso de agregación completamente reversible. Este patrón se observó de manera más clara en el caso del latex catiónico, justamente aquel en el que el SCN^- (que actúa como contraion) provoca un efecto más desestabilizante. En el caso del NO_3^-, se obtuvieron cinéticas intermedias entre la del Cl^- y el SCN^-.

Los procesos de agregación reversible observados con SCN^- se justificaron en base a las fuertes modificaciones estructurales que este ion induce en el agua, creándose en torno al ion estructuras de agua tipo hielo. La fuerte acumulación de entidades SCN^-/agua en torno a la superficie supone una barrera estérica que impide que las partículas se acerquen más allá de una cierta distancia. Como resultado, las partículas quedan, bien en mínimos secundarios de potencial, o bien en regiones donde la curva de potencial no es muy profunda, de manera que es posible la reversibilidad de la agregación. Este efecto es más importante cuanto mayor es el carácter caotrópico del ion, explicando así las diferencias observadas con NO_3^- y Cl^-. Estas suposiciones se comprueban al observar que las curvas de distribución de tamaños experimentales se ajustan a un modelo teórico que contempla la existencia de estos mínimos de potencial poco profundos. Concretamente se resolvió la ecuación maestra, que determina en términos probabilísticos la evolución temporal de la distribución en tamaño de agregados, considerando un kernel de agregación browniano (ya que las medidas se hicieron por encima de la ccc) y otro de fragmentación que contempla la posibilidad de dos tipos de enlace, correspondientes a mínimos primarios y secundarios. La probabilidad de que una reacción de agregación dé lugar a un enlace primario (P_1) y el tiempo de vida medio de los enlaces primarios (τ_1) y secundarios (τ_2) se utilizaron como parámetros de ajuste. El kernel de fragmentación utilizado, que hasta el momento sólo había sido confrontado en el ámbito de los procesos de agregación reversible con resultados de simulación, fue capaz de reproducir satisfactoriamente las curvas experimentales. Además, se observó (fundamentalmente con el sistema catiónico) que al aumentar el carácter caotrópico del ion se obtenían valores inferiores de los tres parámetros, confirmando así la existencia de una barrera estérica entre las partículas.

Las dos facetas asociadas a la estabilidad de sistemas coloidales, concentraciones críticas de coagulación y cinéticas de agregación, pusieron de manifiesto la existencia de los dos mecanismos microscópicos que subyacen a los efectos Hofmeister: fenómenos de acumulación/exclusión y reestructuración del solvente.

Paper VII: "Cationic and Anionic Poly(N-isopropylacrylamide) Based Submicron Gel Particles: Electrokinetic Properties and Colloidal Stability"

En este trabajo se sintetizaron y caracterizaron partículas termosensibles basadas en poly(N-isopropilacrilamida) (PNIPAM). Las excepcionales propiedades de solvencia de estos microgeles los convierte en candidatos idóneos para estudiar fenómenos sensibles a la estructura del agua. El objetivo de este trabajo es estudiar la respuesta de partículas de PNIPAM, desde un punto de vista estructural y electrocinético, ante cambios en las propiedades del solvente, concretamente variaciones en la temperatura y salinidad el medio. Para este estudio se utilizó una sal indiferente, NaCl, mientras que el efecto específico del resto de los iones se analizó en el *paper VIII*.

Las partículas se sintetizaron mediante un procedimiento de polimerización por precipitación. Se estudiaron dos tipos de látex: un aniónico y un catiónico. Este último sistema fue sintetizado utilizando, además de PNIPAM, un comonómero catiónico hidrófilo (AEMH) que proporciona propiedades ligeramente distintas a las de los microgeles aniónicos de PNIPAM comúnmente estudiados. Las diferencias entre los dos sistemas se detallan en el artículo. En primer lugar se analizó el efecto de la sal en los fenómenos de hinchado. La reducción de la temperatura de transición de fase en volumen (T_{VPT}) y el deshinchado del microgel a altas fuerzas iónicas pusieron de manifiesto la disminución de la solubilidad del PNIPAM en presencia de sal. Se observó, además, que en este tipo de microgeles la caída del tamaño de las partículas con la concentración de sal es más fuerte que el comportamiento asintótico $D \sim c_s^{-1/5}$ característico de microgeles iónicos. Esto se debe principalmente a la alteración de la estructura de agua responsable de la solubilidad del PNIPAM como consecuencia de la hidratación de los iones. Las diferencias observadas entre partículas positivas y negativas se interpretaron en base a la presencia del comonómero AEMH en el látex catiónico, que

confiere un carácter más hidrófilo y, por tanto, una mayor solubilidad al sistema. La estabilidad del microgel se estudió en función de dos parámetros: la temperatura y la concentración de sal. Mediante el seguimiento de la evolución temporal del diámetro se determinó, de manera experimental, el diagrama de estabilidad de las partículas. En él se distinguen dos dominios claramente definidos, correspondientes a condiciones de estabilidad e inestabilidad. La reversibilidad de la agregación permitió pasar de un dominio al otro simplemente cambiando la temperatura o la fuerza iónica del medio.

La comparación entre transiciones de fase en volumen y electrocinéticas proporcionó información a cerca de la estructura interna del microgel, ya que estas últimas dependen tanto de las propiedades eléctricas como friccionales de las partículas. Al aplicar un modelo sencillo propuesto por Pelton se observó que las transiciones de fase en el caso de las partículas aniónicas se desarrollan en dos etapas, mientras que una sola etapa se distingue con las catiónicas. Estos resultados ponen de manifiesto diferencias estructurales entre los dos sistemas estudiados. Las partículas catiónicas parecen tener una estructura bastante homogénea. Sin embargo, la red polimérica de las partículas aniónicas está constituida por un núcleo muy entrecruzado rodeado de una capa de polímero mucho menos densa. Otro resultado interesante se obtuvo al estudiar la evolución de la movilidad electroforética con la concentración de sal a distintas temperaturas. El máximo comúnmente observado en partículas tipo *"hard sphere"* a bajas concentraciones de sal, tiende a desaparecer conforme disminuye la temperatura y las partículas adquieren el carácter de *"soft particles"*. La transición de *"hard sphere"* a *"soft particle"* se interpretó utilizando la teoría desarrollada por Ohshima para sistemas que presentan en su superficie una capa polimérica cargada en la que pueden penetrar los electrolitos. Dos parámetros, N y $1/\lambda$, se utilizaron para ajustar este modelo a las curvas de movilidad en función de la concentración sal. El primero representa la densidad de grupos cargados de la superficie y el segundo da cuenta del character "soft" de las partículas. El aumento de la temperatura supuso un aumento de N y una disminución de $1/\lambda$, es decir, el incremento de la densidad de carga superficial y la disminución de las fuerzas de fricción del sistema.

Paper VIII: "*Hofmeister Effects on PNIPAM Microgel Particles: Macroscopic Evidences of Ion Adsorption and Changes in Water Structure*"

Las partículas sintetizadas y caracterizadas en el *paper VII* se utilizaron para investigar, desde un punto de vista macroscópico, los mecanismos microscópicos que subyacen a los fenómenos Hofmeister. Como ya indicábamos en trabajos anteriores, estos fenómenos tienen su origen en *i)* cambios en la estructura del agua que rodea iones y superficies y *ii)* procesos específicos de acumulación/exclusión de iones en interfases. Aunque ambos mecanismos están interrelacionados y actúan simultáneamente, afectan de manera distinta a las diversas propiedades de los sistemas. En este sentido la "naturaleza dual" del PNIPAM fue explotada para investigar de manera independiente los dos mecanismos anteriormente citados. Se trata de sistemas que presentan características propias de polímeros o de partículas duras según las propiedades del solvente. Los cambios estructurales producidos en la red polimérica del microgel que se manifiestan macroscópicamente mediante el cambio de volumen de las partículas están gobernados por interacciones polímero-solvente, y por tanto, son altamente sensibles a cambios en la estructura de agua. Por otra parte, las propiedades interfaciales como el potencial ζ de las partículas íntimamente relacionado con la movilidad electroforética se ven fuertemente afectadas por posibles acumulaciones o exclusiones iónicas.

Los trabajos que existen en la literatura relacionados con efectos Hofmeister en partículas de PNIPAM solo tratan los fenómenos de hinchado. Es por esto que la especificidad iónica en este tipo de sistemas ha sido atribuida exclusivamente a cambios en la estructura del agua. En este artículo se presentan novedosos resultados relacionados con las propiedades electrocinéticas de las partículas. Por una parte, esta propiedad resultó ser extremadamente sensible a la naturaleza de los electrolitos. Se observaron fuertes inversiones en la movilidad electroforética de las partículas con electrolitos monovalentes a concentraciones de sal de sólo 10 mM. Pero lo que es aún más interesante, el estudio conjunto de los fenómenos de hinchado y las propiedades electrocinéticas de las partículas de PNIPAM puso de manifiesto la existencia de mecanismos de acumulación iónica en este tipo de sistemas. Estos resultados fueron contrastados con las predicciones de la teoría de Ninham, poniendo de manifiesto el acuerdo entre teoría y experimentos. Las

fuerzas de dispersión, de carácter universal, que aparecen entre iones y superficie parecen ser un pilar fundamental en este tipo de fenómenos.

Paper IX: "Macroscopically Probing the Entropic Influence of Ions: De-Swelling Neutral Microgels with Salt"

El origen microscópico de las transiciones de fase de geles y microgeles poliméricos constituye un importante ámbito de investigación en la actualidad. Los cambios de fase que experimentan los microgeles iónicos al aumentar la concentración de sal del medio han sido explicados de manera satisfactoria en base a equilibrios de tipo Donnan. Sin embargo, el origen de estas transiciones en el caso de microgeles neutros sigue sin estar claro. En este artículo se propone una interpretación a estos fenómenos fundamentada en la relación existente entre la naturaleza kosmotrópica/caotrópica de los iones y el mayor/menor colapso que éstos provocan en las partículas. Tales resultados ponen de manifiesto la influencia entrópica de los electrolitos en las interacciones polímero-solvente que, en definitiva, controlan el tamaño del microgel. Por tanto, las transiciones de fase inducidas por sal en partículas de PNIPAM se interpretaron mediante la teoría termodinámica de Flory-Rehner para este tipo de sistemas. Concretamente en base a cambios en la contribución entrópica (ΔS) del parámetro de solvencia χ.

El procedimiento seguido se detalla en el artículo. En primer lugar se ajustó la curva experimental D-T (tamaño en función de temperatura, *paper VII*) a la ecuación de cambio fase proporcionada por la teoría de Flory-Rehner. De este ajuste se obtuvieron los valores de algunos parámetros importantes del sistema (temperatura Θ, fracción de volumen en el estado colapsado, etc.) necesarios para el posterior cálculo de ΔS. Además, se puso de manifiesto la necesidad de incluir una dependencia de segundo orden en el parámetro χ con la fracción de volumen del polímero en el microgel. A partir de estos valores y de las curvas D-c (tamaño en función de la concentración de sal, *paper VIII*) se obtuvieron las correspondientes curvas ΔS-c y χ-c para los distintos iones. A partir de estas curvas se concluyó que el mayor carácter kosmotrópico del ion supone el aumento de la entropía correspondiente a interacciones solvente-solvente, lo que se traduce en una disminución del número de contactos polímero-solvente o, lo que es lo mismo, en un colapso de la red polimérica. Este mismo efecto se produce al aumentar la concentración de sal.

Paper X: "Salt interference in co-nonsolvency of poly (N-isopropylacrylamide) microgel particles in mixed ethanol-water solutions"

El PNIPAM, a temperatura ambiente, es soluble tanto en agua como en etanol (o cualquier otro alcohol de bajo peso molecular: metanol, propanol, etc.); sin embargo, no es soluble en algunas mezclas de los dos solventes. A este fenómeno se le denomina co-nonsolvencia y su origen constituye un tema de debate en la actualidad. La explicación más extendida hace referencia a la formación de complejos alcohol-agua debido a la fuerte interacción (tipo enlace de hidrógeno) entre los dos componentes. Como se ha puesto de manifiesto a lo largo de esta tesis, el análisis de los efectos Hofmeister en procesos gobernados por la estructura del solvente resulta ser una herramienta clave para investigar los mecanismos microscópicos responsables de dichos procesos. Concretamente, en este trabajo se estudia cómo diferentes sales pueden alterar los fenómenos de co-nonsolvencia del PNIPAM en mezclas etanol/agua, lo que proporciona interesante información a cerca de las interacciones que gobiernan estos procesos.

La curva de co-nonsolvencia de las partículas de PNIPAM (diámetro en función de la fracción de volumen de etanol (ϕ_e) presenta tres zonas diferenciadas que se corresponden con: i) regiones ricas en agua ($\phi_e < 0.2$), ii) regiones ricas en etanol ($0.5 < \phi_e < 0.7$) y iii) una región de transición ($0.2 < \phi_e < 0.5$). Las distintas tendencias observadas en estas regiones se atribuyen a las propiedades estructurales del solvente. El efecto de la sal en la solubilidad y estabilidad del PNIPAM fue analizado de manera independiente en cada una de estas zonas.

En el intervalo $\phi_e < 0.2$ observamos que tanto la sal como el aumento de la concentración de etanol provocan el deshinchado del microgel. En esta región la solubilidad del PNIPAM está controlada por las interacciones polímero-agua. Por tanto, la hidratación de los iones y la formación de complejos etanol-agua suponen una competencia con el PNIPAM por las moléculas de agua. Las diferencias observadas con las distintas especies iónicas apoyan estos argumentos y ponen de manifiesto la efectividad de las interacciones ion-agua de acuerdo con el carácter caotrópico o kosmotrópico de los iones. Por otra parte, los diagramas de estabilidad muestran una concentración límite de sal por encima de la cual el sistema es inestable. Dicha concentración disminuye conforme ϕ_e aumenta, de tal manera que en el límite

$\phi_e = 0.2$ el sistema es inestable prácticamente a cualquier fuerza iónica. Sólo en el caso del NaSCN se observaron dominios de estabilidad a $\phi_e > 0.2$. Los resultados de estabilidad apoyan las conclusiones obtenidas a partir de las curvas de tamaño.

El comportamiento observado a bajas concentraciones de etanol se asemeja al estudiado en disoluciones acuosas (*paper VIII*), sin embargo, aparecen tendencias totalmente distintas cuando el alcohol es el componente mayoritario ($0.5 < \phi_e < 0.7$). Por una parte, se observaron procesos de hinchado al aumentar la concentración de NaSCN en el medio. Esta tendencia, que se manifiesta incluso a concentraciones de sal de 1 ó 2 M, es contraria a la comúnmente observada en disoluciones acuosas. Por otra parte, las propiedades de estabilidad del NaSCN se invierten cuando $\phi_e > 0.2$. Es decir, el microgel es inestable a bajas concentraciones de sal y estable por encima de una concentración de NaSCN crítica. La simetría entre la curva de co-nonsolvencia del microgel y el diagrama de estabilidad del NaSCN ponen de manifiesto el efecto del ion en la estructura del solvente. Las propiedades excepcionales del NaSCN en mezclas etanol-agua pueden ser explicadas en base al fuerte carácter caotrópico o *structure-breaker* del ion, capaz de romper los enlaces hidrógeno que conforman los complejos etanol-agua.

En la región de transición ($0.2 < \phi_e < 0.5$), en la que la concentración de los dos solventes es importante, las tendencias opuestas observadas cuando el agua o el alcohol son componentes mayoritarios se superponen. Como consecuencia se obtuvieron transiciones de fase en volumen con la concentración de alcohol de tipo re-entrante. El punto de inflexión de estas curvas delimita las regiones en la que la solvencia del PNIPAM se produce vía interacciones con agua ó vía interacciones con etanol. El análisis de la región de transición permitió comparar las diferencias entre los dos tipos de solvatación.

Paper XI: "Thermosensitive Reversible Nanoparticles Formed by Self-Assembly of Poly(N-Isopropylacrylamide) Charged Chains: Testing Hofmeister Effects"

En el *paper VIII* se mostró cómo las propiedades de los microgeles, en tanto que presentan características comunes a polímeros y esferas duras, pueden ser explotadas para investigar de manera independiente procesos de acumulación iónica y cambios estructurales en el agua. Con el fin de acentuar

esta naturaleza dual de los fenómenos Hofmeister se diseñaron y sintetizaron las que hemos denominado como "partículas reversibles de PNIPAM". Se trata de disoluciones de cadenas cargadas de PNIPAM que a temperatura ambiente se encuentran en una configuración extendida. Sin embargo, por encima de la LCST (lower critical solubility temperature) las interacciones hidrófobas se hacen dominantes y las cadenas colapsan y agregan. De esta manera se forman núcleos primarios que crecen hasta que la repulsión eléctrica debido a la carga de las cadenas estabiliza el sistema. Como resultado, a temperaturas superiores a la LCST se tienen partículas coloidales monodispersas de tipo esfera dura. Por tanto, simplemente variando la temperatura se puede pasar de una disolución polimérica a una dispersión coloidal de partículas duras y viceversa. El objetivo de este trabajo es doble. Por una parte se presentan las propiedades de este novedoso sistema, y por otra, se investigan con ellas la física que subyace a los efectos de especificidad iónica. En concreto, se pretende obtener resultados que permitan contrastar la teoría de Ninham basada en fuerzas de dispersión.

Se sintetizó un sistema aniónico y otro catiónico. En primer lugar se examinaron las propiedades de las disoluciones poliméricas. Concretamente la variación de la LCST en función de la concentración de sal con las distintas especies iónicas (en este caso se analizaron sólo los aniones). Los efectos provocados por los distintos iones difieren en órdenes de magnitud. Estas curvas se ajustaron aplicando un modelo teórico propuesto por Zhang y colaboradores en el que el desplazamiento causado por la sal en la LCST se modela con un término lineal y una isoterma de Langmuir. En el caso de iones caotrópicos, estos autores afirman que el término lineal está relacionado con cambios en la tensión superficial del polímero, lo cual se vuelve a confirmar con nuestros datos experimentales. De acuerdo con la teoría de Ninham los cambios que los electrolitos originan en la tensión superficial de la interfase están a su vez relacionados con la polarizabilidad de los mismos. Conectando la teoría de Ninham con el modelo de Zhang pudimos comprobar que existe una correlación entre las pendientes del término lineal obtenidas del ajuste y la polarizabilidad de los iones, que demás siguen la relación funcional que predice la teoría de Ninham. Está correlación se pierde en el caso del sulfato, cuyo carácter kosmotrópico hace que la fuerte interacción con las moléculas de agua provoque efectos que enmascaren el efecto de las fuerzas de dispersión.

A continuación se estudió el cambio de fase del sistema con la temperatura mediante el seguimiento de la evolución del diámetro medio de los

componentes de la dispersión. En este proceso se distinguieron tres etapas una vez superada la LCST: i) una primera región de inestabilidad termodinámica en la que las cadenas se asocian y el diámetro medio crece, ii) seguida de una región de estabilidad cinética en la que el crecimiento de las partículas se detiene debido a la aparición de una barrera de potencial eléctrica repulsiva y iii) una última etapa en la que el diámetro decae hasta alcanzar un *plateau* debido a la relajación del polímero. La presencia de una concentración de sal de sólo 10 mM en el medio dio lugar a tamaños finales de partículas que varían entre 200 nm y 2 μm. Estas diferencias fueron explicadas en base a la acumulación específica de iones capaz de modificar la barrera de potencial repulsiva entre partículas. Los procesos de acumulación iónica se manifestaron de manera explícita al estudiar la movilidad electroforética del sistema durante el cambio de fase. De nuevo, los resultados fueron explicados satisfactoriamente mediante la teoría de Ninham salvo en el caso el sulfato. La resolución de la ecuación no lineal de Poisson Boltzmann, considerando además de la energía potencial eléctrica de los iones un término imagen y otro de dispersión, nos permitió calcular los perfiles de concentración iónica cerca de la interfase.

Por tanto se concluye que las fuerzas de dispersión son una fuente de especificidad iónica, y por tanto, tienen que ser consideradas al estudiar interacciones en presencia de iones. Sin embargo, una explicación general de estos fenómenos debe incluir la naturaleza discreta del agua.

CONCLUSIONES Y PERSPECTIVAS

Las conclusiones y resultados más relevantes extraídos de esta tesis doctoral se enumeran a continuación:

Bloque I: Estabilidad y movilidad electroforética de partículas coloidales tipo "hard sphere".

1. Los estudios de estabilidad y movilidad electroforética realizados con partículas de poliestireno han puesto de manifiesto la existencia de fenómenos Hofmeister en este tipo de sistemas. Los resultados experimentales se escapan a las predicciones de la teoría clásica de estabilidad coloidal DLVO (Derjaguin-Landau-Verwey-Overbeek). Mecanismos basados en una acumulación iónica específica permiten explicar los resultados obtenidos.

2. El estudio realizado con partículas de poliestireno fue extendido a otros sistemas con diversas características superficiales (partículas de poliestireno recubiertas con la proteína IgG, sílice, quitosano, etc.). Aunque la posición relativa de las distintas especies iónicas dentro de las series de Hofmeister resultó ser prácticamente la misma, se observaron series invertidas en función de las propiedades de la superficie coloidal analizada. Se concluyó que dos factores determinan el orden final de las series: i) el signo de carga y ii) el carácter hidrófobo/hidrófilo de la superficie considerada.

3. Las inversiones por signo de carga en sistemas hidrófobos (partículas de poliestireno) pueden ser explicadas mediante la teoría de Ninham y Yaminsky basada en procesos de acumulación/exclusión iónica originados por fuerzas de dispersión entre iones y superficies. Sin embargo, esta teoría no puede explicar las inversiones parciales detectadas en superficies con el mismo signo de carga pero con distinto carácter hidrófilo/hidrófobo. La correlación encontrada entre este tipo de inversiones y procesos de reestabilización a altas concentraciones de sal, puso de manifiesto el papel crucial de la estructura de agua en estos procesos.

4. Por primera vez se observaron fenómenos de reestabilización con aniones caotrópicos (débilmente hidratados) actuando no sólo como contraiones sino también como coiones. Esto ha supuesto la generalización del concepto de fuerzas de hidratación tal y como se emplea para explicar la

reestabilización de sistemas coloidales. La teoría de Ruckenstein, ampliamente utilizada para explicar los fenómenos de reestabilización en sistemas coloidales, queda cuestionada en base a estos novedosos resultados experimentales.

5. La teoría de Ohshima y Kondo explica los resultados de movilidad electroforética correspondientes a complejos poliestireno-IgG y permite un análisis cuantitativo de la acumulación específica de las distintas especies iónicas en la capa de polielectrolito.

Bloque II: Cineticas de agregacion de particulas de poliestireno.

1. La doble naturaleza que subyace a los fenómenos Hofmeister (reestructuración del agua y acumulación/exclusión iónica) se puso de manifiesto de manera clara al estudiar las cinéticas de los procesos de agregación de partículas de poliestireno y comparar estos resultados con las concentraciones críticas de coagulación asociadas (ccc).

2. Se comprobó que distribución de iones en torno a la superficie de las partículas varía considerablemente al incluir las fuerzas de dispersión ion-superficie que contempla la teoría de Ninham y Yamiski. Los perfiles iónicos obtenidos al resolver la ecuación de Poisson-Boltzmann autoconsistente, muestran como los aniones más polarizables tienden a acumularse más intensamente sobre la superficie de las partículas, estabilizando los sistemas aniónicos y desestabilizando los catiónicos.

3. Independientemente del efecto del ion en la estabilidad del sistema, se observó que las cinéticas de agregación se vuelven más lentas cuanto más caotrópica es la naturaleza del anion. Esta conclusión se apoya en valores de constantes cinéticas de agregación y dimensión fractal de los agregados. Estos resultados se confirmaron haciendo uso de técnica SCLS (Single Cluster Light Scattering), que permite analizar la distribución en tamaño de agregados con el tiempo. Resultados sorprendentes se obtuvieron con el ion más caotrópico, el SCN^-, con el que llega a observarse como la agregación se congela a tiempos largos. Estas curvas representan la primera medida directa de un proceso de agregación completamente reversible.

4. A partir de las curvas de distribución en tamaño de agregados se obtuvo información a cerca del potencial de interacción entre partículas. Para ello se hizo uso de la ecuación maestra del método estocático, considerando un kernel de agregación browniano y otro de fragmentación. El ajuste entre teoría

y experimentos resultó ser muy bueno, y puso de manifiesto la existencia de mínimos poco profundos en el potencial de interacción entre partículas cuando los iones son caotrópicos. La agregación en regiones de potencial de poca profundidad se debe a la formación de capas de agua muy estructuradas entorno a estos iones que suponen una barrera estérica a cortas distancias.

Bloque III: Sistemas coloidales basados en PNIPAM.

1. Los comúnmente estudiados microgeles aniónicos de PNIPAM, sintetizados mediante un procedimiento de polimerización por precipitación, manifiestan una estructura más heterogénea, menor tamaño, y una mayor capacidad de hinchado que partículas catiónicas de PNIPAM sintetizadas con el mismo procedimiento pero que además presentan ligeras cantidades del comonómero AEMH (aminoethyl methacrylate hydrochloride).

2. Tras analizar el efecto de la sal en las propiedades físico-químicas de estos microgeles se concluyó:

- La presencia de sal en el medio desplaza la temperatura crítica de transición de fase tanto en volumen (T_{VPT}) como electrocinética (T_{ET}) del PNIPAM a valores inferiores de T.

- Estas partículas presentan un diagrama de estabilidad T-c en el que se distinguen dos dominios claramente diferenciados. El paso de la región de estabilidad a la de inestabilidad es totalmente reversible.

- El deshinchado de las partículas provocado por la sal decrece según una ley de potencias de tipo c^{-m}, con $m > 0.2$ que es el valor característico de microgeles iónicos. La ruptura de la estructura de agua que rodea al grupo isopropilo del PNIPAM se propone como principal responsable de estos procesos de deshinchado.

- El máximo encontrado en curvas de movilidad electroforética en función de la concentración de sal frecuente en sistemas tipo "hard sphere" desparece conforme el carácter de la partícula se hace "soft".

- Las transiciones de fase electroforéticas fueron interpretadas satisfactoriamente mediante la teoría de Ohshima y Kondo.

3. Las partículas basadas en PNIPAM son sistemas altamente sensibles a los fenómenos Hofmeister. La especificidad iónica que se distingue en partículas rígidas resulta llamativa en estos microgeles termosensibles.

Especialmente en lo que respecta a la movilidad electroforética, que hasta ahora no había sido investigada. Por ejemplo, electrolitos monovalentes a concentraciones de tan solo 10 mM son capaces de invertir completamente la movilidad electroforética de las partículas.

4. La naturaleza dual de los microgeles de PNIPAM fueron explotadas para observar, de manera independiente, los dos mecanismos microscópicos responsables de los efectos Hofmeister. Los procesos de hinchado pusieron de manifiesto el efecto de los iones en la estructura del agua. Mientras que medidas de movilidad electroforética demostraron la existencia de procesos de acumulación iónica.

5. El efecto de los iones en los fenómenos de hinchado de estos microgeles no-iónicos fue interpretado mediante la teoría termodinámica de Flory-Rehner. En base a las evidencias experimentales, se propuso que la presencia de iones en el medio modifica el término entrópico del parámetro de Flory, alterando así la solvencia del polímero. A partir de las curvas experimentales de hinchado se pudo determinar cuantitativamente el cambio entrópico asociado a los distintos electrolitos. El aumento de la concentración de sal en el medio resultó tener un efecto equivalente a incrementar la temperatura del sistema.

6. Los procesos de acumulación iónica se explicaron en base a la teoría de Ninham.

7. El fenómeno de cononsolvencia que experimenta el PNIPAM en disoluciones etanol/agua se ve afectado por la presencia de electrolitos en el medio. Los iones Cl^-, NO_3^- y SO_4^{2-}, manifiestan un comportamiento distinto al observado con SCN^-. Dichos iones se comportan como en agua pura cuando $\phi_e < 0.2$ (ϕ_e fracción en volumen de etanol) y precipitan a concentraciones de alcohol superiores.

8. El diagrama de estabilidad c-ϕ_e (c concentración de sal) correspondiente al SCN^- presenta tres regiones claramente definidas: i) $\phi_e < 0.2$, ii) $0.2 < \phi_e < 0.5$ y iii) $0.5 < \phi_e < 0.7$. Cuando $\phi_e < 0.2$ el efecto del SCN- es cualitativamente similar al del resto de los electrolitos. Sin embargo, estas tendencias se invierten a $\phi_e > 0.5$. Concretamente, se ha observado estabilización e hinchado de partículas de PNIPAM como consecuencia del aumento de la concentración de SCN^- en el medio. A concentraciones de etanol intermedias, $0.2 < \phi_e < 0.6$, ambas tendencias se solapan dando lugar a

diagramas de fase re-entrantes. Estos comportamientos anómalos ponen de manifiesto los cambios estructurales que el ion provoca en el solvente y apoya modelos basados en la formación de complejos etanol/agua para explicar los fenómenos de cononsolvencia.

9. Se sintetizaron sistemas reversibles basados en la asociación de cadenas cargadas de PNIPAM a T > LCST, dando lugar a partículas cuyo tamaño final puede ser controlado con la concentración y el tipo de sal empleada.

10. Las modificaciones que los distintos electrolitos provocan en la LCST de la disolución polimérica inicial se ajustan al modelo empírico propuesto por Zhang y colaboradores para cadenas de PNIPAM no cargadas. Dicho modelo fue interpretado haciendo uso de la teoría de Ninham. Se encontró una correlación entre la constante de proporcionalidad del término lineal que aparece en el modelo de Zhang, asociado a cambios en la tensión superficial, y la polarizabilidad de los electrolitos.

11. En el proceso de formación de las partículas se distinguen tres etapas: estabilidad termodinámica, desestabilización, estabilidad cinética y relajación de las cadenas. Los cambios sustanciales en el tamaño final de las partículas pueden ser explicados en base a fenómenos de adsorción específica originados por fuerzas de dispersión. Sólo en el caso del SCN- se obtuvieron partículas estables con el polímero catiónico. La acumulación de este ion en la interfase polímero/agua fue tan importante que invirtió el signo de la carga superficial de las partículas. La acumulación iónica se hace obvia al estudiar la movilidad electroforética. Los perfiles iónicos que resultan de resolver la ecuación autoconsistente de Poisson-Boltzmann incluyendo los términos imagen y de dispersión en la energía potencial de los iones, fueron contrastados con las curvas de movilidad, llegando a un gran acuerdo.

Las perspectivas futuras de este trabajo de investigación son numerosas. Desde un punto de vista experimental, uno de los objetivos que se plantean es la utilización de técnicas experimentales que permitan acceder de manera más directa a las propiedades microscópicas del sistema. Como proyecto futuro se tiene, por ejemplo, la utilización de la técnica RMN (resonancia magnética nuclear) para investigar las propiedades del solvente en el interior de microgeles de PNIPAM en presencia de sales Hofmeister. Desde un punto de vista más teórico se pretende incluir las fuerzas de dispersión, tal y como se proponen en el modelo de Ninham, para explicar ciertos fenómenos relacionados con la especificidad iónica. Una futura colaboración con otros miembros del grupo tiene como objetivo estudiar mediante simulación cómo la concentración local de iones que predice el modelo de Ninham cerca de una interfase se ve afectada por correlaciones iónicas y efecto de tamaño de iones.

REFERENCIAS

[1] R. M. Pashley, P. M. McGuiggan, B. W. Ninham, J. Brady y D. F. Evans, *J. Phys. Chem.*, **1986**, 90 : 1637.

[2] S. Lewith, *Arch. Exp. Pathol. Pharmakol.*, **1888**, 24 : 1.

[3] F. Hofmeister, *Arch. Exp. Pathol. Pharmakol.*, **1888**, 24 : 247.

[4] W. Kunz, P. Lo Nostro y B. W. Ninham, *Current Opinion in Colloid Interface Sci.*, **2004**, 9 : 1.

[5] K. D. Collins y M. W. Washabaugh, *Quarterly Rev. Biophys.*, **1985**, 18 : 323.

[6] M. G. Cacace, E. M. Landau y J. J. Ramsden, *Quarterly Rev. Biophys.*, **1997**, 30 : 241.

[7] J. Lyklema, *Molecular Physics*, **2002**, 100: 3177.

[8] K. D. Collins, *Methods*, **2004**, 34: 300.

[9] Y. Koga, P. Westh, J. V. Davies, K. Miki, K. Nishikawa y H. Katayanagi, *J. Phys. Chem. A*, **2004**, 108 : 8533.

[10] P. Westh, H. Kato, K. Miki, K. Nishikawa y Y. Koga, *J. Phys. Chem. A*, **2006**, 110 : 2072.

[11] R. W. Gurney, *Ionic Processes in Solution* (New York, McGraw-Hill).

[12] J. P. Chatterjee y I. N. Basumallick, *J. chem. Soc. Faraday Trans.*, **1990**, 86 : 3107.

[13] R. Leberman y A. K. Soper, *Nature (London)*, **1995**, 378 : 364.

[14] R. Jimenez, G. R. Fleming, P. V. Kumar y M. Maroncelli, *Nature (London)* **1994**, 369 : 471.

[15] S. E. Jackson y M. C. R. Symons, *Chem. Phys. Lett.*, **1976**, 37 : 551.

[16] N. G. M. Pay y M. C. R. Symons, *J. chem. Soc. Faraday Trans.*, **1993**, 89 : 2417.

[17] J. Davies, S. Ormondroyd y M. C. R. Symons, *Trans. Faraday Soc.*, **1971**, 67 : 3465.

[18] Y. G. Bérubé y P. L. de Bruyn, *J. Colloid Interface Sci.*, **1968**, 28 : 92.

[19] S. Marcelja y N. Radic, Chem. Phys. Lett, **1976**, 42 : 129.

[20] R. Kjellander y S. Marcelja, J. Phys., **1988**, 49 : 1009.

[21] B. W. Ninham y V. Yaminsky, *Langmuir*, **1997**, 13 : 2097.

[22] B. W. Ninham, *Adv. Colloid Interface Sci.*, **1999**, 83 : 1.

[23] B. W. Ninham, *Prog Colloid Polym Sci*, **2002**, 12 : 1.

[24] M. Boström, D. R. M. Williams y B. W. Ninham, Phys. Rev. Letters, **2001**, 87 : 168103-1.

[25] B. V. Derjaguin y L. Landau, *Acta Physiochim.*, 1941 14 : 633.

[26] E. J. Verwey y J. T. G. Overbeek, *Theory of the Stability of Lyophobic Colloids* (Elsevier Publishing Company, Inc., Amsterdam, 1948).

[27] G. Nägele, *Soft Matter: Complex Materials on Mesoscopic Scale*, capítulo B16 (Schriften des Forschungszentrums Jülich Reihe).

[28] E. M. Lifshitz, *Soviet. Phys. JETP* (Trad. Ingl.), **1956**, 2 : 73.

HOFMEISTER EFFECTS IN THE STABILITY AND ELECTROPHORETIC MOBILITY OF POLYSTYRENE LATEX PARTICLES

Teresa López-León, Ana B. Jódar-Reyes, Delfi Bastos-González, and Juan L. Ortega-Vinuesa

Colloid and Fluid Physics Group, Department of Applied Physics, University of Granada, Av. Fuentenueva S/N, 18071 Granada , Spain

Abstract

Specific ionic effects on numerous solid-aqueous solution interfaces have usually been ranked in the so called Hofmeister series. Ion specificity has experimentally been manifested in many ways. In this work, the colloidal stability and electrophoretic mobility of three different polystyrene latex samples are analyzed in presence of different electrolytes. The effects on their colloidal stability and electrokinetic behaviour provoked by four anions (SO_4^{2-}, Cl^-, NO_3^- and SCN^-) and three cations (NH_4^+, Na^+ and Ca^{2+}) located in different positions in the Hofmeister series are shown. Some of these ions specifically modified the pair potential interaction of the colloidal particles yielding results not explained by the Derjaguin, Landau, Verwey and Overbeek (DLVO) theory. A modification in the repulsive electrostatic term of this theory is then proposed to consider the ionic specificity. In addition, general but qualitative explanations about the subjacent mechanisms involved in the Hofmeister effects are also summarized.

I. Introduction

Interactions between particles dissolved in aqueous solutions are sometime significantly affected by the presence of different electrolytes. The nature of the different salts, even those having identical charge characteristics, specifically affects the interaction pair potential between surfaces. This is a phenomenon experimentally known a long time ago, although a satisfactory theoretical interpretation is still missing.

The introduction of this paper can be divided in two clearly different parts. The first one aims to present the state of the art of the specificity of the ions, summarizing the main features of this topic, highlighting the complexity of the problem, and discussing two simple microscopic models that can help to understand the ionic specificity. The second part deals with the specific research developed in this work, in which different ions have been used to destabilize polystyrene latex particles.

1.1. Hofmeister Series.

The ionic effects on the aggregation or stabilization phenomena of particle immersed in aqueous solutions have been extensively studied since 1888. Lewith[1] and Hofmeister[2] published accounts of great differences between the minimum concentration of various salts required to precipitate a given protein from solution, even among those with identical charge characteristics. Many ions have been ranked in sequences called Hofmeister series (henceforth HS), depending on their specific effects on different experimental systems. These effects are manifested by a plethora of experimental measurements (i.e. polymer cloud points, protein solubility, chromatographic selectivity, critical micelle concentration, etc.) as listed in a comprehensive review published by Collins and Washabaugh[3]. Therefore, there should be so many HS as different physical or chemical magnitudes and systems are analysed. Nevertheless, although the relative position of ions in the numerous existing Hofmeister series does not exactly coincide, only slight alterations appear in the characteristic rank ordering. Consequently, a representative Hofmeister series can be given for anions and cations, albeit, as mentioned, their relative positions should be thought of as indicative only.

$$\underset{\text{(kosmotropic anions)}}{\text{Citrate}^{3-} > SO_4^{2-} > PO_4H^{2-} > F^- > CH_3COO^- > Cl^- > Br^- > I^-} > \underset{\text{(chaotropic anions)}}{NO_3^- > ClO_4^- > SCN^-}$$

$$\underset{\text{(chaotropic cations)}}{N(CH_3)_4^+ > NH_4^+ > Cs^+ > Rb^+ > K^+ > Na^+ > H^+} > \underset{\text{(kosmotropic cations)}}{Ca^{2+} > Mg^{2+}}$$

Despite the broad spectrum of experimental results existing at the present date, the molecular origins of the HS remains unravelled. There are some hypotheses about the underlying mechanisms, although a general rule capable of explaining all of them still seems to be elusive. Whatever the molecular mechanism is, the HS emerges from a combination of effects in which the water structure is the cornerstone of the problem. If a Hofmeister series is obtained from systems in which interaction between surfaces takes place, (i.e. adsorption of macromolecules on interfaces, protein crystallization, colloid aggregation, and so on), not only the water structure around the solved ions but also that surrounding the immersed surfaces plays a significant role. This is why establishing a general explanation to all the existing HS becomes almost impossible, because it results from ion-water, water-water, surface-water, surface-ion and surface-surface interactions. What can be done to simplify the study is to analyse separately all these contributions.

Ion – water interactions. It is known that the origin of the HS features lies in the different ways in which ions influence the structure of the water in which they are embedded. Interactions do not arise only from electric ion-dipole forces but also, and sometimes more importantly, from the ability of ions (and even noncharged cosolutes, such as urea) to give or accept a couple of electrons to or from the water molecules. Then the local natural hydrogen bonding network of water changes. That is, the Lewis base or Lewis acid character of the ions, together with their charge and size, must be taken into account[4]. Chromatographic studies[3] and vibrational spectroscopic evidences[5] support a correlation between the HS and water structure. Ions that interact with water more strongly than water itself are known as structure-makers or *kosmotropes*, whereas ions having the opposite effect are known as structure breakers or *chaotropes*. The Hofmeister series shown above have been ordered according to their degree of hydration. Strongly hydrated anions (kosmotropes) are on the left and weakly hydrated anions (chaotropes) are on the right. Cations are just ordered on the contrary; chaotropes, weakly hydrated cations, are on the left and the kosmotropes on the right. It should be noticed that the effects of kosmotrope anions are opposite to kosmotrope cations as, although both of them structure water molecules strongly, the orientation of the oxygen and hydrogen atoms toward the ions surface is also opposite. That is, the water structure induced by a kosmotropic anion must

result similar to that of a chaotropic cation, and viceversa. Finally, the effects shown by the Hofmeister series usually present an inversion at about Cl^- (for anions) and Na^+ (for cations). So, the position of these two ions is usually considered as a null point in the specific ions effects.

Water – water interactions. It should be noted that models that only consider the state of single water molecules immediately adjacent to the ion surface break down for explaining satisfactorily the HS. Therefore, the interaction between the ion and the solvent must be transmitted beyond this first water layer. This is done by a cooperative mechanism by means of water-water hydrogen bonding that is propagated through several molecular layers[6]. The cooperativity of water-water hydrogen bonding is crucial for understanding many conceptual difficulties of different items, not only the nature of the HS, but also the hydrophobic hydration of surfaces, the magnitude of hydrophobic force or the protein folding, as stated by Wiggins[7].

Surface – water interactions. Water also becomes cooperatively structured when it is put into contact at any kind of surface. If the surface is hydrophobic, a particular rearrangement of water molecules is proposed[7-10] leading to aqueous layers adjacent to the surface with a lower density than that found in normal water. The effect of any hydrophilic surface is the opposite, generating a high density layer of water around it. Independently of the surface nature, interfacial water molecules exhibit spatial orientations different from that of bulk water.

Surface – ion and surface – surface interactions. Interactions between surfaces immersed in electrolyte solutions are usually originated by electrical and dispersion forces, and generally they have been studied by continuum theories[11]. The most important feature for the ions is the charge, and those for the surfaces are the Hamaker constant (considering the medium in which they are embedded), and the surface potential. Ion concentrations near a surface differ from those of the bulk, and they are obtained by using a Boltzmann distribution in which only electrical energies are taking into account. However, when two particles approach each other the modified solvent "shells" begin to overlap and the local water structure becomes highly directional[12]. The role of water is probably crucial. Despite that, the structure of water molecules is usually neglected when studying surface interactions, and then, the continuum interfacial theories always fail to explain the Hofmeister effects. To our knowledge, only Ninham and Yaminsky[13] have tried to theoretically justify the

Hofmeister effects that are reflected in changes of the surface potential of an interface. They propose a molecular explanation based on the specific ion adsorption and exclusion by taking into account dispersion interactions between ion and surface, by using a continuum analysis. They argued that the dispersion interactions can be dominant in ion adsorption processes. The dispersion potential essentially depends on the excess polarizability of ions related to water. So, these authors try to present a way to systematize the HS based on the excess of polarizability of the ions. They only, however, attain to properly justify the order of four anions, namely, acetate, Cl^-, Br^-, and I^-, but nothing is said about SCN^- or NO_3^-, which present very striking effects. Because both, surface and ions change the solvent properties around them, the theoretical approaches to the Hofmeister series must be done using discontinuum models and taking molecular considerations. Until now, nobody has solved the problem.

Although there is not any theory that satisfactorily explains how Hofmeister ions specifically affect surface-surface interactions, there are qualitative explanations about how the presence of chaotropic or kosmotropic ions could modify the surface potential (Ψ_0). Concretely, there exist two different molecular mechanisms which are discussed below. Some diagrams have also been included, and although they are rather simple, the schemes can help to understand the HS better.

(1) On one hand, there is a microscopic interpretation of the Hofmeister effects that explains changes in Ψ_0 by means of a specific exclusion or accumulation mechanism of ions at the surface. It should be noted that this mechanism is fundamentally based on entropy changes and thus it differs from that proposed by Ninham and Yaminsky[13] previously commented. To simplify as much as possible this idealization, an uncharged surface is considered, avoiding any Boltzman distribution of ions. In addition, no ion-ion correlation is considered either. Therefore, the accumulation or exclusion of ions will be only led by the structure of the water molecules adjacent to both the surface and the solved ions. As explained above, if a hydrophobic surface is taken into account, the water molecules located at the surface present a modified structure (compared to that of the bulk water) caused by a cooperative mechanism that yields a low density water structure[7]. It is broadly assumed that chaotropic ions disrupt the water structure around them provoking somehow a local "chaos". So, they tend to accumulate in these low density water layers because they prefer to be embedded in this "previously" re-

structured water than to be immersed in "normal" water, which structure they have to reorganize. It should be noted that the surface does not attract chaotropic ions by itself. The accumulation mechanism is mediated by the molecular structures of the water molecules that surround both the surface and the ions. The effect of the hydrophobic surface on a kosmotropic ion is opposite. Kosmotropic ions strongly interact with water, and they do not tend to be immersed in regions where water has a low density. The just discussed mechanism is depicted in the Scheme 1. It becomes easy to understand why the effect induced by a chaotropic anion can be similar to that of a kosmotropic cation. If a non-specific electrolyte is dissolved, that is, NaCl (picture a in Scheme 1), there must not be any specific exclusion or accumulation of ions at the interface, at least as a primary hypothesis. However, if a salt containing a chaotropic anion and a nonspecific cation is now added, that is, NaSCN (Scheme 1, picture b), an accumulation of anions would result near the surface. This would reduce the surface potential, being the Ψ_0 reduction shaper for increasing chaotropic degree. Nevertheless, if the solved salt was formed by a kosmotropic anion and a nonspecific cation, that is, NaF (Scheme 1 picture c), the Ψ_0 value would be higher because anions would be repelled from the surface yielding a local excess of cations. If salts are made of nonspecific anion but chaotropic or kosmotropic cations, that is, NH_4Cl or $CaCl_2$, respectively, the ion distribution would be similar to that shown in Scheme 1, pictures d and e, respectively. (It should be noted that figures have been only depicted for 1:1 electrolytes but not for 2:1 species). Therefore, the effect induced by a chaotropic anion on the Ψ_0 value may be similar to that provoked by a kosmotropic cation. Likewise, a kosmotropic anion would behave as a chaotropic cation. Just compare Scheme 1, pictures b and e, or Scheme 1, pictures c and d. A hydrophilic surface would reorganized the ions just in the opposite way that a hydrophobic surface does. Anyway, the molecular mechanism is similar, although now kosmotropic ions tend to accumulate near the surface, because the water adjacent to a hydrophilic surface have an increased density instead, and chaotropic ions would be located far from this high density water region.

2) On the other hand, there is a second mechanism that can be considered to explain Hofmeister effects in which no ion adsorption considerations are taken into account. As an example we can analyse the surface potential of an air/water interface. It has been argued[14-16] that the

Scheme 1. Modifications in the surface potential induced by means of an ion accumulation or exclusion mechanism[a]

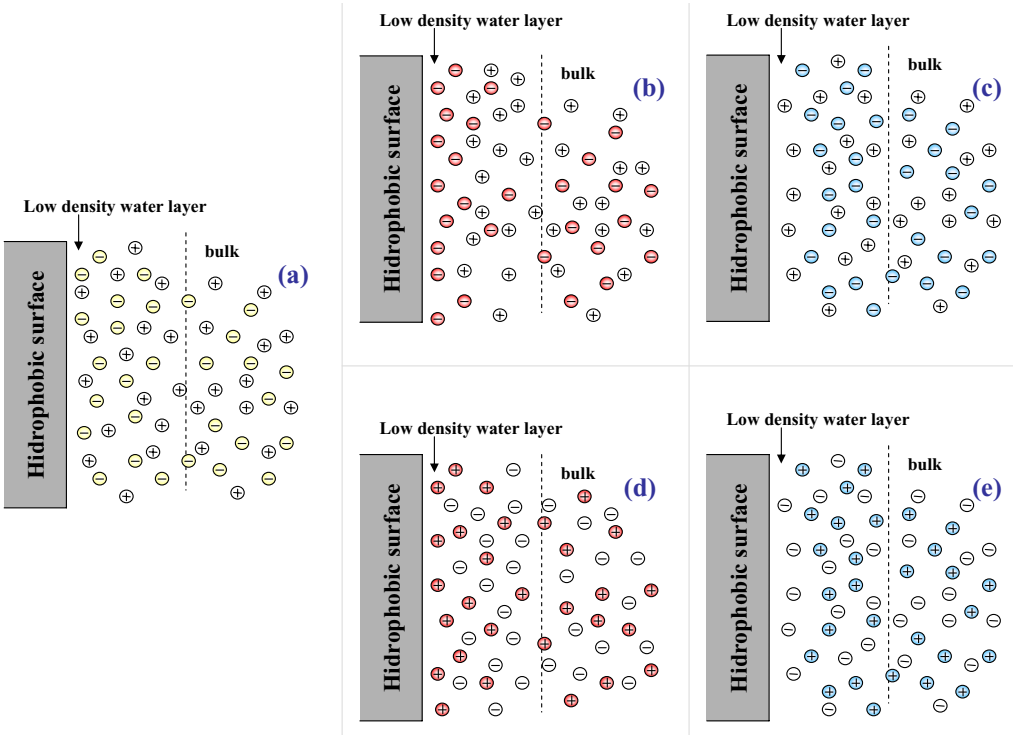

[a] Red circles represent chaotropic ions which tend to accumulate near hydrophobic surfaces; blue circles represent kosmotropic ions, and clear circles represent non-specific ions. Picture (a) depicts nonspecific anions and cations. Picture (b) depicts chaotropic anion and nonspecific cation. Picture (c) depicts kosmotropic anion and nonspecific cation. Picture (d) depicts chaotropic cation and nonspecific anion. Picture (e) depicts kosmotropic cation and nonspecific anion. More details are provided in the main text.

water molecules at the air-water interface have a preferential orientation with the oxygen atoms outermost. A result of this orientation is the establishment of an electrical double layer at the surface with the outermost portion of the double layer being negative and the innermost part being positive. Then, an electrical potential difference ($\Delta\Psi$) can be measured across the air-water

Scheme 2. Modifications in the surface potential induced by changes in the average dipole orientation of the water molecules located at the interface[a]

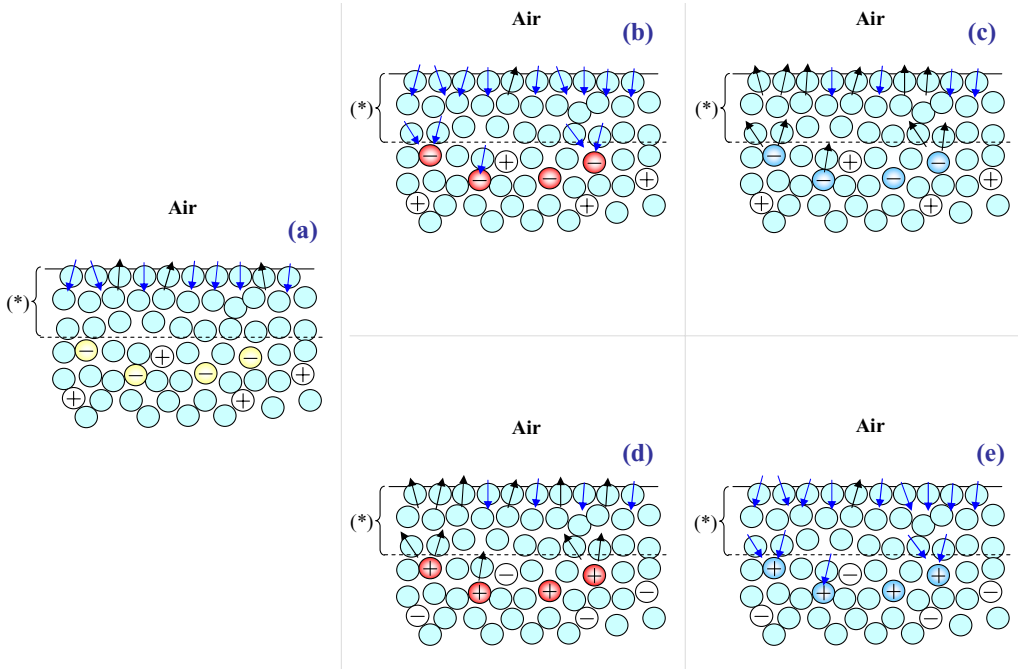

[a] The free ion layer is denoted by (∗). Red circles represent chaotropic ions, blue circles represent kosmotropic ions, clear circles with a charge inside represent nonspecific ions, and cyan circles are the water molecules. The dipoles of some water molecules have been drawn as arrows. Picture (a) represents the situation for nonspecific anions and cations. Picture (b) depicts the effect of chaotropic anions and nonspecific cations. Picture (c) depicts the effect of kosmotropic anions and nonspecific cations. Picture (d) depicts the effect of chaotropic cations and nonspecific anions. Picture (e) depicts the effect of kosmotropic cations and nonspecific anions. More details are provided in the main text.

interface. If water contains an electrolyte, the surface potential can be modified if the solvated ions specifically disrupt the water organization at the interface. It is also assumed that there is deficiency of electrolytes in the surface layer, obtaining a pure water layer about 4 Åthick [17-19]. The way that Hofmeister ions rearrange the interface water dipoles is explained by a cooperative mechanism. Local changes in water structure are transmitted cooperatively by water-water hydrogen bonding[6] through several molecular

layers. Collings and Washabaugh[3] purposed different models that took into account at least three water layers. Scheme 2 shows how this molecular mechanism would act. Nonspecific electrolytes would not modify the structure of pure water, either in bulk or at interface, and then a reference $\Delta\Psi$ value is obtained. If a chaotropic anion is added the local water restructuring is transmitted to the interface water molecules, partially changing their dipole orientations, and then modifying the surface potential. Experimental measurements[20] have shown that chaotropic anions reduce $\Delta\Psi$. Kosmotropic anions rearrange local water molecules in the opposite way that chaotropic anions do, despite having identical sign of charge. This could be understood by remembering that Hofmeister ions restructure the water molecules not only by means of charge and size but also by its Lewis base or acid character. So, a kosmotropic anion would lead to an increase of the $\Delta\Psi$ value (Scheme 2c). The effects induced by cations are just on the contrary of the anions, because of their different charge sign. This has been reflected in Scheme 2d,e. This explanation given for an air/water interface could be extended to any hydrophobic material immersed in water, for example polystyrene.

1.2. Goals of the Paper.

Although there exist numerous references in the literature that use Hofmeister ions to study many systems, few papers can be found presenting a systematic analysis of Hofmeister series using latex particles. This paper is the first part of a broader study centered on the colloidal stability of polystyrene latex particles in the presence of different salts related to the HS. There are three important aspects that have been analysed, namely, (i) the hydrophobic/hydrophilic degree, (ii) the charge sign, and (iii) the surface charge density (σ_0) of the immersed surfaces, to elucidate how they affect ranking of the chosen Hofmeister ions. The work presented in this paper is actually concerned with two of these items, namely, the analysis of the charge sign and the σ_0, because the hydrophobic character of the latex particles has been kept almost constant. The influence of the hydrophobic/hydrophilic character has been extensively evaluated in a second part[21], in which the hydrophobic surface of latex particles was changed to hydrophilic by adsorbing a protein. The Hofmeister salts selected for the study are listed below. On one hand, the salts Na_2SO_4, NaCl, $NaNO_3$, and NaSCN were chosen to analyse the effects of four anions with different positions in the HS. On the other hand,

$Ca(NO_3)_2$, $NaNO_3$, and NH_4NO_3 were selected for comparing cations. In addition, three different latexes have been employed in this work. All of them were synthesized using styrene as unique or major monomer, and their main differences are related to their surface ionic groups. Two of them were anionic with different acid groups at the surface, and the other one presents a positive surface charge having a weak base character. These latex pools allow us to test independently the effect of charge sign and σ_0 of the surfaces on ordering the Hofmeister ions by means of their destabilizating properties. As will be shown, the interaction pair potential between the latex particles is specifically modified by each of these Hofmeister ions, which is reflected on reliable differences regarding the colloidal stability of the latex samples. This is why stating a theoretical model that accounts for the Hofmeister effects would be advisable.

The paper has been structured as follows. First, a complete characterization of the latex particles is described. Then, an extensive study on the aggregation patterns of the latex particles is presented. Subsequently, the electrophoretic mobility behaviour of our samples is evaluated, which can help to corroborate some conclusions arisen from the colloidal stability studies. Finally, the paper finishes with a theoretical section, in which a modification in the electrical term of the Derjaguin, Landau, Verwey, and Overbeek (DLVO) theory is proposed to include in such a theory the Hofmeister effects.

II. Materials and Methods

2.1. Reagents.

Styrene and sodium styrenesulfonate (NaSS) monomers were obtained from Merck and Fluka, respectively, and they were used without further purification. The initiators used in this work were 4,4'-azobis (4-cyanopentanoic acid) (ACPA) purchased from Aldrich and azo N,N'-dymethyleneisobutyramidine hydrochloride (AMDBA) which was kindly donated by Dr. J. W. S. Goosens from Bayer, A. G. A cationic lipid, distearoyl dimethyl ammonium bromide (DSDMA) from Fluka, was also employed in this study. The rest of the salts were of analytical grade and purchased from different firms: Sigma, Panreac, and Scharlau. Double distilled and deionised (DDI) water was used throughout.

2.2. Preparation and Characterization of Latex Particles.

Three different polystyrene latexes have been used in this work. All of them were synthesized in our laboratories. There are two anionic latexes, namely, **ABJ2** and **AMJ5**. The former has strong acid groups (sulfonate) in the surface, and the latter possesses weak acid groups (carboxyl). The third latex, **AMJ10**, is cationic and the nature of its surface charged group is amidine, a weak base group. All of them were prepared by emulsifier-free polymerisation in a discontinuum reaction. The sulfonate latex is a styrene/NaSS co-polymer, and the surface charged groups come from both the initiator molecules and the NaSS co-monomer. **AMJ5** and **AMJ10** were synthesized using styrene as the only monomer. For both latexes, the surface charged groups come from the initiators. ACPA initiator provides carboxyl groups to the **AMJ5** latex, and the cationic groups of **AMJ10** latex derives from the AMDBA molecules. The reactor was a spherical vessel (maximum volume = 1 L), and solutions were stirred with a palette located at 2 cm over the bottom of the vessel. Synthesis conditions were established following studies of different authors[22-24], and they are summarised in Table 1.

A comprehensive cleaning process was followed after the synthesis. It is well known that the diverse methods to prepare clean latexes could provide polymer colloids with quite different electrokinetic and stability properties. For this reason, to clean our latexes, we have followed the recommendations given by Wilkinson et al.[25] in their extensive paper dedicated to reviewing a wide range of cleaning and characterization techniques. After synthesis, the latexes were filtered through glass wool, and then they underwent repeated cycles of centrifugation-decantation-redispersion (except for **ABJ2** latex, due to its small size). Subsequently, serum replacement was employed in several steps: first with DDI water until the electrical conductivity of the samples was below 2 $\mu S\ cm^{-1}$. Then, a strong acid solution was added to serum replacement to replace the cations with protons. Finally, DDI water was added to remove the excess acid until the electrical conductivity was, again, below 2 $\mu S\ cm^{-1}$.

The average particle diameter was obtained by transmission electron microscopy (TEM) using a H-7000 FA Hitachi microscope. The mean diameter of each latex sample was obtained averaging over 500 individual particles (automatically analyzed with Bolero software, AQ Systems).

Table 1. Syntesis conditions of the latexes[a]

latex	H_2O (mL)	St (g)	NaSS (mg)	$K_2S_2O_3$ (mg)	$NaHSO_3$ (mg)	$NaHCO_3$ (mg)	ACPA (mg)	ADMBA (mg)	NaOH (mg)	HCl (μL)	Stirring rpm.	T (°C)	Time (h)
ABJ2	567	90	775	820	320	508					250	45	14
AMJ5	720	25					300		225		350	80	20
AMJ10	720	35						200		390	350	60	15

[a] Abbrevation: st, styrene; NaSS Sodium Styrenesulfonate; ACPA, 4,4'-azobis (4-cyanopentanoic acid); ADMBA, azo N,N'-dymethyleneisobutyramidine hydrochloride.

Surface charge densities of the latexes were determined by conductimetric and potentiometric automatic titrations employing a pH-meter (Crison Instruments, model 2002) and a conductimeter (Crison Instruments, model 525) and a Dosimat 665 (Metrhom) to add the tritant agent.

2.3. Electrophoretic Mobility.

Electrophoretic mobility measurements were performed with a Zeta-Sizer IV (Malvern Intruments). Latex particles were diluted in the desired electrolyte solution and data were obtained from the average of six measurements at the stationary level in a cylindrical cell. Standard deviations were always lower than 5%. It should be noted that no buffered solutions were used in both mobility and coagulation experiments to avoid the presence of other salt species different from the chosen Hofmeister ions.

2.4. Colloidal Stability.

Particle aggregation studies were carried out using a low-angle light-scattering technique. Scattering light intensity was observed at 10^o for 120 s. The scattering cell was rectangular with a 2 mm path length. The cell was thoroughly cleaned with chromic acid, rinsed with distilled water, and then dried using an infrared lamp. Equal volumes (1 mL) of salt and latex solutions were mixed and introduced into the cell by an automatic mixing device. Aggregation analysis were performed in two nonbuffered solutions at pH 4 (HCl 10^{-4} M) and pH 10 (NaOH 10^{-4} M) freshly prepared.

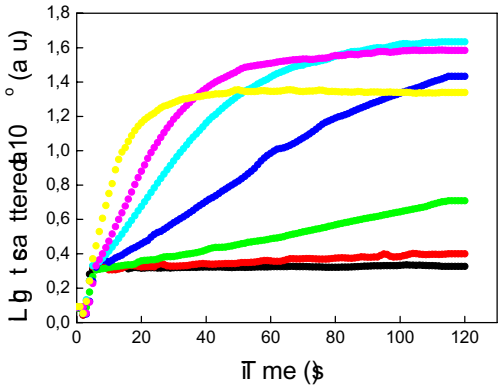

Figure 1. Aggregation kinetic of **ABJ2** particles for increasing NaCl concentration: (●) 100,(●) 150, (●) 200, (●) 250, (●) 300, (●) 400, and (●) 625 mM.

The latex dispersions used for such coagulation experiments were diluted enough to minimize multiple scattering effects. The light scattered at 10° behaves linearly for the first steps of the coagulation. However, linearity was rapidly lost in the aggregation kinetics in which aggregates of large size were formed quickly. A typical coagulation experiment is shown in Figure 1.

The stability ratio, also called Fuch's factor (W), is a criterion broadly used to study the stability of colloidal systems. It can be obtained by the following expression

$$W = \frac{k_r}{k_s} \tag{1}$$

in which the rate constant k_r corresponds to rapid coagulation kinetic, and k_s is the rate constant for slow coagulation regime. The ratio of both constants is equal to that of the ratio of the initial slopes in our coagulation experiments (see Figure 1). The critical coagulation concentration (CCC), that is, the minimum salt concentration needed to rapidly aggregate the colloidal system, can be easily obtained by plotting the logarithm of W versus the logarithm of the salt concentration and locating that point where log W reduces to zero.

Table 2. Some characteristics of latex particles[a]

Latex	Mean diameter (nm)	PDI	σ_0 at pH 4 ($\mu C/cm^2$)	σ_0 at pH 10 ($\mu C/cm^2$)
ABJ2	138 ± 7	1.007	-9.6 ± 0.4	-9.6 ± 0.4
AMJ5	364 ± 13	1.004	-6.1 ± 0.3	-20.5 ± 0.8
AMJ10	320 ± 15	1.007	+18.3 ± 1.2	+4.0 ± 0.6

[a] Abbrevation: PDI, polydispersity index; σ_0, surface charge density.

III. Results and Discussions

3.1. Surface Characterization of Latex Particles.

A complete surface characterization of latex particles were performed to quantify the surface charge density and its dependence on pH. Strong acidic and weak acidic and basic characters of surface groups were also corroborated measuring the electrophoretic mobility as a function of pH. First, the mean diameter of the particles was measured by TEM. The obtained results are shown in Table 2. The three latex samples were highly monodisperse, their polydispersity index (PDI) being extremely close to unity.

The surface charge density (σ_o) of latexes **AMJ5** and **AMJ10** were obtained by conductometric back titration. The σ_o calculation for latex particles with weak acid or base groups must not present any difficulty, and details on how it can be obtained are described in ref 26. However, the calculus of σ_o for a sulfonate latex by means of conductometric titration may become unreliable because the strong acid groups on the surface are not possible to determine directly. What is evaluated is the concentration of H_3O^+ ions that act as counterions. Hence, correlating the H_3O^+ concentration to the surface charge density may become a difficult task because the usual counterions, Na^+ or K^+ (which arise from those electrolytes used in the particle synthesis), must previously be completely replaced by protons. Whatever the method used to replace the cations (usually incubation with ion-exchange resins or, as in our case, by addition of a strong acid to the serum replacement device), it is really difficult to ensure a total exchange of protons. Therefore, a shadow of a doubt always remains when σ_o values of sulfonate latexes are

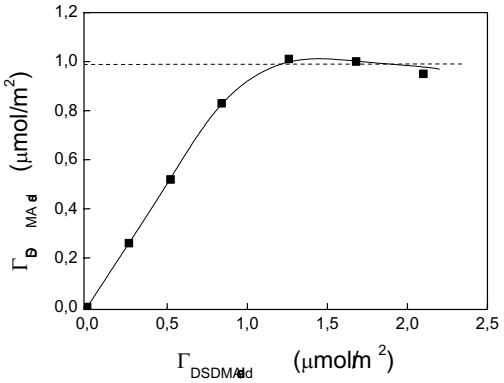

Figure 2. Adsorption isotherm of DSDMA in 50% ethanol/water solutions (v/v), for the **ABJ2** latex.

calculated. This is why the surface charge density of the **ABJ2** was obtained by in alternative way: adsorbing a cationic lipid, namely, DSDMA, in a 50% (v/v) ethanol/water mixture. Details are given elsewhere,[27] and what is shown is that in 50% ethanol/water solutions the adsorption of DSDMA on a polystyrene latex with sulfonate groups is mainly led by pure electrostatic attraction. At maximum DSDMA coverage, latex-lipid complexes are totally unstable because a complete charge cancellation takes place. Obtaining σ_o is immediate knowing the number of lipid molecules adsorbed per unit area, assuming that each sulfonate group is balanced by one DSDMA. Such a DSDMA adsorption onto the **ABJ2** particles is shown in Figure 2.

The surface charge density of latexes with weak acid or base groups depends on pH. This dependence can be analyzed by potentiometric titrations, as also described in ref 26. The σ_o values versus pH for the three latexes are plotted in Figure 3a. In addition, the σ_o dependence on pH has been corroborated by electrophoretic mobility (μ_e) measurements, shown in Figure 3b. It can be observed that for sulfonate latex the μ_e remains constant in all of the pH range studied, while for carboxyl and cationic latexes, a decrease in μ_e values is perceived when their σ_o values diminish. From these measurements, it is easy to identify the weak acidic and basic character of the

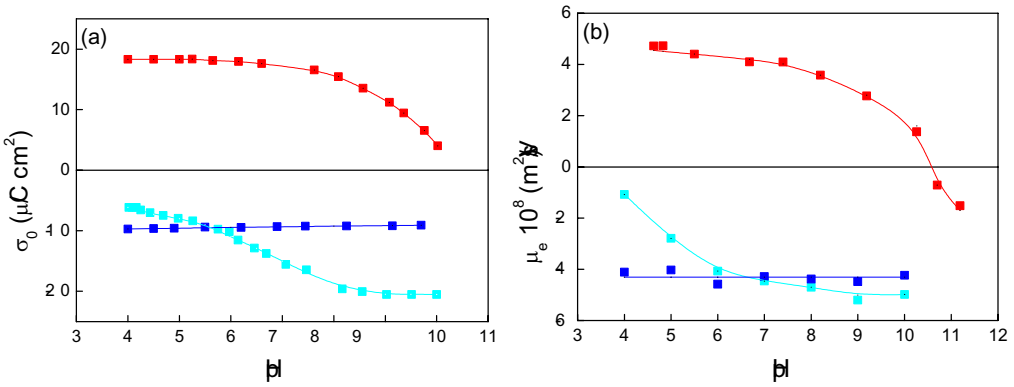

Figure 3. Dependence of (a) the surface charge density and (b) the electrophoretic mobility on pH for the (■) **ABJ2**, (■) **AMJ5,** and (■) **AMJ10** latexes.

latexes, although it should be noted that there is not an exact correspondence between σ_o and μ_e data because mobility is related to ζ potential and not to the surface potential.

3.2. Colloidal Aggregation Results.

Because **AMJ5** and **AMJ10** latexes change their σ_o values with pH, the stability studies were carried out at two of them, pH 4 and pH 10, to check whether Hofmeister effects could also depend on different surface charge densities. Table 2 collects the σ_o values obtained by titration at these pHs. As it was previously commented, the **ABJ2** latex does not modify its σ_o value, and thus stability of this sulfonate latex can be studied at only one pH. We chose pH 4 for its analysis. It is broadly assumed that NaCl is an inert electrolyte with regard to its interaction with polystyrene surfaces. Therefore, experiments of colloidal aggregation performed with such a salt have been taken as a reference for comparing the specific effect of the rest of the salts. Aggregation results are shown in Figures 4 (**ABJ2**), 5a,b (**AMJ5** at pH 4 and 10, respectively), and 6a,b (**AMJ10** at pH 4 and 10, respectively). The CCC values obtained from these figures are indicated in Table 3. Some conclusions can be extracted from this vast set of experiments. The most relevant of them are listed in the following.

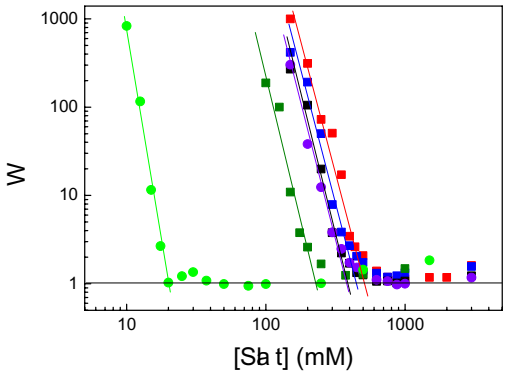

Figure 4. Stability ratio (Fuch's factor) versus electrolyte concentration for the **ABJ2** latex at pH 4: (■) NaSCN, (■) $NaNO_3$, (■) NaCl, (■) Na_2SO_4, (●) NH_4NO_3, and (●) $Ca(NO_3)_2$.

(1) First, the stability patterns obtained by NaCl are discussed. The CCC values are practically in the same order as those of the σ_o values, the most stable latex being the most charged. There is, however, a slip in such ranking. The cationic latex (**AMJ10**) at pH 4 presents a quite low stability (CCC being equal to 210 mM with NaCl) while its surface charge density is high (18.3 μC/cm^2), that is, actually near the carboxyl latex when it is totally charged (20.5 μC/cm^2). Besides, the mobility data shown in Figure 3b would prompt the thought that **AMJ10** should show a higher stability at acid pH than that obtained. At least, electrostatic arguments would aim to this conclusion. Some authors[28], however, have found flocculation phenomena in situations in which measured ζ-potential was still sufficient to ensure electrostatic repulsion between colloidal particles. Such a coagulation was justified by means of hydrophobic attraction. In principle, this reasoning should not be applied to our latexes because all them are made of polystyrene and, thus, no important differences in the hydrophobic character among their surfaces should be expected. Nevertheless, it has been demonstrated[24, 29, 30] that cationic polystyrene particles synthesized with the AMBDA initiator present a more hydrophobic surface. Justification lies in the fact that their charged groups (amidine) are placed in an organic heterocycle, and then they are

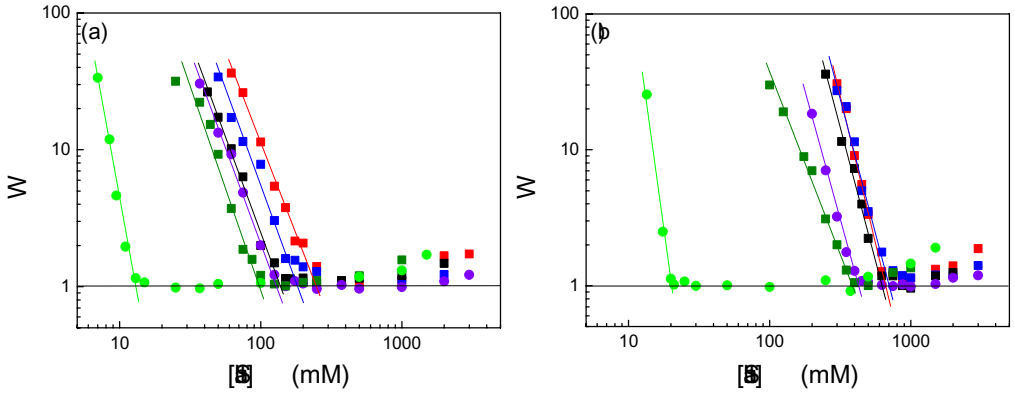

Figure 5. Stability ratio (Fuch's factor) versus electrolyte concentration for the AMJ5 latex at (a) pH 4 and (b) pH 10: (■) NaSCN, (■) $NaNO_3$, (■) NaCl, (■) Na_2SO_4, (●) NH_4NO_3, and (●) $Ca(NO_3)_2$.

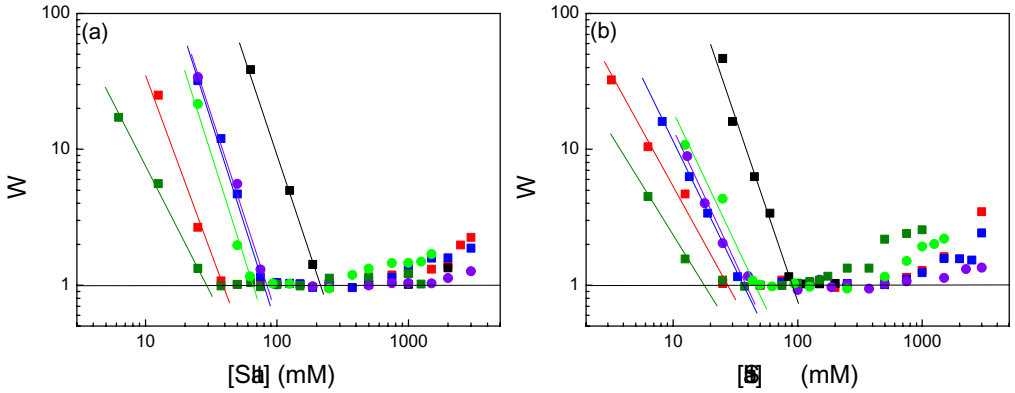

Figure 6. Stability ratio (Fuch's factor) versus electrolyte concentration for the **AMJ10** latex at (a) pH 4 and (b) pH 10: (■) NaSCN, (■) $NaNO_3$, (■) NaCl, (■) Na_2SO_4, (●) NH_4NO_3, and (●) $Ca(NO_3)_2$.

Table 3. Critical coagulation concentration for the latexes at pH 4 and pH 10[a]

ABJ2 latex at pH 4			
Hofm. ion	CCC (mM)	Ψ_0 (mV)	$\Delta\Psi_0$ (mV)
SCN^-	505	-27.0	-1.8
NO_3^-	445	-26.1	-0.9
Cl^-	390	-25.2	0
SO_4^{2-}	225	-29.2	-4.0
NH_4^+	385	-25.1	+1.0
Na^+	445	-26.1	0
Ca^{2+}	20	-14.6	+11.5

	AMJ5 latex at pH4			AMJ5 latex at pH10		
Hofm. ion	CCC (mM)	Ψ_0 (mV)	$\Delta\Psi_0$ (mV)	CCC (mM)	Ψ_0 (mV)	$\Delta\Psi_0$ (mV)
SCN^-	240	-22.7	-3.0	675	-29.6	-0.7
NO_3^-	170	-20.8	-1.1	700	-29.9	-1.0
Cl^-	140	-19.7	0	610	-28.9	0
SO_4^{2-}	100	-24.0	-4.3	370	-33.5	-4.6
NH_4^+	130	-19.4	+1.4	430	-26.3	+3.6
Na^+	170	-20.8	0	700	-29.9	0
Ca^{2+}	13	-14.1	+6.7	21	-15.4	+14.5

	AMJ10 latex at pH4			AMJ10 latex at pH10		
Hofm. ion	CCC (mM)	Ψ_0 (mV)	$\Delta\Psi_0$ (mV)	CCC (mM)	Ψ_0 (mV)	$\Delta\Psi_0$ (mV)
SCN^-	40	14.2	-7.6	27	12.6	-4.9
NO_3^-	80	17.0	-4.8	35	13.6	-3.9
Cl^-	210	21.8	0	90	17.5	0
SO_4^{2-}	30	17.6	-4.2	18	15.3	-2.2
NH_4^+	85	17.1	+0.1	40	14.1	+0.5
Na^+	80	17.0	0	35	13.6	0
Ca^{2+}	72	22.0	+5.0	45	19.5	+5.9

[a] Ψ_0 is the corresponding surface potential obtained by application of the DLVO theory. $\Delta\Psi 0$ is surface potential difference with regard to that obtained for chloride when anions are compared, and that obtained for sodium when cations.

embedded in a more apolar environment than sulfonate or carboxyl groups. Therefore, this more hydrophobic character of the **AMJ10** latex would make particles less stable than predicted by their σ_o value.

(2) Another important feature is that the stability of the latexes is specifically influenced by the nature of the electrolyte used. Whatever latex was chosen, the CCC values differ for different salts. The DLVO theory, extensively used to explain the stability of colloidal particles, does not account the specificity effect of ions, and it predicts the same CCC for 1:1 electrolytes. Likewise, no CCC differences should be obtained between different 2:1 salts. Actually, no classical theory of colloid science can explain quantitatively the experimental results that we have obtained.

(3) In relation to the stability sequence obtained with the Hofmeister ions employed in our latexes, we have found the following results: (i) for negative latexes, **ABJ2** and **AMJ5** at both pH values, the CCC values obtained can be ranked as (more stable) $SCN^- \geq NO_3^- > Cl^- > SO_4^{2-}$ (more unstable) and (more stable) $Na^+ > NH_4^+ > Ca^{2+}$ (more unstable) (with the only exception being carboxyl latex at pH 10 for which the CCC value of NO_3^- was higher than that of SCN^-) and (ii) for the positive latex, **AMJ10**, the order can listed as (more stable) $Cl^- > NO_3^- > SCN^- > SO_4^{2-}$ (more unstable) and (more stable) $NH_4^+ > Na^+ > Ca^{2+}$(more unstable) (with the exception of pH 10 at which Ca^{2+} showed a slightly higher stability that Na^+).

It can be concluded that the order in stability is practically reversed for the cationic latex in comparison to anionic ones. Moreover, taking into account the rank of HS given in the Introduction, it can be seen that for 1:1 electrolytes the sequence coincides with that obtained with our cationic latex and it is opposite for the anionic ones. For divalent anions it can be observed that they always induce the most destabilizing effects. To clarify as much as possible the discussion of the results, the monovalent ions analysis will first be presented. The inversion found in our Hofmeister series when the sign of the surface changes has been also obtained in studies of crystallization of proteins and in the stability of inorganic colloids, despite polystyrene and protein or inorganic surfaces presenting interfacial characteristics that are totally different. On one hand, Riès-Kautt and co-workers showed that a positive protein ordered anions in agreement with HS,[31] but a negative one reversed the order of HS.[32] On the other hand, Franks[33] observed that ζ-potential of negative silica evaluated with different Hofmeister cations showed an ion

ordering that was inverted for positive materials such as alumina, hematite or zirconia. All these patterns can be understood if the presence of Hofmeister ions modifies the surface potential, whatever microscopic mechanism takes place. Jarvis and Scheiman[20] showed numerous experimental data in which the air/water interface potential changed for different added salts. A representative selection of those results obtained with the same ions used by us is shown in Figure 7. As can be seen, SCN^- reduces the surface potential compared to Cl^-, which practically does not change it. NO_3^- also diminishes it, although not as much as SCN^-. If the behaviour of NH_4^+ and Na^+ cations is compared, the ammonium ion slightly increases the surface potential. These features are also observed in our polystyrene/water interface. Compared to Cl^-, the presence of SCN^- ions reduces the surface potential (making it more negative) and thus generates more stable systems if latex particles are negatively charged and less stable once if they are positively charged. NO_3^- behaves as SCN^-, although its effect is not as drastic. The opposite effect is shown by the ammonium ion when compared to sodium, as it slightly increases the potential, improving the stability of cationic latex particles and diminishing that of anionic ones. As shown, monovalent ions seem to induce similar effects in both the air/water and the polystyrene/water interface. Anyway, this behaviour should not be extrapolated to any hydrophobic surface in contact with an aqueous solution because an oil/water interface behaves differently to the air/water interface with regard to the Hofmeister effects.[34]

In relation to the influence of surface charge densities on the stability order, it seems that the sequence was not exceptionally affected when pH, and hence σ_0, was varied because only few exceptions have been found with this variation.

The analysis of the instability induced by divalent ions is not as simple as that previously discussed for the monovalent ions. In this case, the valency of sulphate or calcium ions is more important by means of the reduction of the electric potential associated with the diffuse layer than the modification induced by these ions in the surface potential by means of their "Hofmeister" effect. What is clear is that both ions destabilize dramatically the system when they act as counterions. It would be possible to give a plausible explanation of this phenomenon, at least qualitatively. The concentration of divalent ions near a surface of opposite charge must be much higher than that of those interfaces having the same sign. Then, their divalent nature would

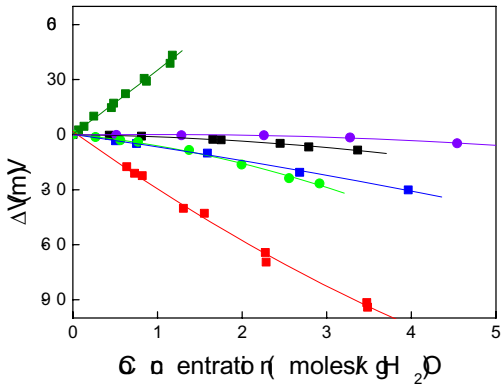

Figure 7. Surface potential difference versus solution concentration of the electrolytes (■) NaSCN, (■) $NaNO_3$, (■) NaCl, (■) Na_2SO_4, (●) NH_4NO_3, and (●) $Ca(NO_3)_2$ for an air/water interface at 20 °C. Data obtained from ref 16.

considerably reduce the electrical potential in the proximity of the surface, facilitating the approximation of the particles and thus triggering aggregation for much lower salt concentrations comparing to 1:1 electrolytes or to situations in which the divalent specie acts as coion. The strong Hofmeister effect shown by these two ions in other systems seems to be a little masked in the coagulation of polystyrene particles. At least, it would not be possible to predict whether the Hofmeister effect of these divalent ions could imply a reduction or an increment of the surface potential, as shown by the monovalent species. Accordingly to the air/water experiments (see Figure 7), sulfate should increase the potential and calcium would reduce it. Nevertheless, a more rigorous analysis must be done prior to stating such a conclusion with our latex particles. That analysis will be shown in the next section.

(4) A general feature of the HS is that they are dominated by anion effects, instead of cations effects.[3,4] Our results aim in the same direction. Comparing our cations, only clear differences among CCC values are obtained when they act as counterions, and thus their local concentration near the surface is high. Differences become questionable, however, when they act as co-ions. This does not happen with the anions, which show significant differences however they act, as counterions or co-ions. In fact, even for anionic latexes

when the local concentration of anions in the proximity of the surface is supposed to be low, nonnegligible variations in the CCC values are obtained.

3.3. Electrophoretic Mobility

The major effect of the anions has also been demonstrated measuring the electrophoretic mobility (μ_e) of the particles versus different salts concentrations. These measurements were performed to support the stability results, although technical limitations of our mobility instrument made it impossible to exactly reproduce the CCC conditions because reliable data can only be obtained for ionic strengths lower than 100 mM (that is, 33 mM for a 2:1 electrolyte). Additionally, much lower concentration of particles than those used in the stability experiments were used in the mobility measurements. These μ_e data are shown in Figure 8. Mobility is plotted versus salt concentration for **ABJ2** and **AMJ10** latexes at pH 4. Results obtained with the **AMJ5** sample gave very similar patterns to those obtained with the other anionic latex. For the sake of clarity, the mobility of this carboxylated latex has not been shown in this Figure 8. From these μ_e data, it is worth highlighting three points that will be independently commented on: (1) The cationic latex shows significant differences among the several salts analysed even at low salt concentration. For the anionic latexes, although these differences exist, they are much less important. (2) In general terms, the differences in the μ_e data observed between cationic and anionic latexes cannot be explained in the basis on their σ_0 values previously obtained. (3) For all the latexes studied, the divalent ions, when acting as counterions, depicted constant μ_e values in all range of concentrations tested, despite their very low CCC values.

In relation to the first point, it can be clearly observed that differences are more significant in the cationic latex, where variations of even 3 mobility units are obtained between NaCl and NaSCN salts. The μ_e data corroborate that SCN^- and NO_3^- make the surface potential of the polystyrene/water interface more negative, always compared to the Cl^- results. As can be also checked in these mobility experiments, the potential reduction induced by the SCN^- ion (which even produces an inversion in the sign of the mobility at high concentrations) is sharper than that of nitrate. This feature also appears in the anionic latexes, although the differences are not as clear as those for the

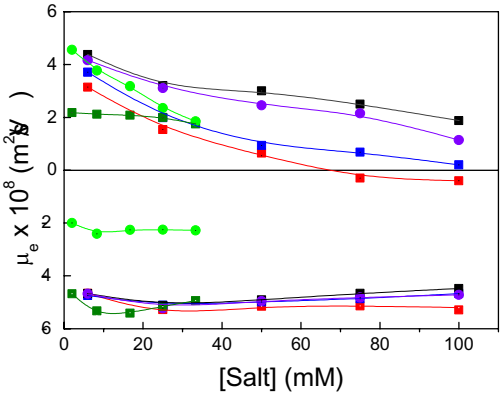

Figure 8. Electrophoretic mobility versus electrolyte concentration for the **ABJ2** latex (negative region) and **AMJ10** latex (positive region) at pH 4. (■) NaSCN, (■) $NaNO_3$, (■) NaCl, (■) Na_2SO_4, (●) NH_4NO_3, and (●) $Ca(NO_3)_2$.

cationic latex for which anions act as counterions. Anyway, in the anionic latexes as the SCN^- concentration becomes higher, the difference with regard to the μ_e data of other monovalent ionic species becomes more significant. If NH_4^+ and Na^+ cations are compared, nitrate being the common anion, mobility data also reflect the stability patterns, that is, the ammonium increases (makes more positive) the polystyrene surface potential, independently of its charge sign. However, differences between monovalent ions are not as noticeable in the anionic latexes. Probably, major differences would be obtained if mobility data could be taken at salt concentrations proximate to the corresponding CCC values. It can also be observed that, as a general feature, the mobility decreases (in absolute value) as the electrolyte concentration becomes higher because of the compression of the electrical double layer. This behaviour is more pronounced for the cationic latex, which presents much lower CCC values than the anionic one. Curiously, no zero mobility was exactly obtained when measured at the corresponding CCC values. The different method used to obtain the mobility, in which particle concentrations are more diluted than those used in the aggregation experiments, could justify these discrepancies. In addition, to obtain the μ_e values the particles are forced to move in an external field. This field could

influence and modify somehow the interaction and the structure of the electric double layer depending on the type of ions surrounding the particles.

A short discussion is now presented to clarify why the mobility patterns of the cationic latex are quite different from that shown by the anionic one. It has been demonstrated[22, 26] that polystyrene latex particles with surface charge density values in the 10-20 μC/cm^2 range and sulfonate or carboxyl groups on the surface show identical μ_e data despite their σ_0 difference. Therefore, changes in mobility are only detectable if changes in σ_0 values take place below (approximately) 10 μC/cm^2. This feature is related to the ion condensation mechanism explained by Maning[35] for linear particles and extended by Belloni,[36] Robert and co-workers[37, 38] and Levin[39] to spherical geometric. Both experimental events, the significant differences found in μ_e data of **AMJ10** latex as a result of small changes in surface potential induced by the Hofmeister ions (which were almost negligible in the **ABJ2** and **AMJ5** samples), and the low CCC value shown by the cationic latex compared to the other two, question the validity of the σ_0 value obtained for the former by titration, despite titration results being repeatedly confirmed.

Anyway, the most striking result shown in Figure 8 is the apparent lack of sensitivity in mobility when divalent ions act as counterions. That is, the mobility of calcium for the **ABJ2** latex behaves as SO_4^{2-} for the cationic one, given an approximately constant μ_e value in the concentration range tested. Surprisingly, in both cases the mobility values at concentrations beyond their corresponding CCC are not zero. We have not found any plausible explanation for this behaviour, although a similar feature was obtained by Wu et al.[28] after adsorbing Ca^{2+} on montmorillonite because coagulation took place in situations in which mobility data showed sufficient electrostatic repulsion to keep stable the colloidal system. They argued that such a lack of stability was due to hydrophobic attraction, because these authors consider the surface interaction to be constituted by three terms: an electrical contribution, which arises from the overlapping of two electrical double layers, a London-van der Waals term, and an interaction potential the origin of which lies on the donor/acceptor electron properties of the surface with the surrounding water. This third contribution is responsible for the (in)stability related to the overlap of solvent shell structured layers and thus is what originates such an non-DLVO attraction between hydrophobic surfaces.

IV. A theoretical approach

As commented previously, the elaboration of a novel theory about surface interactions that explains properly and quantitatively the role played by each of the ions of the Hofmeister series is actually a utopia. Water cooperativity yields spatial orientations in which hydrogen bonds are structured leading to either low or high density water layers. This depends on several properties of the surface and ions such as those related to donor/acceptor electron, charge, and hydrophobic/hydrophilic character, and on the ability of ions to be adsorbed or excluded from interfaces. Nowadays, no theory can undertake these considerations. Because of the complexity discussed above about the establishment of a new theory and for the sake of simplicity, we have chosen to use a DLVO model in which a modification will be introduced to consider the salt specificity of the Hofmeister series. This *modus operandi* can be criticized because this simple theory usually fails because of its own numerous limitations and approximations.[34] Despite this handicap, "extra-DLVO" forces are commonly included when DLVO theory breaks down, as can be checked after perusing the literature. As an example, Molina-Bolívar et al.[40-42] have recently published in prestigious journals a modification on the DLVO theory with the goal of including the effect of hydrated cations on the restabilization of hydrophilic colloids at high salt concentrations. Independently, Franks[33] and Lyklema[43] also had to modify the potential that appears in the repulsive electrostatic term of the DLVO theory to account the Hofmeister effects of monovalent cations on the stability and mobility of inorganic colloids. Changes in the surface or ζ-potential or both were explained by these authors considering an ion adsorption mechanism. Concretely, Lyklema justified this specific adsorption on changes in the configurational entropy of the water molecules adjacent to the solid surface after binding of the ion to the surface sites. Tardieu et al.[44] also used the DLVO theory in protein crystallization studies, and they were obeyed to vary either the charge or the potential attraction to account the salt series. Our strategy aims in the same direction because DLVO interactions will be somehow modified by the presence of specific cations and anions. We have clearly seen in the aggregation experiments that the specificity of the HS modifies the pair potential. Whatever microscopic mechanisms takes place, reorientation of water dipoles at the interface or ion adsorption or exclusion, Hofmeister ions change the electrostatic term of the total interaction potential.

The inclusion of the ionic specificity in the DLVO theory can be done as follows.

Fitting strategy. The total potential energy (V_T) of the interaction that determines the colloidal stability between two identical particles is defined by the DLVO theory as a sum of two terms:

$$V_T = V_A + V_E \tag{2}$$

The V_A term corresponds to the energy of interaction caused by the van der Waals dispersion forces, which is attractive between identical materials, and can be expressed for spherical particles as[45]

$$V_A = -\frac{A}{6}\left[\frac{2a^2}{H(4a+H)} + \frac{2a^2}{(2a+H)^2} + \ln\frac{H(4a+H)}{(2a+H)^2}\right] \tag{3}$$

where A is the Hamaker constant for the interacting particles immersed in a medium, a is the particle radius, and H is the distance between the surfaces of both particles.

The V_E term represents the repulsive interaction created by the overlap of the electrical double layers of the particles. According to the constant surface potential model and assuming moderate potential (that is, lower than 50 mV), the following approximated expression can be used:[46]

$$V_E = 2\pi\varepsilon_0\varepsilon_r a\Psi_0^2 \ln\left[1+\exp(-\kappa H)\right] \tag{4}$$

ε_r being the relative permittivity of the electrolyte solution, ε_0 the permittivity of the vacuum, Ψ_0 the surface potential (or the Stern potential, if Stern model is considered), and κ is the Debye parameter given by

$$\kappa = \left(\frac{\sum_i \rho_i e^2 z_i^2}{\varepsilon_r\varepsilon_0 k_B T}\right)^{1/2} \tag{5}$$

where ρ_i is the concentration of ion "i" in the bulk, e the elementary electric charge, z_i the ion valency, k_B the Boltzmann constant, and T the temperature. In fact, eq 4 is applicable in the case of large particle radii and small surface separations, that is, $\kappa a >> 1$ and $H << a$.

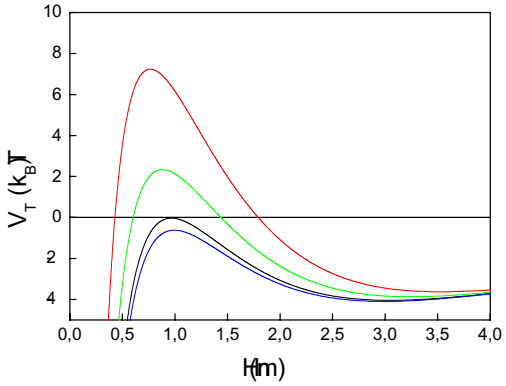

Figure 9. DLVO total interaction potential (V_T in k_BT units) versus distance. Concentration of the 1:1 electrolyte is 390 mM, and the Hamaker constant being equal to 5.5×10^{-21} J. Surface potential was used as the fitting parameter: Ψ_0 = 27.0 mV (red line); Ψ_0 = 26.1 mV (green line); Ψ_0 = 25.2 mV (black line); and Ψ_0 = 25.1 mV (blue line).

As known, CCC is defined by the DLVO theory as that salt concentration at which both the maximum value of V_T and is derivative $\mathrm{d}V_T/\mathrm{d}H$ are equal to zero. Starting from this, surface potential was taken as the fitting parameter to fit the theoretical CCC to that obtained by experiments. Other parameters were set at fixed values. The relative permittivity of pure water was selected for ε_r, and the Hamaker constant for the polystyrene-water-polystyrene (PS-W-PS) interface was taken from literature being equal to 5.5×10^{-21} J.[47] The exactitude of this A value may be questionable because a plethora of Hamaker constant values (both experimental and theoretical) for the PS-W-PS interaction can be found in the literature. Anyway, what must be pointed out is that whatever its value was, it must be practically the same for our three polystyrene latexes. Then, differences in stability will never be originated by variations in A, but changes in the electrical term.

Figure 9 shows the DLVO potential versus distance for a salt concentration of a 1:1 electrolyte equals to 390 mM. A surface potential of 25.2 mV (in absolute value) fits such a concentration as the CCC. Because that is the experimental CCC of the **ABJ2** latex in a NaCl solution, the Ψ_0 value so obtained will be assigned for such a latex in the presence of that salt.

In the same way, different Ψ_0 values have been obtained for each of our experiments, and results are shown in Table 3. Taking Cl^- as a reference ion because of its position in the HS, changes in the surface potential induced by the presence of other anions with specific effects can be evaluated. These surface potential differences ($\Delta\Psi_0$) are also shown in Table 3. The same strategy has been followed for comparing cations using sodium as the reference ion.

Most of the Hofmeister effects on different systems present linear dependences with the salt concentrations. Protein solubility,[48] protein melting temperature,[49] the B_2 virial coefficient of the osmotic pressure in protein solutions,[50] or even the air/water interface potential[20] shown in Figure 7 behaves linearly. Therefore, a linear dependence of the polystyrene/water surface potential on the concentration of Hofmeister salts could also be expected. Our surface potential differences, $\Delta\Psi_0$ (with regard to Cl^- and Na^+ ions), as a function of salt concentration are depicted in Figure 10a-c. Surprisingly, some linear tendencies arise despite the roughness of the fitting strategy employed. It should be noted, however, that the problem of fitting this kind of curves is doubled because it is necessary to know not only the effective surface potential, but also the concentration of ions near the interface at the CCC. Bulk concentration is used in noncharged surfaces,[20] but charged surfaces distribute ions heterogeneously. The experimental results have shown how the specific influence of the Hofmeister ions is different depending on whether they act as co-ions or conterions. This is why in Figure 10a-c the shown ion concentration is that obtained at the proximity of the surface after performing a Boltzmann distribution.[11] No ion size consideration or electric charge correlations between ions have been taken into account. Therefore, the lack of linearity could also have its origin in the calculus of the local ion concentration instead of errors in obtaining the surface potential. The best results were obtained for cations (Figure 10a). In this figure, the data obtained for the anionic and cationic latexes are plotted together and a rough linearity was obtained, which implies that cations have a similar behaviour acting as co- or counterions and, therefore, independently of the surface nature of the latex. But when anions are compared (Figure 10b,c) the tendencies are not as clear. First, it is not possible to represent in one single linear plot both type of latexes. There is no correlation between the surface potential differences, $\Delta\Psi_0$, obtained for cationic and anionic latexes. A possible explanation could be that,

as it was previously commented, the cationic latex (**AMJ10**) presents a more

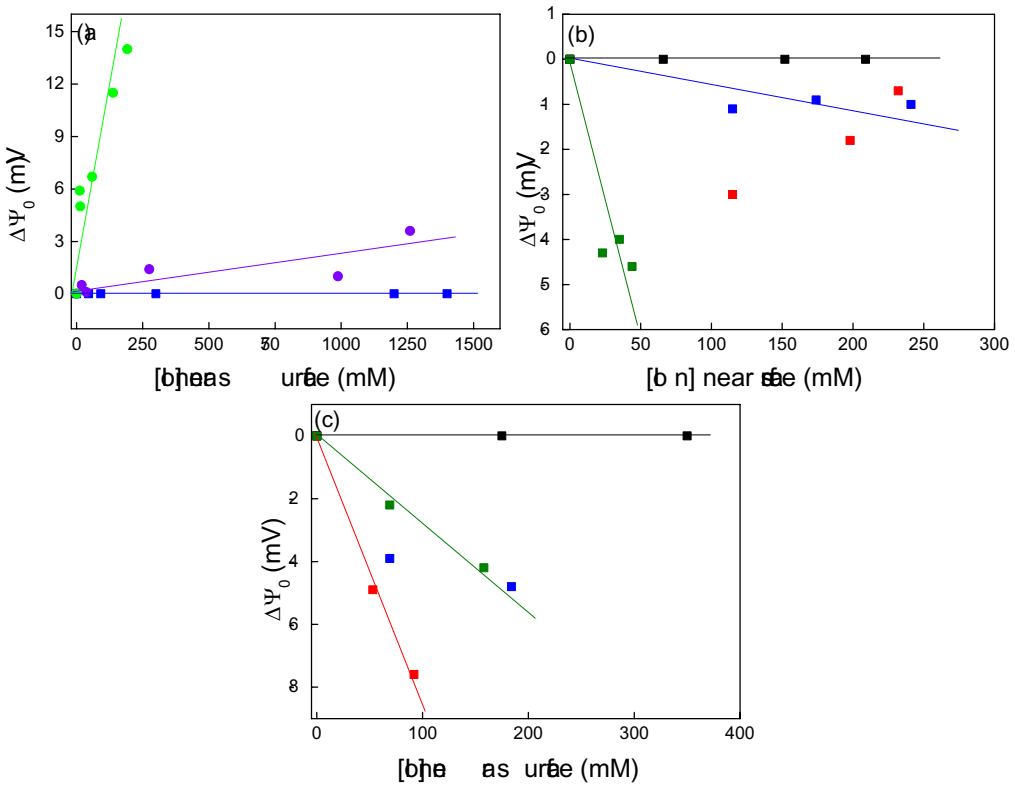

Figure 10. Surface potential difference obtained by using DLVO theory (see the fitting strategy in the text) (a) for polystyrene/water interfaces in which only effects of cations are evaluated, the common anion being NO_3^- ((■) Na^+, (●) NH_4^+, and (●) Ca^{2+}), (b) for negatively charged polystyrene/water interfaces in which only effects of anions are evaluated, the common cation being Na^+ ((■) SCN^-, (■) NO_3^-, (■) Cl^-, and (■) SO_4^{2-}) and (c) for positively charged polystyrene/water interfaces in which only effects of anions are evaluated, the common cation being Na^+ ((■) SCN^-, (■) NO_3^-, (■) Cl^-, and (■) SO_4^{2-}).

hydrophobic surface than the anionic particles. This difference could make Hofmeister ions behave in such a way that anions present patterns in the **AMJ10** sample that are different from that shown for the anionic latexes. Such a difference in hydrophobicity would explain the marked potential reduction

induced by the most chaotropic anion SCN^- in the **AMJ10** latex. It should be noted that the Ψ_0 reduction is even more drastic than that given by SO_4^{2-} ions, despite the fact that the valency of the latter doubles that of the former. This feature also supports the experimental fact that says that chaotropic ions (i.e., SCN^-) tend to accumulate into the low density water layer at hydrophobic surfaces, while kosmotropic ions (i.e., SO_4^{2-}) are usually excluded from it. Cations seem not to distinguish this hydrophobic difference among our cationic and anionic latexes. Once more, the Hofmeister effect of cations seems to be less specific than that shown by anions. Only a couple of exceptions were found regarding the observed linear tendencies and only for anions, the SCN^- ion for anionic latexes (Figure 10b) and the NO_3^- ion for the cationic particles (Figure 10c). Concretely, the SCN^- ion acting as co-ion gave an opposite tendency to the rest of the ions (anion or cations) showing an increase of $\Delta\Psi_0$ for increasing ion concentration. Again, this most extreme ion in the HS seems to show a major sensitivity to any possible change in surface characteristics.

All the data shown in this paper supports the previous ideas that a modification on the DLVO theory should be done to be able to consider the Hofmeister effects. From the experimental results, a linear dependence of surface potential on the salt concentration (C_0) could be proposed, that is $\Psi_0 = a + bC_0$, as in the case of air/water interface (Figure 7). If linear dependence was accepted, keeping in mind that this model is rather simplistic and that there are some experimental exceptions, the surface potential should change in such a way that the slope of the linear behaviour of the surface potential should depend on (at least) two factors: (i) On one hand, the slope depends on one term that accounts for the nature of the interface and that would take different positive or negative values depending on the hydrophobic/hydrophilic character of the surface. The capital letter S can be assigned for such a factor. (ii) On the other hand, the slope also depends on the ion nature, patterns being different for identical interfaces if the ion is changed. The capital letter I can be then assigned. Therefore, the surface potential Ψ_0 in eq 4 could be changed by this expression:

$$\Psi_0 = \Psi_{0\,NaCl} + SIC_0 \tag{6}$$

where $\Psi_{0\mathrm{NaCl}}$ is the surface potential of the interface in the presence of a nonspecific electrolyte, (i.e., NaCl) and C_0 is the concentration of a Hofmeister ion at the proximity of the surface. C_0 could be assumed the be the bulk concentration only for uncharged surfaces, such as air/water or oil/water

interfaces. Eq 6 should be only used for salts having Na^+ or Cl^-; that is, when the cation is sodium, the salt would be Na_iX (where X can be any anion and i its valency); electrolytes with chloride as the common anion would be YCl_j.

The main problem on applying eq 6 is that both factors, S and I, become fitting parameters with the additional handicap that an arbitrary value must be assigned to S for a given surface to be able to analyse the values of I for different ions.

V. Conclusions

The dependence on colloidal stability of different latex particle using several ions of Hofmeister series has been analysed. The results show that the positive or negative nature of the surface is important to determine the stability sequence. We have found that for 1:1 electrolytes the positive particles rank ions (from high to low stabilizing properties) in agreement with HS while negative particles reverse this order. Anyway, divalent ions have always shown the most destabilizing results. Thus, it can be concluded that for these systems, when SO_4^{2-} or Ca^{2+} act as counterions, the effect of double layer compression is more important that any possible water structure effect. The sign of charge does exert an important influence on ranking the Hofmeister ions. The HS order, however, seems not to depend significantly on the surface charge density of the immersed surfaces. Another conclusion that can be stated is that the cationic latex surface is more hydrophobic than that of negative latexes. This is supported by both the CCC values and the electrophoretic mobility results obtained. Mobility measurements have been also useful to corroborate that the effectiveness on changing the surface potential is more pronounced for the most chaotropic anion and kosmotropic cation.

Finally, an extension of DLVO theory has been proposed, modifying the electrical term where the surface potential appears, in order to include the Hofmeister effects.

Acknowledgements

We appreciate the financial support from the projects MAT99-0662-C03-02 and MAT2000-1550-C03-01 given by the Comisión Interministerial de Ciencia y Tecnología (CICYT).

References and Notes

(1) Lewith, S. Arch. Exp. Pathol. Pharmakol. **1888**, 24, 1.

(2) Hofmeister, F. *Arch. Exp. Pathol. Pharmakol.* **1888**, 24, 247.

(3) Collins, K.D.; Washabaugh, M.W. *Quarterly Rev. Biophys.* **1985**, 18, 323.

(4) Cacace, M.G.; Landau, E.M.; Ramsden, J.J. *Quarterly Rev. Biophys.* **1997**, 30, 241.

(5) Pay, N.G.M; Symons, M.C.R. *J. Chem. Soc. Faraday Trans.* **1993**, 89, 2417.

(6) Barnes, P.; Finney, J.L.; Nicholas, J.D.; Quinn, J.E. *Nature* **1979**, 282, 459.

(7) Wiggins, P.M. *Physica A* **1997**, 238, 113.

(8) Lumry, R.; Battistel, E.; Jolicoeur, C. *Faraday Symp. Chem. Soc.* **1982**, 17, 93.

(9) Wiggins, P.M. *Langmuir* **1995**, 11, 1984.

(10) Wiggins, P.M. *Cell Biol. Internat.* **1996**, 20, 429.

(11) Israelachvili, J. *Intermolecular & Surface Forces*, 2nd ed.; Academic Press: London, 1991; Chapter 12.

(12) Kim, J.; Cremer, P.S. *Chem. Phys. Chem.* **2001**, 8/9, 543.

(13) Ninham, B.W.; Yaminsky, V. *Langmuir* **1997**, 13, 2097.

(14) Weyl, W.A. *J. Colloid Sci.* **1951**, 6, 389.

(15) Good, R.J. *J. Chem. Phys.* **1957**, 61, 810.

(16) Fletcher, N.H. *Phil. Mag.*, **1962**, 7, 255.

(17) Langmuir, I. *J. Am. Chem. Soc.* **1917**, 39, 1848.

(18) Harkins, W.D.; McLaughlin, H.M. *J. Am. Chem. Soc.* **1925**, 47, 2083.

(19) Harkins, W.D.; Gilbert, E.C. *J. Am. Chem. Soc.* **1926**, 48, 604.

(20) Jarvis, N.L.; Scheiman, M.A. *J. Phys. Chem.* **1968**, 72, 74.

(21) López-León, T.; Jódar-Reyes, A.B.; Ortega-Vinuesa, J.L.; Bastos-González, D. *Hofmeister effects on the un-stabilisation and re-stabilisation of a cationic latex covered by IgG.*, sent to be published in *J. Chem. Phys.*, **2002**.

(22) Bastos, D.; de las Nieves, F.J. *Colloid Polym. Sci.* **1993**, 271, 860.

(23) Guthrie, W.H. *New free radical initiators and their use in the preparation of polystyrenes polymer colloids* Ph. D Disssertation, University of Lehigh (USA), 1985.

(24) Ortega-Vinuesa, J.L.; Gálvez-Ruiz, M.J.; Hidalgo-Álvarez, R. *Langmuir* **1996**, 12, 3211.

(25) Wilkinson, M.C.; Hearn, J.; Steward, P. *Adv. Colloid Interface Sci.*, **1999**, 81,77.

(26) Bastos-González, D.; Ortega-Vinuesa, J.L.; de las Nieves, F.J.; Hidalgo-Álvarez, R. *J. Colloid Interface Sci.* **1995**, 176, 232.

(27) Ortega-Vinuesa, J.L.; Gálvez-Ruiz, M.J.; Hidalgo-Álvarez, R. *J. Materials Sci.: Materials Medicine* **1995**, 6, 754.

(28) Wu, W.; Giese, R.F.; van Oss, C.J. *Colloids Surfaces A* **1994**, 89, 241.

(29) Holgado, J.A.; Martín, A.; Martínez, F.; Cabrerizo, M.A. *Proceedings of the Solid/Fluid Interfaces Capillarity and Wetting Congress* September 1-6, Arnhem (The Nederland) **1992.**

(30) Martín-Rodríguez, A.; Cabrerizo-Vílchez, M.A.; Hidalgo-Álvarez, R. *Colloids Surfaces A.* **1996**, 108, 263.

(31) Riès-Kautt, M.; Ducruix, A. *J. Biol. Chem.* **1989**, 264, 745.

(32) Carbonnaux, C.; Riès-Kutt, M.; Ducruix, A. *Protein Sci.*, **1995**, 4, 2123.

(33) Franks, G.V. *J. Colloid Interface Sci.* **2002**, 249, 44.

(34) Ninham, B.W. *Adv. Colloid Interface Sci.* **1999** 83, 1.

(35) Manning, G.S. *Ber. Bungenses. Phys. Chem.* **1996**, 100, 909.

(36) Belloni, L. *Colloid Surf. A*, **1998**, 140, 227.

(37) Roberts, J.M.; Sierzputowskagracz, H.; Stejskal, E.O.; Osteryoung, J.G. *J. Phys. Chem. B* **1998**, 102, 7735.

(38) Aoki, K.; Roberts, J.M.; Osteryoung, J.G. *Langmuir* **1998**, 14, 4445.

(39) Levin, Y.; Barbosa, M.C.; Tamashiro, M.N. *Europhys. Lett.* **1998**, 41, 123.

(40) Molina-Bolívar, J.A.; Galisteo-González, F.; Hidalgo-Álvarez, R. *Phys. Rev. E* **1997**, 55, 4522.

(41) Molina-Bolívar, J.A.; Galisteo-González, F.; Hidalgo-Álvarez, R. *Colloids Surf., B* **1999**, 14, 3.

(42) Molina-Bolívar J.A.; Ortega-Vinuesa, J.L. *Langmuir* **1999**, 15, 2644.

(43) Lyklema, J. *Specificity in the statics and dynamics of surface confined ions, Molecular Physics*, in press **2002**.

(44) Tardieu, A.; Le Verge, A.; Malfois, M.; Bonete, F.; Finet, S.; Ries-Kautt, M ; Belloni, L. *J. Crystal Growth* **1999**, 196, 193.

(45) Hiemenz P.C.; Rajagopalan, R. *Principles of Colloid and Surface Chemistry*, 3rd ed., Marcel Dekker: New York, 1997; Chapter 10.

(46) Ohshima, H. In *Electrical Phenomena at Interfaces: Fundamentals, Measurements, and Applications;* Ohshima, H., Furusawa, K., Eds.; Surfactant Science Series, Vol. **76**; Marcel Dekker: New York, 1998, Chapter 3.

(47) Gregory, J.; *Adv. Colloid Interface Sci.* **1969**, 2, 397.

(48) Setschenow, J. *Z. Phys. Chem.* **1889**, 4, 117.

(49) von Hippel, P.H.; Wong, K.-Y *Science* **1964**, 145, 577.

(50) Piazza, R. Pierno, M.; *J. Phys.: Condens. Matter* **2000**, 12, 443.

HOFMEISTER EFFECTS ON THE COLLOIDAL STABILITY OF AN IGG-COATED POLYSTYRENE LATEX

T. López-León, A.B. Jódar-Reyes, J.L. Ortega-Vinuesa and D. Bastos-González

Colloid and Fluid Physics Group, Department of Applied Physics, University of Granada, Av. Fuentenueva S/N, 18071 Granada , Spain.

Abstract

The effect of various ions related to the Hofmeister series (HS) on different properties of a cationic latex covered with a protein (IgG) has been analyzed in this study. $NaNO_3$, NH_4NO_3 and $Ca(NO_3)_2$ were used to compare the specificity of the cations, and NaCl, NaSCN, $NaNO_3$, and Na_2SO_4, to compare the specificity of the anions. Two pH values, pH 4 and pH 10, were chosen to analyze the behavior of these ions acting as counter and coions. At pH 4, the total surface charge is positive, whereas at pH 10 it is negative. Three different phenomena have been studied in the presence of these Hofmeister ions: (1) colloidal aggregation, (2) electrophoretic mobility, and (3) colloidal restabilization. The specific effect of the ions was clearly observed in all experiments, obtaining ion sequences ordered according to their specificity. The most important parameter for ion ordering was the sign of the charge of the colloidal particle. Positively charged particles displayed an ion order opposite to that observed for negatively charged surfaces. Another influential factor was the hydrophobic/hydrophilic character of the particle surface. IgG-latex particle surfaces at pH 10 were more hydrophilic than those at pH 4. The SCN^- ion showed a peculiar specific effect on the phenomena studied (1)-(3) at pH 10. With respect to the restabilization studies at high ionic strengths, new interesting results were obtained. Whereas it is commonly known that cations may provoke colloidal restabilization in negative particles when they act as counterions, our experiments have demonstrated that such a restabilization is also possible with positively charged particles. Likewise, restabilization of negative surfaces induced by the specific effect of chaotropic anions (acting as coions) was also observed.

I. Introduction

The presence of any electrolyte in aqueous solutions disrupts the molecular structure of pure liquid water. The structural modifications induced by different electrolytes are not at all identical; in fact, they can be extremely different depending on the nature of the dissolved salt. The changes induced in the water layers adjacent to the ions are reflected by a plethora of macroscopic phenomena. Many ions have been ranked in the so-called Hofmeister series (HS) depending on their specific effects tested by numerous experimental measurements of different physical phenomena. Many of these results have been analyzed in a comprehensive review published by Collins and Washabaugh [1]. One of the main features of the HS is that the relative positions of the ions usually coincide for the different properties studied and only slight alterations appear in the characteristic rank ordering. Another broadly observed feature is that the specific effects caused by the anions are more significant than those caused by the cations. A representative HS is given below for anions and cations, although, as mentioned, their relative positions should only be thought of as indicative.

$$\underset{\textbf{(kosmotropic anions)}}{\mathrm{Citrate}^{3-} > \mathrm{SO_4}^{2-} > \mathrm{PO_4H}^{2-} > \mathrm{F}^- > \mathrm{CH_3COO}^-} > \underset{\textbf{(chaotropic anions)}}{\mathrm{Cl}^- > \mathrm{Br}^- > \mathrm{I}^- > \mathrm{NO_3}^- > \mathrm{ClO_4}^- > \mathrm{SCN}^-}$$

$$\underset{\textbf{(chaotropic cations)}}{\mathrm{N(CH_3)}^{4+} > \mathrm{NH}^{4+} > \mathrm{Cs}^+ > \mathrm{Rb}^+ > \mathrm{K}^+} > \underset{\textbf{(kosmotropic cations)}}{\mathrm{Na}^+ > \mathrm{H}^+ > \mathrm{Ca}^{2+} > \mathrm{Mg}^{2+}}$$

Although the first Hofmeister series was proposed more than one century ago [2, 3], no general conceptual framework providing a complete explanation about the origin of these specific effects is yet available. Different studies [1, 4-6] however, have clearly evidenced a correlation between the HS and water structure. An explanation broadly accepted is that HS emerges from the disturbance of water structure induced by the ions. The ions shown in the HS above have been ordered according to their degree of hydration. Strongly hydrated anions (kosmotropes) are on the left and weakly hydrated anions (chaotropes) are on the right. It should be noted that cations are ordered in the opposite way; chaotropic or weakly hydrated cations are on the left and

the kosmotropes on the right. This means that the effect of kosmotropic anions is opposite to that of kosmotropic cations. Although both of them structure water molecules strongly, the orientations of the oxygen and hydrogen atoms toward the ion are opposite. However, the water structure induced by a kosmotropic anion is similar to that of a chaotropic cation, and vice versa. Finally, the effects shown by the HS usually present an inversion at Cl^- (for anions) and Na^+ (for cations). So, the position of these two ions is usually considered null points in the specific ion effects. The fact that the Hofmeister effects are observed in macroscopic phenomena suggests that the interaction between ions and water is transmitted through the solvent beyond the first hydration layer. This is done by a cooperative mechanism of water-water hydrogen bonding [7].

Explaining some properties of colloidal particles immersed in media containing Hofmeister ions becomes a puzzle almost impossible to solve. As an example, the colloidal stability is modulated by the *surface-surface* interactions [8], which depend on the *surface-water* [1, 9] and *surface-ion* interactions [10], which in turn are also related to the mentioned *ion-water* and *water-water* interactions. Therefore, the specific restructuring of water and the ionic distribution around a colloidal particle modify its interfacial potential. This change in the potential can be experimentally observed in colloidal stability and electrokinetic studies. There are two qualitative explanations for why the presence of chaotropic or kosmotropic ions can modify surface potentials. On the one hand, potentials can be changed by a mechanism of specific exclusion or accumulation of ions at the surface. Some authors justify it by dispersion forces [10-13], while others [9, 14] state that it arises from entropic contributions. On the other hand, there is a second mechanism based on the cooperative orientation of water molecules adjacent to the surface induced by the presence of Hofmeister ions [1, 9]. This generates a polarization gradient that can be translated into a change in the surface potential [15-17]. Recent molecular-dynamics simulations support this mechanism based on the local structuring of water [18-20]. These molecular mechanisms must not be thought of as mutually exclusive. Actually, it is more than likely that ion specificity comes from a combination of both.

The goal of the present work is to supply experimental results on how the nature of some ions located at different positions in the Hofmeister series specifically affects three important phenomena in a colloidal sample. Hofmeister effects on (1) colloidal aggregation, (2) electrokinetic properties,

and (3) restabilization patterns at high salts concentrations of a polystyrene latex covered by IgG are analyzed in depth.

II. Materials and methods

2.1 Reagents

Na_2SO_4, NaCl, $NaNO_3$, NaSCN, $Ca(NO_3)_2$, and NH_4NO_3 salts were of analytical grade and purchased from different firms: Merck, Sigma and Scharlau. Double deionized water was used throughout. Non-buffered solutions were obtained by adding to water the amount of HCl or NaOH necessary to get pH 4 or pH 10, respectively. When necessary, intermediate pH values were obtained by mixing appropriately the above solutions, maintening the ionic strength of all of them constant.

2.2 Latex particles.

The polystyrene latex sample was synthesized and characterized in our laboratory as described in reference [21]. It had an amphoteric nature with positive charge in the pH range 4 to 10 and an isoelectric point (pI) at pH 10.5. Superficial positive charges presented weak base character (amidine). Consequently, the surface charge density (σ_0) changed as the pH value varied. In fact, the σ_0 value was 18.3 ± 1.2 μC/cm2 at pH 4 and 4.0 ± 0.6 μC/cm2 at pH 10, respectively [21]. The mean diameter, obtained by TEM, was 320 ± 15 nm, with a polydispersity index extremely close to unity (1.007).

2.3 Protein.

Rabbit polyclonal IgG was purified and kindly donated by Biokit S.A. (Spain). The isoelectric point determined by isoelectric focusing was in the range 6.1-8.5. The protein adsorption onto the latex surface was performed as follows. The protein concentration before and after adsorption was determined by UV spectrophotometry at 280 nm using a DU 7040 (Beckman) spectrophotometer. The IgG extinction coefficient was 1.40 ml/mg cm. Dialyzed IgG was added to 8-ml volumes of aqueous solutions at different pH containing latex particles with a total polystyrene area of 0.3 m^2 each. Two sets of samples were prepared. Incubation was carried out at 25 °C for 21 hours. After incubation, samples were spun at 25.000 × g for 30 minutes,

and all the pellets of one set were redispersed and stored at pH 4, and the other set at pH 10. The protein desorption induced by this pH change was also quantified.

2.4 Electrophoretic mobility.

Electrophoretic mobility measurements at ionic strengths below 100 mM were performed with a Zeta-Sizer IV (Malvern Instruments). For measurements at high ionic strengths (up to 1 M), a ZetaPALS (Brookhaven Instruments), based on phase analysis light scattering, was used instead. Latex particles were diluted in the desired electrolyte solution and data were obtained from the average of six measurements. Standard deviation was always lower than 5 %

2.5 Colloidal Stability.

Particle aggregation studies were carried out using a low-angle light-scattering technique. Aggregation was analyzed by monitoring the light scattered by the samples at 10° for 120 s. The scattering cell was rectangular with a 2-mm path length. Equal volumes (1 ml) of salt and latex solutions were mixed and introduced into the cell with an automatic mixing device. The latex dispersions used for such coagulation experiments had to be diluted enough to minimize multiple scattering effects. The increment in light scattered at 10º is linear for the first steps of the coagulation. The stability ratio (W), also called Fuch's factor, was experimentally obtained as the ratio between the rate constants of rapid and slow coagulation kinetics, as described elsewhere [21]. The critical coagulation concentration (CCC) can be easily obtained by plotting the logarithm of W versus the logarithm of the salt concentration and by locating that point where log W decreases to zero.

III. Results and discussion

3.1 IgG adsorption and desorption.

The first goal was to cover as much of the polystyrene surface with protein molecules as possible. An excess of IgG molecules was added to the latex samples dispersed at different pH solutions and the amount of protein

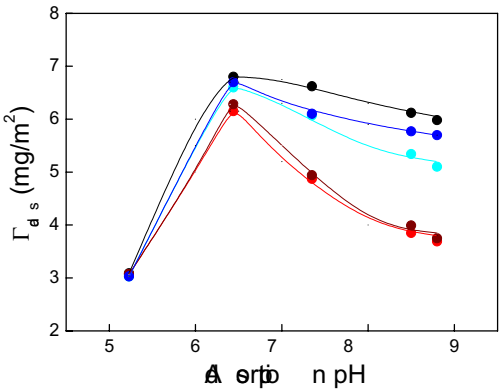

Fig. 1. Maximum amount of adsorbed IgG as a function of the adsorption pH (●). Amounts that remain adsorbed after resuspending the IgG-latex complexes in pH 4 (●) and pH 10 (●) for 90 minutes, and pH 4 (●) and pH 10 (●) for 24 hours.

adsorbed was then measured. Data are plotted in Fig. 1. Maximum adsorption was obtained at pH 6.3. Actually, the maximum amount of adsorbed protein is usually obtained at the pH value at which the protein charge matches the charge of the sorbent surface. That is, the maximum is placed at the isoelectric point of the protein-latex complex [22, 23]. This feature is also revealed by our system, as will be shown with the electrophoretic mobility data.

Desorption results are illustrated in Fig. 1. Adsorption was not fully irreversible when the pH was changed. If freshly prepared IgG-latex complexes were immersed in acidic media (pH 4) - below the pI of IgG - a significant amount of positive IgG molecules were released from the cationic surface. Desorption was higher in those samples having high initial protein coverage, that is, in those complexes formed at neutral or basic pH. If samples were immersed at pH 10 instead, where electrostatic and hydrophobic interactions between protein and surface are favorable, desorption was significantly reduced. The experiments reported little desorption at both pH values (4 and 10) when the adsorption was performed at pH 6, obtaining particles with a high protein coverage. Thus, only two pools of IgG-latex particles were used afterwards in the colloidal stability and electrophoretic mobility studies. Both were obtained by adsorbing IgG at pH 6, and redispersed and stored at different pHs (pH 4 and pH 10).

3.2 Colloidal destabilization.

The CCC values of our particles were obtained by adding independently $NaNO_3$, NH_4NO_3 and $Ca(NO_3)_2$, for comparing cations, and NaSCN, $NaNO_3$, NaCl, and Na_2SO_4, for comparing anions. The results obtained at pH 4 (positive surface) and pH 10 (negative surface) are shown in Figs. 2a and 2b, respectively. The corresponding CCC values are listed in Table 1. These values demonstrate that IgG-latex complexes at pH 4 are significantly more stable than those at pH 10. This agrees with the electrical state of the particles. Both protein molecules and latex patches free of IgG are positively charged at pH 4. At pH 10, however, protein molecules have a negative charge whereas latex surface is positive. Therefore, the total charge of the complex at this basic pH must be low, as must its colloidal stability.

The experimental results also make evident the clear influence exerted by the nature of the aggregating salt on colloidal stability. The DLVO theory predicted identical CCC values whatever 1:1 electrolytes were used; likewise, different 2:1 salts must give identical aggregation patterns. However, the destabilization induced by these salts gave different CCC values, in such a way that ions could be ordered according to the HS.

At pH 4 (positive surface), the ion ranking given by the coagulation results was:

$$\text{(more stable)}\quad Cl^- > NO_3^- > SCN^- > SO_4^{2-}\quad \text{(more unstable)}$$

$$\text{(more stable)}\quad NH^{4+} > Na^+ > Ca^{2+}\quad \text{(more unstable)}$$

As shown, the order of the CCC values almost fits the HS given in Section 1. The only exception in the HS ranking is the sulfate. The effect on the colloidal stability of this divalent ion, acting as counterion, is a result manely of its valency, not of its capacity to restructure the surrounding water molecules. An extensive and detailed discussion on the above ion ranking can be found in Ref. [21].

One of the most important points to discuss concerns the influence of surface hydrophobicity on HS ranking. The external surface of the IgG molecules is more hydrophilic than polystyrene [24, 25]. Therefore, the adsorbed protein layer reduces the overall hydrophobicity of the primitive latex surface. If the specific effects of the ions depended on the

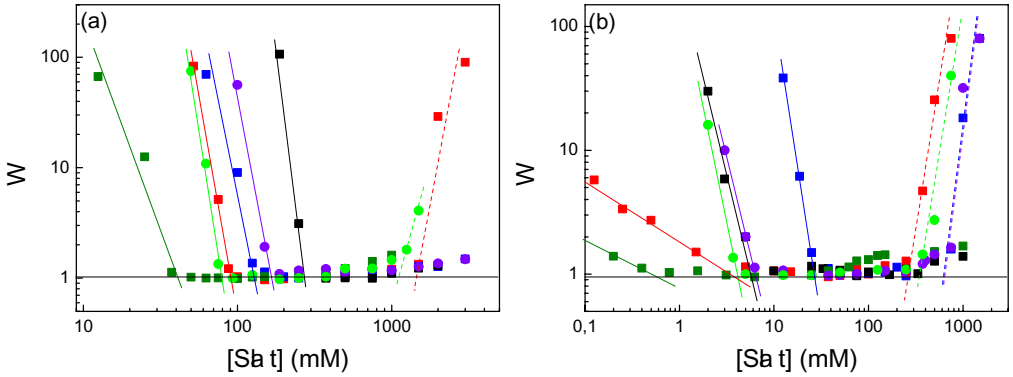

Fig. 2. Stability ratio (Fuch's factor) versus electrolyte concentration for the IgG-latex complexes at (a) pH 4 and (b) pH 10: (■) NaSCN, (■) $NaNO_3$, (■) NaCl, (■) Na_2SO_4, (●) NH_4NO_3, and (●) $Ca(NO_3)_2$. Solid lines are used for de-stabilization and segmented lines for restabilization.

Table 1. Critical coagulation concentration (CCC) and critical stabilization concentration (CSC) for the IgG-latex complexes at pH 4 and pH 10.

Hofm. ion	IgG-latex at pH4		IgG-latex at pH10	
	CCC (mM)	CSC (mM)	CCC (mM)	CSC (mM)
SCN^-	90	1500	4	260
NO_3^-	130	–	25	700
Cl^-	275	–	6	–
SO_4^{2-}	40	–	< 1	–
NH_4^+	165	–	7	700
Na^+	130	–	25	–
Ca^{2+}	80	1100	4	350

hydrophobic/hydrophilic character of the surface, the presence of the IgG should modify the ion ranking with respect to the bare (and highly hydrophobic) polystyrene particles. However, the Hofmeister ion ranking obtained with the CCC values of the IgG-latex complexes fully coincides with that obtained for the bare hydrophobic polystyrene at pH 4 [21]. Hence, the change toward a more hydrophilic surface promoted by the IgG adsorption seems not to modify the Hofmeister ion ranking, at least at pH 4. This point is taken up again later.

The order in the stability results obtained at pH 10 (negative surfaces) was different:

$$\text{(more stable)}\ \ NO_3^- > Cl^- > SCN^- > SO_4^{2-}\ \ \text{(more unstable)}$$
$$\text{(more stable)}\ \ \ Na^+ > NH^{4+} > Ca^{2+}\ \ \text{(more unstable).}$$

The monovalent ions, excepting SCN^-, are ordered in an inverse sequence compared with that given by our positive surfaces. When negative surfaces are used to analyze the Hofmeister effects, the sequence order is usually the inverse of that obtained for positive surfaces. This feature has been observed not only on negative hydrophobic polystyrene [21], but also on amphiphilic (Hypoderma lineatum collegenasa) [26] or hydrophilic materials, such as silica [27] or TiO2 [28, 29]. Therefore, the sign of charge of the surface is one of the most crucial parameters controlling the HS ranking. With respect to divalent ions, the exception in the inverse sequence is the calcium ion, because it acts as counterion at pH 10. Reasoning identical to that given for sulfate at pH 4 can now be applied to Ca^{2+}.

The most striking point, however, is the exception obtained for the SCN^- ion, which induces aggregation on negatively charged particles at very low salt concentrations. This pattern is opposite to that found in all our previous experiments working with hydrophobic particles when using thiocyanate. Our experiments showed that this chaotropic ion (compared with Cl^-) had a clear tendency to make more negative the surface potential of hydrophobic surfaces [21]. That is, thiocyanate reduced the surface potential of positive particles inducing destabilization, but increased (in absolute value) the surface potential of negative ones, making the system more stable. In the case of positive IgG-latex complexes (pH 4), SCN^- also showed a clear tendency to aggregate the system, which is totally similar to that observed for positive bare latex particles [21], but surprisingly SCN^- did not improve the stability of the negatively charged system when the IgG was absorbed (pH 10). Actually, negative IgG-latex particles are clearly unstable at very low thiocyanate concentrations. This result (repeatedly confirmed) shows that the increase in surface hydrophilicity due to the protein adsorption modified the specific effect exerted by the SCN^- ion. One may wonder why this feature (if caused by a change in surface hydrophobicity) was not observed in the IgG-latex sample incubated at pH 4. A possible explanation is that the samples stored at pH 10 had a higher hydrophilicity than those at pH 4. As shown in Fig. 1 and discussed above, IgG desorption was higher in those samples resuspended at

pH 4. So, the complexes stored at pH 4 would have more hydrophobic patches of polystyrene than those at pH 10. In addition, the desorption studies shown in Fig.1 were carried out for incubation periods no longer than 24 hours, while the pools used in the aggregation experiments were stored for periods as long as one week. Thus, it is more than likely that the total amount of IgG adsorbed in the complexes incubated at pH 4, where electrical protein-surface repulsions exist, would be even lower than the values shown in Fig. 1. As SCN^- is the most chaotropic anion, it may have a higher sensitivity to surface hydrophobicity changes. The modification in the water structure at the particle interface induced by the presence of the protein layer would alter the tendency of SCN^- to accumulate at hydrophobic surfaces. A deeper analysis of the hydrophilic character of the surface of both IgG-latex pools is provided under Section 3.4.

Finally, it should be noted that protein solubility and conformational stability are known to be sensitive to the chemical environments in which the proteins reside. Both important parameters depend on the ionic nature of the electrolyte solution in which proteins are immersed [1, 6]. As our latex particles are covered by IgG, the colloidal stability of the particles might be influenced by the salting-in/salting-out effects on immunoglobulin solubility. Therefore, the salt effects in this protein must be taken into account to properly discuss the stability results. As a rule, chaotropic ions improve protein solubility, but do so at the expense of conformational stability. On the other hand, kosmotropic ions stabilize the protein structure, although they behave as strong precipitants (salting-out agents) [30, 31]. Gagnon et al. [32] experimentally showed that chaotropic ions improve the solubility of IgG molecules. Specifically, these authors reported that negatively charged IgG showing a good solubility in presence of ClO_4^-, a chaotropic ion usually located at the extreme of the HS together with SCN^-. Chaotropic ions are able to penetrate a protein's hydration sheath and bind directly to peptide bonds and hydrophobic residues. This increases the net charge on the protein, increasing its interactivity with the polar solvent, thus improving its solubility [30, 31]. This maximizes solubility, although it does so at the expense of internal stability: a loss of local hydrophobicity due to chaotropic ion-binding disrupts the protein's native conformation. Nevertheless, our stability results at pH 10 (where IgG is negatively charged) do not obey this pattern at all. Considering the salting-in effect, the presence of SCN^- should help to prevent the aggregation of IgG molecules, and thus, to avoid the collapse between two

contacting surfaces covered by IgG. However, thyocianate induces aggregation even at very low concentrations. So, the stability behavior shown by our system seems not to be affected by the salting-in effects on immunoglobulin. It should be also noted that we have very recently tested the stability of negative silica particles on addition of the same salts. The CCC values of the highly hydrophilic silica particles (unpublished data) order the monovalent anions exactly as the negative IgG-latex complexes do. Therefore, the specific effects of these ions on our IgG-latex samples at pH 10 seem to be related to the hydrophilicity of the surface, but not to the salting-in/salting-out effects on protein solubility.

3.3 Electrophoretic mobility.

Electrokinetic studies often help to clear up and support results concerning colloidal stability. If Hofmeister effects have been observed in destabilization, they could be also present in electrophoretic mobility measurements.

Two different sets of mobility experiments were performed. The first set of μ_e measurements was aimed at evaluating the isoelectric point (pI) of the IgG latex complexes in the presence of Hofmeister salts. Only the most stable complexes, those stored at pH 4, were used in this study. If Hofmeister ions modify surface potential, this must be also reflected in a change in ζ-potential, which, in turn, must vary the mobility behavior, producing differences in the pI values. Figs. 3a and 3b illustrate mobility as a function of the medium pH. All of the solutions were identical in ionic strength. Despite the low salt concentration used (6 mM for 1:1 electrolytes and 2 mM for 2:1 electrolytes), differences in pI values were observed. These pI values are listed in Table 2. A pI equal to 6.0 was obtained in the presence of sodium chloride; note that this pH coincides with the value at which the maximum adsorption of the protein was observed (see Fig. 1). The pI values obtained with the other ions support all the stability patterns. In fact, the ion ranking given by the pI values of the particles stored at pH 4 coincides exactly with that given by the CCC values (except Ca^{2+}). As mentioned before, one of the microscopic interpretations of the effects of chaotropic ions is based on the accumulation of these ions in water layers adjacent to hydrophobic surfaces. The accumulation of chaotropic ions at the proximity of the IgG-latex surfaces stored at pH 4 causes the pI to

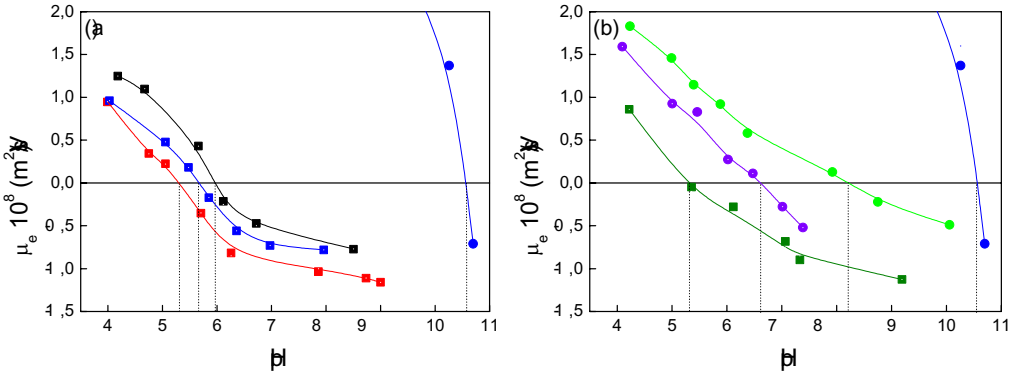

Fig. 3. Electrophoretic mobility of IgG-latex complexes as a function of pH in presence of different 1:1 electrolytes at an ionic strength equal to 6 mM: (a) (■) NaSCN, (■) $NaNO_3$, and (■) NaCl and (b) (■) Na_2SO_4, (●) NH_4NO_3, and (●) $Ca(NO_3)_2$.The data of the bare latex particles (●) were obtained with $NaNO_3$.

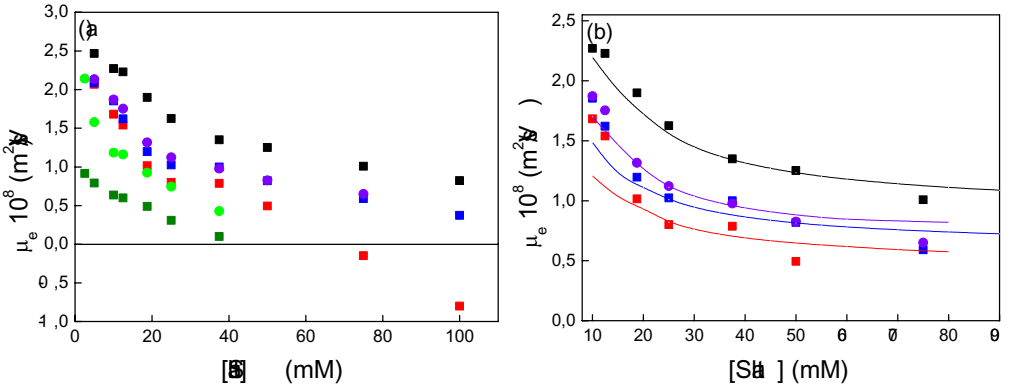

Fig. 4. Electrophoretic mobility of the IgG-latex complexes incubated at pH 4 versus salt concentration: (a) (■) NaSCN, (■) $NaNO_3$, (■) NaCl, (■) Na_2SO_4, (●) NH_4NO_3, and (●) $Ca(NO_3)_2$; (b) lines correspond to the theoretical fitting made by using Ohshima's theory : d = 100 Å $\lambda = 0.3$ nm^{-1}; N values are given in Table 2.

Table 2. Isoelectric points of bare latex and IgG-latex particles, stored at pH 4, obtained by electrophoretic mobility measurements. "N" was the average charge density of the adhered protein layer calculated by using the Ohshima theory.

Sample	Bare latex	IgG-latex						
Ion	NO_3^- (Na^+)	SCN^-	NO_3^-	Cl^-	SO_4^{2-}	NH_4^+	Na	Ca^{2+}
i.e.p.	10.5	5.3	5.7	6.0	5.3	6.6	5.7	8.2
N (mM)	–	11	13	21	–	15	13	–

shift to more acid values for chaotropic anions (SCN^- and NO_3^-) or to more basic values for chaotropic cations (NH_4^+). This justification is plausible only if our system incubated at pH 4 behaves as a hydrophobic surface, since hydrophilic interfaces behave in the opposite manner.

The second set of mobility experiments was planned to analyze the variation in μ_e with electrolyte concentration, keeping the pH constant. Fig. 4a shows the results obtained at pH 4. It can be seen that μ_e decreased by increasing electrolyte concentration, independently of the nature of the salt. This pattern results from the double layer compression. As expected, SO_4^{2-} acting as a counterion, had the lowest mobility in the range studied. The μ_e of the remaining ions also behaved according to the stability results, SCN^- being the anion that reduced mobility the most when comparing 1:1 electrolytes. The effect of this chaotropic ion is so drastic that it changed the sign of the mobility even at moderately high salt concentrations. This result would agree with the accumulation mechanism proposed for chaotropic ions at the proximity of hydrophobic surfaces. This feature was also observed in bare latex particles [21], which would again support that the hydrophobicity of the polystyrene surface was not markedly modified by the IgG adsorption when samples were stored at pH 4.

This set of mobility measurements can also be used to quantify Hofmeister effects by applying a theoretical treatment developed by Ohshima et al. [33-36]. As a result of the accumulation or exclusion of ions at the particle surface due to Hofmeister effects, the values of the average charge density in the adsorbed protein layer should change. Ohshima and colleagues' theory allows prediction of such a charge density from the μ_e data, and is a useful tool in evaluating this specific ion accumulation / exclusion processes. The theory can be summarized as follows. Consider a colloidal particle with a polyelectrolyte layer of thickness d adsorbed on its surface. The charged

groups of this superficial layer are supposed to be uniformly distributed with a density N. These charged groups have a valency of z. The particle surface is assumed to be a plane with the applied electric field parallel to it. The charged colloidal particles are moving in a liquid containing a symmetrical electrolyte of valency ν and bulk concentration n. Ohshima et al. obtained an analytical expression for the electrophoretic mobility of such a system [33] by using two Poisson-Boltzmann equations and hydrodynamics considerations. Nevertheless, it is quite difficult to calculate μ_e with that equation, as there is an integral that seldom gives an analytical solution. Anyway, the authors managed to obtain various simpler expressions for the mobility of structured interfaces. The best equation to be applied to protein-latex complexes is [37]:

$$\mu_e = -\frac{\varepsilon_r\,\varepsilon_0\,k_BT}{\nu e\eta}\ln\left(\frac{|\sigma|}{2\nu end}+\left[\left(\frac{\sigma}{2\nu end}\right)^2+1\right]^{1/2}\right)+\frac{\varepsilon_r\,\varepsilon_0\,k_BT}{\nu e\eta}\left(\left[\left(\frac{2\nu end}{\sigma}\right)^2+1\right]^{1/2}-\frac{2\nu end}{|\sigma|}\right)$$
$$\times\ \frac{(\kappa/\lambda)\left[1+(\sigma/2\nu end)^2\right]^{1/4}\tanh\lambda d-1}{(\kappa/\lambda)^2\left[1+(\sigma/2\nu end)^2\right]^{1/2}-1}-\frac{|\sigma|}{\eta d\lambda^2}\left(1-\frac{1}{\cosh\lambda d}\right) \tag{1}$$

The equation has been expressed considering a negatively charged polyelectrolyte layer. If positive, the absolute value must be taken. σ is the amount of fixed charge in the surface layer per unit area,

$$\sigma = zeNd \tag{2}$$

and λ is a hydrodynamic parameter equal to

$$\lambda = \left(\frac{\gamma}{\eta}\right)^{1/2} \tag{3}$$

where η and γ are the viscosity of the fluid and the frictional coefficient of the adsorbed polyelectrolyte layer, respectively. κ is the reciprocal of the double layer thickness, and e, ε_r, ε_0, k_B and T have their usual meaning.

Experimental μ_e data can be fitted by Eq. (1) using three fitting parameters: N, λ and d. For a given IgG-latex complex d and λ values are constant. However, N could change if disolved ions penetrate or are excluded from the adsorbed protein layer, depending on its Hofmeister nature. It should be noted that Eq. (1) is applicable only to symmetrical electrolytes, and thus, the fitting process could not be performed with 2:1 salts. Results for 1:1 salts are shown in Fig. 4b, where symbols correspond to experimental data and lines

are the theoretical mobilities predicted by Eq. (1). Values for d and λ were set to 100 Åand 0.3 nm $^{-1}$, respectively, for layers of adsorbed antibody [36, 37]. Hence, the net charge density in the protein layer (N) was used as the only fitting parameter. If the pH of medium is stationary, the total surface charge of the particles remains constant, and only a specific accumulation or exclusion of ions in this layer modifies the net charge in this region. This is reflected in the N values. These values at pH 4 are also listed in Table 2. As expected, the SCN^- ion showed the most significant reduction in the N value compared with Cl^-. As chaotropic ions tend to accumulate at the proximity of hydrophobic surfaces, this result also confirms that IgG-latex complexes incubated at pH 4 must have a non-hydrophilic surface. Again, and according to N values obtained, all the monovalent ions are ordered as usual HS ($Cl^- > NO_3^- > SCN^-$ for anions, and $NH_4^+ > Na^+$ for cations). Consequently, a change in interfacial potentials induced by ion specificity is once more evidenced.

3.4 Colloidal restabilization.

Finally, there is another macroscopic phenomenon where Hofmeister effects can be evaluated. It is related to the restabilization of colloidal particles at high salt concentrations. Restabilization is attributed to hydration forces. The origin of this structural force has been associated with the structuring of water in the vicinity of the surfaces. They are not only correlated with the hydrophilicity degree of the surface, but also strongly depends on the nature and concentration of the hydrated counterions that surround the surface [38-42]. So, these restabilization phenomena depend, on the one hand, on the water structure around the surface of the colloidal particles, which, in turn, depends on the hydrophilic/hydrophobic of the surface; and on the other hand, on the structural state of the water molecules that surround the solved ions at the proximity of the surface. As Hofmeister effects are related to ion-water interactions, restabilization experiments on IgG-latex complexes can be a good option to test the HS.

The restabilization of latex particles covered by proteins has been extensively studied by Molina-Bolívar et al. [25, 42-45]. As mentioned above, the role played by the presence of hydrated ions at the solid/water interface is crucial in the restabilization process. Cations, but not anions, have usually been considered responsible for hydration restabilization when they act as counterions. Actually, the hydration numbers are larger for cations than for

anions, and it has been experimentally confirmed that the hydration forces increase with the hydration number of the cations [38]. Molina-Bolívar et al. showed that protein-latex complexes restabilize due to the presence of cations, and restabilization is observed only in negatively charged particles, that is, when cations acted as counterions having a high local concentration near surface.

One of the most characteristic features analyzed in restabilization studies is the minimum electrolyte concentration at which restabilization starts, which is referred to as the critical stabilization concentration (CSC). Returning to Figs. 2a and 2b, it can be seen that at high salt concentration the restabilization occurred for both latex pools (pH 4 and pH 10), this non-DLVO stabilization being more evident at pH 10. The corresponding CSC data are summarized in Table 1. As can be seen, only NaSCN and $Ca(NO_3)_2$ salts induced restabilization at pH 4. Four salts (NaSCN, $Ca(NO_3)_2$, NH_4NO_3 and $NaNO_3$), however, caused complete restabilization of the particles at pH 10. It should be noted that restabilization by hydration forces had been observed only in hydrophilic materials [38]. Restabilization did not occur in the bare latex samples at all [21], but it did so in the IgG-latex complexes. Consequently, adsorption of IgG has effectively increased the hydrophilicity of the particle surface. Moreover, (taking into account the CSC values at both pH values), one may state that the hydrophilic of samples stored at pH 4 is lower than that at pH 10, as restabilization is quite more significant in the latter than in the former. Therefore, these restabilization results confirm our previous assumptions regarding the differences on the surface hydrophobicity among our two IgG-latex pools.

Two remarkable results, which had never been seen in previous protein-latex restabilization studies, should be highlighted:

i) $Ca(NO_3)_2$ (but not $NaNO_3$) and NaSCN (but not NaCl) salts induce restabilization in positively charged IgG-latex complexes (pH 4 data). In addition, both salts have a similar and strong tendency to restabilize particles at pH 10. Considering the results at acid pH, the ionic specificity must be due to the presence of Ca^{2+} and SCN^- ions. There are two possible explanations of how these $Ca(NO_3)_2$ and NaSCN salts induce restabilization. The first one is related to the role played by specific ions in the hydration forces associated with the water structure at the surface, independent of whether these ions act as counterions or coions. In this case, Ca^{2+} and SCN^- (even acting as coions at

pH 4 and pH 10, respectively) would directly alter water's hydrogen-bonding network at the proximity of the surface. The structured water shell induced around the particles would prevent aggregation [38]. Curiously, only these two ions, which strongly interact with water molecules (each one in a different way), show restabilization at the two pH values tested. According to second explanation proposed by other authors, only hydrated counterions are able to restabilize. In this sense, when $Ca(NO_3)_2$ is present at pH 4, nitrate would be responsible for the restabilization, as it is the counterion. Its adsorption may be enhanced when Ca^{2+} is present (compared to Na^+) due to rejection of Ca^{2+} from the positive surface relative to the rejection of Na^+. So, nitrate would directly stabilize, although its high accumulation at the surface is indirectly caused by the presence of calcium. When NaSCN is present, thiocyanate preferentially absorbs because it is a strong chaotropic ion. However, this second mechanism fails to explain the stability phenomena with the positive bare latex particles [21], as restabilization at high salt concentration is never observed even though the local SCN^- concentration is supposed to be higher at the highly hydrophobic surface.

ii) At pH 10, SCN^- and $NO3^-$ restabilize the system, whereas Cl^- is not able to do it. As all of them are balanced by the same cation (Na^+), the CSC differences can only be attributed to the anions. The same two possible explanations just discussed above can be now considered, although it is more than likely that Ca^{2+}, SCN^- and NO_3^- exert their corresponding specific effects by means of their capacity to change the structure of the water molecules around the particles. Therefore, our experiments reveal a negatively charged system in which anions but not cations control restabilization. Stenkamp et al. [46], working with electrosterically stabilized latex, also proved the importance of anions in the restabilization process. However, in their case the mechanism for such a restabilization was related to the presence of micelles or agglomerates, and not hydration forces.

To corroborate that restabilization is completely initiated by structural forces and not by electrical forces, the electrophoretic mobility of some samples was measured at high salt concentrations using the ZetaPALS instrument, which allows collection of μ_e data even in extremely high ionic strength media. Fig. 5 shows the electrophoretic behavior of the samples incubated at pH 10 for increasing thiocyanate and calcium concentrations. Two features is worth highlighting. First, the mobility was almost negligible at high electrolyte

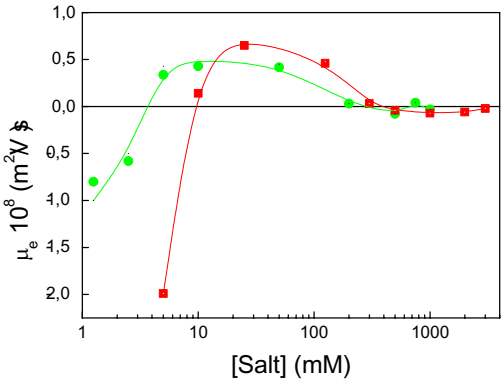

Fig. 5. Electrophoretic mobility of IgG-latex complexes at pH 10 as a function of NaSCN (■) and $Ca(NO_3)_2$ (●) concentrations.

concentrations. Therefore, the restabilization phenomena induced by these ions at high concentrations do not have an electrical origin. Second, with respect to the mobility, the complexes behaved similarly with both ions, inverting the μ_e sign in a broad salt concentration range. This is a peculiar pattern observed only with these two ions, and may not be easily explained. Samples are negative at pH 10, and consequently their mobility was also negative at very low salt concentration. The change in the μ_e sign, however, occurred as soon as SCN^- and Ca^{2+} concentrations began to increase. This feature could support the proposed mechanism of exclusion for strongly chaotropic ions (SCN^-) and of accumulation for kosmotropic ones (Ca^{2+}) at hydrophilic surfaces. If SCN^- (which now acts as coion) is excluded from the proximity of the protein surface, the vicinity of the particle/water interface would be enriched by counterions (Na^+) in such a way that the sign of the ζ-potential would be inverted while the surface potential Ψ_0 remained negative. The inversion of the μ_e sign produced by calcium could also be interpreted in terms of an accumulation mechanism.

Finally, our restabilization results should also be contrasted with the known effects of salts on protein solubility and conformational stability. As previously mentioned, chaotropic ions improve protein solubility but disrupt the protein's native architecture. On the contrary, kosmotropic ions stabilize protein structure but behave as strong precipitants. Keeping that in mind, two

points should be discussed. On the one hand, the restabilization observed at high concentrations of calcium is an effect opposite to that expected considering the protein solubility in the presence of calcium, as this kosmotropic ion is a salting-out agent, that is, it provokes aggregation at high salt concentration. So, the stability induced by Ca^{2+} must be caused by means of hydration forces on hydrophilic surfaces, but not of salting effects on the IgG layer. On the other hand, the stability observed at high concentrations of chaotropic ions (i.e. SCN^-) would agree with the high solubility shown by the IgG in presence of this kind of ions [32]; however, the low colloidal stability observed over a wide range of chaotropic salt concentrations (see Figs. 2a and 2b) would question this point. That is, the typical salting-in/salting-out processes usually observed in protein solutions are the opposite in IgG-latex particles: a salting-out/salting-in mechanism for increasing salt concentrations is found instead. This feature is qualitatively depicted in Figs. 6a and 6b.

Despite the fact that hydration forces are considered to be the main factor responsible for restabilization, an additional factor could contribute to stabilize our particles at high concentrations of chaotropic ions (SCN^- and $NO3^-$). Proteins undergo conformation changes in the presence of chaotropic ions. Hence, at high salt concentrations, adsorbed IgG molecules could become partially denatured originating a steric stabilization. However, this hypothetical mechanism is not very plausible. Pérez-Amodio et al. [47] measured the immuno-reactivity of IgG-latex particles in solutions containing, independently, 100 mM of NaCl, $NaNO_3$ and NaSCN. If conformational changes occurred in the antibody molecules, a loss in immuno-reactivity should be observed. There were, however, only marginal differences in reactivity between the anionic species: NaCl = 100 %reactivity, NaNO3 = 98 %and NaSCN = 87 % Therefore, there are no significant modifications in the protein structure to justify the steric stabilization as the mechanism subjacent in restabilization phenomena. As shown, the specific effects of salts on the protein itself seem not to significantly support the main stability features of the IgG-latex complexes. At least, there is no clear correspondence between the protein salting-in/salting-out effects and the colloidal coagulation and restabilization phenomena.

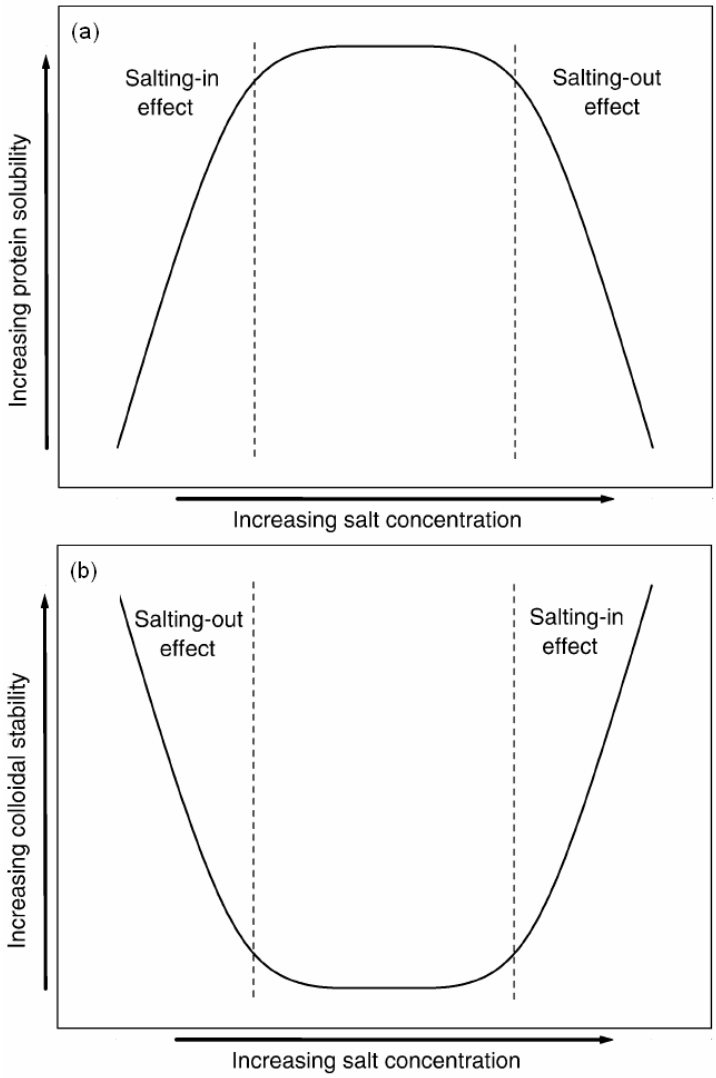

Fig. 6. (a) Typical salting-in/salting-out effects on protein solubility; (b) Typical salting-out/salting-in effect on the colloidal stability of protein-latex particles.

IV. Summary

It has been demonstrated that specific ionic effects play an important role in colloidal aggregation, electrophoretic mobility, and restabilization phenomena of polystyrene particles covered by IgG. The results often order the ions according to the Hofmeister series. The highest ionic specificity has been shown by the most chaotropic anion (SCN^-) and the most kosmotropic cation (Ca^{2+}). One of the main conclusions is related to the importance of the surface sign in destabilization processes: the aggregation results working with positive surfaces gave an ionic sequence that was almost inverted by negative particles. Actually, the most stabilizing ions acting as coions destabilize the system when they act as counterions. This feature was also observed in bare latex particles [21]. The electrokinetic studies also gave an ion ranking that agrees with that obtained in destabilization experiments. Nevertheless, there has been a surprising exception with thiocyanate in the system stored at pH 10. This strange behavior can be understood by assuming that IgG-latex complexes do not have similar hydrophilicity (or hydrophobicity) at the two experimental pH values tested. Restabilization caused by hydration forces confirms that particles incubated at pH 10 are actually more hydrophilic than those immersed in pH 4. Restabilization experiments have also provided interesting results never observed previously in latex-protein systems: anions are able to restabilize acting not only as coions but also as counterions.

Acknowledgements

We appreciate the financial support from the MAT2003-01257 project of the Comisión Interministerial de Ciencia y Tecnología (CICYT). We are greatly indebted to Miguel Vega Expósito for supervising the final English version. Of course, only the authors are responsible for those errors which may have passed unnoticed.

References

[1] Collins, K. D., Washabaugh, M. W., Q. Rev. Biophys., 18 (1985) 323.

[2] Lewith, S., Arch. Exp. Pathol. Pharmakol., 24 (1888) 1.

[3] Hofmeister, F., Arch. Exp. Pathol. Pharmakol., 24 (1888) 247.

[4] Luck, W.A.P., in A. Pullman, V. Vasilescu, L. Packer, (Eds.), Water and ions in biological systems, Plenum Press, New York, 1985.

[5] Pay, N. G. M., Symons, M. C. R., J. Chem. Soc., Faraday Trans., 89 (1993) 2417.

[6] Cacace, M.G., Landau, E.M., Ramsden, J.J., Quarterly Rev. Biophys., 30 (1997) 241.

[7] Barnes, P., Finney, J.L., Nicholas, J.D., Quinn, J.E., Nature, 282 (1979) 459.

[8] Hiemenz P. C., Rajagopalan, R., Principles of Colloid and Surface Chemistry, 3rd ed., Marcel Dekker, New York, 1997.

[9] Wiggins, P.M., Physica A, 238 (1997) 113.

[10] Ninham, B. W., Yaminsky, V., Langmuir, 13 (1997) 2097.

[11] Boström, M., Williams, D.R.M., Stewart, P.R., Ninham, B.W., Phys. Rev. E, 68 (2003) 041902.

[12] Boström, M., Craig, V.S.J., Albion, R., Williams, D.R.M., Ninham, B.W., J. Phys. Chem. B, 107 (2003) 2875.

[13] Maheshwari, R., Sreeram, K.J., Dhathathreyan, A., Chem. Phys. Lett., 375 (2003) 157.

[14] Lyklema, J., Mol. Phys., 100 (2002) 3177.

[15] Ruckenstein, E., Manciu, M., Langmuir, 18 (2002) 7584.

[16] Huang, H., Manciu, M., Ruckenstein, E., J. Colloid Interface Sci., 263 (2003) 156.

[17] Ruckenstein, E., Huang, H., Langmuir, 19 (2003) 3049.

[18] Hribar, B., Southall, N.T., Vlachy, V., Dill, K.A., J. Am. Chem. Soc., 124 (2002) 12302.

[19] Karlström, G., Hagberg, D., J. Phys. Chem. B, 106 (2002) 11585.

[20] Karlström, G., Phys. Chem. Chem. Phys., 5 (2003) 3238.

[21] López-León, T., Jódar-Reyes, A. B., Bastos-González, D. Ortega-Vinuesa, J.L., J. Phys. Chem. B, 107 (2003) 5696.

[22] Buijs, J., Lichtenbelt, J. W. T., Norde, W., Lyklema, J., Colloids Surf. B, 5 (1995) 11.

[23] Ortega-Vinuesa, J. L., Gálvez-Ruiz, M. J., Hidalgo-Álvarez, R., Langmuir, 12 (1996) 3211.

[24] Ortega-Vinuesa, J. L., Tengvall, P., Lundström, I., J. Colloid Interface Sci., 207 (1998) 228.

[25] Molina-Bolívar, J. A., Ortega-Vinuesa, J. L., Langmuir, 15 (1999) 2644.

[26] Carbonnaux, C., Riès-Kautt, M., Ducruix, A., Protein Sci., 4 (1995) 2123.

[27] Franks, G. V., J. Colloid Interface Sci., 249 (2002) 44.

[28] Dumont, F., Warlus, J., Watillon, A., J. Colloid Interface Sci., 138 (1990) 543.

[29] Bourikas, K., Hiemstra, T., van Riemsdijk, W. H., Langmuir, 17 (2001) 749.

[30] Arakawa, T., Timasheff, S., Biochemistry, 21 (1982) 6545.

[31] Arakawa, T., Timasheff, S., Biochemistry, 23 (1984) 5914.

[32] Gagnon, P., Mayes, T., Danielsson, Å. J. Pharm. Biomed. Anal., 16 (1997) 587.

[33] Ohshima, H., Kondo, T., J. Colloid Interface Sci., 116 (1987) 305.

[34] Ohshima, H., Kondo, T., J. Colloid Interface Sci., 130 (1989) 281.

[35] Ohshima, H., Nakamura, M., Kondo, T., Colloid Polym. Sci., 270 (1992) 873.

[36] Nakamura, M., Ohshima, H., Kondo, T., J. Colloid Interface Sci., 149 (1992) 241.

[37] Ortega-Vinuesa, J. L., Hidalgo-Álvarez, R., J. Non-Equilib. Thermodyn., 21 (1996) 339.

[38] Israelachvili, J., Intermolecular & Surface Forces, 2nd ed., Academic Press, London, 1992.

[39] Pashley, R.M., J. Colloid Interface Sci., 83 (1981) 531.

[40] Pashley, R. M., Adv. Colloid Interface Sci., 16 (1982) 57.

[41] Christenson, H.K., J. Dispersion Sci. Technol., 9 (1988) 171.

[42] Molina-Bolívar, J.A.; Galisteo-González, F.; Hidalgo-Álvarez, R., Colloids Surf. B, 21 (2001) 125.

[43] Molina-Bolívar, J. A., Galisteo-González, F., Hidalgo-Álvarez, R., Phys. Rev. E, 55 (1997) 4522.

[44] Molina-Bolívar, J. A., Galisteo-González, F., Hidalgo-Álvarez, R., J. Colloid Interface Sci., 206 (1998) 518.

[45] Molina-Bolívar, J. A., Galisteo-González, F., Hidalgo-Álvarez, R., Colloids Surf. B, 14 (1999) 3.

[46] Stenkamp, V. S., McGuiggan, P., Berg, J.C., Langmuir, 17 (2001) 637.

[47] Pérez-Amodio, S., Holownia, P., Davey, C.L., Price, C.P., Anal. Chem., 73 (2001) 3417.

HOFMEISTER EFFECTS IN THE RESTABILIZATION OF IgG-LATEX PARTICLES: TESTING RUCKENSTEIN'S THEORY

T. López-León, P.M. Gea-Jódar, D. Bastos-González, and J.L. Ortega-Vinuesa

Biocolloid and Fluid Physics Group, Department of Applied Physics, University of Granada, Av. Fuentenueva S/N, 18071 Granada , Spain

Abstract

The hydration interaction is responsible for the colloidal stability observed in protein coated particles at high ionic strengths. The origin of this non-DLVO interaction is related not only to the local structure of the water molecules located at the surface, but also the structure of those molecules involved in the hydration of the ions that surround the colloidal particles. Ruckenstein and co-workers have recently developed a new theory based on the coupling of double-layer and hydration interactions. Its validity was contrasted by their fitting experimental data obtained with IgG-latex particles restabilized at high salt concentration. The theory details the important role played by the counterions in the stability at high salt concentrations by proposing an ion pair reaction forming surface dipoles. These surface dipole are responsible of repulsive interactions between two approaching surfaces. This paper checks the theory with recent data where some ions associated with the Hofmeister series, (NO_3^-, SCN^- and Ca^{2+}), restabilize the same kind of IgG-latex systems by means of hydration forces. Surprisingly, these ions induce stability acting even as coions, likely by modifying the water structure at the surface, but not forming surface ion pairs. Therefore, these experimental evidences would question Ruckenstein's theory based on the surface dipole formation for explaining the observed restabilization phenomena.

I. Introduction

Repulsive hydration forces between hydrophilic surfaces have been extensively observed in many systems for the last 25 years. These forces were first studied between clay surfaces by van Olphen.[1] Israelachvili and Adams[2] were the first who directly measured the hydration forces between two mica surfaces immersed in aqueous KNO_3 solutions. The origin of this force has been associated with the structuring of water in the vicinity of the surfaces. It is a structural force that arises from the local order of water layers adjacent to the surface. It is not only correlated to the hydrophilicity degree of the surface, but also it strongly depends on the nature and concentration of the hydrated counterions that surround the surface.[3-7] In fact, this force is usually attributed to the hydration shells of (i) adsorbed counterions and (ii) ionic and/or polar functional groups in the surface. Despite its perception as a short-range force, compared to the classical forces accounted in the DLVO theory,[8,9] its effective range goes from 0 to as much as 5-10 nm.[3,10] This "relatively" long-range interaction is believed to arise from a cooperative mechanism of water-water H-bonding.[11] The hydrophilic surface restructures the first adjacent water layer, which in its turn modifies the H-bonding network of subsequent water molecules. This cooperative mechanism propagates the hydration forces a few nanometers from the surface. Experimentally, an exponential decay of the hydration interactions has been often found.[2,3,5,12-15] The decay length is in the 0.2-1.1 nm range,[16] while the preexponential factor varies by more than an order of magnitude, depending on the hydration of the surface.

Regarding hydration in colloidal dispersions, the effects of different electrolytes on the hydration forces between colloidal particles can determine whether they will coagulate or not. Highly hydrophilic surfaces (e.g., silica, lecithin)[3,17] cannot be coagulated by changing the ionic conditions. Less hydrophilic surfaces, for example, polystyrene particles totally covered by globular proteins, show destabilization with increasing ionic strength, as predicted by the DLVO theory, but restabilization at sufficiently large electrolyte concentrations.[7,15,18,19] The role played by the presence of hydrated ions at the solid/water interface is crucial in the restabilization process. Cations, but not anions, have been usually considered responsible for the hydration restabilization when they act as counterions. Actually, the hydration numbers are bigger in cations than anions. It has been experimentally

confirmed that the hydration forces increase with the hydration number of the cations.[3]

There have been several theoretical approaches to included the hydration interaction in the colloidal stability framework. Most of them are based on adding a "hydration" term (V_H), given by an exponential equation, to the usual repulsive (V_R) and attractive (V_A) terms shown by the DLVO theory.[20,15] V_R considers the repulsive interactions coming from the overlapping of the double layers, while V_A is related to the attractive van der Waals interactions. Thus, the total interaction can be described by the algebraic sum of three potentials:

$$V_T = V_A + V_R + V_H \tag{1}$$

Nevertheless, Ruckenstein et al.[21-25] have recently demonstrated that this simple equation would be incorrect, as double layer and hydration interactions are interrelated and they cannot be considered independent terms. These authors demonstrated an elaborated theory based on a set of coupled equations dependent on the polarization of water molecules, where the electric fields generated by the surface charges and surface dipoles, as well as the field due to the neighboring dipoles in structured water layers were taken into account. These equations were satisfactorily used in refs 24 and 25 to explain the restabilization phenomena observed at large ionic strengths for colloidal particles covered by IgG molecules shown in ref 18. The average field and polarization generated by the dipoles on the surface, which act on the first water layer, is the cornerstone of the theory. This polarization is transmitted from the surface to the liquid medium through dipole-dipole interactions giving a gradient of polarization. The gradient polarization, related to the water structure, affects via Poisson equation the macroscopic electric field and, hence, the double layer interaction. According with this theory, the restabilization of IgG-latex complexes is triggered by the formation of surface dipoles, which are originated by the formation of ion pairs (dipoles) between fixed negative charged groups on the surfaces and the cations that act as counterions. It must be pointed out that this theory combines simultaneously the two parameters affecting the hydration forces: the water structure and the presence of ions.

On the other hand, it is worth mentioning that there are a plethora of phenomena associated to the correlation between ions and water structure. Over a century ago, Hofmeister and Lewith[26,27] published accounts of great

differences between the minimum concentration of various salts required to precipitate a given protein from solution. The specific ionic effects are nonnegligible at all, and they are always present in intermolecular or surface interactions. Polymer cloud points, protein solubility, chromatographic selectivity, critical micelle concentrations, etc., are dependent on how the ions specifically interact and/or structure the surrounded water molecules. Many ions have been ranked in sequences called Hofmeister series, depending on their specific effects (usually referred to as Hofmeister effects) on different experimental systems. Despite the broad spectrum of results existing at this point, the molecular origin of the Hofmeister effects still remains unraveled, as shown in comprehensive reviews.[28,29] Whatever the molecular mechanism is subjacent, they do emerge from a combination of effects in which the water structure and/or specific ionic adsorption or exclusion from a surface are the cornerstones.[30] Therefore, the Hofmeister effects and the hydration forces just discussed above must be related. However, there is a controversial point. The Hofmeister effects are dominated by anions instead of cations,[28] while hydration forces between interfaces are associated mainly to cations.[3] To elucidate this controversial item, we very recently designed different experiments where anions associated to the Hofmeister series were used to restabilize latex particles covered by IgG at high ionic strength.[31] Restabilization induced by anions was found and, to our knowledge, these experiments become the first report where anions are responsible for hydration forces in this kind of system. This is a clear example that corroborates the interrelation between the Hofmeister effects and hydration interactions.

The goal of the present paper is, therefore, to apply the theory developed by Ruckenstein et al.[21-25] to colloidal restabilization phenomena given by some Hofmeister anions. As previously commented, Hofmeister effects are associated with molecular mechanisms related to water structure and/or ion adsorption or exclusion. Ruckenstein's theory also is based on the same points. So, it could be interesting to test this theory with novel results concerning to colloidal restabilization.

II. Materials and methods

NaCl, $NaNO_3$, NaSCN, and $Ca(NO_3)_2$ salts were of analytical grade and purchased from Sigma and Scharlau. Deionized water was used throughout.

Freshly nonbuffered solutions were obtained when required by adding HCl or NaOH to water in the desired quantity to get pH 4 or pH 10, respectively.

Polystyrene latex particles were synthesized, cleaned and characterized in our laboratories. Details are given in ref 30. Size and surface charge density data are briefly described below. The mean diameter, obtained by transmission electron microscopy, was 320 ± 15 nm, having a polydispersity index extremely close to unity (1.007). It showed an anfoteric nature with positive charge in the pH 4 to 10 range, and had an isoelectric point (iep) at pH equal to 10.5. Consequently, the positive surface charge density (σ_0) was not constant. The σ_0 values at the two pHs tested in the present work were equal to 18.3 ± 1.2 μC/cm^2 at pH 4 and 4.0 ± 0.6 μC/cm^2 at pH 10, respectively.

Polyclonal IgG from rabbit was obtained, purified and kindly donated by Biokit S.A. (Spain). The isoelectric point determined by isoelectric focusing was in the 6.1-8.5 range. An excess of protein was added to the latex particles in order to cover the polystyrene surface with IgG as much as possible. The protein loads of the latex particles were around 6 mg/m^2. Details are given in ref 31.

Particle aggregation studies were carried out using a low-angle light-scattering technique. Scattering light intensity was observed at 10º for 120 s. The scattering cell was rectangular with a 2 mm path length. Equal volumes (1 ml) of salt and IgG-latex solutions were mixed and introduced into the cell by an automatic mixing device. The light scattered at 10ŋbehaves linear for the first steps of the coagulation. The stability ratio, also called Fuch's factor, (W) is a criterion broadly used to study the stability of colloidal systems. It can be obtained by the following expression

$$W = \frac{k_r}{k_s} \tag{2}$$

in which the rate constant "k_r" corresponds to rapid coagulation kinetic, and "k_s" is the rate constant for the slow coagulation regime. The scattered light intensity at low angles increases linearly with time during a coagulation process.[32] Thus, the coagulation rate constants can be easily obtained from the slopes. The critical coagulation concentration "CCC", defined as the minimum salt concentration needed to rapidly aggregate the colloidal system, can be obtained by plotting the logarithm of W versus the logarithm of the salt

concentration and locating that point where log W reduces to zero. Likewise, the critical stabilization concentration "CSC" is defined as the minimum salt concentration at which restabilization starts.

III. The basic equations

It should be noted that the following theoretical framework must be thought of as a very brief summary. Complete information can be found in refs 23 and 24. It should be also noted that the vectorial notation of vectors have been intentionally removed for the sake of clarity, as only one spatial dimension is considered.

Traditional double-layer theory combines the Poisson equation with the assumption that the polarization is proportional to the macroscopic electric field. However, this is only applicable when the electric field is sufficiently uniform, and hence when the polarization gradient is sufficiently small. When this condition is not satisfied, the polarization gradient generates an additional electric field, because the fields acting on a water molecule due to the neighboring water dipoles do not compensate each other any longer. Actually, a large polarization gradient is generated in an aqueous electrolyte solution, either when the surface charge density is large and/or when there are dipoles on the surfaces. Ruckenstein's theory assumes that near a surface the water is composed of a succession of icelike layers. The electric field E_p that acts on a water molecule and that is generated by the neighboring structured water molecules through their dipoles can be approximately expressed as [23,24]

$$E_p \approx C_1 \Delta^2 \frac{\partial^2 m}{\partial z^2} \tag{3}$$

where Δ is the distance between the centers of two adjacent water layers, $m(z)$ is the dipole moment as a function of z, which is the normal component of the distance, and C_1 is given by:

$$C_1 = \frac{1.827}{4\pi\varepsilon_0\varepsilon'' l^3} \tag{4}$$

l is the distance between the centers of two adjacent water molecules, and ε'' is the dielectric constant for the interaction between neighboring molecules, taken as unity in the present calculations. It should be noted that only the fields of the neighboring dipoles are important because those caused by more

remote ones are screened. This is why the electric constant is unity between two adjacent dipoles, but very large for the remote ones.

On one hand, by introducing the field E_p (Equation 3) in the traditional Lorentz-Debye theory and relating the dipole moment m with the local electric field via the water polarizability, one finally obtains [23,24]

$$m(z) = \varepsilon_0 \upsilon_0 (\varepsilon - 1) E(z) + \varepsilon_0 \upsilon_0 (\varepsilon - 1) C_1 \Delta^2 \frac{\partial^2 m}{\partial z^2} \tag{5}$$

where υ_0 is the volume of a water molecule, ε is the dielectric constant of water, and $E(z)$ is the macroscopic electric field.

On the other hand, assuming Boltzmann distributions for the ions, one can write

$$\rho = -2 c_E e \sinh\left(\frac{e\Psi}{kT}\right) \tag{6}$$

where ρ is the volume charge density, c_E the bulk electrolyte concentration, Ψ the electrical potential, and k, T and e have its usual meaning. Introducing Equation 6 in the Poisson equation, this last one becomes

$$\frac{\partial^2 \Psi(z)}{\partial z^2} = \frac{2 e c_E}{\varepsilon_0} \sinh\left(\frac{e\Psi}{kT}\right) + \frac{1}{\varepsilon_0 \upsilon_0} \frac{\partial m(z)}{\partial z} \tag{7}$$

Equations 5 and 7 (see Appendix) constitute a system of differential equations for Ψ and m. To obtain the solutions some boundary conditions must be set. These conditions, described in ref 24, are based in electroneutrality and symmetry impositions when two surface approach each other. The key for solving the system of Equations 5 and 7 is given by the average electric field E_s generated by dipoles on the surface and that is acting in the first water molecules. It affects to the boundary conditions and it is indirectly used as the fitting parameter to explain the experimental results. Its expression is given by[22]

$$E_s = \left| \frac{\left(p \big/ \varepsilon'\right)}{2\pi\varepsilon_0 \left(\frac{A}{\pi} + \Delta'^2\right)^{3/2}} \right| \tag{8}$$

where p is the normal component of the dipole moment of the surface dipoles, ε' is the local dielectric constant of the medium, A is the surface area per dipole of the surface ($1/A$ is the surface dipole density), and Δ' is the distance between a surface dipole and the center of the first layer of water molecules. As will be shown afterward, (p/ε') and A will be actually the two fitting parameters of this theory, while many other parameters will be set at constant values.

Once the system of nonlinear equations is numerically solved, the potential interaction between two colloidal particles can be obtained from the free energy of the system per unit area F, which contains three contributions

$$F = F_{chem} + F_{ele} + F_{entropy} \tag{9}$$

where F_{chem} is the chemical, F_{ele} the electrostatic and $F_{entropy}$ the entropic contribution. Their values depend on $E(z)$, $\Psi(z)$ and $m(z)$, and their analytical expressions are given in refs 33,24 and 34, respectively. By using the Derjaguin approximation, the repulsive interaction energy between two identical spheres of radius a is given by

$$V_R = \pi a \int_{H_0}^{\infty} (F - F_\infty)\, dH \tag{10}$$

where H_0 is the minimum distance between the surfaces of two approaching spheres and F_∞ is the repulsive free energy per unit area between two infinitely separated plates. The van der Waals attractive interaction between two spherical particles has the form[35]

$$V_A = -\frac{A_H}{6}\left[\frac{2a^2}{H(4a+H)} + \frac{2a^2}{(2a+H)^2} + \ln\frac{H(4a+H)}{(2a+H)^2}\right] \tag{11}$$

A_H being the Hamaker constant.

The total interacting free energy between the two particles is therefore given by

$$V_T = V_A + V_R \tag{12}$$

The main difference between Equation 12 and Equation 1 is that hydration interactions and the electrical term associated to the overlapping of the double layers are now dependent. The surface dipoles polarize the nearby

water molecules, which in turn polarize the next layer and so on. Thus, water and ionic effects are simultaneously considered in this theory in the V_R term.

The experimental value of the stability ratio W is easily accessible through aggregation experiments monitored by optical devices (see Equation 2). To be able to compare theory and experiments, a theoretical expression for such a factor is required. The stability ratio is related to the interaction potential via the expression[36,37]

$$W = \frac{\int_0^\infty \frac{\beta(u)}{(u+2)^2} \exp\left(\frac{V_T}{kT}\right) du}{\int_0^\infty \frac{\beta(u)}{(u+2)^2} \exp\left(\frac{V_A}{kT}\right) du} \tag{13}$$

where β is a hydrodynamic correction factor, and $u = H_0/a$. For the sake of simplicity, the hydrodynamic factor has been taken as unity.

Finally, as our colloid particles are covered by protein, some parameters related to the IgG molecules are needed to definitively quantify the theoretical value of W. They are the surface density of basic sites (N_B), the surface density of the acidic sites (N_A), and the acidic constant of the acidic sites (K_H). Although they are not known, Ruckenstein et al.[24] assumed some constant values that match in typical experimental ranges. These variables control the value of the surface charge density, that is, a parameter that appears in the boundary conditions used to solved the system of Equations 5 and 7. In addition, authors mentioned above consider that surface dipoles are formed through the adsorption of counterions, forming the following ion pairs:

$$\begin{aligned} S_{A^-} + C^+ &\rightleftarrows S_{A^-}C \\ S_{B^+} + A^- &\rightleftarrows S_{B^-}A \end{aligned} \tag{14}$$

where S_A^- is a dissociated acidic site of the surface, C^+ a cation, S_B^+ a dissociated basic site, A^- an anion, and S_A-C and S_B-A the corresponding ion pairs. The first reaction is proposed for negatively charged surfaces and the second one for positive. These authors quantify this surface dipole formation proposing an equilibrium constant (K_C for cation union and K_A for anions), which is used as a fitting parameter in their theory. Actually, the value of K_C (or K_A) control the value of the dipole density on the surface ($1/A$), which in turn, and together with p/ε', governs the E_S value via Equation 8. As

previously commented, the E_S value is the key for solving the system of Equations 5 and 7, and then for obtaining the theoretical W values.

IV. Results and discussion

NaCl, $NaNO_3$, and NaSCN, were chosen to analyze the effect of three anions located in different positions of the Hofmeister series. The specific effects shown by ions usually present an inversion at about Cl^- (for anions) and Na^+ (for cations) in the Hofmeister series. So, these two ions are usually considered as null points in the specific ionic effects. Thiocyanate is a strongly chaotropic ion. That is, it is a weakly hydrated anion that greatly disturbs the order of the surrounding water molecules.[28,29] Nitrate behaves as SCN^-, although its chaotropic character is less pronounced. $Ca(NO_3)_2$ was used to analyze the specific effects of calcium comparing the experimental results with those obtained with $NaNO_3$. As both salts share the same anion, experimental differences must be attributed to the cations. Calcium is strongly hydrated. It belongs to the so-called kosmotropic ions. Its strong interaction with water molecules also modifies the local order of the solvent around it. It should be noticed that the effect of kosmotropic anions is opposite to that of the kosmotropic cations. Although both of them interact with water molecules strongly, the orientation of the oxygen and hydrogen atoms toward the ions surface is opposite due to its difference in charge sign. However, the water structure induced by a chaotropic anion results similar to that of a kosmotropic cation, and vice versa.[28,29] This is why SCN^- and Ca^{2+} usually show similar specific effects.

The experimental stability ratio W was obtained in aggregation experiments adding independently the chosen salts to samples containing the IgG-latex particles. Figure 1 shows the results obtained at pH 4, at which particles exhibit positive charge. The results obtained at pH 10, particles showing a negatively charged surface, are plotted in Figure 2. The corresponding CCC and CSC values are given in Table 1. As shown, restabilization phenomena at high salts concentrations (not explained by the DLVO theory) are observed at both pHs. These patterns are a consequence of the hydration forces. This can be confirmed taking into account that the ions that most change the water structure, that is those located at the extreme of the Hofmeister series (SCN^- and Ca^{2+}), show the most restabilizing effects.

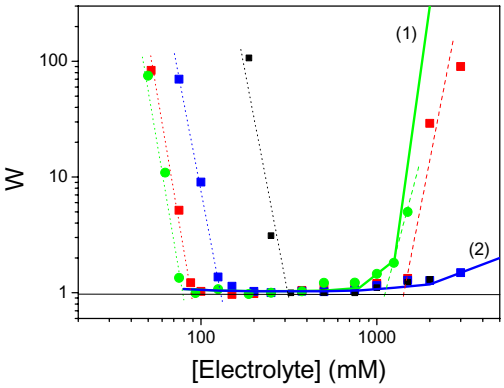

Figure 1. Stability ratio (Fuch's factor) versus electrolyte concentration for IgG-latex complexes buffered at pH4. NaSCN NaSCN (■), $NaNO_3$ (●), NaCl (■), and $Ca(NO_3)_2$ (■). Dotted and segmented lines are used only to guide the eye to get the CCC and CSC values, respectively. Solid lines correspond to theoretical predictions using K_A and (p/ε') as the fitting parameters. $(p/\varepsilon') = 3$ Debye; (1) $K_A = 0.8$ M; (2) $K_A = 1.4$ M.

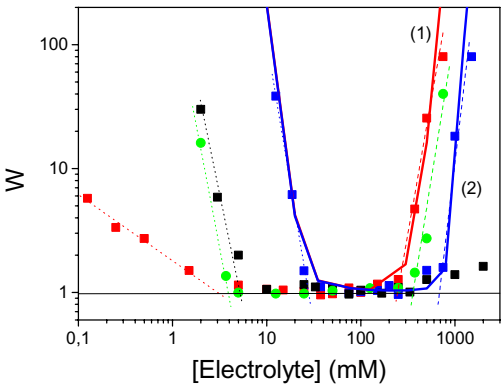

Figure 2. Stability ratio (Fuch's factor) versus electrolyte concentration for IgG-latex complexes buffered at pH10. NaSCN (■), $NaNO_3$ (●), NaCl (■), and $Ca(NO_3)_2$ (■). Dotted and segmented lines are used only for a guide to get the CCC and CSC values, respectively. Solid lines correspond to theoretical predictions using K_A and p/ε' as the fitting parameters. $(p/\varepsilon') = 3$ Debye; (1) $K_A = 0.2$ M; (2) $K_A = 0.5$ M.

Table 1. Critical coagulation concentration (CCC) and critical stabilization concentration (CSC) for the IgG-latex particles.

	IgG-latex at pH 4				IgG-latex at pH 10			
	SCN^-	NO_3^-	Cl^-	Ca^{2+}	SCN^-	NO_3^-	Cl^-	Ca^{2+}
CCC (mM)	90	130	270	80	4	25	6	4
CSC (mM)	1500	---	---	1100	260	700	---	350

Surprisingly, not only cations but also anions can induce colloidal restabilization. Thus, these data support the relation between hydration forces and Hofmeister effects. If the 1:1 electrolytes are compared, the observed differences in CCC and CSC values can be only attributed to the specific effects of the anions. As SCN^-, NO_3^- and Cl^- specifically modify the surrounding water molecules structure despite of possessing identical valency, only hydration interactions must be responsible for the stability differences, discarding any electrical origin. The structure of water molecules at the surface must be specifically modified by the presence of these ions, causing observable changes between the surface interactions of two approaching particles. A more extensive discussion about this item can be found elsewhere.[30,31]

The goal of this paper actually aims to the application of the theory developed by Ruckenstein and co-workers summarized before. These authors attained to explain the restabilization of IgG-latex particles induced independently by sodium and calcium at high concentrations.[24,25] Restabilization was theoretically explained by considering the adsorption of sodium (or calcium) on a negative surface forming ion pairs. The concentration at which the ion pair formation starts was selected by controlling the value of the equilibrium constant K_C. The adsorption of cations onto negatively charged groups of the surface, which is stimulated by higher salt concentrations, increases the density of surface dipoles. The surface dipoles polarize the nearby water molecules, which in turn polarize the next layer and so on. The force generated by the overlap of the polarization layers of the two plates (hydration force) is responsible for the restabilization of the colloidal system as soon as the salt concentration becomes higher than a critical stabilization concentration. Therefore, the theory combines adsorption of ions and structuration of water (dipole-dipole interactions). Actually, these are the same mechanisms usually proposed for explaining Hofmeister effects.

Unfortunately, the theory has many parameters that must be set. Some of them are not known. As an example, Δ (the distance between the centers of two adjacent water layers), l (the distance between the centers of two adjacent water molecules), Δ'(the distance between a surface dipole and the center of the first layer of water molecules), p (the normal component of the dipole moment of the surface dipoles), ε' (the *local* dielectric constant of the medium), A_H (the Hamaker constant), N_B (the surface density of basis sites in the IgG molecule), N_A (the surface density of the acidic sites), K_H (the acidic constant of the acidic sites), and K_C (the equilibrium constant for surface dipole formation for cation adsorption). The last 4 parameters are needed to get a value for $1/A$, which will be responsible for colloidal restabilization. This important drawback of the theory is solved by Ruckenstein et al. keeping constant many of these parameters giving them plausible values and only using (p/ε') and K_C (for cation adsorption) as fitting parameters. Then, we will apply their theory using the same procedure, as our experimental system is completely similar to that used by them. However, K_A instead of K_C will be used for explaining the effects caused by the anions. Consequently, most of the following data were taken from refs 21 and 24: $l = 2.76$ Å $\Delta = 3.68$ Å $\Delta' = 1.0$ Å $N_A = N_B = 2 \times 10^{18}$ m^{-2}; $K_H = 8 \times 10^{-10}$ M. $A_H = 3.2 \times 10^{-20}$ J. The data shown in Figures 1 and 2 were theoretically fitted optimizing the values of (p/ε') and K_A. Both of them control the E_S and subsequently the W values at high ionic strengths. On one hand, Figure 3 shows the influence of the (p/ε') parameter for a given K_A value. On the other hand, Figure 4 shows the K_A effect keeping constant (p/ε').

The theoretical description based on surface dipole formation could satisfactorily explain the restabilization at pH 4 (Figure 1) induced by the presence of SCN^-. Particle surface are positive at this acidic pH, and this anion, acting as counterion, could form ion pairs in the surface triggering the stabilizing mechanism previously discussed. However, the theory would fail for justifying the stabilizing effect given by the calcium. In this case, calcium acts as co-ion, and the formation of surface dipoles to restabilize the colloidal particles makes no sense. It should be highlighted that it is the co-ion calcium and not the counterion nitrate that is responsible for this non-DLVO phenomenon, since restabilization did not take place when $NaNO_3$ was used. The same problem appears at pH 10 (Figure 2). At this basic pH the particles clearly exhibit a negatively charged surface.[31] Now, both thiocyanate and

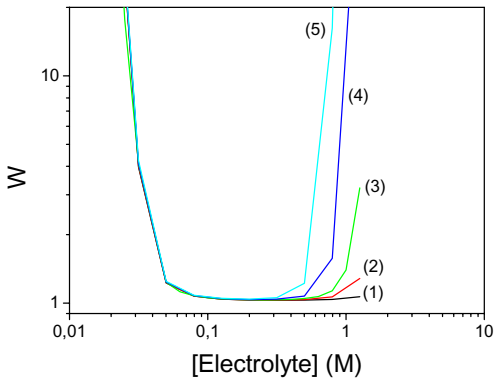

Figure 3. Theoretical stability ratio versus electrolyte concentration. l = 2.76 Å Δ = 3.68 Å Δ' = 1.0 Å $N_A = N_B$ = 2 x 10^{18} m^{-2}; K_H = 8 x 10^{-10} M; A_H = 3.2 x 10^{-20} J; pH10; K_A = 1.0 M. (1) (p/ε') = 3 Debye; (2) (p/ε') = 5 Debye; (3) (p/ε') = 7 Debye; (4) (p/ε') = 10 Debye; (5) (p/ε') = 15 Debye.

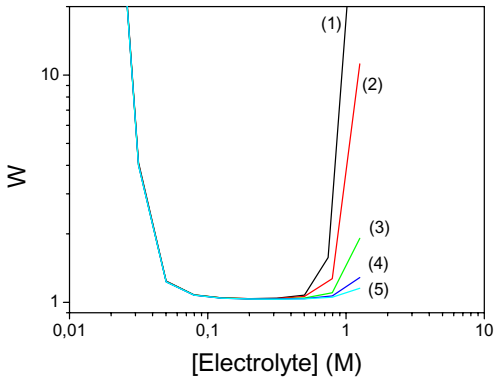

Figure 4. Theoretical stability ratio versus electrolyte concentration. l = 2.76 Å Δ = 3.68 Å Δ'= 1.0 Å $N_A = N_B$ = 2 x 10^{18} m^{-2}; K_H = 8 x 10^{-10} M; A_H = 3.2 x 10^{-20} J; pH10; (p/ε') = 3 Debye. (1) K_A = 0.5 M; (2) K_A = 0.6 M; (3) K_A = 0.8 M; (4) K_A = 1.0 M; (5) K_A = 1.2 M.

nitrate acting as coions provoke restabilization. The ion pair formation on negative surfaces (S_A^- + C^+ ⇆ S_A-C), which is one of the cornerstones of the Ruckenstein theory, cannot be the mechanism subjacent to this colloidal stability at high SCN^- and NO_3^- concentrations. Again, the stability cannot come from the counterion (sodium), as the restabilization does not happen when using NaCl. This corroborates that SCN^- and NO_3^- (but not Na^+) are the stabilizing ions. At this basic pH, only calcium could form the ion pairs. Therefore, there would be only two cases supporting the Ruckenstein theory (SCN^- at pH 4 and Ca^{2+} at pH 10), while three exceptions are found (Ca^{2+} at pH 4, NO_3^- and SCN^- at pH 10). Therefore, the theory should be revised. It should be noted that considering the ion valency in the theory for application to the calcium experiments complicates the mathematical equations.[25] This additional effort was not made for fitting our data, since (shown) the theory fails to explain restabilization by means of ion pair formation even for the 1:1 electrolytes.

The value of E_s, obtained from the fitting parameters via Equation 8, is crucial to control the theoretical behavior of the stability ratio W. Therefore, any modification affecting this equation could be planned at least as a first approximation. However, the fact that the ions that strongly modify the water structure (those located at the extreme of the Hofmeister series), show higher stabilizing features would question another important point of this theory. The theory is based on a succession of icelike water layers parallel to the surface.[22] However, it is known that these specific ions disrupt the structure of water,[28,29] and thus, it is more than likely that the virtual structured water layers proposed by the theory do not actually exist. This point would also invalid the theory for explaining the restabilization given by chaotropic and kosmotropic ions at high concentrations.

IV. Conclusions

As shown, the formation of surfaces dipoles can hardly be accepted as an explanation of the colloidal stability of protein-latex particles at high ionic strengths. The hydration interaction must be thought of as coming from changes in the structure of water molecules induced by specific ions. The repulsion that originated for the overlapping of structured water layers when two particles approach could have different, but interrelated, origins. On one hand, there could be a steric component associated with the rupture of the

liquid structure at the surface when to particles collapse. This sterical repulsion not only would account for entropic contributions but also would include the energy needed to dehydrate the ions near the surfaces before contacting. In addition, one could also take into account repulsive solvation forces of the solvent molecules behaving as hard sphere forces.[38,39] In our case, however, these hard sphere forces should be only associated to the ions, but not to the water molecules, as restabilization only occurs in the presence of high salt concentrations, while the system aggregates at intermediate ionic strengths. On the other hand, there could be an electrical component coming from structured dipoles. These orientated dipoles would generate an additional electric field, as shown by Ruckenstein et al., yielding electrical repulsive forces and preventing aggregation. Both mechanisms are not independent as they are based on the local orientation of the water molecules. This is why the hydration interaction could be thought of electrosteric origin. What can be inferred is that the hydration force is not of a simple nature, and it may be fair to say that it is probably the least understood of all the forces in water.

Acknowledgements

The authors would like to thank the MAT2003-01257 projects given by the Ministry of Science and Technology (Spain).

Appendix

Equations 5 and 7 are basic equations used in this paper. They can be obtained from other elementary equations of physics, as demonstrated below.

Equation 5 of the main text comes from a known relation for dielectric materials:[40]

$$\boldsymbol{D} = \varepsilon_0 \boldsymbol{E} + \boldsymbol{P} = \varepsilon \varepsilon_0 \boldsymbol{E} \qquad (15)$$

where "$\mathbf{D}$" is the electric displacement vector, "ε_0" the vacuum permittivity, "$\mathbf{E}$" the macroscopic electric field, "$\boldsymbol{P}$" the polarization of the medium and "ε" the electric constant of the medium.

So, the polarization vector can be expressed as:

$$\boldsymbol{P} = \varepsilon\varepsilon_0\boldsymbol{E} - \varepsilon_0\boldsymbol{E} = \varepsilon_0(\varepsilon - 1)\boldsymbol{E} \tag{16}$$

Polarization is defined as the average dipole moment per unite volume,

$$\boldsymbol{P} = \frac{\boldsymbol{m}}{\upsilon_0} \tag{17}$$

Thus, Equation A.2 can be written as

$$\boldsymbol{m} = \varepsilon_0\upsilon_0(\varepsilon - 1)\boldsymbol{E} \tag{18}$$

If only one spatial dimension is considered, this equation reduces to:

$$m(z) = \varepsilon_0\upsilon_0(\varepsilon - 1)E(z) \tag{19}$$

Ruckenstein's theory suggest that the electric field acting on a water molecule located at "*z*" position must include the field $\mathbf{E_p}$ generated by the neighboring dipoles. If this new term is added, then:

$$m(z) = \varepsilon_0\upsilon_0(\varepsilon - 1)\big[E(z) + Ep(z)\big] \tag{20}$$

The expression for $E_p(z)$ was shown in the Equation 3 (see main text), and demonstrated by Ruckenstein et al. in refs 23 and 24. Consequently, finally one obtains

$$m(z) = \varepsilon_0\upsilon_0(\varepsilon - 1)E(z) + \varepsilon_0\upsilon_0(\varepsilon - 1)C_1\Delta^2\frac{\partial^2 m}{\partial z^2} \tag{21}$$

which is the first of the differential equations for Ψ and m, knowing that

$$E(z) = -\frac{\partial\Psi}{\partial z} \tag{22}$$

The second differential equation (Equation 7) can be obtained from the Maxwell equations. The Gauss law in differential form says:

$$\nabla.\boldsymbol{D} = \rho \tag{23}$$

where ρ is the volume charge density. Taking into account Equation A.1, the Gauss law becomes

$$\varepsilon_0\nabla.\boldsymbol{E} + \nabla.\boldsymbol{P} = \rho \tag{24}$$

which is the Poisson equation for dielectric materials:

$$\varepsilon_0\nabla.\boldsymbol{E} = \rho - \nabla.\boldsymbol{P} \tag{25}$$

If only one dimension is considered and multiplying everything by –1, one can write

$$-\varepsilon_0 \frac{\partial E}{\partial z} = -\rho + \frac{\partial P}{\partial z} \tag{26}$$

Changing $\mathbf{E}$ and $\mathbf{P}$ for their corresponding expressions, that is using Equations A.8 and A.3, one obtains

$$\frac{\partial^2 \Psi}{\partial z^2} = -\frac{\rho}{\varepsilon_0} + \frac{1}{\varepsilon_0 \upsilon_0} \frac{\partial m}{\partial z} \tag{27}$$

If a Boltzmann distribution for the ions is assumed (see Equation 6 in the main text), the sought equation is finally obtained.

References

(1) Van Olphen, H. *An Introduction to Clay Colloid Chemistry*, Wiley: New York, 1977.

(2) Israelachvili, J.N.; Adams, G.E. *J. Chem. Soc. Faraday Trans.* **1978**, *74*, 975.

(3) Israelachvili, J.N. *Intermolecular & Surface Forces*, Academic Press: London, 1992.

(4) Pashley, R.M. *J. Colloid Interface Sci.* **1981**, *83*, 531.

(5) Pashley, R.M. *Adv. Colloid Interface Sci.* **1982**, *16*, 57.

(6) Christenson, H.K. J. Dispersion Sci. Technol. **1988**, *9*, 171.

(7) Molina-Bolívar, J.A.; Galisteo-González, F.; Hidalgo-Álvarez, R. *Colloids Surf. B* **2001**, *21*, 125.

(8) Derjaguin, B.V.; Landau, L. *Acta Physicochim. URSS* **1941**, *14*, 633.

(9) Verwey, E.J.; Overbeek, J.Th.G. *Theory of Stability of Lyophobic Colloids*, Elsevier: Amsterdam, 1948.

(10) Israelachvili, J.N.; Pashley, R.M. *J. Colloid Interface Sci.* **1984**, *98*, 500.

(11) Wiggings P.M. *Physica A* **1997**, *238*, 113.

(12) Marcelja, S.; Radic, N. *Chem. Phys. Lett.* **1976**, *42*, 129.

(13) Parsegian, V.A. *Adv. Colloid Interface Sci.* **1982**, *16*, 49.

(14) Derjaguin, B.V.; Rabinovich, Y.I.; Churaev, N.V. *Adv. Colloid Interface Sci.* **1982**, *16*, 63.

(15) Molina-Bolívar, J.A.; Galisteo-González, F.; Hidalgo-Álvarez, R. *Phys. Rev. E* **1997**, *55*, 4522.

(16) van Oss, C.J. *Colloids Surf.* **1993**, *78*, 1.

(17) Yotsumoto, H.; Yoon, R.H. *J. Colloid Interface Sci.* **1993**, *157*, 434.

(18) Molina-Bolívar, J.A.; Ortega-Vinuesa, J.L. *Langmuir* **1999**, *15*, 2644.

(19) Dávalos-Pantoja, L.; Ortega-Vinuesa, J.L.; Bastos-González, D.; Hidalgo-Álvarez, R. *Colloids Surf. B* **2001**, *20*, 165.

(20) Churaev, N.V.; Derjaguin, B.V. *J. Colloid Interface Sci.* **1985**, *103*, 542.

(21) Manciu, M.; Ruckenstein, E. *Langmuir* **2001**, *17*, 7061.

(22) Manciu, M.; Ruckenstein, E. *Langmuir* **2001**, *17*, 7582.

(23) Ruckenstein, E.; Manciu, M. *Langmuir* **2002**, *18*, 7584.

(24) Huang, H.; Manciu, M.; Ruckenstein, E. *J. Colloid Interface Sci.* **2003**, *263*, 156.

(25) Ruckenstein, E.; Huang, H. *Langmuir* **2003**, *19*, 3049.

(26) Hofmeister, F. *Arch. Exp. Pathol. Pharmakol.* **1888**, *24*, 247.

(27) Lewith, S. *Arch. Exp. Pathol. Pharmakol.* **1888**, *24*, 1.

(28) Collins, K.D.; Washabough, M.W. *Q. Rev. Biophys.* **1985**, *18*, 323.

(29) Cacace, M.G.; Landau, E.M.; Ramsden, J.J. *Q. Rev. Biophys.* **1997**, *30*, 241.

(30) López-León, T.; Jódar-Reyes, A.B.; Bastos-González, D.; Ortega-Vinuesa, J.L. *J. Phys. Chem. B* **2003**, *107*, 5696.

(31) López-León, T.; Jódar-Reyes, A.B.; Ortega-Vinuesa, J.L.; Bastos-González, D. "Hofmeister effects on the colloidal stability of an IgG-coated polystyrene latex", *J. Colloid Interface Sci.*, submitted.

(32) Lips, A.; Willis, E.J. *J. Chem. Soc. Faraday Trans.* **1971**, *67*, 2979.

(33) Manciu, M.; Ruckenstein, E. *Langmuir*, **2003**, *19*, 1114.

(34) Overbeek, J.Th.G. *Colloids Surf.* **1990**, *51*, 61.

(35) Hiemenz, P.C.; Rajagopalan, R. *Principles of Colloid and Surface Chemistry*, Marcel Dekker: New York, 1997.

(36) Fuchs, N.Z. *Phys.* **1934**, *89*, 736.

(37) Honing, E.P.; Roebersen, G.I.; Wiersema, P.H. *J. Colloid Interface Sci.* **1971**, *36*, 97.

(38) Qin, Y.; Fichthorn, K.A. *J. Chem. Phys.* **2003**, *119*, 9745.

(39) Henderson, D.; Trokhymchuk, A.D.; Wasan, D.T. J. Mol. Liq. 2004, 112, 21.

(40) Albella-Martín, J.M.; Martínez-Duart, J.M. *Física de Dieléctricos*, Marcombo: Barcelona, 1984.

INVERSIONS IN THE HOFMEISTER ORDER OBSERVED IN COLLOIDAL SYSTEMS

T. López-León*, J.L. Ortega-Vinuesa, and D. Bastos-González

Colloid and Fluid Physics Group, Department of Applied Physics, University of Granada, Av. Fuentenueva S/N, 18071 Granada , Spain

Abstract

The original Hofmeister series concerned the effectiveness of different salts to precipitate negatively charged proteins. Although the relative position of the species in the series has shown to be approximately universal, reversed Hofmeister sequences have been observed with many systems: an example can be found when working at pHs above and below the isoelectric point of any protein. Another example is shown in an earlier work, where it was reported how polystyrene cationic particles led to a Hofmeister sequence while anionic particles ordered the ions in the other way around. In this paper we show evidence of inversions in the Hofmeister series induced not only by changing the sign of the surface charge, but also by varying the hydrophobic/hydrophilic character of the surface keeping constant the surface charge sign. Four colloidal systems have been analyzed: a polystyrene latex, an IgG-coated polystyrene latex, silica particles and chitosane particles. They are systems with differing hydrophilic/hydrophobic character and with a pH-dependent sign of charge. Particularly, the effect of these two factors on the ion ranking has been analyzed by studying the colloidal stability of the systems. The typical inversions induced by modifying the sign of charge of the particle were observed; in addition, and more interestingly, the series observed with negatively charged hydrophobic systems turned into inverted series as the surface became more hydrophilic, at least for the most chaotropic anions. The correlation found between these inversions and restabilization processes at high salt concentrations evidenced the solvent structural nature of these phenomena. Interesting conclusions about the origin of these specific ionic effects have been drawn from a comparative analysis in which results concerning other colloidal systems have also been considered.

I. Introduction

Hofmeister effects or lyotropic sequences refer to the relative effectiveness of anions and cations on a wide range of phenomena (i.e. ionic ability to change the CMC value of micellar systems). In the original Hofmeister's work [1,2] ions were ordered according to their ability to stabilize protein solutions, providing the following rankings:

$$\underset{\text{(kosmotropic anions)}}{Citrate^{3-} > SO_4^{2-} > PO_4H^{2-} > F^- > CH_3COO^-} > \underset{\text{(chaotropic anions)}}{Cl^- > Br^- > I^- > NO_3^- > ClO_4^- > SCN^-}$$

$$\underset{\text{(chaotropic cations)}}{N(CH_3)_4^+ > NH_4^+ > Cs^+ > Rb^+ > K^+ > Na^+} > \underset{\text{(kosmotropic cations)}}{H^+ > Ca^{2+} > Mg^{2+}}$$

The origin of these series has been traditionally attributed to what Hofmeister called the *water withdrawing power* of ions, i.e., the capability of ions to interact with the water molecules so disturbing the hydrogen-bonded structure of bulk water. On this basis, ions have been classified in two main groups: i) those promoting water structure, called structure makers or kosmotropes, and ii) those disrupting such structure named structure-breakers or chaotropes. There are several mechanisms by means of which electrolytes can modify the water structure. First, ions induce via electrostatic interactions a dipolar orientation of the surrounding solvent molecules. In addition, they can induce via ion size and shape hydrogen bonding rearrangements. Finally, as it has been recently proposed, they can also cause solvent order via dispersion forces [3]. The influence exerted by ions on the neighboring water molecules has been experimentally determined by a number of techniques and methods ranging from entropies of solution to H-H correlation function measurements [4]. The Jones and Dole empiric equation has been commonly used to quantify the kosmotropic/chaotropic character of ions:

$$\frac{\eta}{\eta_w} = 1 + A\sqrt{c} + Bc$$

where η_w and η are respectively the viscosity of water and the saline solution, c is the salt concentration, and A and B are coefficients empirically determined. The coefficient A seems to be related with ion-ion electrostatic interactions and it is always positive. The coefficient B is interpreted as the

effect that salt has on the water in the vicinity of ions, and it is positive for kosmotropes and negative for chaotropes.

This scenario becomes more complicated when a third component (polymers, colloidal particle, gas bubbles, etc.) is involved in the solution. In this case, the surface-water, surface-ion, and surface-surface interactions may totally alter the picture emerging from the properties of ions in solution. The complexity of the problem makes that a complete understanding of the origin of the Hofmeister series is still missing [5]. The order of the lyotropic series has been shown to depend on the nature of the surface in solution. In fact, investigations performed with a wide variety of oxide surfaces indicate that ion specific effects give both direct and inverse Hofmeister sequences depending on the charge properties of the surface analyzed. Materials with high isoelectric point, such as alumina or rutile, are typified by "inverse series", whereas "direct series" are characteristic of inorganic materials with low isoelectric point, such as silica [6]. Similar results are observed with proteins below and above their corresponding isoelectric points (*iep*). For example, the relative effectiveness of different ions in crystallizing proteins follows a reversed Hofmeister sequence for pH $<$ *iep* and a direct Hofmeister sequence for pH $>$ *iep* [7,8]. Direct and inverse series recently observed with hydrophobic colloidal particles (polystyrene particles, PNIPAM microgel particles, etc.) have also shown to be related with the cationic or anionic character of the particle surface [9,10]. A quantitative explanation of the Hofmeister phenomena has not been provided until very recently [11]. Such explanation is due to Ninham and co-workers, who account for the Hofmeister effects considering the universal electrodynamic fluctuation forces or dispersion forces in the ion-surface interaction. The inclusion of the dispersion forces in the ion-surface potential energy modifies the ion distribution near the interface according to the Poisson-Boltzmann equation. With these modified ion profiles they calculate the double layer pressure at the middle plane between two surfaces (considered like planar plates) and find net positive and negative pressures when anions act like co-ion or counter-ion respectively.

Although generally cationic particles lead to Hofmeister sequences that are reversed when working with anionic surfaces, in the current work, we show experimental evidence of direct and inverse series which origin cannot be only attributed to the sign of charge of the surface. Specifically, it is reported how alterations in the lyotropic series become apparent when modifying the

hydrophobic/hydrophilic character of the surface keeping constant the surface charge sign.

For this investigation, several colloidal systems possessing different surface properties were employed. Essentially, the influence of the sign of charge and the hydrophobic/hydrophilic character of the surface on the Hofmeister ranking was examined. The analysis of the specific ion effects was mainly focused on the colloidal stability of the particles, although some electrophoretic mobility measurements have also been performed. Colloidal stability seems to be especially useful since it is dependent on changes in the particle surface potential, but it can also be affected by structural modifications in the solvent. In a typical aggregation process, an increase in the ionic strength entails the system destabilization. This is basically due to a reduction in the interparticle interaction potential responsible for the system stability, as explained by the well-known DLVO theory. However, when the system has a certain hydrophilic character it is possible to achieve a stable state on further salt addition. These restabilization processes at high salt concentrations have their origin in the so called "hydration forces", which are structural forces arising from the interaction of the particle surface and ions with water [12,13]. The existence and intensity of restabilization phenomena is a good indicative not only of the hydrophilic character of the surface, but also of the hydration shell formed around the dissolved ions.

This paper has been divided in two parts. In the first one, we shall present independently the results concerning the stability and, occasionally, the electrophoretic mobility of the different colloidal systems in the presence of several electrolytes. Five salts occupying different positions in the Hofmeister series were used in this study: i) NaCl, $NaNO_3$, NaSCN to contrast behaviors among anions, and ii) $NaNO_3$, NH_4NO_3, $Ca(NO_3)_2$ to compare cations. The analyzed systems were: an amphoteric polystyrene latex, a protein-coated polystyrene latex, chitosane particles, and silica particles. They are surfaces with different hydrophilic character and a pH-dependent sign of charge. The most relevant conclusions can be drawn from a comparative analysis of the results obtained with the different systems. Such analysis is presented in the second part of the paper in which, in addition, results concerning other surfaces reported in previous papers have also been considered in the discussion, in order to set a more general context. Hence, for the comparative analysis, different colloidal systems were chosen to run a broad spectrum from hydrophobic to hydrophilic character with positive and negative surfaces.

II. Materials and Methods

2.1. Salts and Solutions.

NaCl, $NaNO_3$, NaSCN, $Ca(NO_3)_2$, and NH_4NO_3 salts were of analytical grade and purchased from different firms: Merck, Sigma and Scharlau. Deionized Milli-Q water was used throughout. Non-buffered solutions were obtained by adding HCl or NaOH to water in the desired quantity to get pH 4 or pH 10, respectively. When necessary, intermediate pH values were obtained by mixing appropriately the above solutions. Only with the IgG-latex complex, which shows an enormous sensitivity to changes in pH, the medium acidity or basicity was controlled using different buffers (acetate at pH 4-5, phosphate at pH 6-7, borate at pH 8-10) at constant ionic strength (0.002 M).

2.2. Polystyrene, Silica, and Chitosan Particles.

Two polystyrene latex samples were synthesized, cleaned and characterized in our laboratory as described in references [9] and [14]. The amphoteric latex [14] showed an isoelectric point (i.e.p.) around 6, so that at any pH below 6 particles are positively charged, while they are negatively charged over this value. The surface groups come from the initiator molecules used in the synthesis: methacrylic acid (carboxyl groups) and N,N-diethylaminoethyl methacrylate (amine groups) in a 1:1 molar relation. Consequently, the surface charge density (σ_0) was not constant on pH. The σ_0 value at pH4 (at which the stability studies were performed) was equal to 33 ± 2 $\mu C/cm^2$. The mean diameter, obtained by transmission electron microscopy (TEM), was 210 ± 10 nm, having a polydispersity index (*PDI*) very close to unity (1.010), which gives an idea about its size homogeneity.

The sulfonate polystyrene latex was synthesized using styrene (St) as principal monomer and sodium styrenesulfonate (NaSS) as co-monomer [9]. The surface charge groups are strong acid groups (sulfonate) coming from both, the initiator molecules and the NaSS co-monomer. Thus its surface density charge remains constant in all the pH range considered (from 4 to 10) and it was equal to -9.6 ± 0.4 $\mu C/cm^2$. The average particle diameter obtained by TEM was 138 ± 7 nm and the *PDI* equal to 1.007 indicated a really monodisperse system.

Silica particles under the commercial name of Nyacol were kindly donated by EKA Nobel for Westbond Corporation. These particles were roughly spherical with an average diameter around 100 nm.

Nanoparticles of chitosan were produced following an ionic gelation process of tripolyphosphate (TPP) and chitosan. Nanoparticles were spontaneously obtained upon the addition of 1.2 mL (0.84 mg/mL w/v) of a TPP aqueous basic solution to 3 mL of the chitosan acidic solution (2 mg/mL w/v) under magnetic stirring at room temperature. Nanoparticles were concentrated by centrifugation at 16,000 g in a 10 µL glycerol bed, for 30 min. The supernatants were discarded and nanoparticles resuspended in water with 5 %trehalose for further freeze-dry (Labconco, Kansas City, MI, United States) under the following conditions: a primary drying step for 48 h at -30ºC, and a secondary drying step until the temperature gradually rose to +20ºC.

2.3. IgG Adsorption onto the Sulfonate Latex.

Purified polyclonal IgG from rabbit was purchased from Biokit S.A. (Spain). The isoelectric point, determined by isoelectric focusing, was in the 6.1 - 8.5 range. Dialysis against distilled water was carried out to remove precipitating salts. The protein concentration before and after adsorption were determined by UV spectrophotometry at 280 nm using a DU 7040 (Beckman) spectrophotometer. In order to cover as much as possible the polystyrene surface, the incubation was performed at pH 4, at which the adsorption isotherm versus pH had its maximum. This is reasonable since, at pH 4, both the electrostatic and hydrophobic interactions between the protein and the particle surface are favorable. The Hofmeister effects were studied in two situations where the sign of charge of the particles was opposite: pH 4 (positive surface) and pH 10 (negative surface). Adsorption was carried out at follows: Dialyzed IgG was added to 8 ml of aqueous solution at pH 4 containing latex particles with a total polystyrene area of 0.3 m^2. The IgG concentration was high enough to guarantee maximum coat (5.7 mg/m^2). Two sets of samples were then prepared. Incubation was carried out at 25ºC for 21 hours. After that, samples were spun at 25.000 × g for 30 minutes, and all the pellets of one set were redispersed and stored at pH 4, and the other set at pH 10.

2.4. Electrophoretic Mobility.

Electrophoretic mobility measurements at ionic strengths below 100 mM were performed with a Zeta-Sizer IV (Malvern Instruments). For measurements at high ionic strengths (up to 1 M) a ZetaPALS (Brookhaven Instruments), based on phase analysis light scattering, was used instead. Latex particles were diluted in the desired electrolyte solution and data were obtained from the average of six measurements. Standard deviation was always lower than 5%.

2.5. Colloidal Stability.

Latex and silica particle aggregation studies were carried out using a low-angle light-scattering technique. Scattering light intensity was observed at 10º for 120 s. The scattering cell was rectangular with a 2 mm path length. Equal volumes (1 ml) of salt and latex solutions were mixed and introduced into the cell by an automatic mixing device. The dispersions used for such coagulation experiments was diluted enough to minimize multiple scattering effects. The stability ratio (W), also called Fuch's factor, is a criterion broadly used to study the stability of colloidal systems. It is defined by

$$W = \frac{k_r}{k_s}$$

in which the rate constant "k_r" corresponds to rapid coagulation kinetics, and "k_s" is the rate constant for a slow coagulation regime. The scattered light intensity at low angles increases linearly with time during a coagulation process [15]. Thus, the coagulation rate constants can be easily obtained from the slopes of the scattered light intensity versus time curves. The critical coagulation concentration "*CCC*", defined as the minimum salt concentration needed to rapidly aggregate the colloidal system, can be easily obtained by plotting the logarithm of W versus the logarithm of the salt concentration and locating that point where log W reduces to zero. In a similar way, when restabilization occurs the critical stabilization concentration "*CSC*" can be calculated. *CSC* is the minimum electrolyte concentration at which restabilization starts.

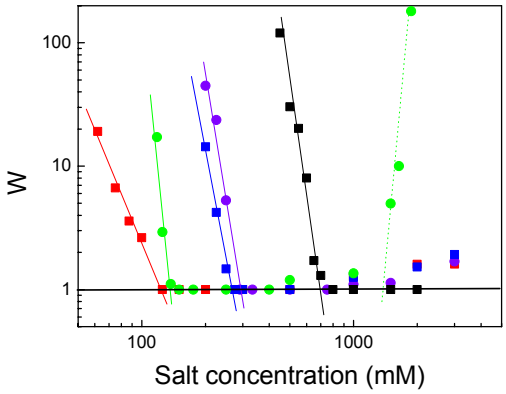

Figure 1. Stability ratio (Fuch's factor) versus electrolyte concentration for the amphoteric latex at pH 4: (■) NaSCN; (■) $NaNO_3$; (■) NaCl; (●) NH_4NO_3; (●) $Ca(NO_3)_2$.

Aggregation of chitosan particles was studied by static light scattering with a commercial light scattering set up, 4700C (Malvern Instruments), working with an argon laser of wavelength equal to $\lambda_0 = 488$ nm.

III. Results and Discussions

3.1. Amphoteric Polystyrene Latex.

De-stabilization and re-stabilization processes were first investigated with the amphoteric latex. Figure 1 shows, for all the electrolytes, the Fuch's factor W versus salt concentration at pH 4, where particles are positively charged. Important differences among the salts can be detected. If anions and cations are ordered separately according to their CCC values (see Table 1), the following ranking is obtained:

$$\text{(more stable) } Cl^- > NO_3^- > SCN^- \text{ (more unstable)}$$

$$\text{(more stable) } NH_4^+ > Na^+ > Ca^{2+} \text{ (more unstable)}$$

The previous sequences exactly coincide with that of Hofmeister series. It is possible to understand the stability results taking into account the Ninham's model [11], which states that dispersion forces acting between ions

Table 1. Critical coagulation concentrations (in mM units) obtained with our four systems using different electrolytes as aggregating agents. Isoelectric point (*iep*) data are also shown for the bare polystyrene latex system. For the chitosan case, the shown values (marked with an asterisk) are not exactly CCC data; they refer to the minimum salt concentration needed to completely disintegrate the chitosan-TPP particles.

	Polystyrene Particles		**IgG-coated Polysterene Particles**		**Silica Particles**	**Chitosan Particles**
	CCC (pH4)	*iep*	*CCC* (pH4)	*CCC* (pH10)	*CCC* (pH4)	*CCC** (pH4)
SCN^-	120	5.6	80	60	1500	500
$NO3^-$	270	5.9	90	130	3000	150
Cl^-	700	6.1	125	130	2000	250
NH_4^+	300	7.2	---	---	---	130
Na^+	270	5.9	90	130	3000	150
Ca^{2+}	135	7.5	85	5	90	100

and particle surface (and where the magnitude of these forces depend on the ionic polarizability), are not negligible at all. That is, the most polarizable anions tend to accumulate at the vicinity of the latex/water interface due to these attractive dispersion forces, screening more effectively the positive surface potential of the particles; consequently, the system becomes more unstable, whereas the less polarizable anions have an opposite tendency, enhancing the diffuse potential which improves the colloidal stability. As the polarizability of anions increases in this way $Cl^- < NO_3^- < SCN^-$, the Ninham's model perfectly can explain our CCC results. On the contrary, accumulation of cations at the interface increases the stability, while an exclusion of them produces destabilization at lower salt concentrations. Similar sequences as that observed with our latex were previously obtained working with other positive colloidal particles [9]. In this case, cation polarizability increases as $Na^+ < Ca^{2+} < NH_4^+$. Therefore, the Ninham's model would justify why the CCC obtained

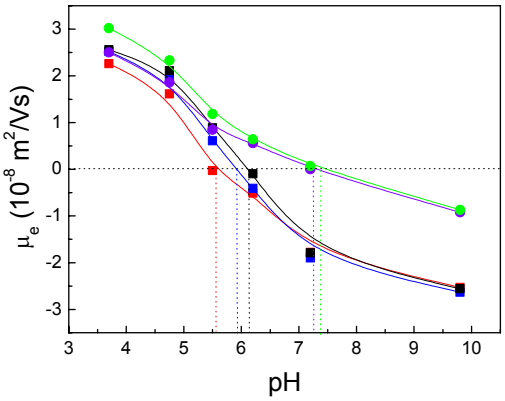

Figure 2. Electrophoretic mobility versus pH for the amphoteric latex at 30 mM ionic strength: (■) NaSCN; (■) $NaNO_3$; (■) NaCl; (●) NH_4NO_3; (●) $Ca(NO_3)_2$.

with NH_4^+ is higher than that of Na^+. However, it would fail to explain the calcium CCC. It is worthy to note that, in the case of Ca^{2+}, the stabilizing effect associated to its polarizability is strongly counteracts by the desestabilizing effect given by its double valence. This last factor seems to be dominant, and this is why calcium coagulates this system at relatively low concentration.

At high salt concentrations restabilization processes were only observed with $Ca(NO_3)_2$. This result is quite significant, since it contrasts with a previous study performed with different polystyrene particles, in which re-stabilization phenomena were not observed with any of the salts employed [9]. Nonetheless, it seems that the high surface charge density of this amphoteric latex makes particles hydrophilic enough to experiment repulsive hydration forces at high salt concentrations. Evidences of hydration forces on polystyrene particles have also been observed by other authors [16-19]. However, in all the cases the surfaces studied were anionic, and the existence of restabilization phenomena has been always ascribed to the presence of highly hydrated cations acting as counterions. In the current case, the surface of the polystyrene latex is positive, which evidences that cations, even acting as coions, can also induce restabilization. In an earlier work concerning latex particles coated with protein, we already concluded that cations acting as

coions are able to provoke restabilization [19], but it is the first time, to our knowledge, that this effect is observed on bare latex particles.

Electrophoretic mobility (μ_e) measurements were performed as a function of pH at a constant ionic strength (30 mM). If dispersion forces alters the ionic distribution around the particles, they also must modify the ζ-potencial, what in turn must change in the electrophoretic mobility curves. The μ_e-results are displayed in Figure 2. From these curves, clear differences among the ions can be distinguished, since very different isoelectric points are obtained. The *iep* values (see Table 1) show again the Hofmeister order for the anions ($Cl^- > NO_3^- > SCN^-$), although exceptions are found for the cations ($Na^+ > NH_4^+ > Ca^{2+}$). As a general feature, divalent ions located close to the particle surface modify the ζ-potential stronger than monovalent ions [20]; for that reason Ca^{2+} increases the ζ-potential in all the pH range and gives the highest *iep* value. Surprisingly ammonium resembles calcium effect above pH 5. This is due to a chemical reaction that takes place between the carboxylic groups of particles and the dissolved NH_4^+ ions that produces non-charged amide groups. This reaction is speeded up above the pK of the carboxyl groups (around pH 4-5), which yields to a surface charge cancellation, and thus, it is expected a electrophoretic mobility approaching to zero, as experimentally observed.

3.2. IgG-coated Polystyrene Particles.

The hydrophobic character of a sulfonate polystyrene latex was modified by adsorbing a moderate hydrophilic protein (IgG). It is should be noted that the stability patterns of these (hydrophobic) bare latex was already studied and reported in reference [19]. The adsorption of protein will allow us to analyze what happens, with regard to Hofmeister effects, when a hydrophobic surface is changed into a hydrophilic one. The stability experiments of the IgG-latex particles were studied in two situations where the sign of charge of the protein was opposite: at pH4 (positive surface) and pH10 (negative surface). Figures 3a and 3b show the stability curves at both pHs, respectively. The corresponding CCC values are also listed in Table 1. From these values, the ions can be ranked in the same sequence independently of the sign of charge of de surface, since at both pHs the obtained order is given by:

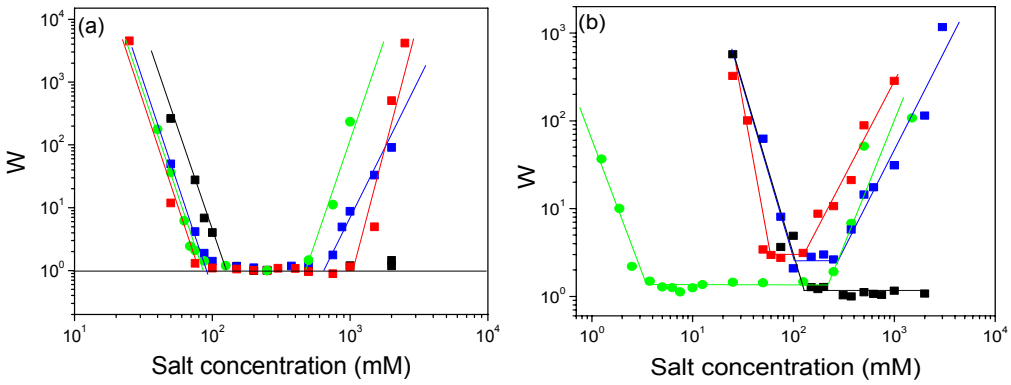

Figure 3. Stability ratio (Fuch's factor) versus electrolyte concentration for the IgG-latex complexes at **(a)** pH 4 and **(b)** pH 10: (■) NaSCN; (■) $NaNO_3$; (■) NaCl; (●) NH_4NO_3; (●) $Ca(NO_3)_2$.

$$\text{(more stable)}\ Cl^- \geq NO_3^- > SCN^-\ \text{(more unstable)}$$

$$\text{(more stable)}\qquad Na^+ > Ca^{2+}\qquad \text{(more unstable)}$$

It is should be noted that Cl^- destabilizes the system less strongly than NO_3^- at pH 4, whereas at pH 10 both ions behave similarly. Hence, there is here a system where the direct Hofmeister series typically observed in negative hydrophilic surfaces does not invert when the surface turns into a positive one. It is important to remark that with the bare sulfonate particles, the stability results revealed just the opposite order for the anions to that found with the negatively charged IgG-latex particles. From these observations it can be inferred that the inversions of the lyotropic series traditionally attributed to changes from positive to negative surfaces can be also observed if the hydrophobic/hydrophilic character of the surface is modified without varying its sign of charge. This feature can be explained considering the structural changes that surfaces and ions induce in the neighboring water. In terms of entropies, the "like seeks like" rule determines that chaotropic ions tend to accumulate near hydrophobic surfaces whereas they tend to be excluded from hydrophilic ones [6,21]. Thereby, it is possible that anions like SCN^- can less approximate to the particle surface as it becomes more hydrophilic. In the case of anionic systems, this fact would imply that the screening effect of counterions (cations) on the particle surface charge becomes much more

effective, and thus, the SCN^- has a high destabilizing effect. Nevertheless, this point will be discussed in more depth in the next section.

Restabilization processes at high salt concentrations were observed at both pHs, although these processes were especially intense at pH 10, where the restabilization conditions were observed at moderately low salt concentration (around 100 mM). Three salts were involved in these processes at both pHs: $Ca(NO_3)_2$, $NaNO_3$, and NaSCN. It is important to emphasize that, no restabilization was observed in the presence of NaCl. Therefore, it can be inferred that neither Na^+ nor Cl^- are in this case responsible for the restabilization phenomena. Hence, the resurgence of stabilizing forces must be attributed to the SCN^-, NO^-_3 and Ca^{2+} influence. The two former are strong chaotropes, whereas the latter possesses an intense kosmotropic character. The connection between Hofmeister effects and restabilization processes was also reported in the case of IgG-coated cationic polysterene particles [19]. Traditionally, restabilization phenomena have been thought to be controlled by kosmotropic cations (more hydrated cations) when acting as counterions [22-24]. However our results have revealed that i) cations can cause restabilization even acting as coions, and that ii), more surprisingly, chaotropic anions can also induce restabilization acting either as coions or counterions.

3.3. Silica Particles.

The following system analyzed was a silica suspension, which represents the most hydrophilic of the surfaces investigated (especially at very acid pH). These systems are characterized by isoelectric point values around 2-3, although they may vary depending on the type of silica employed (amorphous or quartz). This feature has been attributed to the dissociation equilibria of surface silanols and, presumably, their eventual neutralization at low pH. The silica dispersions present unusual properties regarding stability [25,26]. At the *iep*, where the electrostatic repulsions are negligible and one could expect rapid aggregation due to attractive van der Waals forces, the particles remain stable upon salt addition. Although there is still debate about the origin of this *anomalous* stability, it seems to be related with structural repulsive forces due to the hydration layer formed next to the silica surface or steric repulsions due to silicic acid hairs [27-30]. Isoelectric points and stability both can be specifically altered by the presence of electrolytes [31].

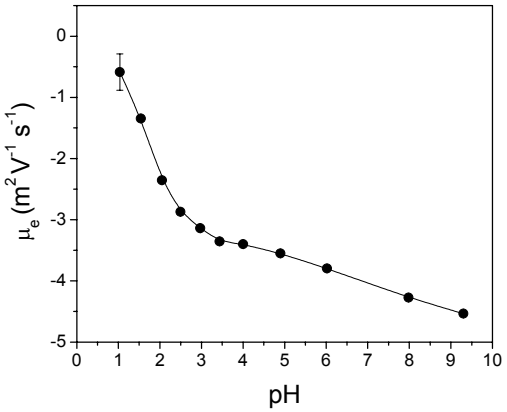

Figure 4. Electrophorectic mobility versus pH for the silica particles. Buffered solutions with low ionic strength (2mM) were employed at pH ⩾ 4.

The *iep* of our silica suspension was first determined. Figure 4 shows the electrophoretic mobility (μ_e) dependence with pH. In this curve, it can be observed a decrease in magnitude of the negative value of μ_e as the pH progressively diminishes more acid. However, no *iep* was detected within the analyzed pH range. This feature indicates that the silanols groups at silica particle surface must be highly dissociated. Colloidal stability in the presence of different electrolytes was investigated at three representative pH values: 1, 4 and 10.

At pH 1 silica particles were completely stable at any salt concentration value; even ionic strengths as high as 2 or 3 M were unable to destabilize the system. On the other hand, at pH 4 or 10, particles showed lower stability and aggregation processes could be observed. When comparing stability curves corresponding to pH 4 and pH 10, no meaningful differences were found. Thus, only data measured at pH 4 are displayed in Figure 5, which represents the evolution of the Fuch's factor (W) with the salt concentration for the different electrolytes. The most destabilizing effect was exerted by the $Ca(NO_3)_2$, because the calcium possesses double valence and acts like a counterion. Regarding monovalent electrolytes Cl^-, NO_3^-, and SCN^-, all them sharing the same cation (Na^+) remarkable differences were

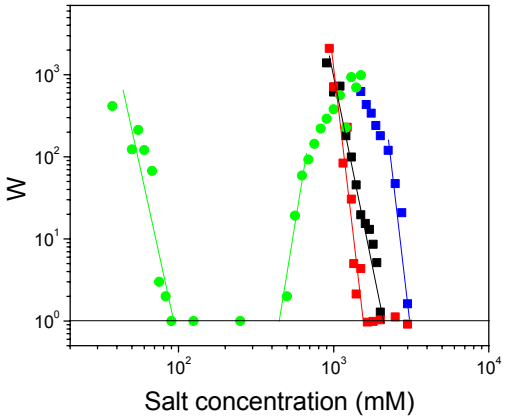

Figure 5. Stability ratio (Fuch's factor) versus electrolyte concentration for the silica particles at pH 4: (■) NaSCN; (■) $NaNO_3$; (■) NaCl; (●) $Ca(NO_3)_2$.

found. Although aggregation processes were observed with the three electrolytes, only in the case of SCN^- the fastest aggregation kinetic was reached (with a *CCC* value above 1M, as shown in Table 1). In these experiments NH_4NO_3 was not used. According to the electrolyte capability to induce aggregation, ions can be ranked as:

(more stable) $NO_3^- > Cl^- > SCN^-$ (more unstable)

(more stable) $Na^+ > Ca^{2+}$ (more unstable)

This order does not coincide with classical series, as two chaotropic ions (NO_3^- and SCN^-) are located at both sides of the chloride (a non-specific anion). Once more, the SCN^- displays the most destabilizing effect, contrary to what happens in hydrophobic anionic systems. It should be noted that the same series as that obtained with silica was also observed with another negative hydrophilic system (see the IgG-latex system at pH 10 in reference [19]). The fact of having obtained the same pattern with systems of such different nature but identical sign of charge and high surface hydrophilicity emphasizes the general character of the observed tendencies.

In this case, only the Ca^{2+} made the system restabilize at high salts concentrations. The high CCC values found for the 1:1 electrolytes entails a

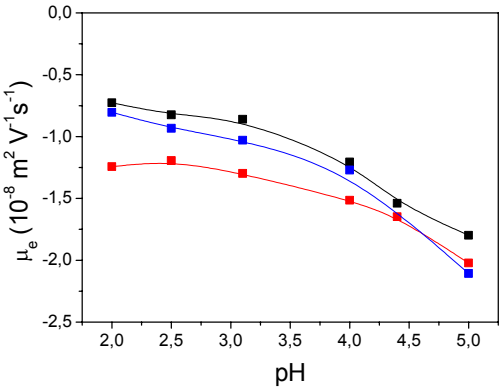

Figure 6. Electrophorectic mobility versus pH for the silica particles at 6 mM ionic: (■) NaSCN; (■) $NaNO_3$; (■) NaCl; (●) $Ca(NO_3)_2$.

hypothetic values of CSC extremely high, probably beyond their corresponding solubility constant. This is why restabilization with symmetrical electrolytes, although expected, was not detected.

Finally, the great stability of the system allowed us to perform the electrophoretic mobility experiments at a relative high ionic strength, 100 mM (with the limitations of the experimental devise). Figure 6 shows the μ_e-versus-pH curves corresponding to three different salts. Surprisingly, the destabilizing effect of SCN^- was not reflected in the μ_e measurements, as this anion gave higher μ_e values in spite of producing relatively low *CCC* data. This feature was also observed in IgG-latex complexes [19].

3.4. Chitosane Particles.

Chitosane particles were lastly employed as a representative hydrophilic positive surface. This system substantially differs from the other colloidal particles analyzed. While polystyrene and silica particles are hard-sphere systems, chitosan particles are pH-dependent microgels, and thus, they exhibit typical behaviors related with their soft nature (such as swelling processes). Because of the enormous interest that chitosane particles offer as drug delivery systems, the methods of synthesis concerning chitosane

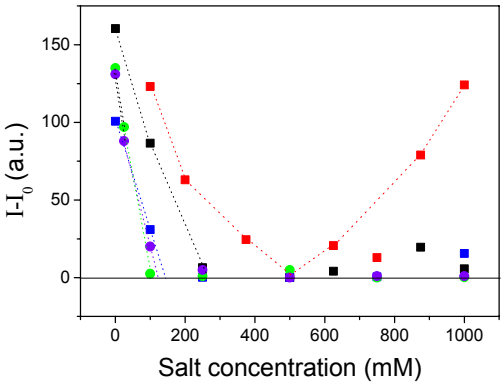

Figure 7. Normalized light intensity ($I-I_0$) scattered by a dispersion of chitosane particles at pH 4 as a function of salt concentration: (■) NaSCN; (■) $NaNO_3$; (■) NaCl; (●) NH_4NO_3; (●) $Ca(NO_3)_2$.

nanospheres have been focused to obtain systems with the physico-chemical characteristics appropriated to the this purpose. Particularly, the chitosan particles used in this study fall into the category of physical microgels: the crosslinking points between polymers are not given by covalent bonds, but they are established by means of electrostatic interactions between the positively charged chitosane chains and a polyanion employed as crosslinkers (tripolyphosphate, TPP). These electrostatically stabilized chitosane-TPP nanogels, although with a great practical interest, possessed a very labile character. It has been proved that the TPP-chitosan attractive interactions can be weaken upon increasing the ionic strength of the medium, so that at low/moderate salt concentrations the chitosane particles completely lose their integrity [32]. This happens before colloidal destabilization processes arise, what makes impossible to analyze the specific ion effects on *CCC* values. Nonetheless, it is possible to determine the salt concentration at which each elctrolyte provokes the total disintegration of the particles. This value would be indicative of the screening provoked by the ions on the attractive electrostatic interaction between the chitosane and the TPP polyanion. Figure 7 shows the normalized light intensity scattered at 90º by a dispersion of chitosan particles as a function of the salt concentration. The several curves refer to the different electrolytes. Since these particles have an amphoteric character (with *iep* about 7.5), measurements were made at pH 4 to assure the

positive charge of the particle surface. In all the cases, the increase in the ionic strength of the medium involves a diminution in the light intensity scattered by the colloidal dispersion, revealing the progressive erosion of the chitosan particles. At a certain critical salt concentration, the light intensity scattered by the dispersion coincides with that obtained with a blank (pure solvent) evidencing that particles are completely disaggregated. Such critical concentration allows us to rank the ions in the following series:

(more stable) $SCN^- > Cl^- > NO_3^-$ (more unstable)

(more stable) $Na^+ \geq NH_4^+ \geq Ca^{2+}$ (more unstable)

Cations behave approximately similar. It is should be noted that the accuracy of these experiments where chitosan particles disaggregate makes impossible to establish a reliable series for cations. Therefore, the values given for the chitosan system in Table 1 must be considered only as indicative. However, reliable differences are observed with the anions (see Fig. 7). When comparing the series for anions with those observed in other positive surfaces (see the results corresponding to the amphoteric latex or the IgG-latex complexes at pH 4), the SCN^- behaves as a stabilizing ion instead of being the most destabilizing one. This striking behavior (never observed previously with positive surfaces) is similar to that exhibited by the SCN^- with anionic systems, where the position of this chaotropic ion in the Hofmeister series is altered when increasing the hydrophilic character of the surface. In addition, this ion is also responsible for the re-stabilization phenomena observed with the chitosane particles at high salt concentrations. The interest of these results is double. Firstly, it has been found a positive surface in which alterations in the lyotropic series are evidenced. Furthermore, they reinforce the idea that a common mechanism related to the hydrophilic character of the surface must be responsible for these alterations.

3.5. Comparative Analysis.

The rationalization of the alterations that different surfaces provoke in the lyotropic series requires a comparative analysis of the experimental data. Indeed remarkable conclusions can be drawn from comparing the results presented in this paper with those reported in earlier works, where analogous studies with different other colloidal particles were accomplished [9,19]. In this investigation we are emphasizing the effect of the hydrophilic character of the

surface. Hence, for the comparative analysis, very different colloidal systems were selected to cover as much as possible from hydrophobic to hydrophilic characters. Positive and negative surfaces were analyzed separately. The negative surfaces considered, ordered from the most hydrophobic to the most hydrophilic one, are: a sulfonate polystyrene latex at pH 4 (ABJ2) [9], a carboxylic polystyrene latex at pH 4 and pH 10 (AMJ5) [9], an amidine polystyrene latex covered by IgG at pH 10 (IgG-AMJ10) [19], silica at pH 4 [present work], and a sulfonate polystyrene latex covered by IgG at pH 10 (IgG-ABJ2) [present work]. The three formers, although all them being polystyrene surfaces, present different surface charge densities

$$\sigma_{AMJ5\ at\ pH4} \simeq -6.1\mu C/cm^2, \sigma_{ABJ2} \simeq -9.6\mu C/cm^2, \sigma_{AMJ5\ at\ pH10} \simeq -20.5\mu C/cm^2$$

what slightly alters the hydrophobic character of the particles. Although *a priori* silica must be the most hydrophilic material, the systems have been ordered according to the efficiency of the restabilization processes exhibited by the particles at high salt concentrations which, as already discussed, is a good indicative of the hydrophilic nature of the system. Therefore, the negative systems are ordered as follows according to the hydrophobic/hydrophilic criteria:

AMJ5 (4) ≥ ABJ2 (4) ≥ AMJ5 (10) > IgG-AMJ10 (10) > silica (4) > IgG-ABJ2 (10)

(more hydrophobic) (more hydrophilic)

The number in brackets refers to the pH value where the stability experiments were carried out. Likewise, the positive surfaces can be ordered as follows: an amphoteric latex of low charge (AMJ10) [9], the amphoteric latex shown in this work (AJ25), the AMJ10 latex coated by IgG (IgG-AMJ10) [19], the IgG-ABJ2 system mentioned above, and chitosan, all them at pH 4:

AMJ10 (4) > AJ25 (4) > IgG-AMJ10 (4) > IgG-ABJ2 (4) > chitosan (4)

(more hydrophobic) (more hydrophilic)

With regard to chitosan, the restabilization phenomena could not be measured due to the labile nature of the particles. Nevertheless, this N-deacetylated version of chitin is certainly the most hydrophilic of the positive surfaces compared; (note that this polymer forms gels due to its high water solvency). The lyotropic series, obtained from the CCC values induced by the different electrolytes, are listed in Table 2 for the anionic systems, and Table 3 for the cationic ones.

Table 2. Positions of Hofmeister ions ordered according to the *CCC* values obtained with negatively charged systems differing in the hydrophobic/hydrophilic character. Changes with regard to usual negative hydrophobic surfaces have been highlighted in bold. The arrows serve to guide the eye.

	NEGATIVE SURFACE	Hofmeister order
more hydrophobic	AMJ5 (pH 4)	$Cl^- < NO_3^- < SCN^-$ $Ca^{2+} < NH_4^+ < Na^+$
	ABJ2 (pH 4)	$Cl^- < NO_3^- < SCN^-$ $Ca^{2+} < NH_4^+ < Na^+$
	AMJ5 (pH 10)	$Cl^- < SCN^- < NO_3^- < SCN^-$ $Ca^{2+} < NH_4^+ < Na^+$
	IgG-AMJ10 (pH 10)	$SCN^- \leq Cl^- < NO_3^- < SCN^-$ $Ca^{2+} < NH_4^+ < Na^+$
	Silica (pH 4)	$SCN^- \leq Cl^- < NO_3^- < SCN^-$ $Ca^{2+} < Na^+$
more hydrophilic	IgG-ABJ2 (pH 10)	$SCN^- < NO_3^- < Cl^- < NO_3^- < SCN^-$ $Ca^{2+} < Na^+$

Table 3. Positions of Hofmeister ions ordered according to the *CCC* values obtained with positively charged systems differing in the hydrophobic/hydrophilic character. Changes with regard to usual positive hydrophobic surfaces have been highlighted in bold. The arrows serve to guide the eye.

	POSITIVE SURFACE	Hofmeister order
more hydrophobic	**AMJ10 (pH 4)**	$SCN^- < NO_3^- < Cl^-$ $Ca^{2+} < Na^+ \leq NH_4^+$
	AJ25 (pH 4)	$SCN^- < NO_3^- < Cl^-$ $Ca^{2+} < Na^+ < NH_4^+$
	IgG-AMJ10 (pH 4)	$SCN^- < NO_3^- < Cl^-$ $Ca^{2+} < Na^+ < NH_4^+$
	IgG- ABJ2 (pH 4)	$SCN^- < NO_3^- < Cl^-$ $Ca^{2+} < Na^+$
more hydrophilic	**Chitosan (pH 4)**	$SCN^- < NO_3^- < Cl^- < \mathbf{SCN^-}$ $Ca^{2+} \leq \mathbf{NH_4^+} \leq Na^+ < NH_4^+$

Let first analyze cations. Calcium always produces the lower stability irrespective of the surface charge sign and the hydrophobic/hydrophilic character. In this case, the double valence of this ion dominate the stability of all the systems at moderate salt concentrations and possible modifications in the particle surface potential due to specific accumulation/exclusion mechanisms are masked by the electrostatic interaction. This is the reason why this ion shows the most destabilizing effect with all the surfaces studied. If only Na^+ and NH_4^+ ions are evaluated, it is worthy to highlight that their relative positions always invert when the sign of charge of the surface change from positive to negative, but changes in the surface hydrophobicity/hydrophilicity do not provoke any alteration; (only chitosan could invert this order, although, as mentioned above, this result would be questionable due to the low accuracy of the experimental method). These global results strengthen the belief that surfaces with opposite sign of charge lead to reversed lyotropic series. According to a model based on ion accumulation by dispersion forces, this can be readily explained considering that the adsorption of positive ions on negative surfaces involves a reduction in the surface potential (destabilizing) whereas it has an opposite effect in positive particles (stabilizing). A deeper analysis of the traditional order exhibited by both cations and anions in positive and negative colloidal particles can be found elsewhere [11]. Therefore, the cationic series can be basically explained invoking ion valences and ionic polaryzabilities.

On the contrary, the main observation regarding anions is that the sequence does depend on the hydrophobic/hydrophilic character of the surface (of course, keeping constant the sign of charge). Let first analyze the negative surfaces (Table 2). With hydrophobic polystyrene particles, where restabilization phenomena do not occur, a typical $Cl^- > NO_3^- > SCN^-$ series is obtained. However, the thiocyanate ranking becomes altered as the hydrophilic character of the surface increases and the restabilization phenomena arise. With an intermediate hydrophilic surface (see the AMJ5 (pH10) latex in Table 2), this ion changes only one position. However, for higher hydrophilic systems, the SCN^- moves two positions, reversing its original position in "hydrophobic" series in all cases, whereas the rest of the anions manifest the same order observed in negative hydrophobic surfaces. Only with the system displaying the strongest restabilizacion processes, i.e., the ABJ2-IgG (pH10), we find a completely reversed anion order, since the NO_3^- also changes its position. The order now obtained fully coincides with the usual Hofmeister

series obtained with protein solubility studies. Therefore, inversions by an increase in hydrophilicity and restabilization processes seem to be correlated. The anomalous behavior exhibited by SCN^-, and occasionally by NO_3^-, entails that these chaotropic anions, instead of stabilizing negative surfaces by an accumulation mechanism derived from dispersion forces, favours the particle aggregation, since they appears to be excluded from the hydrophilic interface as explained as follows. On the basis of a model explaining specific ion effects by means of the relative accumulation of anions and cations at surfaces, this result would imply that the concentration of SCN^- and NO_3^- anions (acting as co-ions) at the particle-water interface is lower than that of Na^+ cations (counter-ion). This would reduce particle surface potential and would enhance colloidal aggregation. The "negative adsorption" or exclusion (with respect to Na^+) of these anions cannot be explained just considering their respective ion excess polarizabilities. SCN^- and NO_3^- are the most polarizable ions analyzed, and thus, they should experiment stronger attractive dispersion forces. It should be noted that, taking into account the Ninham's model, in all cases the refraction index of the colloidal surface is higher than that of water, so dispersion forces felt by ions are always attractive [5,33]. Hence, electrodynamics fluctuation forces can explain the unaltered series observed with hydrophobic surfaces, but not those alterations manifested in more hydrophilic systems. The fact that the strong destabilizing effects of SCN^- and NO_3^- are associated to important restabilization phenomena, suggests that the mechanism responsible for the exclusion of this chaotropic ions has a steric origin associated to the water structure at the surface vicinity and around the ions. As a consequence, a consistent interpretation can be given considering the effect induced by ions and colloidal particles on water structure. The chaotropic/kosmotropic concept is readily extendible from ions to any type of surface. Hydrophobic colloidal particles behave as chaotropic systems, inasmuch as the surface-water interactions are weaker than the water-water interactions. Analogously, hydrophilic surfaces interact strongly with water and cause similar arrangement in the neighboring solvent molecules as kosmotropic ions. The general "like seeks like" rule was adapted by Bérubé and De Bruyn to the association of ions with surfaces within this context [34]. When a surface is immersed in a saline solution, the ions promoting similar water rearrangements than those induced by the surface on the adjacent water layers can be easily accommodated at the interface. Conversely, ions causing dissimilar solvent environment tend to be excluded from the interfacial zone

[6,34-37]. These entropically controlled processes would explain why the adsorption of chaotropic ions is favored in hydrophobic surfaces and precluded in hydrophilic ones. The Jones-Dole viscosity B coefficients enable to quantify these phenomena. The B-coefficients corresponding to the anions are:

$$B(SCN^-) = \text{-}0.103,\ B(NO_3^-) = \text{-}0.043,\ B(Cl^-) = 0.007$$

From these values it can be inferred that the SCN^- influences the water structure much more intensely than the rest of the anions considered. This is why effects related with structural incompatibilities were clearly observed with this ion, and not only for negative surfaces, but also for positive ones (see the chitosan case in Table 3). In addition, given the negative sign of the B-coefficient, they become more evident on increasing the hydrophilic surface character of the particles. In the case of NO_3^- they are more attenuated, and hence, more hydrophilic surfaces are necessary to observe any exclusion phenomenon.

Restabilization phenomena can be understood in these terms. At high salt concentrations, the electric double-layer is completely compressed and all the electrolytes are confined at short distances from the surface. In the proximities of a hydrophilic interface, water molecules are orientated to maximize the number of surface-water bonds. Such water organization must be compatible with the highly directional order induced by chaotropic ions, what eventually results in an ice-like rigid structure of water molecules and ions firmly attached to the surface. In the case of kosmotropic ions, such as calcium, both surface and ion have strong tendency to be hydrated, and thus, a dense structure of water molecules and ions is formed instead. Whichever the case, this structure means a steric barrier when two particles approach which is responsible for the system stability at high salt concentrations. This argument justifies the existence of restabilization phenomena regardless the sign of charge of ions and particles, and generalize the traditional concept of colloidal restabilization.

Finally, the lyotropic series displayed by anions in positive surfaces (Table 3) can be easily rationalized according to the previous discussion. It is important to note that in this case anions act as counterions, and thus, not only the dispersion forces but also the electrostatic interactions between particles and anions favour the approximation of these species toward the surface. This feature makes that, with positive surfaces, alterations in the

lyotropic series only were observed with the most hydrophilicic surface (chitosan) in the presence of the most chaotropic anion (SCN^-). Taking into account that this anion is supposed to be surrounded by a water shell of significant rigidity and size [38,39], a strong structured water layer at the particle surface is also needed to overcome the attractive SCN^--surface interactions promoted by both dispersion and electrostatic forces. Only highly hydrophilic surfaces, as that of chitosan, are capable to create such structured water layer that origins a steric repulsion. Otherwise, direct Hofmeister series were obtained. The unusual stabilizing properties displayed by the SCN^- when added to the chitosane dispersions evidence once again the existence of exclusion mechanisms driven by entropic forces, as previously described. This hypothesis is reinforced with the restabilization processes observed not only with chitosa, but also with the latex-IgG complexes in the presence of SCN^-, (and even NO_3^-, although only with the ABJ2-IgG complex). With these less hydrophilic systems (IgG- AMJ10 and IgG-ABJ2), it appears as though high salt concentrations are necessary to observe effects related with the ion influence on water structure.

Acknowledgements

Financial support from the "Comisión Interministerial de Ciencia y Tecnología" Project MAT2003-01257 (European FEDER support included) and from the "Consejería de Innovación, Ciencia y Tecnología de la Junta de Andalucía" Project FQM 392 is gratefully acknowledged.We would like to thanks to Juan José Valle Delgado for the synthesis and characterization of the amphoteric AJ25 latex.

References

[1] Lewith S. Arch. Exp. Pathol. Pharmakol **1888**, 24, 1.

[2] Hofmeister F. Arch. Exp. Pathol. Pharmakol **1888**, 24, 247.

[3] Ahn-Ercan, G.; Krienke, H.; Kunz W. Current Opinion in Colloid Interface Sci **2004**, 9, 92.

[4] Cacace, M. G.; Landau E. M.; Ramsden, J. J. Quarterly Rev. Biophys. **1997**, 30, 241.

[5] Kunz, W.; Lo Nostro P.; Ninham, B. W. Current Opinion in Colloid Interface Sci. **2004**, 9, 1.

[6] Lyklema, J. Molecular Physics **2002**, 100, 3177.

[7] Riés-Kautt, M. M.; Ducruix, A. F. J. Biol. Chem. **1989**, 264, 745.

[8] Carbonnaux, C.; Riés-Kautt, M. M.; Ducruix, A. F Protein Sci. **1995**, 5, 2123.

[9] López-León, T.; Jódar-Reyes, A. B.; Bastos-González, D.; Ortega-Vinuesa, J. L. J. Phys. Chem. B **2003**, 107, 5696.

[10] López-León, T.; Elaïssari, A.; Ortega-Vinuesa, J.L.; Bastos-González, D. ChemPhysChem **2006**, accepted.

[11] Boström, M.; Tavares, F. W.; Finet S.; Skouri-Panet, F.; Tardieu A.; Ninham B.W. Biophys. Chem. **2005**, 117, 217.

[12] Israelachvili J. Intermolecular & Surface Forces (second ed., Academia Press, London, **1992**).

[13] Molina-Bolívar, J. A.; Galisteo-González, F.; Hidalgo-Álvarez, R.; Colloids Surf. B **2001**, 21, 125.

[14] Valle-Delgado, J. J.; Molina-Bolivar, J. A.; Galisteo-González, F.; Gálvez-Ruiz M. J. Colloid Polym Sci **2003**, 281, 708.

[15] Lips, A.; Smart, C.; Willis, E.; Trans. Faraday Soc. **1971**, 67, 2979.

[16] Healy, T. W.; Homola, A.; James, Hunter, R. J. Farday Discuss. **1978**, 65, 156.

[17] Elimelech, M. J. Chm. Soc. Farday Trans. **1990**, 86, 1623.

[18] Delgado-Calvo-Flores, J. M.; Peula-García, J. M.; Martínez-García, J.; Callejas-Fernández, J. Colloid Interface Sci. **1997**, 189, 58.

[19] López-León, T.; Jódar-Reyes, A. B.; Ortega-Vinuesa, J.; Bastos-González, D. L. J. Colloid. Interface Sci. **2005**, 284, 139.

[20] Hunter, R. J. in "Foundations of Colloid Science", **1987**, vol.1 Oxford University Press, Nueva York.

[21] Wiggins, P. M. Physica A **1997**, 238, 113.

[22] Molina-Bolívar, J. A.; Galisteo-González, F.; Hidalgo-Álvarez, R. Phys. Rev. E **1997**, 55, 4522.

[23] Molina-Bolívar, J. A.; Galisteo-González, F.; Hidalgo-Álvarez, R. J. Colloid Interface Sci. **1998**, 206, 518.

[24] J.A. Molina-Bolívar, F. Galisteo-González, R. Hidalgo-Álvarez, Colloids Surf. B **1999**, 14, 3.

[25] Iler R. K. The Chemistry of Silica; Wiley: New Cork, 1979.

[26] Healy, T. W. In The Colloid Chemistry of Silica ACS Advances in Chemistry Series No. 234; Bergna, H. E. Ed.; American Chemical Society: Washington, 1994.

[27] Pashley, R.M. J. Colloid Interface Sci. **1981**, 83, 531.

[28] Pashley, R.M. Adv. Colloid Interface Sci. **1982**, 16, 57.

[29] H.K. Christenson J. Dispers. Sci. Technol. **1988**, 9, 171.

[30] Israelachvili, J. N. ; Wennerstrom, H. Nature **1996**, 379, 219.

[31] G.V. Franks, J.Colloid Interface Sci. 249 (2002) 44.

[32] López-León, T.; Carvalho, E. L. S.; Seijo, B.; Ortega-Vinuesa J. L.; Bastos-Gonzalez J Colloid Interface Sci **2005**, 283, 344.

[33] Boström, M.; Williams, D. R. M.; Ninham, B. Langmuir **2001**, 17, 4475.

[34] Bérubé, Y. G.; De Bruyn, P. L. J. Colloid Interface Sci. **1968**, 28, 92.

[35] Dumont, F. ; Warlus, J. ; Watillon, A. J. Colloid Interface Sci. **1990**, 138, 543.

[36] Dumont, F.; Contreras, S.; Díaz-Alonso, M. An. Quim. **1995**, 91,635.

[37] Franks, G. V.; Johnson, S. B.; Scales, P. J.; Boger, D. V.; Healy, T. W. Langmuir **1999**, 15, 4411.

[38] López-León, T.; Bastos-González, D.; López-López. J.M.; Schmitt, A.; Odriozola, G.; Ortega-Vinuesa, J.L. "Hofmeister effects in colloidal suspensions: experimental evidences in aggregation kinetics" J. Phys. Chem. B **2006**, submitted.

[39] López-León, T.; Santander-Ortega, M.J.; Gea-Jódar, P.; Bastos-González, D.; Ortega-Vinuesa, J.L. "Specific ionic effects on aggregation kinetics and

fractal dimensions of polystyrene nanoparticles" Langmuir **2006**, submitted. Matter **2000**, 12, 443.

SPECIFIC IONIC EFFECTS ON AGGREGATION KINETICS AND FRACTAL DIMENSIONS OF POLYSTYRENE NANOPARTICLES

T. López-León, M.J. Santander-Ortega, P.M. Gea-Jódar, D. Bastos-González and J.L. Ortega-Vinuesa

Colloid and Fluid Physics Group, Department of Applied Physics, University of Granada, Av. Fuentenueva S/N, 18071 Granada , Spain

Abstract

The aggregation of a polystyrene latex dissolved in saline solutions containing different electrolytes (Na_2SO_4, NaCl, $NaNO_3$, NaSCN, $Ca(NO_3)_2$ and NH_4NO_3) has been studied using static light scattering. Different aggregation parameters have been evaluated, namely, i) the critical coagulation concentration (*ccc*), ii) the rate constant for rapid aggregation regimes ($k_{R\text{-}r}$), and iii) the fractal dimension (d_f) of those aggregates generated at salt concentrations above the *ccc*. All these results order the anions according to classical Hofmeister series, albeit some exceptions are found for the cations. The microscopic origin of Hofmeister effects is still controversial. Although they have usually been attributed to alterations in the water structure around the ions, Hofmeister effects have also been recently explained by considering the role played by high frequency dispersion forces in the ionic distribution at interfaces. In this paper, the experimental results can be perfectly explained when both microscopic mechanisms (water restructuration and dispersion forces) are taken into account. This suggests that the ionic specificity subjacent to the Hofmeister effects has a dual origin where both mechanisms simultaneously participate.

I. Introduction

It is well known that the specific nature of different ions (even with the same valence) can have a great influence on the forces acting between molecules or colloidal surfaces.[1,2] These ion-specific effects are related to the characteristic behavior of ions in solution, which has given rise to the Hofmeister lyotropic sequences. From these sequences, ions can be divided in two broad classes according to their ability to structure the neighboring water molecules:[3,4] structure-maker or kosmotropic ions and structure-breaker or chaotropic ions. However, several fundamental studies have demonstrated that these specific effects are not only associated to the structure of water around the electrolytes but also they are related to the high frequency dispersion forces that act on the ions.[5-9] In fact, the usual ionic distribution at the proximities of any charged interface predicted by the Poisson-Boltzmann equation is altered when the van der Waals dispersion forces are considered.[10] The importance of the dispersion forces significantly augments in systems where the ionic strength is high (i.e biological systems); in this case, electrostatics is strongly screened and ion-surface dispersion forces can be expected to dominate. Since dispersion forces depend on the ion polarizability, this parameter becomes crucial to explain the ion distribution next to a interface, which at the end governs the interaction between surfaces and molecules in colloidal suspensions. Nevertheless, and despite all the efforts made in the scientific community to fully explain the Hofmeister effects, its origin is not totally understood yet. Water structure and dispersion forces appear to be the cornerstones of these phenomena; this microscopic duality turns the Hofmeister problem into a complicated puzzle to resolve.

Intercolloidal forces have been traditionally studied in an indirect way by analyzing aggregation kinetics and evaluating the structure of the formed aggregates, both factors depending on the interaction potential between two approaching particles.[11] This particle clustering may occur by a non-equilibrium process (irreversible aggregation) or by an equilibrium cluster formation (reversible aggregation). The type of kinetics will depend on the existence or absence of repulsive interaction barriers. It is now generally accepted that there are two limiting regimes of aggregation: (i) diffusion-limited cluster aggregation (DLCA) in which there is no repulsive barrier and every collision between particles results in the formation of a permanent contact, and (ii) reaction-limited cluster aggregation (RLCA), in which

barriers exist and only a small fraction of particle collisions leads to the formation of a contact. A fast aggregation process, in which the particles or clusters stick to each other upon contact as a result of diffusion, results in a loose, ramified structure with a fractal dimension of 1.78, in conformity with the predictions of the DLCA model.[12,13] On the other hand, a slow aggregation process, in which more than one collision is required to form permanent contacts, yields a more compact structure with a fractal dimension of 2.1, as predicted by the RLCA model.[12,13] In addition, it is possible to find systems in which a rapid aggregation process gives initially a low fractal dimension (i.e. 1.75) that grows up with time: if particles remain in minima of little depth, aggregates can restructure after certain time to more compact clusters with a higher fractal dimensions of 2.1[14,15] or 2.4.[16] In this case, the aggregation can be considered partially reversible, as clusters can loosen and re-form repeatedly after the first collision.

In this paper, aggregation kinetics and fractal dimensions of polystyrene (PS) latex particles have been analyzed using different salts as coagulating agents. The aim was investigating how the Hofmeister effects can modulate the interparticle interaction and show that these modifications are connected with both dispersion forces and water structure around ions. Na_2SO_4, NaCl, $NaNO_3$ and NaSCN salts were chosen to evaluate the specific effect of the anions, which differ in kosmotropic/chaotropic character. On the other hand, the specific effects exerted by different cations were studied by comparing the results obtained with $Ca(NO_3)_2$ $NaNO_3$ and NH_4NO_3. The effects of different electrolytes on the fractal aggregation of polystyrene latexes have already been studied by Zhu and Napper,[17] although in this case the PS particles were completely coated by a poly(N-isopropylacrilamide) (PNIPAM) shell. Therefore, the results reflected the peculiar solvency properties of this last polymer but they did not show any dependence on the PS characteristics. The particles showed a decrease in the thickness of the steric PNIPAM layers as a consequence of the reduction in the polymer solvency upon salt addition. This feature led to differences in fractal dimensions at long time. Results were ascribed to the kosmotropic/chaotropic properties of the added ions, that is, the results showed macroscopically the microscopic competition for the water molecules between the PNIPAM backbone and the solved ions.[18] However, only the water-structure origin of the Hofmeister effects was detected, and no mention to the accumulation / exclusion of ions due to dispersion forces was done by these authors. Nevertheless, the microscopic duality of the Hofmeister

effects appears to be clearer and clearer in a variety of systems at the present. As an example, López-León et al. have recently reported in different works[19-21] irrefutable data of the two mechanisms underlying the specific ionic effects by using hydrophobic, hydrophilic and anfoteric materials. The present paper shows new experimental data on intercolloidal interactions between bare PS particles that can help to gain more insight in the microscopic dual origin of the Hofmeister effects.

II. Materials and Methods

2.1. Regents and PS particles.

Salts (Na_2SO_4, NaCl, $NaNO_3$, NaSCN, $Ca(NO_3)_2$ and NH_4NO_3) were of analytical grade and purchased from different firms: Merck, Sigma and Scharlau. Polystyrene particles were purchased from Ikerlat S.A. (Spain). They were cleaned by repeated centrifugation/redispersation cycles. The surface charge came from strong acid groups (sulfonate) given by the initiator molecules. The mean diameter was 85 nm and the corresponding polydispersity index was 1.008. All the experiments were carried out in pH 5 buffered solutions, using acetate/acetic acid at a very low ionic strength (1 mM). Water was of Milli-Q quality.

2.2. Static Light Scattering Measurements.

Two different sets of static light experiments were performed. The first one was designed to calculate coagulation rate constants and critical coagulation concentrations (*ccc*), while the second set aimed to obtain quantitative structural information, such as the fractal dimension d_f of the aggregates.

In the first set, the aggregation rate constant of the latex particles immersed in different saline media was measured using a low-angle light scattering technique developed by Lips and Willis.[22] With this technique, the total light intensity scattered at an angle θ by a dispersion of identical primary particles with a time varying distribution of sizes depends on time according to the expression:

$$\frac{I(t,\theta)}{I(0,\theta)} = 1 + 2k_R n_0 t \tag{1}$$

where $I(0,\theta)$ is the initial intensity of light scattered at the selected angle, n_0 is the number of primary particles, and k_R is the rate constant. These aggregation experiments were carried out in an apparatus working with a He/Ne laser, using a rectangular scattering cell with a 2 mm path length, and measuring the light scattered at an angle equal to 5º. Equal volumes (1 mL) of salt and latex solutions were mixed and introduced into the cell by an automatic mixing device. The initial particle concentration was set at $n_0 = 6.9\ 10^{11}$ mL^{-1}, and the agglutination processes were analyzed for 120 s. According to eq. 1, the scattered light intensity $I(t,\theta)$ increases linearly with time, and thus, an absolute coagulation rate can be obtained from the slope if the number of primary particles is known. However, the linearity in the aggregation kinetics was rapidly lost when aggregates of large size were formed. Figure 1 shows a representative experiment in which different salt concentrations provoked different aggregation kinetics.

On the other hand, these experiments also allowed us to obtain the stability ratio W, (often called Fuchs factor), which can be calculated from the following expression:

$$W = \frac{k_{R-r}}{k_{R-s}} \tag{2}$$

where the rate constant "$k_{R\text{-}r}$" corresponds to rapid coagulation kinetics, and "$k_{R\text{-}s}$" is the rate constant for a slow coagulation regime. The ratio of both constants is equal to that derived from the ratio of the initial slopes in our coagulation experiments. The critical coagulation concentration (*ccc*) can be easily determined by plotting the logarithm of W versus the logarithm of the salt concentration and locating that point where *log* W reduces to zero.

In the second set, the angular dependence of the scattered light intensity $I(q)$ was measured, where q is the scattering wave vector. This wave vector is related to the scattering angle θ by the following expression: $q = (4\pi n/\lambda)\ \sin(\theta/2)$, where n is the refractive index of the solvent and λ the wavelength of light in the vacuum. If multiple scattering is negligible and the intensity scattered by a cluster of mass M is expressed as $I_M(q)$, the total intensity scattered by a distribution $N(M)$ of clusters of mass M is given by

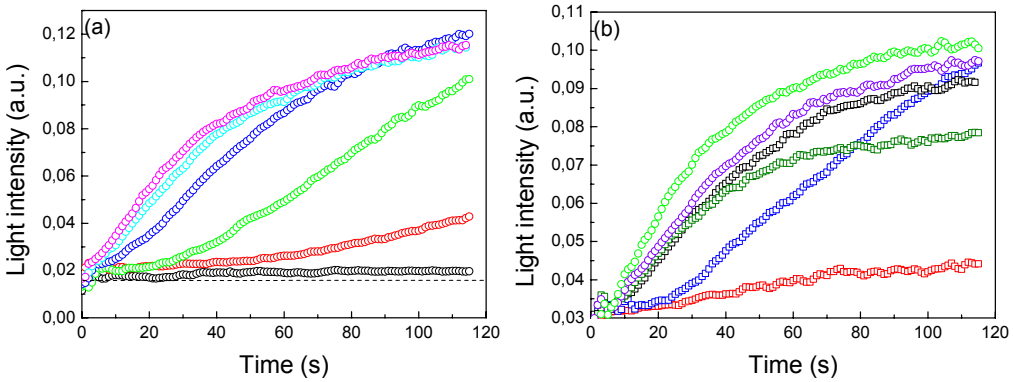

Figure 1. Aggregation kinetics of the PS particles detected by means of changes in the intensity of light scattered at 5º. **(a)** Using $Ca(NO_3)_2$ as aggregating salt: (○) 20 mM, (○) 30 mM, (○) 37 mM, (○) 50 mM, (○) 75 mM and (○) 100 mM. **(b)** Salt concentration was set at 600 mM. (□) NaSCN, (□) $NaNO_3$, (□) NaCl, (□) Na_2SO_4, (○) NH_4NO_3 and (○)$Ca(NO_3)_2$.

$$I(q) = \sum_{M} N(M)\, I_M(q) \tag{3}$$

The expression for $I_M(q)$ depends on the qR_g value, where R_g is the radius of gyration of an aggregate. $I_M(q)$ can be expressed as $M^2S(qR_g)$, where $S(qR_g)$, called structure factor, has a complicated form that depends on the type of aggregation kinetics.[23,24] The total intensity is then given by:

$$I(q) \propto \sum_{M} N(M)\, M^2\, S(qR_g) \tag{4}$$

It can be shown that for $qR_g >> 1$ the structure factor satisfies the following expression:[25]

$$S(qR_g) = \left(qR_g\right)^{-d_f} \tag{5}$$

where d_f is the fractal dimension of the aggregates. As the measured intensity $I(q)$ is proportional to the structure factor $S(qR_g)$, there exists an asymptotic behaviour:[26,27]

$$I(q) \propto S(qR_g) \propto q^{-d_f} \tag{6}$$

in the $R_g^{-1} < 1 < R_o^{-1}$ range, where R_o is the radius of a single particle. Thus, the fractal dimension of the aggregates can be obtained by plotting $I(q)$ versus q on a double-logarithmic scale. The negative slope in the region where the power-law is satisfied gives d_f.

The measurements of the scattered light intensity as a function of the scattering angle θ (or scattering wave vector q) were carried out with a He/Ne laser operating at a 632.8 nm wavelength. All the experiments were performed at constant temperature (25ºC) in a thermostatic optical cell. To ensure the validity of eq. 4, the $\{30° < \theta < 85°\}$ angular range was chosen to extract the d_f data. The intensity measurements were collected from different angular runs (each of one lasted 15 min), which were continuously repeated during a few hours until an asymptotic time independent behaviour was achieved. Agglutination was initiated by rapid mixing 1 mL of a stable latex dispersion buffered at pH 5 and 1 mL of a saline solution with a constant ionic strength equal to 3 M (that is, a concentration of 3 M for the 1:1 electrolytes and a 1 M concentration for the 2:1 salts). Therefore, the final ionic strength in the aggregating medium was 1500 mM, which corresponded to a saline concentration above the *ccc* of the samples (as will be shown afterwards).

III. Results and Discussions

Figure 1a shows a typical aggregation experiment in which the intensity of scattered light increases as a consequence of particle coagulation. The increase in the aggregation kinetics with the increment of the salt concentration is a logical result predicted by the DLVO theory. The presence of electrolytes in the medium screens the electrical interactions that govern the repulsive DLVO term, which leads to a reduction in the height of the interaction potential barrier.[3] If this barrier disappears, every collision between particles will result in the formation of a contact, and the aggregation kinetics will speed up. The contact will be permanent or not depending on the depth of the energy minimum at which the particles remain stuck.[28] This common behavior was proved not to be affected by ion specificity, and thus, only curves corresponding to one salt are shown in Fig. 1a; the rest of the electrolytes gave the same pattern. Ion specific effects, however, were clearly manifested when the PS particles were induced to collapse under identical salt concentrations. Figure 1b shows the aggregation kinetics using different

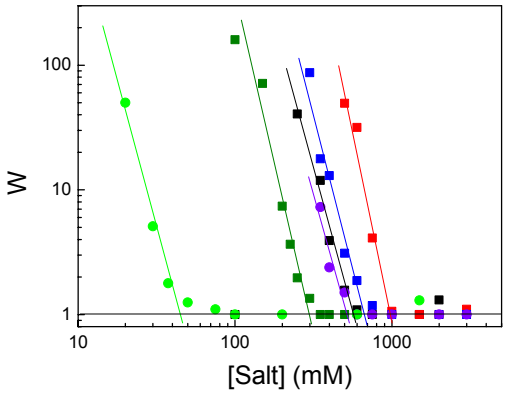

Figure 2. Stability ratio (Fuchs factor) versus electrolyte concentration: (■) NaSCN, (■) $NaNO_3$, (■) NaCl, (■) Na_2SO_4, (●) NH_4NO_3 and (●) $Ca(NO_3)_2$. Straight lines are only used to guide the eye toward the corresponding *ccc* value.

electrolytes at the same saline concentration (600 mM). If the rate constants (directly related to the initial slope of the curves) are considered, a typical Hofmeister series is found for the anions, that is, they are ordered as follows: $SO_4^{2-} > Cl^- > NO_3^- > SCN^-$: the rapidest coagulation regime is given by the sulphate while the thiocyanate produces the lowest aggregation kinetics. Cations, however, are ordered according to the following sequence: $Ca^{2+} > NH_4^+ > Na^+$, which does not exactly coincide with the usual Hofmeister series (which would be $Ca^{2+} > Na^+ > NH_4^+$).

Figure 2 shows the stability ratio as a function of the salt concentration. This figure allows us to estimate the *ccc*, that is, the lowest salt concentration needed to aggregate the system at maximum velocity. The so obtained *ccc* values are shown in Table 1. These *ccc* values also order our ions in the same sequences as those given by the experiment shown in Fig. 1b. That is, anions are placed in the following ranking $SO_4^{2-} > Cl^- > NO_3^- > SCN^-$, while the cations are situated as follows: $Ca^{2+} > NH_4^+ > Na^+$. This means that one needs a 1000 mM concentration of NaSCN to get the rapidest aggregation kinetics while this rapid aggregation regime is obtained with only 575 mM of NaCl. The DLVO theory is unable to explain why different salts with identical charge characteristics (i.e. the 1:1 electrolytes) produce so different aggregation

Table 1. Critical coagulation concentrations, constante rates and fractal dimensions associated to the different ions.

Hofmeister ion	*ccc* (mM)	k_R (mL/s) x10^{14}	d_f
SCN^-	1000	3.08	1.97
NO_3^-	675	3.75	1.85
Cl^-	575	3.88	1.81
SO_4^{2-}	300	3.89	1.71
NH_4^+	525	4.08	1.77
Na^+	675	3.75	1.85
Ca^{2+}	50	4.19	1.74

kinetics and *ccc* values. However, these phenomena can be understood when dispersion forces acting between the PS surface and the ions are taken into account. A quantitative (or at least semiquantitative) explanation based on these forces is presented below.

Inclusion of the dispersion potentials of the ions has a very important influence on ion distribution, self-consistent potential, and on the double-layer force. Hence, these dispersion interactions significantly alter the forces appearing when two charged surfaces come close together being responsible, as will be shown afterwards, for the *ccc* differences found in our experiments (with ions of the same valence). The dispersion force contribution to the double electric layer ionic distribution can be estimated according to the Ninham's model. It should be noticed that this model is built under certain approximations that might be questioned, although the simplicity of this treatment helps to gain much clarity. For example, water is assumed to be a dielectric continuum. Correlations between ions by electric, dispersion or hard-sphere interactions are also neglected. In addition, we will consider that the ions are much smaller than our polystyrene particles, and therefore, ion distributions will be estimated at a planar surface. If we take an x axis perpendicular to the surface with its origin ($x = 0$) at the surface so that the region $x > 0$ corresponds to the liquid phase, then dispersion potential between an ion and a surface is approximately:[6]

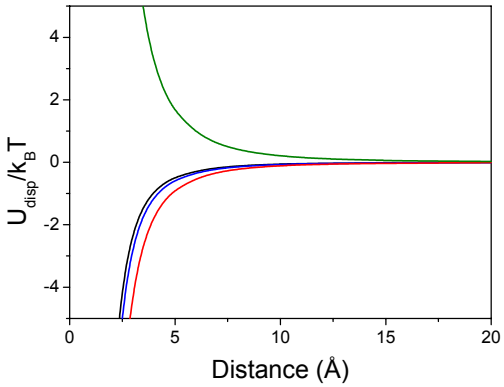

Figure 3. Dispersion potential as a function of distance to the polystyrene-water interface: NaSCN (red line), $NaNO_3$ (blue line), NaCl (black line), Na_2SO_4 (green line).

$$U_{disp}(x) \approx \frac{\left(n_w^2 - n_p^2\right)}{8x^3}\alpha^*(0)h\nu_i \tag{7}$$

Here, $n_w = 1.33$ and $n_p = 1.54$ are the refractive indexes of water and polystyrene, respectively. $\alpha^*(0)$ is the static excess polarizability of the ion in water, h is the Planck constant and ν_i is the ionization frequency of the ion in water; that is, $h\nu_i$ is the ionization energy in water. This ionization energy is similar and positive for monovalent anions (around 9.0 10^{-12} erg), but negative for the sulfate (-16.4 10^{-12} erg).[29] However, the static excess polarizability of the studied monovalent anions in water significantly differ: ($\alpha^*(0)_{SCN^-}$= 6.61, $\alpha^*(0)_{NO3^-}$ = 4.30, $\alpha^*(0)_{Cl^-}$ = 3.59). The product "$\alpha^*(0)\ h\nu_i$", which vary for each ion, is the key point of this interaction, since it alters the dispersion potential between the ion and the surface, as shown in Figure 3. This dispersion potential considerably changes the typical ionic distribution obtained when only electrostatic forces between charged surfaces and dissolved ions are considered, and thus, yield a possible explanation about the microscopic origin of the Hofmeister effects. The physical background is summarized below. If dispersion forces are taken into account, a new local ion concentration ($c(x)$) can be obtained using a Boltzmann distribution:

$$c(x) = c_b \exp\left(-\beta U_T(x)\right) \tag{8}$$

where $\beta = 1/k_B T$ (being k_B the Boltzmann constant and T the absolute temperature), $U_T(x)$ is the total potential energy of the ions and c_b is the bulk concentration. According to Ninham's model, $U_T(x)$ embodies three major energetic contributions: the mentioned energy potential originated by dispersion forces ($U_{disp}(x)$); a second one ($U_{elec}(x)$) that comes from electrical interactions between the charged interface and the ion; and finally, a term ($U_{image}(x)$) arising from the image force between the ion and the dielectric material (polystyrene in this case). If these terms are assumed additive, then:

$$c(x) = c_b \exp\left(-\beta\left[U_{elec}(x) + U_{image}(x) + U_{disp}(x)\right]\right) \tag{9}$$

The electric term is given by

$$U_{elec}(x) = z\, e\, \Psi(x) \tag{10}$$

where z is the ion valency, e the elementary charge and $\Psi(x)$ is the electric potential at the x position.

The $U_{image}(x)$ term can be derived from the original Onsager-Samaris' theory.[30] It invokes the repulsive electrostatic image force seen by an ion near an air-water interface. The expression is readily adapted for a polystyrene-water interface, leading to:

$$U_{image}(x) \approx \frac{1}{4\pi\varepsilon_0\varepsilon_w}\frac{e^2}{4x}\Delta \exp(-2\kappa x) \tag{11}$$

which is a repulsive and screened potential. Here, $\Delta = (\varepsilon_w - \varepsilon_p)/(\varepsilon_w + \varepsilon_p)$, ε_0 is the electric permittivity of a vacuum, ε_w the relative permittivity of the electrolyte solution (which has been assumed equal to that of pure water: 78.5), ε_p is the relative permittivity of polystyrene ($\varepsilon_p = 2.6$) - and then, $\Delta \approx 1$ -, and κ is the well-known Debye-Hückel parameter. To obtain the self-consistent electrostatic potential $\Psi(x)$ we need to solve the nonlinear Poisson-Boltzmann equation taking into account all the terms:

$$\frac{d^2\Psi(x)}{dx^2} = -\frac{(c(x)_+ - c(x)_-)}{\varepsilon_0\varepsilon_w} \tag{12}$$

where the cation and anion concentration profiles ($c(x)_+$ and $c(x)_-$, respectively) are given by eq. [7]. There are some possible boundary

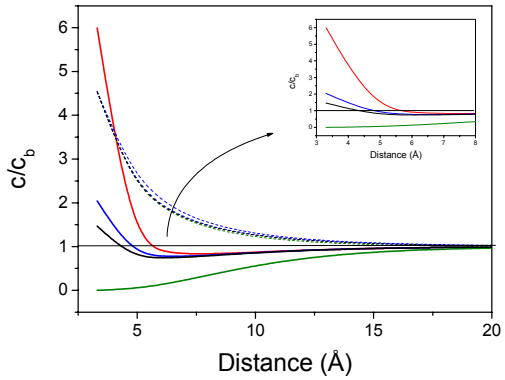

Figure 4. Ion specific self-consistent relative concentration profile as a function of distance to the polystyrene-water interface: Solid lines are for anion and dashed lines for cation: NaSCN (red line), $NaNO_3$ (blue line), NaCl (black line), Na_2SO_4 (green line).

conditions. Here we will use the fixed potential boundary conditions, that is, $\Psi(0) = constant$ and $\Psi(L) = 0$ with L much larger than any other length scale in the problem. The potential at the surface was set at - 30 mV, which is a reasonable value for anionic PS particles with a *ccc* around 600 mM in NaCl solutions.[31] We solve the Poisson-Boltzmann equation numerically using the method of relaxation. Figure 4 shows the local concentration of anions near the surface when dispersion forces are considered. As can be seen, SCN^- accumulates at the proximity of the particle surface much more effectively than Cl^-, while the NO_3^- exhibits an intermediate behavior. The origin of these divergences has to be seen in the different excess polarizabilities of the ions. The ionic accumulation predicted by the Ninham's theory satisfactorily explains the *ccc* results obtained with our latex. The higher accumulation of SCN^- at the water/particle interface enhances the negative electric potential of the particles, what makes increase the colloidal stability of the system. The same effect, although less pronounced, is exerted by the NO_3^-. On the contrary, the negative "$\alpha^*(0)\ h\nu_i$" value associated to the SO_4^{2-} involves a weak concentration of these ions close to the particle-water interface (see Fig. 3). This fact, together with the high screening effect produced by the double charge of SO_4^{2-}, justifies that this ion the the stability be the lowest for the tested anions. The same pattern was observed with cations (curves not shown) although differences in the ion local concentrations were much more

attenuated. High frequency dispersion forces can totally explain the stability results obtained with the monovalent cations. The most polarizable cation, NH_4^+ ($\alpha^*(0)_{NH4}{}^+ = 1.86$), accumulates more effectively at the proximities of the negative latex than the sodium ion ($\alpha^*(0)_{Na}{}^+ = 0.15$), screening more intensively the surface potential, and then, giving rise to a less stable system. Conversely, in the calcium case, although the ionic polarizability also contributes to the system stability, it is the valence of this counter-ion the main responsible for the low *ccc* observed.

Nevertheless, if high frequency dispersion forces were the only responsible for the ionic specificities, Hofmeister series would be always ordered according to the product of ionic polarizabilities and ionization energies, at least for 1:1 electrolytes. However, exceptions have often been found as discussed in ref. 20.[20] Ions can alter the water structure around them, which can give rise to repulsive structural forces not considered in the Ninham's model when two surfaces approach to contact. It should be noted that even very weak perturbations in the water structure can give rise to strong hydration forces between large surfaces. This kind of forces appear to require only about two layers of perturbated water to give hydration forces in approximately one nanometer range.[11] Differences in the way that ions change the solvent order seems to be the origin of the specific effects found in the following experiments. López-León et al.[20] have very recently demonstrated that aggregation kinetics of positive and negative large PS particles (550 nm in diameter) were different when using three different 1:1 electrolytes working in the rapidest aggregation regime. This feature has been also evaluated in the present work. The kinetics rate constant shown in eq. 1 was calculated in other aggregation experiments similar to those shown in Fig. 2, although in this case they were carried out in 1500 mM ionic strength media. It should be noted that this ionic concentration was higher than any *ccc* value, independently of the electrolyte nature. The corresponding $k_{R\text{-}r}$ values are shown in Table 1. In these saline conditions, if no structural forces took place, no repulsive barrier should exist, and subsequently the aggregation kinetics should coincide among all the salts with a pure DLCA model. However, differences in $k_{R\text{-}r}$ exist among the different ionic species, which makes plausible the assumption of the appearance of any kind of weak repulsive barrier or steric hindrance given by structured ion-solvent entities located between two contacting particles. Curiously, the $k_{R\text{-}r}$ values order the ions in

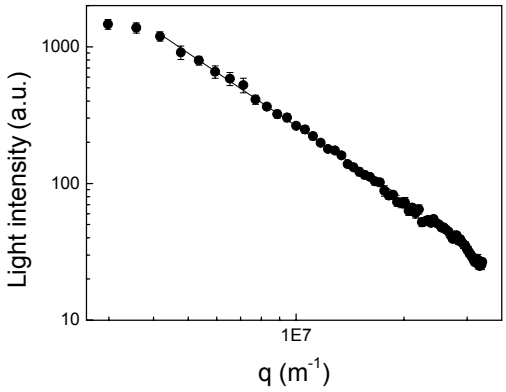

Figure 5. Typical log-log plot of the intensity of scattered light versus the scattering wave vector for a steady state obtained at long time. The aggregates of this figure were obtained with NaCl at 1500 mM.

the same sequences as those given by the *ccc*: $SO_4^{2-} = Cl^- > NO_3^- > SCN^-$ for anions and $Ca^{2+} \geq NH_4^+ > Na^+$ for cations. As mentioned above, the high ionic strength used screens any electrostatic interaction, and thus, the differences in aggregation kinetics could be ascribed to the presence of structured ion-water clusters at the proximities of the particle surface, which originates repulsive structural forces that slows down the coagulation process. In order to confirm the $k_{R\text{-}I}$ results, the fractal dimensions of the aggregates formed in these experiments were also calculated. Figure 5 shows a typical experiment where the intensity of scattered light is plotted versus the scattering wave vector, and from which the d_f values can be determined, Table 1. Ions are ordered once more in the sequences: $SO_4^{2-} < Cl^- < NO_3^- < SCN^-$ for anions and $Ca^{2+} \leq NH_4^+ < Na^+$ for cations. It should be noted that fractal dimensions decreased with an increase in the rate constant, which is an expected result coincident with the usual models for aggregation of electrostatically stabilized particles.[32] In the case of relatively slow aggregation processes (i.e. that obtained with SCN^-), the data cannot distinguish whether the clusters are formed irreversibly with low sticking probability or represent something closer to an aggregate distribution that results from reversible cluster aggregation. It should be noted that if structured ion-solvent entities exits, they must force two contacting particles to stay at larger distances where the depth of the interaction potential curve is small, and consequently favoring partial reversibility in the

aggregation. Previous studies with larger PS particles[20] points out this last hypothesis. Recent molecular dynamics simulations carried out by Bastea[33] demonstrate that short-range repulsive interactions given by the rigidity of solvent "particles" with non-negligible size produce steric forces that can give rise by themselves to coagulation-fragmentation reversible dynamics. This would also produce higher fractal dimensions in the formed clusters. The role played by the solvent particles in the Bastea's study may be played by the ion-water clusters in our aggregation experiments. Our ions in solution interact with the surrounding water molecules in different ways due to their kosmotropic/chaotropic character, forming ion-solvent structures of different size and rigidity. For example, thiocyanate appears to form a shell of partially immobilized water around it similar to those water cages (or ice-like clathrates) generated by hydrophobic molecules.[34] This is why this ion, located at the extreme of the Hofmeister series owing to its low tendency to be hydrated, is capable of generating important structural forces that stabilize other colloidal systems (i.e. PS particles coated by IgG)[19] at high salt concentrations. Previous aggregation studies shown in ref. 19 and 21 clearly suggest the formation of this kind of ion-water cages responsible of structural repulsive forces. The size and/or stiffness of the SCN^--water clusters appears to be higher than that of NO_3^- and Cl^- (in this order). Therefore, if aggregation of colloidal particles is carried out in the presence of a large number of these structures, that is to say, at high salt concentrations (i.e. 1500 mM), the contact between two approaching nanospheres will be partially obstructed. Figure 6 shows a scheme about it. This figure represents the total interaction potential curve for two colliding particles at high salt concentrations. At 1500 mM our latex particles rapidly aggregate independently on the salt nature. Therefore, no repulsive barrier has been drawn in Fig. 6. However, if the presence of ion-water clusters prevents a total contact between the surfaces of two particles, the distance at which the particles remain stuck will vary. The structural hindrance induced by larger ion-water entities will make this distance also larger. At that position, the depth of the interaction curve is small, which favors partial aggregation reversibility, which finally will give rise to lower kinetic rate constants and higher fractal dimensions. This explanation supports the results obtained with our monovalent anions, given that thyocianate alters more efficiently the water molecules around it forming bigger clathrates than nitrate and chloride, respectively. The results reported

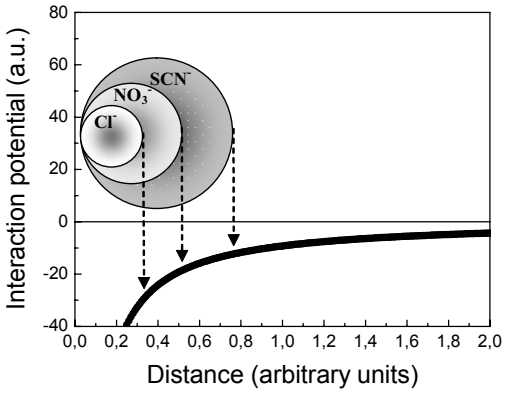

Figure 6. Interaction potential for two approaching particles versus distance in arbitrary units. Arrows indicate hypothetic maximum approximations between the particle surfaces due to repulsive structural hindrances given by the stiffness and size of different ion-water clathrates. Note that this is only a schematic representation that supplies qualitative but not quantitative information.

in ref. 21 also support this idea. Nevertheless, lower k_R and higher d_f values should be expected for the sulphate, a large hydrated anion, if this explanation is taken into account. However, it should be noted that the k_R and d_f experiments performed with our divalent ions were carried out at a 500 mM concentration (that is, a 1500 mM ionic strength), and thus the number of water-sulphate species is three time lower than the other anions coming from 1:1 salts. According to the experimental results, these structural repulsive forces are almost negligible, obtaining high k_R and low d_f values. In fact, a high local concentration of ion-water species in the vicinity of the particle surface is an important factor that enhances structural repulsion interactions between two colliding particles. As shown in Fig. 4, dispersion forces also contributes to increase or decrease the ion concentration in this order: $SCN^- > NO_3^- > Cl^- > SO_4^{2-}$, which modulates the repulsive forces between particles in such a way that is concordant with the obtained k_R and low d_f values. Therefore, not only the size and rigidity of the ion-water clusters, but also its concentration near the surface are responsible of structural repulsive interactions that affect the aggregation kinetics and fractal dimensions.

Acknowledgements

Financial support from the "Comisión Interministerial de Ciencia y Tecnología" Project MAT2003-01257 (European FEDER support included) and from the "Consejería de Innovación, Ciencia y Tecnología de la Junta de Andalucía" Project FQM 392 is gratefully acknowledged.

References and Notes

(1) Collins, K.D.; Washsabough, M.W. *Q. Rev. Biophys.* **1985**, *18*, 323.

(2) Cacace, M.G.; Landau, E.M.; Ramsden, J.J. *Q. Rev. Biophys.* **1997**, *30*, 241.

(3) Israelachvili, J.N. *Intermolecular & Surface Forces*; Academic Press: London, 1992.

(4) Franks, G.V.; Johnson, S.B.; Scales, P.J.; Boger, D.V.; Healy, T.W. *Langmuir* **1999**, *15*, 4411.

(5) Ninham B.W.; Yaminsky, V. *Langmuir* **1997**, *13*, 2097.

(6) Böstrom, M.; Williams, D.R.; Ninham, B.W. *Langmuir* **2001**, *17*, 4475.

(7) Böstrom, M.; Williams, D.R.; Ninham, B.W. *Langmuir* **2002**, *18*, 6010.

(8) Kunz, W.; Lo Nostro, P.; Ninham B.W. *Current Opinion Colloid Interface Sci.* **2004**, *9*, 1.

(9) Böstrom, M.; Kunz, W.; Ninham, B.W. *Langmuir* **2005**, *21*, 2619.

(10) Böstrom, M.; Williams, D.R.; Ninham, B.W. *Phys. Rev. Lett.* **2001**, *87*, 168103.

(11) Parsegian, V.A.; Evans, E.A. *Current Opinion Colloid Interface Sci.* **1996**, *1*, 53.

(12) Meaking, P. *Phys. Rev. Lett.* **1983**, *51*, 1119.

(13) Kolb, M.; Botet, R.; Jullien, R. *Phys. Rev. Lett.* **1983**, *51*, 1123.

(14) Aubert, C.; Cannell, D.S. *Phys. Rev. Lett.* **1986**, *56*, 738.

(15) Martin, J.E.; Wilconxon, J.P.; Schaefer, D.; Odinek, J. *Phys. Rev. A* **1990**, *41*, 4379.

(16) Dimon, P.; Sinka, S.K.; Weitz, D.A.; Safinya, C.R; Smith, G.S.; Varady, W.A.; Lindsay, H.M. *Phys. Rev. Lett.* **1986**, *57*, 595.

(17) Zhu, P.W.; Napper, D.H. *Colloids Surf. A* **1995**, *98*, 93.

(18) Daly, E.; Saunders, B.R. *Langmuir* **2000**, *16*, 5546.

(19) López-León, T.; Jódar-Reyes, A.B.; Ortega-Vinuesa, J.L.; Bastos-González, D. *J. Colloid Interface Sci.* **2005**, *284*, 139.

(20) López-León, T.; Elaïssari, A.; Or tega-Vinuesa, J.L.; Bastos-González, D. "Hofmeister effects on PNIPAM microgel particles: experimental evidences of ion adsorption and changes in water structure" *ChemPhysChem* **2006**, in press.

(21) López-León, T.; Bastos-González, D.; López-López. J.M.; Schmitt, A.; Odriozola, G.; Ortega-Vinuesa, J.L. "Hofmeister effects in colloidal suspensions: experimental evidences in aggregation kinetics"

(22) A. Lips and E.J. Willis, *J. Chem. Soc. Faraday Trans. 1*, **1971**, *67*, 2979.

(23) Schmidt, P.W. *The Fractal Approach to Heterogeneous Chemistry*, Avnir, D. Ed., Wiley: New York, 1989.

(24) Teixeira, J. *On Growth and Form*, Stanley, H.E.; Ostrowsky, N. Eds., Nijhoff: Dordrecht, 1986.

(25) Martin, J.E.; Ackerson, G.J. *Phys. Rev. A* **1985**, *31*, 1180.

(26) Amal, R.; Raper, J.A.; Waite, T.D. *J. Colloid Interface Sci.* **1990**, *140*, 158.

(27) Zhang, J.; Buffle, J. *J. Colloid Interface Sci.* **1995**, *174*, 500.

(28) Molina-Bolívar, J.A.; Galisteo-González, F.; Hidalgo-Álvarez, R. *J. Chem. Phys.* **1999**, *110*, 5412.

(29) Tavares, F.W.; Bratko, D.; Blanch, H.W.; Prausnitz, J.M. *J. Phys. Chem. B* **2004**, *108*, 9228.

(30) Onsager, L.; Samaris, N.T. *J. Chem Phys.* **1934**, *2*, 528.

(31) López-León, T.; Jódar-Reyes, A.B.; Bastos-González, D.; Ortega-Vinuesa, J.L., *J. Phys. Chem. B.* **2003**, *107*, 5696.

(32) Tirado-Miranda, M.; Schmitt, A.; Callejas-Fernández, J.; Fernández-Barbero, A. *Phys. Rev. E* **2003**, *67*, 011402.

(33) Bastea, S. *Phys. Rev. Lett.* **2006**, *96*, 028305.

(34) Franks, F.; Reid, D. S. *Water – A Comprehensive Treatise*, ed. Franks: Plenum, New York, 1973.

HOFMEISTER EFFECTS IN COLLOIDAL SUSPENSIONS: EXPERIMENTAL EVIDENCES IN AGGREGATION KINETICS

T. López-León[1], D. Bastos-González[1], J.M. López-López[1], A. Schmitt[1], G. Odriozola[2], and J.L. Ortega-Vinuesa[1]

[1] *Biocolloid and Fluid Physics Group, Department of Applied Physics, Faculty of Sciences, University of Granada, Campus Fuentenueva S/N, 18071 Granada , Spain*

[2] *Programa de Ingeniería Molecular, Instituto Mexicano del Petróleo, Eje Lázaro Cárdenas 152, 07730 México DF, México*

Abstract

Specific ionic effects (also called Hofmeister effects) are present in chemical and biological sciences. Explaining their microscopic origin has become a major challenge for the scientific community in the last decades. Although the Hofmeister puzzle has not been totally unravelled today, its elucidation appears to be nearer and nearer. Hofmeister effects stem from two combined phenomena that not only coexist, but also seem impossible to disentangle. One of them appears as a consequence of the molecular water structure around ions and other boundaries, i.e. at the water-particle interface in the case of colloidal suspensions. The other one is related to the specific accumulation/exclusion of ions at interfaces, which mainly depends on the dispersions forces acting on the ions. Traditionally, the analysis of aggregation kinetics of colloidal particles has represented a recurrent and useful way to indirectly measure intercolloidal forces. Experimental techniques such as turbidimetry or nephelometry have generally been used to analyse the aggregation processes. However, much more accurate information can be obtained when using a single cluster light scattering (SCLS) apparatus. Actually, valuable information about the inter-particle pair potentials can be gathered when both techniques are combined. In this work, aggregation kinetics of polystyrene particles has been studied using NaCl, $NaNO_3$, and NaSCN as aggregating salts. These three electrolytes behave different with regard to the Hofmeister character, which allows us to investigate their specific effects on the inter-particle interactions. The experimental setup reveals that the Hofmeister effects are crucial in the colloidal interactions. In addition, the results emphasize and corroborate the existence of the two mechanisms underlying the Hofmeister effects. Differences in critical coagulation concentrations (ccc) evidence ionic accumulation-exclusion phenomena, whereas differences in aggregation kinetics confirm the presence of structural forces caused by the specific solvent arrangement that ions induce on their neighbouring water molecules. Surprisingly, a reversible aggregation has been found working with NaSCN above the ccc of the particles. Although this aggregation regime has been predicted by both theory and computer simulations, it has never been clearly observed in experiments. To our knowledge, this is the first time that a reversible aggregation process has been detected in a direct way. These new experimental results have also made possible to test the theory accounting for these phenomena. A well concordance between experiments and simulations has been found.

I. Introduction

Colloidal suspensions are common in biological, chemical, and geological systems. Their unusual properties are intensely exploited in many industrial applications, from pharmaceutics to food processing. One of the remarkable features of colloids is the possibility of easily control the interparticle interactions [1], which ultimately govern the colloidal equilibrium and kinetic behaviour. The well known DLVO theory has been extensively used to explain the colloidal stability of lyophobic materials. This theory combines a repulsive and an attractive term that have different origins. The repulsive term comes from electrostatic forces affecting the double layer organization, while the attractive one is given by quantum mechanical forces. These two contributions determine the net interaction potential between two approaching particles. However, there is a large number of experimental data that can not be explained by this simple idealized DLVO theory. The lack of concordance might be in part due to a fundamental inconsistency, even at the continuum level, which arises from treating the electric double layer via a non-linear theory (through the Poisson-Boltzmann equation), and the van der Waals – Lifschitz forces by a linear theory [2]. Where the theory apparently fails, new terms to describe "non-DLVO" forces (i.e. hydration, structural, hydrophobic, depletion) are usually added. As an example, the original theory does not account for specific ion effects embraced by the term Hofmeister effects or Hofmeister series. Hofmeister effects are present not only in colloidal systems; they also participate in a plethora of phenomena (stability and solubility of proteins, water activity coefficients, surface tension at the air-water interface, lipid solubility, chromatographic selectivity, polymer cloud points, polymer swelling, heats of hydrations, etc) [3,4]. Much attention has been paid to Hofmeister effects, especially during the last decade, where the number of related publications has grown exponentially. Despite they have been known for over a century, their microscopic origin has not been totally understood until nowadays. The specific ionic effects were originally attributed to changes in the solute-induced water structure. However, it is currently known that their microscopic origin must be sought not only in the structure of the solvent molecules surrounding the ions, but also in other factors that Ninham et al. have explained in some recent papers [5-9]. These authors state that ions experience not just an electrostatic interaction with an interface but also a short ranged dispersion interaction that can lead to either ionic adsorption or exclusion, which in turn modifies the double layer structure.

Actually, dispersion forces must play an important role in the Hofmeister effects, since many of these phenomena have been found to be correlated with the ion polarisability. Most of the recent efforts have been made to explain Hofmeister effects in terms of the high-frequency or dispersion part of the Lifshitz forces acting on ions in adsorption [6,9-11]. However, for aqueous solutions, it turned out that this high-frequency contribution is only a small part of the full dispersion interaction [12]. The lower frequency contribution, - i.e. dipolar and induced dipole-dipole – responsible for the hydration of ions, are evidently more important here. Therefore, a complete and correct description of all the dispersion forces would be necessary to properly explain the behaviour of colloidal systems, although the problem becomes much more complicated when the structure of the water molecules is taken into account. Most theories treat water as a continuum, ignoring short ranged hydration repulsive interactions that come from overlapping inhomogeneous surface-induced water structures [13]. This hydration interaction is a non-negligible structural force that arises from the local order of water in the vicinity of the surfaces, and which is capable by itself to stabilize colloidal systems even at experimental conditions where the DLVO theory predicts aggregation. This interaction is not only correlated with the hydrophilic degree of the surface, but also strongly depends on the nature and concentration of the ionic species near the surface [14-17]. Ions can firmly influence the water structure. They can induce via electrostatic interactions a dipolar orientation of the neighbouring solvent molecules, but they can also induce, via size, shape and heterogeneous charge distribution, hydrogen bonding rearrangements and, via dispersion forces, (dipole-"induced dipole" and "induced dipole"-"induced dipole"), solvent order. This ionic specificity, which contributes in many ways to the total interparticle interaction potential in colloidal suspensions, turns Hofmeister effects into an unsolved puzzle. This is why developing a theoretical framework accounting for all the ion effects is a very difficult task and one of the basic problems of the colloidal science nowadays. In any case, there is no doubt that the Hofmeister series emerge from a combination of effects in which water structure and specific ionic accumulation/exclusion are the cornerstones. Both mechanisms always coexist, and thus, only a hybrid model will be able to account for the Hofmeister phenomena.

In this paper, we provide experimental evidence of this double underlying mechanism by investigating the aggregation of hydrophobic colloidal particles. Polystyrene (PS) nanospheres were chosen for this study

because of their model behavior. One of the main advantages of using these particles is that they minimize as much as possible any extra-DLVO forces, which would complicate the problem even more. The PS nanospheres present a smooth surface in aqueous media, and thus, the possibility of steric hindrance between extended polymer chains can be dismissed. In addition, the hydration forces that usually appear in hydrophilic materials are not important here – it is worth noting that such "hydration forces" only refer to the repulsive forces arising from the overlapping of the structured water layers originated by the hydrophilic nature of the solid surface. Hence, it can be assumed that there are no steric or hydration forces participating in the stability of the particles. Aggregation of the PS particles was induced by adding (independently) three different sodium salts (NaSCN, $NaNO_3$, and NaCl). As all of them share the same cation, the differences observed in our experiments must be caused by the specific effects produced by the monovalent anions. Sodium is considered a non-specific ion with regard to the Hofmeister series [3,4]; the anions, however, are located in different positions in these series, as they differ in the strength of the ion-water interaction. Ions that interact with water more weakly than water itself are called chaotropes, as their presence in solution disrupt the original H-bonding network. Under this definition, thiocyanate is the most chaotropic ion, nitrate is an intermediate chaotrope and chlorate is considered a non-specific anion. In order to analyze differences appearing when the anions acted either as counter- or co-ions, the study was developed working in parallel with positive and negative PS particles. Aggregation results are presented into two parts. On the one hand, those obtained with a nephelometer that allowed us to determine the critical coagulation concentrations (ccc). On the other hand, those obtained with a single cluster light scattering apparatus, where the salt concentration used was above the ccc. Although the two mechanisms underlying the Hofmeister effects always appear together, their effect is different depending on the phenomenon analyzed. Certain physical properties are highly sensitive to the charge density at the surface proximities but not so dependent on water structure variations, and viceversa. In this paper, this fact has been exploited to investigate individually both mechanisms. As will be shown, the first set of experiments reflects ionic accumulation-exclusion mechanisms, while the second one manifests differences in the water structure around the ions.

II. Materials and Methods

Two different polystyrene latices were used in this work. One of them was an anionic latex, while the other presented a positive surface. Both were synthesized without any added surface active agents, and thus, the particles were electrostatically stabilized by the charged groups derived from the initiator molecules used in the polymerization reaction. The anionic sample was manufactured at the laboratories of Granada University (Spain) using potassium persulfate as the initiator. Details about its synthesis and main characteristics are given elsewhere [18]. The cationic sample was purchased from the Interfacial Dynamics Corporation (IDC, USA). Amidine groups are responsible of the surface charge of these particles. The mean diameter of both systems coincided, which was (525 ± 5) nm. In addition, they presented extremely narrow size distributions, as reflected in their corresponding polydispersity index values, which were very close to unity: 1.005 and 1.002 for the anionic and cationic samples, respectively.

Electrolytes (NaCl, $NaNO_3$, and NaSCN) were of analytical grade and purchased from Sigma. The particles were solved in buffered solutions (pH 5) with a rather low ionic strength (acetate / acetic acid at 0.002 M). These solutions kept the surface charge of the anionic and cationic particles at its maximum value, since sulfate and amidine groups are fully charged at this acid pH [18].

The aggregation phenomena were analyzed by using two different instruments. The first set of experiments was performed with a low-angle light scattering technique (a nephelometer). This apparatus allowed us to monitor the temporal evolution of the light intensity scattered by a sample at a fix angle (5º, 10º or 20º). The reaction between the particles and the destabilizing saline solution took place in a rectangular scattering cell with a 2 mm path length. Equal volumes (1 mL) of non-buffered electrolyte and buffered latex solutions were mixed and introduced into the cell by an automatic mixing device. The particle concentration in the cell was 4 10^9 mL^{-1} for both latices. The aggregation process was detected for 120s. During the first steps of the coagulation the light scattered behaves linearly with time. At low scattering angles the slope of this curve is related with the aggregation kinetic constant k. The stability ratio, also called Fuchs factor (W) [19], is a criterion broadly used to evaluate the colloidal stability. It can be calculated from the following expression: $W = k_r/k_s$, where the rate constant k_r corresponds to rapid

coagulation kinetics, and k_s is the rate constant for a slow coagulation regime. A W value equal to unity means maximum instability, while $W \to \infty$ refers to a stable colloidal system. The W data versus salt concentration are usually plotted using logarithmic scales. The critical coagulation concentration (ccc), that is, the minimum salt concentration needed to produce a rapid coagulation kinetics, corresponds with the salt concentration at which log W reduces to zero.

The second set of experiments was obtained with a single cluster light scattering (SCLS) instrument. A detailed description of this technique can be found elsewhere [20,21]. It allowed us to obtain the cluster size distribution (CSD) for small aggregates without any assumption about the cluster structure. When salt was added to the solution, the colloidal dispersion was then injected into a water flow by means of a computer-controlled peristaltic pump. The clusters, separated by hydrodynamic focusing, were forced to flow across a focused laser beam. The light pulses that clusters scatter were detected at a small angle and counted and classified according to their intensity. Since the scattered light intensity at low angle is monotonically related to the cluster volume, the CSD can be obtained. This type of experiments lasted 16 h. Our instrument is capable of distinguishing aggregates composed of up to eight particles [$c_n(t)$, $n \leq 8$]. Furthermore, the total number of scattered light pulses, that is the total number of clusters ($\Sigma_n c_n$), is also available.

III. Results and Discussions

As mentioned above, the first set of aggregation experiments were analysed by using a nephelometer. The stability ratio W versus salt concentration was obtained for both latices and the results are shown in Figure 1. The corresponding ccc values are given in Table 1. The NaCl will be used as a reference electrolyte, as both species (Na^+ and Cl^-) do not present any ionic specificity; (in fact, the position of these two ions is usually considered as a null point in the Hofmeister series). The NaCl data will be discussed first and, thus, no Hofmeister effects will be considered in this case. The anionic latex showed a ccc value slightly higher than that of the cationic latex. This result agrees with the electrophoretic mobility values of both latices at pH 5, since the mobility of the anionic sample is slightly higher [18].

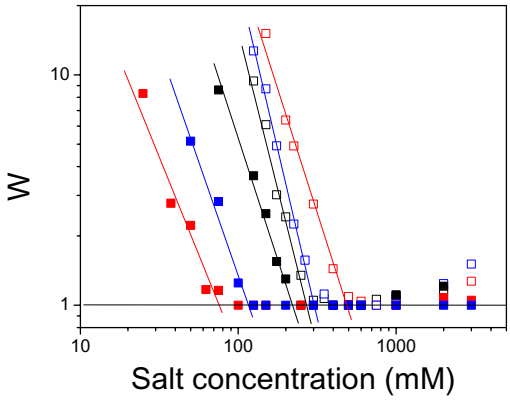

Figure 1. Stability ratio (W) versus electrolyte concentration for the cationic (solid symbols) and anionic (open symbols) latex using NaCl (black), $NaNO_3$ (blue) and NaSCN (red) as aggregating salts.

Table 1. *ccc*, d_f, k_{11}, P_1, τ_1 and τ_2 values of both latices when aggregation is induced by different electrolytes. Details about these parameters are given in the main text.

	ccc values (mM)		d_f values	
	Anionic latex	cationic latex	Anionic latex	cationic latex
NaCl	275	225	1.8	1.8
$NaNO_3$	300	115	2.0	2.0
NaSCN	500	75	2.0	2.0
	k_{11} values (m^3/s)		P_1 values	
	Anionic latex	cationic latex	Anionic latex	cationic latex
NaCl	$9.0\ 10^{-18}$	$9.0\ 10^{-18}$	0.28	0.35
$NaNO_3$	$9.0\ 10^{-18}$	$9.0\ 10^{-18}$	0.06	0.07
NaSCN	$9.0\ 10^{-18}$	$9.0\ 10^{-18}$	0.035	0.04
	τ_1 values (s)		τ_2 values (s)	
	Anionic latex	cationic latex	Anionic latex	cationic latex
NaCl	200000	Infinite	400	2000
$NaNO_3$	200000	100000	150	600
NaSCN	200000	25000	100	370

Hence, the cationic latex possesses a lower ζ-potential value, (that can be translated into a lower surface potential in a NaCl solution), which ultimately is responsible of the stability of lyophobic (and smooth) colloidal particles. Therefore, the ccc values are concordant with the surface potential of the particles. Nevertheless, the most interesting results are those coming from the ionic specificity exerted by the anions. The different values of ccc obtained with the several species allow us to order electrolytes according their stabilizing/destabilizing effect. For the anionic latex, where anions act as coions, a classical Hofmeister series is obtained: $Cl^- < NO_3^- < SCN^-$ (see Table 1). Otherwise, when the anions act as counterions (in the cationic latex), the inverted series is observed: $SCN^- < NO_3^- < Cl^-$. This Hofmeister phenomenon can be explained on the basis of an ion accumulation mechanism. It should be noted that the instability induced by salinity is governed by the effectiveness with which the ions that surround the colloidal particles screen the surface potential. The usual ionic Boltzmann distribution (given solely by electrostatic interactions) is altered when dispersion forces between the surface and the ions are considered. In this case the ionic specificity will depend on the static excess polarizability of the ion in water ($\alpha^*(0)$). This parameter represents the change in polarizability of an ion compared to an equivalent volume of water. The ionic polarizability in aqueous solution is (6.61 ± 0.14) $Å^3$, (4.30 ± 0.18) $Å^3$ and (3.59 ± 0.17) $Å^3$ for SCN^-, NO_3^-, and Cl^-, respectively [8]. A higher excess of polarizability implies a stronger attraction (or repulsion) between the ion and the surface by means of high-frequency dispersion forces. Attraction or repulsion depends on the dielectric properties of the adjoining media as a function of frequency [8]. For the water - polystyrene case, this ion-surface interaction is attractive, making thiocyanate accumulate at the particle-water interface in greater concentration than nitrate and chloride (in this order). When anions act as counterions, this accumulation mechanism screens more effectively the surface potential, leading to more instable particles. When acting as coions the opposite effect is observed, as this accumulation enhances the potential at the proximities of the surface, enhancing the system stability. Electrokinetic mobility measurements (which are related ζ-potential values) also support this explanation. For instance, López-León et al. [22] working with other anionic and cationic polystyrene particles showed that the most polarizable anions augmented the mobility of negatively charged latices, while they diminished the mobility of positive particles.

In order to give quantitative information, some calculations can be done to estimate the dispersion force contribution in the double electric layer ionic distribution according to the Ninham's model. It should be noticed that this model is built under certain approximations. For example, water is assumed to be a dielectric continuum. Correlations between ions by electric, dispersion or hard-sphere interactions are also neglected. In addition, we will consider that the ions are much smaller than our polystyrene particles, and therefore, ion distributions will be estimated at a planar surface. As a consequence, the results must be considered only as a guide in order to gain clarity. Calculations are performed for a cationic latex, where anions act as counterions, at a constant ionic strength (250 mM, which was chosen arbitrarily). If we take an x axis perpendicular to the surface with its origin ($x = 0$) at the surface so that the region $x > 0$ corresponds to the liquid phase, then the concentration of anions for a plate-like particle is given by a Boltzmann distribution:

$$c(x) = c_b \exp\left(-\beta U_T(x)\right) \tag{1}$$

where $\beta = 1/k_B T$ (being k_B the Boltzmann constant and T the absolute temperature), $U_T(x)$ is the total potential energy of the ions and c_b is the bulk concentration. When ions in an aqueous solution are located at the proximity of a dielectric material (i.e. polystyrene) with fixed charges located at its surface, there are three major contributions for the $U_T(x)$ energy: i) a $U_{elec}(x)$ coming from electrical interactions between the charged surface and the ion, ii) a $U_{image}(x)$ arising from the image force between the ion and the dielectric material, and iii) a $U_{disp}(x)$ originated by dispersion forces between ions and the interface. If these terms are assumed additive, then:

$$c(x) = c_b \exp\left(-\beta\left[U_{elec}(x) + U_{image}(x) + U_{disp}(x)\right]\right) \tag{2}$$

The electric term is given by

$$U_{elec}(x) = z\, e\, \Psi(x) \tag{3}$$

where z is the ion valency, e the elementary charge and $\Psi(x)$ is the electric potential at the x position.

The $U_{image}(x)$ term can be derived from the original Onsager-Samaris' theory [23]. It takes into account the repulsive electrostatic image force seen

by an ion near an air-water interface. The expression is readily adapted for a polystyrene-water interface, leading to:

$$U_{image}(x) \approx \frac{1}{4\pi\varepsilon_0\varepsilon_w}\frac{e^2}{4x}\Delta\exp(-2\kappa x) \tag{4}$$

which is a repulsive and screened potential. Here, $\Delta = (\varepsilon_w - \varepsilon_p)/(\varepsilon_w + \varepsilon_p)$, ε_0 is the electric permittivity of a vacuum, ε_w the relative permittivity of the electrolyte solution (which has been assumed equal to that of pure water: 78.5), ε_p is the relative permittivity of polystyrene ($\varepsilon_p = 2.6$) - and then, $\Delta \approx 1$ -, and κ is the well-known Debye-Hückel parameter.

Finally, the dispersion potential between an ion and a surface is approximately [6]:

$$U_{disp}(x) \approx \frac{\left(n_w^2 - n_p^2\right)}{8x^3}\alpha^*(0)h\nu_i \tag{5}$$

Here, $n_w = 1.33$ and $n_p = 1.54$ are the refractive indexes of water and polystyrene, respectively. $\alpha^*(0)$ is th e static excess polarizability of the ion in water, h is the Planck constant and ν_i is the ionization frequency of the ion in water; that is, hνi is the ionization energy in water. This ionization energy is similar for monovalent anions (around 9.0 10-12 erg) [24]. However, the polarizability of our anions in water does differ, and this parameter is ultimately the responsible of changing the ionic distribution and the electric potential at the surface proximities. To obtain the self-consistent electrostatic potential $\Psi(x)$ we need to solve the nonlinear Poisson-Boltzmann equation taking into account all the terms:

$$\frac{d^2\Psi(x)}{dx^2} = -\frac{(c(x)_+ - c(x)_-)}{\varepsilon_0\varepsilon_w} \tag{6}$$

where the cation and anion concentration profiles ($c(x)_+$ and $c(x)_-$, respectively) are given by Eq. 2. There are some possible boundary conditions. Here we will use the fixed potencial boundary conditions, that is, $\Psi(0) =$ *constant* and $\Psi(L) = 0$ with L much larger than any other length scale in the problem. The potential at the surface was set at 20 mV, which is a reasonable value for cationic PS particles with a ccc around 200 mM in NaCl solutions [22]. We solve the Poisson-Boltzmann equation numerically using the method

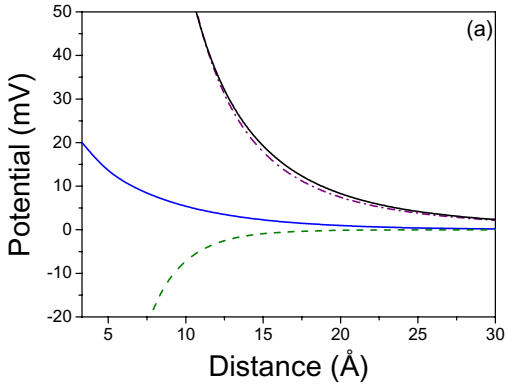

Figure 2a. Total interaction energy potential $U_T(x)$ (solid line) between an ion (Cl^- in this case) and a positive PS surface. The three major contributions for this total potential are also shown: $U_{elec}(x)$ (˙ ˙ ˙ ˙), $U_{image}(x)$ (- - - -) and $U_{disp}(x)$ (˙ - ˙ -).

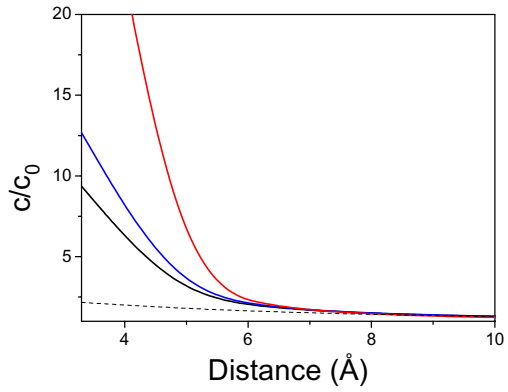

Figure 2b. Local concentration of anions at the particle surface proximities when dispersion forces between the ions and the surface are considered: Cl^- (black), NO_3^- (blue) and SCN^- (red). The ion concentration obtained by a Poisson-Boltzmann distribution where only electrostatic (but no dispersion) forces are taking into account is also shown as a reference (dashed line).

of relaxation. Figure 2a shows the total interaction potential $U_T(x)$ and it also compares the three U(x) terms for the Cl^- case. Figure 2b shows the local concentration of anions near the surface when dispersion forces are considered. As the polarizability of thiocyanate almost doubles that of chloride, and taking into account Eq. 2, SCN^- accumulates at the proximity of the particle surface much more than Cl^-, while nitrate is an intermediate case. This ionic accumulation predicted by the Ninham's theory satisfactorily explains the ccc results obtained with our latices. That is, the higher accumulation of SCN^- at the water/particle interface screens more effectively the charge of the positive particles whereas it enhances the electric potential near the negative ones. This makes the colloidal stability diminish in the positive sample while it is increased in the negative system. Therefore, the inverted Hofmeister series obtained with our two latices with regard to the ccc values is fully justified by this theory.

Nevertheless, if high frequency dispersion forces were the only responsible of the ionic specificities, Hofmeister series would be always ordered according to the ionic polarizabilities. However, exceptions have often been found. An example can be found when studying the ccc of negative colloidal particles with different hydrophobic-hydrophilic degrees. For polystyrene particles with low surface charge density (high hydrophobicity) the ccc values give an order coincident to that of our anionic latex [22]: $Cl^- < NO_3^- < SCN^-$. However, if the surface charge density is increased (which in turn augments the surface hidrophilicity) the order changes: $Cl^- < SCN^- < NO_3^-$, (i.e. see the AMJ5 latex at pH 10 in reference [22]). Finally, if the surface hydrophilicity is increased even more (i.e. by adsorbing a protein onto a polystyrene surface) the stability changes as follows: $SCN^- < Cl^- < NO_3^-$ [25]. This last sequence was also obtained in our labs working with highly hydrophilic silica particles (unpublished data), but all these results are in conflict with the predictions given by the dispersion theory. This controversial point can be solved when the other Hofmeister underlying mechanism is taking into account, that is, the presence of ions near the surface may specifically alter the water structure leading to short ranged hydration repulsive forces. This is why the second set of experiments was designed to investigate this structural force. It is worth to remind that our particles are not hydrophilic at all, and thus, a stabilizing mechanism based on structured water induced by the surface itself should be discarded.

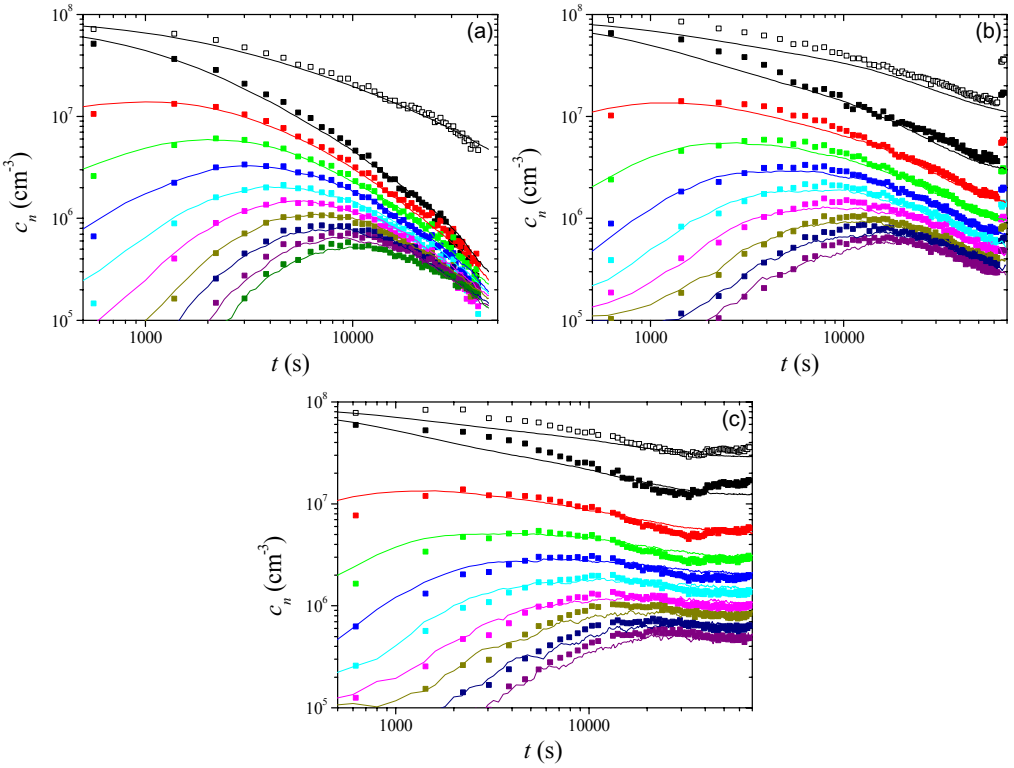

Figure 3a-c. Time evolution of the weight average cluster size for the cationic sample aggregating at 600 mM using the following electrolytes: (a) NaCl, (b) $NaNO_3$ and (c) NaSCN; (■) monomers, (■) dimmers, (■) trimmers (■) tetramers, (■) pentamers, (■) hexamers, (■) heptamers, (■) octamers, (■) nonamers and (□) total number of clusters. Symbols correspond to experimental data and lines come from the stochastic solution using as fitting parameters P_1, τ_1 and τ_2, (see the corresponding values in Table 1).

The aggregation kinetics was now evaluated by using the SCLS apparatus. The salt concentration was set at 600 mM, which is above the ccc values of our systems (see Table 1). This salt concentration was chosen in order to work with the fastest aggregation kinetics regime for each salt. Experimental results are shown in Figures 3a-c and 4a-c for the cationic and the anionic latex, respectively. The experimentally obtained time evolution of the cluster size

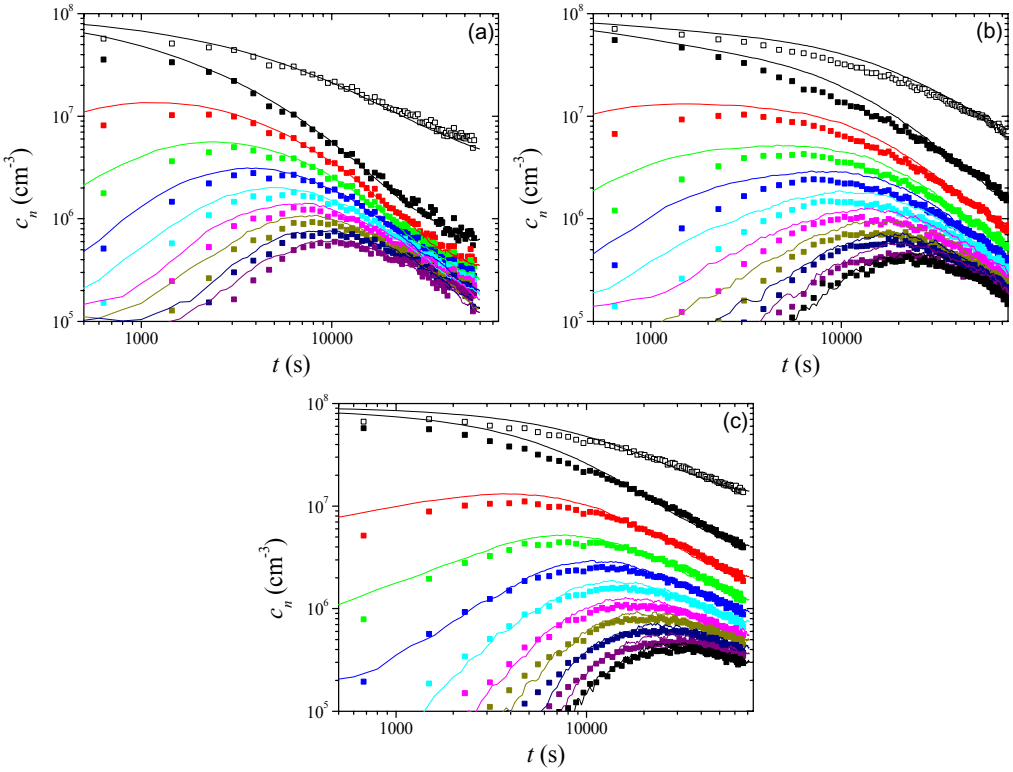

Figure 4a-c. Time evolution of the weight average cluster size for the anionic sample aggregating at 600 mM using the following electrolytes (a) NaCl, (b) $NaNO_3$ and (c) NaSCN; (■) monomers, (■) dimmers, (■) trimmers (■) tetramers, (■) pentamers, (■) hexamers, (■) heptamers, (■) octamers, (■) nonamers and (□) total number of clusters. Symbols correspond to experimental data and lines come from the stochastic solution using as fitting parameters P_1, τ_1 and τ_2, (see the corresponding values in Table 1).

distribution is represented by symbols, while the lines correspond to theoretical predictions. Before analysing the results theoretically, a qualitative interpretation can be done. The CSD clearly differs between the three tested anions. Coagulation in presence of chloride shows characteristic patterns of an irreversible aggregation, as clusters of small sizes tend to disappear at long time due to collision between them to form bigger clusters. However, the presence of SCN^- generates a clear reversible aggregation, above all in the

cationic latex (see Figure 3c). The population of small clusters remains constant at long time, indicating an equilibrium phase where aggregation and break up processes occur. Finally, nitrate shows an intermediate behaviour between the other two anions. Hofmeister effects are ubiquitous in chemical systems and, as seen in Figures 3 and 4, they also participate in aggregation kinetics phenomena of hydrophobic colloidal suspensions. In fact, the irreversibility of the aggregation orders the anions according to an inverted classical Hofmeister series, $SCN^- < NO_3^- < Cl^-$, independently of the surface sign of charge. This difference in kinetics can be accounted by the ability of these anions to rearrange the surrounding water molecules in different manners. The most chaotropic the anion, the most altered the adjacent water shell around it. López-León et al. [25] have recently shown that thyocianate, acting either as co-ion or counterion, was capable to re-stabilize IgG coated polystyrene particles at high salt concentrations. Nitrate only re-stabilized when acting as counterion, while chloride was unable to re-stabilize. These re-stabilization phenomena in hydrophilic particles are highly dependent on the hydration shell of the dissolved ions located at the proximities of the surface [13-17]. Cations but not anions are usually considered responsible for the hydration re-stabilization. However, López-León et al. [25] experimentally evidenced that also chaotropic anions are able to re-stabilize by means of water-induced structural forces. Re-stabilization at high ionic strengths does not occur in our latices (see Figure 1), as they possess hydrophobic surfaces, but it is more than likely that the structured water layers around the different anions placed at the surface proximities were responsible for the different aggregation patterns observed in Figures 3a-c and 4a-c. The most chaotropic anion (SCN^-) would reorganize the water molecules around itself in a more effectively way than nitrate and chloride (in this order). Therefore, latex particles aggregate in presence of ion-water clusters (only one central ion per cluster) with different effective sizes depending on the anion nature. These induced solvent structures obstruct the particle approaching, which is translated into a modification in the interparticle interactions. Even if the interaction potential did not change, the depth of the potential curve where the particles remain stuck would vary. If approximation between two particles is totally allowed (i.e. the Cl^- case) aggregation can take place in a primary minimum of significant depth, and thus, the collision would be irreversible. On the other hand, if a protective "ion-water" shell avoids total approximation (i.e. the SCN^- case), particles would remain in secondary minima or positions

where the potential curve is not deep enough and reversibility in the aggregation must be expected. Therefore, the structured water-ion entity is then responsible of the maximum approximation distance between colliding particles, and thus, responsible of the differences observed in the aggregation kinetics. The higher the chaotropic properties of an anion, the higher the stiffness and size of the water-ion cluster and consequently the higher the distance at which particles collapse and the higher the reversibility of the aggregation. All this explanation has been supported by simulation studies, at least under a qualitative point of view. Bastea [26] has just published a paper accounting for the so-called cluster phases in colloidal systems. This author shows with molecular dynamics simulations that short-range repulsive interactions alone can give rise to the appearance of low-dimensionality clusters in a final equilibrium state. In this case, a binary mixture consisting of two types of spherical particles (colloid "c" and solvent "s") is considered. The interactions between all the particles are based on the inverse-12, "soft-sphere", potential. For low colloid volume fractions and a colloid solvent "diameter (d)" ratio $d_c/d_s = 5$, this author demonstrated that a final phase of low dimensionality colloidal clusters (whose evolution is driven by aggregation and break up processes) is obtained considering only short-range repulsive potentials. These simulated results are similar to those experimentally observed with our two latices working with SCN^- (Na^+) at 600 mM. At such an ionic strength, electrical repulsions are negligible. Therefore, the repulsive interaction could be given by a "soft-sphere" potential where the role played by the "solvent" particles in the molecular dynamics simulations is played by the "ion-water clusters" in the real system. When NaCl is used instead, no reversible aggregation is observed. In this case, the water cage formed around an unspecific ion (Cl^-) must be loose, (it should be reminded that an unspecific ion is assumed that does not disrupt the original H-bonding network). If these ion-water clusters do not exist (or their existence is negligible) the commented short-range repulsive interaction disappears and a typical irreversible process occurs. As the chaotropic properties of nitrate are intermediate between those of thiocyanate and chloride, its aggregation patterns are placed between the two corresponding aggregations regimes.

Finally, a quantitative analysis of the aggregation kinetics can be also done. Since some data clearly show cluster breakup, we have performed a theoretical fit of the experimental results shown in Figures 3 and 4 employing the reversible model given in reference [27] section 4.3. This model considers

two kinds of bonds, primary and secondary ones, that can be formed and must be treated separately. These bonds have different breakup probabilities. The model assumes all collisions to be effective (i.e., collisions always lead to primary or secondary bond formation), and hence, the Brownian kernel is used for the aggregation kinetics. This kernel is given by

$$k_{ij}^{Brow} = \frac{1}{4} k_{11} \left(i^{1/d_f} + j^{1/d_f} \right) \left(i^{-1/d_f} + j^{-1/d_f} \right) \tag{7}$$

where $k_{11} = 8k_B T/3\eta$ is the dimmer formation rate constant, d_f is the cluster fractal dimension, $k_B T$ is the thermal energy, and η is the solvent viscosity. The fragmentation kernel f_{ij} is given by

$$f_{ij} = e_{ij} \left(1 + \delta_{ij} \right) \left[\frac{E_1}{\tau_1 \left(E_1 + E_2 \right)} + \frac{E_2}{\tau_2 \left(E_1 + E_2 \right)} \right] \left(1 - P_c \right) \tag{8}$$

where E_1 and E_2 are the number of primary and secondary bonds in the system, τ_1 is the average life time of primary bonds, and τ_2 is the average life time of secondary bonds. e_{ij} is the average number of bonds that, on breakup, leads to *i*- and *j*-size fragments. This function can be obtained by averaging over all fragmentation possibilities of a vast collection of simulated cluster structures. This was done in reference [28], and the function reads

$$e_{ij} \left(1 + \delta_{ij} \right) = p_1 \left(i^{p_2} + j^{p_2} \right) \left(i^{p_3} + j^{p_3} \right) (ij)^{p_4} \tag{9}$$

where $p_1 = 0.4391$, $p_2 = 1.006$, $p_3 = -1.007$, and $p_4 = -0.1363$. Here and in Eq. 8, δ_{ij} is the Kronecker delta function. Finally, P_c in Eq. 8 is the probability for two recently produced clusters to collide and reaggregate. This probability is size dependent and it is given by

$$P_c = 1 - \frac{1}{6.1 \, (ij)^{0.35}} \tag{10}$$

as was determined from computer simulations [28]. This expression has been tested with experimental data [30, 31], and contrasted with detailed theoretical models [32]. Hence, both kernels are used to obtain the time evolution of the cluster size distribution according to [33]:

$$\frac{dP(\vec{M},t)}{dt} =$$

$$\frac{1}{2V}\sum_{i,j} k_{ij}\left\{\left(N_i+1\right)\left(N_j+1+\delta_{ij}\right)\left[P(\vec{M}_{ij}^{+1},t)P_1+P(\vec{M}_{ij}^{+2},t)(1-P_1)\right]-N_i\left(N_j-\delta_{ij}\right)P(\vec{M},t)\right\}$$

$$+\frac{1}{2}\sum_{n=2}^{\infty}\left[\left(N_n+1\right)\sum_{i=1}^{n-1} f_{i(n-i)}\left[P(\vec{M}_{i(n-i)}^{-1},t)P_{b1}+P(\vec{M}_{i(n-i)}^{-2},t)(1-P_{b1})\right]-N_n\sum_{i=1}^{n-1} f_{i(n-i)}P(\vec{M},t)\right]$$

$$+\frac{1}{2}\sum_{n=2}^{\infty} N_n\sum_{i=1}^{n-1}\frac{f_{i(n-i)}P_{Ci(n-i)}}{1-P_{Ci(n-i)}}[P(\vec{M}^{*1},t)P_{b1}(1-P_1)+P(\vec{M}^{*2},t)(1-P_{b1})P_1$$

$$-P(\vec{M},t)(P_{b1}(1-P_1)+(1-P_{b1})P_1)], \qquad (11)$$

where $P(\vec{M},t)$ is the probability for finding the system in the state $\vec{M}=(N_1,N_2,...,N_n,E_1,E_2)=(\vec{N},E_1,E_2)$ at time t and $P_{b1}=E_1/\tau_1(E_1/\tau_1+E_2/\tau_2)$ is the probability that a given fragmentation event breaks a primary bond. The displaced states $\vec{M}_{ij}^{+1}$, $\vec{M}_{ij}^{+2}$, $\vec{M}_{ij}^{-1}$, $\vec{M}_{ij}^{-2}$, $\vec{M}^{*1}$, and $\vec{M}^{*2}$ are given by

$$\vec{M}_{ij}^{+1}=\left(\vec{N}_{ij}^{+},E_1-1,E_2\right),$$
$$\vec{M}_{ij}^{+2}=\left(\vec{N}_{ij}^{+},E_1,E_2-1\right),$$
$$\vec{M}_{ij}^{-1}=\left(\vec{N}_{ij}^{-},E_1+1,E_2\right),$$
$$\vec{M}_{ij}^{-2}=\left(\vec{N}_{ij}^{-},E_1,E_2+1\right),$$
$$\vec{M}^{*1}=\left(\vec{N},E_1+1,E_2-1\right),$$
$$\vec{M}^{*2}=\left(\vec{N},E_1-1,E_2+1\right).$$

A flow diagram for obtaining the time evolution of the cluster size distribution and bound population is given in reference [27]. It should be noted that k_{11}, d_f, P_1, τ_1 and τ_2 are unknown parameters. However, k_{11} must be the same for all data, since this model states that all collisions lead to the

formation of primary or secondary bonds. In addition, for those systems where the breakup is important, we fixed $d_f = 2.0$; $d_f = 1.8$ was selected when the kinetics practically followed a diffusion limited cluster aggregation (DLCA) regime. Therefore, P_1, τ_1 and τ_2 parameters are free. It should be noted that handling these parameters one may produce the well known DLCA ($P_1 = 1$ and $\tau_1 \rightarrow \infty$, for all τ_2 values; or $\tau_1 \rightarrow \infty$, and $\tau_2 \rightarrow \infty$ for all P_1; or $P_1 = 0$ and $\tau_2 \rightarrow \infty$, for all τ_1), and RLCA (reaction limited cluster aggregation) ($\tau_2 \rightarrow 0$ and $\tau_1 \rightarrow \infty$, being in this case P_1 the sticking probability) models. This was done (not shown here) to make sure the correctness of the algorithm. Hence, this reversible model contains DLCA and RLCA as limiting cases.

We start the discussion for the aggregation of the cationic latex with the three different salts (Figures 3a-c). In particular, for the aggregation under NaCl, which is the salt composed by non-specific ions. These results are shown in Figure 3a, where the corresponding stochastic solutions are represented by lines. The figure also includes the evolution of the total number of clusters (crosses), and the corresponding theoretical prediction. The best fit was obtained for k_{11} = 9.0 10-18 m3/s, $P_1 = 0.35$, $\tau_1 = \infty$, and τ_2 = 2000 s. The obtained agreement is good. It should be mentioned that, for this particular case, a DLCA model having k_{11} = 6.0 10-18 m3/s, i.e. making $P_1 = 1$ and $\tau_1 = \infty$, would also show a poorer but still relatively good agreement with the experimental data. Hence, we should say that the gain produced by considering the extra fitting parameters is not enough to justify them. However, we also observed that $k_{11} = 9.0\ 10^{-18}$ m^3/s improves the matches for all conditions. Since differences between viscosities among all solutions here employed are small, and since our model assumes all collisions to produce bonds (primary or secondary ones), k_{11} must take a single value. Finally, we should also mention that the value employed for the dimmer formation rate constant is just in the boundary of the generally accepted value of 6.0 ± 3.0 10^{-18} m^3/s [34]. This value, which is practically half the Smoluchowsky's one (11.8 10^{-18} m^3/s) can be justified by the presence of hydrodynamic forces. Our k_{11} value suggests that for the very dilute conditions here imposed, hydrodynamic interactions are somewhat less important. Instead, our fit suggests that even for the fastest aggregation kinetics, there is always a small particle-particle potential barrier that impedes reaching a hundred percent of effectiveness between collisions. This belief is supported by the large and repulsive contact force contribution found for the interaction between macroparticles in a model electrolyte solution at small separation distances

[35]. This finding is obtained by means of integral equations and computer simulations, which properly account ion-ion and surface-ion correlations. The force peak appears at a surface-surface distance of a single hydrated counterion, and is due to the simple fact that they resist leaving this preferable place (their adsorption not only diminish the system energy but also decreases entropy by producing more free space for the other bulk ions). This contact force contribution, of course, is not accounted by the classic DLVO theory.

When the aggregation of the cationic latex is induced by the addition of $NaNO_3$, the overall aggregation kinetics strongly slows down. The time evolution of the cluster size distribution for this case is presented in Figure 3b. The fit produces the following parameter values: $P_1 = 0.07$, $\tau_1 = 100000$ s, and $\tau_2 = 600$ s. That is, since the counterion hydrated size has enlarged, the non DLVO contact force contribution peak has moved farther from the particle surfaces where the influence of the van der Waals attractive contribution is smaller, and hence the effective potential barrier enhances. This explains the P_1 and τ_2 decrease. On the other hand, τ_1 has also decreased as compared with the NaCl case, suggesting a weaker bonding of the naked surfaces. This may be related with the many counterions that place very close to the contact point, which are responsible of a still large (not at its maximum) repulsive contact force contribution (see references 35, 36). Hence, these hydrated counterions might modulate the effective depth of the particle-particle potential at contact. This trend is confirmed with the analysis of the aggregation data performed by the addition of NaSCN. The water structure around the SCN^- ions is supposed to be larger, (even larger that that of the NO_3^-), which produce a very slow overall kinetics. In fact, it produces an almost constant cluster size distribution at long times. This behavior makes clear the effect of reversibility in the time evolution. Moreover, the evolution of the small species slightly increases at long times. This effect is surely produced by gravity, as explained in references [37,38]. The model cannot predict such increase and hence, the agreement is not as good as in previous cases. The fitted parameters are $P_1 = 0.04$, $\tau_1 = 25000$ s, and $\tau_2 = 370$ s, which confirm the trends and hypothesis above handled. All the fitting parameters are shown in Table 1.

On the other hand, the time evolution of the cluster size distribution for the aggregation of the anionic latex by the addition of the three salts is shown in Figures 4a-c. It should be noted that anions act as coions in this

case. Therefore, the local concentration at the surface proximities must not as high as that found in the cationic latex. This is why the anionic particles could approach more effectively to each other, which in general makes the average life time of primary bonds higher (see Table 1). Figure 4a shows the aggregation with NaCl. Here, the aggregation is relatively fast, and the fitted parameters read $P_1 = 0.28$, $\tau_1 = 20000$ s, $\tau_2 = 400$ s. As for the case of Figure 3a, this curve may be fitted by a DLCA model, although deviations are even more pronounced since the slow down of the overall kinetics is strong for long times. Additionally, the monomer concentration is always larger than that predicted by DLCA, supporting that breakup is always produced. This explains why this reversible model properly fit the data. In this case, parameters are similar to that found for the cationic latex. The only major difference is that a finite value for τ_1 was found. This can be possible, since now sodium is the counterion instead of chloride.

Data for the aggregation under $NaNO_3$ is given by Figure 4b. It is seen that, as for the cationic latex, the overall kinetics slows down. Hence, coions are influencing the aggregation behavior. The obtained parameters are $P_1 = 0.07$, $\tau_1 = 20000$s, and $\tau_2 = 150$ s. It should be noted that τ_1 is not affected by the change of the coion. This supports our belief that just conterions affects the pair potential at very short interparticle distances. Hence, it seems that only counterions would place close to the adjacent surfaces when they are in touch. However, P_1 and τ_2 are very dependant on the coion, indicating that at slightly larger interparticle distances coions play an important role. The higher its hydrated size by structuring water layers around them, the lower the P_1 and τ_2 values. This, in turn, is interpreted as an increase of the effective potential barrier peak and a shallow secondary minimum. We also expect the potential barrier and the secondary minima to shift towards larger distances, as a result of the larger occupied volume between interfaces due to the interposition of ion-water clusters. Finally, Figure 4c shows the SCN^- results, where the observed trends are definitively confirmed.

IV. Conclusions

The present paper shows experimental evidences of the microscopic duality of Hofmeister effects. Dispersion forces related to ion polarizability together with ion-specific solvation effects have been identified as a major

cause of Hofmeister phenomena. The analysis of aggregation processes of model colloidal suspensions appears to be a useful via to examine these microscopical mechanisms in real systems. The ionic accumulation / exclusion mechanism modifies the electrical potential at the proximities of the particle surface. This modification is translated into differences in the ccc values. Niham et al. [2,5-11] has demonstrated that dispersion forces between the ion and the surface play a major role in the ionic distribution. This is why more polarizable anions accumulate more effectively near the polystyrene surface, reducing the ccc value of positive nanospheres and increasing such a value for negatively charged particles, when results are compared with those obtained with an unspecific anion (i.e. Cl^-). In addition, the analysis of the aggregation kinetics in salt concentrations above the ccc corroborates the existence of short-range structural forces that appear to come from how the ions specifically rearrange the surrounding solvent molecules. The experimental results have been satisfactorily contrasted with a theoretical model capable of reproducing the aggregation kinetics with different degrees of break up. In addition, it must be emphasized the fact that a latex colloidal system showing clear reversible aggregation kinetics is, to the best of our knowledge, reported for the first time in this work. The reversibility has been justified by the presence of ion-water clusters of different size, depending on the anion nature.

Acknowledgements

The authors wish to thank the financial support granted by "FEDER" and "Comisión Interministerial de Ciencia y Tecnología" (CICYT, Spain), projects MAT2003-01257 and AGL2004-01531/ALI and from the "Consejería de Innovación, Ciencia y Tecnología de la Junta de Andalucía" Project FQM 392. In addition, authors are in debt with Dr. Pedro Gea Jódar, who has unselfishly helped to solve some mathematical problems.

References and Notes

[1] See, e.g., P.C. Hiemenz and R. Rajagopalan, Principles of Colloid and Surface Chemistry (Dekker, New York, 1997).

[2] B.W. Ninham, Adv. Colloid Interface Sci. **83**, 1 (1999).

[3] K.D. Collins and M.W. Washabough, Q. Rev. Biophys. **18**, 323 (1985).

[4] M.G. Cacace, E.M. Landau and J.J. Ramsden, Q. Rev. Biophys. **30**, 241 (1997).

[5] B.W. Ninham and V. Yaminsky, Langmuir **13**, 2097 (1997).

[6] M. Böstrom, D.R. Williams and B.W. Ninham, Langmuir **17**, 4475 (2001).

[7] M. Böstrom, D.R. Williams and B.W. Ninham, Langmuir **18**, 6010 (2002).

[8] W. Kunz, P. Lo Nostro and B.W. Ninham, Current Opinion Colloid Interface Sci. **9**, 1 (2004).

[9] M. Böstrom, W. Kunz and B.W. Ninham, Langmuir **21**, 2619 (2005).

[10] M. Böstrom, D.R. Williams and B.W. Ninham, J Phys Chem B **106**, 7908 (2002).

[11] M. Böstrom, D.R. Williams, P.R. Steward and B.W. Ninham, Phys Rev E **68**, 0419021 (2003).

[12] W. Kunz, L. Belloni, O. Bernard and Ninham, J Phys Chem B **108**, 2398 (2004).

[13] See, e.g. J.N. Israelachvili, Intermolecular & Surface Forces (Academia Press, London, 1992), 2nd ed.

[14] R.M. Pashley, J. Colloid Interface Sci. **83**, 531 (1981).

[15] R.M. Pashley, Adv. Colloid Interface Sci. **16**, 57 (1982).

[16] H.K. Christenson, J. Dispersion Sci. Technol. **9**, 171 (1988).

[17] J.A. Molina-Bolívar, F. Galisteo-González and R. Hidalgo-Álvarez, Phys. Rev. E **55**, 4522 (1997).

[18] J.M. López-López, A. Schmitt, J. Callejas-Fernández and R. Hidalgo-Álvarez, *Phys. Rev. E* **69**, 011404 (2004)

[19] N. Fuchs, Z. Phys. **89**, 736 (1934).

[20] A. Fernández-Barbero, M. Cabrerizo-Vílchez and R. Martínez García and R. Hidalgo-Álvarez, Phys. Rev. E **53**, 4981 (1996).

[21] A. Fernández-Barbero, A. Schmitt, M. Cabrerizo-Vílchez and R. Martínez García, Physica A **230**, 53 (1996).

[22] T. López-León, A.B. Jódar-Reyes, D. Bastos-González and J.L. Ortega-Vinuesa, J Phys Chem B **107**, 5696 (2003).

[23] L. Onsager and N.T. Samaris, J. Chem Phys. **2**, 528 (1934).

[24] F.W. Tavares, D. Bratko, H.W. Blanch and J.M. Prausnitz, J Phys Chem B **108**, 9228 (2004).

[25] T. López-León, A.B. Jódar-Reyes, J.L. Ortega-Vinuesa and D. Bastos-González, J Colloid Interface Sci **284**, 139 (2005).

[26] S. Bastea, Phys. Rev. Lett. **96**, 028305 (2006).

[27] G. Odriozola, A. Schmitt, J. Callejas-Fernández, R. Martínez-García, R. Leone and R. Hidalgo-Álvarez, J. Phys. Chem. B **107**, 2180 (2003).

[28] G. Odriozola, A. Schmitt, A. Moncho-Jordá, J. Callejas-Fernández, R. Martínez García, R. Leone and R. Hidalgo-Álvarez, Phys. Rev. E **65**, 031405 (2002).

[29] G. Odriozola, A. Moncho-Jordá, A. Schmitt, J. Callejas-Fernández, R. Martinez-García and R. Hidalgo Álvarez, Europhys. Lett. **53**, 797 (2001).

[30] M. Lattuada, P. Sandkuhler, H. Wu, J. Sefcik and M. Morbidelli, Adv. Colloid Interface Sci. **103**, 33 (2003).

[31] M. Lattuada, H. Wu, P. Sandkuhler, J. Sefcik and M. Morbidelli, CES **58**, 1783 (2004).

[32] M. Lattuada, H. Wu, J. Sefcik and M. Morbidelli, J. Phys. Chem. B **110**, 6574 (2004).

[33] G. Odriozola, R. Leone, A. Schmitt, J. Callejas-Fernández, R. Martínez-García, and R. Hidalgo-Álvarez, J. Chem Phys. **121**, 5468 (2004).

[34] H. Sontag and K. Strenge, Coagulation Kinetics and Structure Formation (Plenum Press, New York, 1987).

[35] F. Jiménez-Ángeles, G. Odriozola and M. Lozada-Cassou, J. Chem. Phys. **124**, 134902 (2006).

[36] G. Odriozola, F. Jimenez-Angeles and M. Lozada-Cassou, Phys. Rev. Lett. **97,** 018102 (2006).

[37] R. Leone, G. Odriozola, L. Mussio, A. Schmitt and R. Hidalgo-Alvarez, Eur. Phys. J. E **7**, 153–161 (2002).

[38] G. Odriozola, R. Leone, A. Moncho-Jorda, A. Schmitt and R. Hidalgo-Alvarez, Physica A **335**, 35, (2004).

CATIONIC AND ANIONIC POLY(N-ISOPROPYLACRYLAMIDE) BASED SUBMICRON-GEL PARTICLES: I. ELECTROKINETIC PROPERTIES AND COLLOIDAL STABILITY

Teresa López-León[1,2], Juan L. Ortega-Vinuesa[1], Delfi Bastos-González[1] and Abdelhamid Elaïssari[2]

[1] *Biocolloid and Fluid Physics Group, Department of Applied Physics, University of Granada, Av. Fuentenueva S/N, 18071 Granada , Spain*

[2] *CNRS bioMérieux, UMR 2714, ESCPE Lyon , 43 Boulevard du 11 Novembre 1918, Villeurbanne Cedex 69616, France*

Abstract

A cationic and an anionic poly(N-isopropylacrylamide) (poly(NIPAM)) microgel latex were synthesized via batch radical polymerization under emulsifier-free conditions. The hydrodynamic properties, colloidal stability and electrokinetic characteristics of these two samples were studied. The hydrodynamic particle size variation was discussed by considering the effect of salinity and temperature on the shrinkage of the thermally sensitive polymer domains. The colloidal stability also depended on temperature and electrolyte concentration. A stability diagram with two well-defined domains (stable and unstable) was obtained. The flow from one domain to the other was fully reversible due to the peculiar (de)hydration properties of the polymer. The electrokinetic behavior, which depends on electrical and frictional properties of the particles, was analyzed via electrophoretic mobility measurements. Results were discussed by considering both: the particle structure dependence on temperature and salinity, and the electric double layer compression. In addition, the electrophoretic mobility data were analysed using Ohshima's equations for particles covered by an ion-penetrable surface charged layer, as well as using another simpler equation for charges located on a hydrodynamic equivalent hard sphere. Differences between the properties of both latexes were justified by the presence of a hydrophilic comonomer, aminoethyl methacrylate hydrochloride (AEMH), in the cationic microgel.

I. Introduction

Microgels are cross-linked polymer particles in the colloidal size range that swell in a good solvents and that have a large number of applications in fields as diverse as medicine biology,[1, 2] industry,[3, 4] or environmental clean-up.[5] One of the most striking properties of microgels is their ability to undergo large volume transitions. This phase change is controlled by competing elastic, solvency, and ionic contributions.[6] Special attention has been paid to temperature-sensitive aqueous microgels since cross-linked poly(N-isopropylacrylamide) (poly(NIPAM)) particles were prepared by Chibante in 1978, and subsequently reported in 1986.[7] Poly(NIPAM) particles exhibit a temperature-induced volume transition. It is generally believed that hydration of the poly(NIPAM) chains originates local ordering in the water molecules around the amide group by means of hydrogen bonding. However, an increase in temperature increases molecular agitation, which in turn causes a disruption of the H-bonding between water and the amide groups. This leads to a break down of local water structure around the poly(NIPAM) chains that triggers hydrophobic attraction among isopropyl groups. This feature causes hydration of polymer chains below the lower critical solution temperature (LCST) and, consequently, microgel particles are swollen, while above the LCST the particles collapse. The LCST for poly(NIPAM) in water is around 32 ° C.[8, 9]

There are numerous publications which refer to the characterization of anionic poly(NIPAM) particles, many of them reviewed by Saunders and Vincent[10] and recently by Pelton.[11] Characterization can involve gel structure, swelling, surface activity, rheology, electrical properties, colloidal stability and interactions with other molecules (surfactants, drugs, proteins, etc). However, characterization of cationic poly(NIPAM) microgels is not so usual in the literature, as these kind of particles have appeared in the past decade. Cationic poly(NIPAM) latexes are usually obtained by adding a positive comonomer together with the NIPAM in the polymerization reaction[12] as well as a cationic initiator, commonly the 2-2'-Azobis-(amidinopropane) di-hydrochloride (V50).[13-15] Some cationic comonomers that can be found in the literature are (in acronyms) MADAP,[16,17] DMAEMA,[18] and DMAPAA,[19] but few authors[14, 15] use the aminoethyl methacrylate hydrochloride (AEMH) employed in the present work.

Some properties of cationic and anionic poly(NIPAM) microgels have been analyzed as a function of salinity, temperature, and ionic specificity.

Specifically, this paper aims to establish the hydrodynamic properties, the electrokinetic characteristics and colloidal stability of a cationic poly(NIPAM) latex, comparing the results with those of a classic anionic one. This analysis is only performed as a function of salinity (using an inert electrolyte, NaCl) and temperature. A second part[20] will be focused on evidencing ionic specificities[21-23] in the two poly(NIPAM) samples working with different electrolytes. It should be noted that Daly and Saunders[24] published an excellent paper in which they studied the electrophoretic mobility and hydrodynamic diameter of anionic polyNIPAM particles, presenting a novel model for polyNIPAM volume phase transitions. Some mobility measurements were analyzed by applying Ohshima's theory. In fact, Ohshima et al.[25,26] previously used such a theory to analyze the mobility of hard polystyrene particles coated by a polyNIPAM shell and obtained promising results. Thus, part of the present work follows in the footsteps of these authors and, subsequently, some results will be compared with those shown in ref 24.

II. Materials and Methods

2.1. Reagents.

N-isopropylacrylamide (NIPAM) from Kodak was recrystallized from a toluene/hexane mixture (60/40). N,N-methylenebisacrylamide (MBA) and aminoethyl methacrylate hydrochloride (AEMH) from Sigma and Polyscience, respectively, were used without further purification. 2-2'-Azobis amidinopropane) di-chloride (V50) from Wako Chemical Group (Germany) was recrystallized from a water/acetone mixture. Potassium persulfate initiator (KPS) and sodium chloride (NaCl) from Sigma (France) were used as received. Water of Milli-Q grade (Millipore, France) was boiled for 2 h under a nitrogen stream before use.

2.2. Poly(NIPAM) Microgel Particles Preparation.

Two poly(NIPAM) microgel latexes were prepared via batch radical polymerization. Polymerizations were performed under emulsifier-free conditions and were carried out in a 250 mL thermostated reactor, round-bottomed four-necked flask, equipped with a glass anchor-shaped stirrer,

Table 1. Masses and volumes of each reactant used in the particle synthesis.

	Water (ml)	NIPAM (mg)	MBA (mg)	KPS (mg)	V50 (mg)	AEMH (mg)
Anionic particles	52	1380	23	33	-	-
Cationic particles	53	1380	23	-	33	77

condenser, thermocouple, and nitrogen inlet. Well boiled and deoxygenated water was introduced under a constant stream of nitrogen. Monomers (NIPAM/MBA for anionic particles or NIPAM/MBA/AEMH for cationic particles) were first dissolved in water and added in the polymerization reactor. The amounts of each reactant used are given in Table 1. The polymerization temperature was set constant at 70 °C; after temperature equilibrium, the initiator (KPS for anionic particles or V50 for cationic particles) dissolved in water was introduced. The agitation rate was 200 rpm during all the polymerization reaction. The duration of the polymerization reaction in both cases was about 4 h.

2.3. Morphology and Size Distribution Analysis.

Transmission electron micrographs (TEM) were carried out using a Hitachi electron microscope (Hitachi S 800, CMEABG at Claude Bernard University Lyon 1, France). This technique was used to determine the particle size and size distribution of dried microgel particles. Photographs from TEM were analyzed with a digitizer (Bolero software, AQ Systems) which supplied the number and weight average diameters (D_n and D_w, respectively):

$$\overline{D_n} = \frac{\sum(n_i \cdot D_i)}{\sum n_i} \qquad \overline{D_W} = \frac{\sum(n_i \cdot D_i^4)}{\sum(n_i \cdot D_i^3)}$$

where n_i is the number of species i with diameter D_i. The polydispersity index (PDI) of the latex particles was defined by the ratio $PDI = \overline{D_w}/\overline{D_n}$. The mean diameter of each latex sample was obtained by analyzing over 500 individual particles.

2.4. Hydrodynamic Particle Size Analysis.

Particle size was measured by quasi-elastic light scattering (QELS) using a Zetasizer 3000HS from Malvern Instruments (Malvern UK). The hydrodynamic diameter of a highly diluted latex dispersion was measured as a function of temperature and salt concentration. The samples were prepared using fresh Milli-Q water. The QELS measurements directly give information about the diffusion coefficient (D) of the particles. The mean hydrodynamic diameter (D_h) can be calculated from the D data by using the Stokes-Einstein equation.

$$D = \frac{kT}{3\pi\eta D_h}$$

where k is the Boltzmann constant, T the absolute temperature, and η the viscosity of the medium.

(a) Swelling Processes. To compare the swelling capacity of the two microgels synthesized (cationic and anionic), the swelling ratio (S_W) was obtained via:

$$S_W = \frac{V}{V_c}$$

where V is the particle volume calculated from the hydrodynamic diameter in a swollen state and V_c in a collapsed state.

(b) Volume Phase Transition Temperature. The volume phase transition temperature (T_{VPT}) was obtained by measuring the hydrodynamic particle size variation induced by changing the medium temperature. As usual, the volume phase transition occurs in a relatively wide range of temperatures, and thus there is a need for a criterion to select the T_{VPT} as objectively as possible. The maximum of the $\delta D_h/\delta T$ curve versus temperature was chosen as the best criterion.

(c) Colloidal Stability. Colloidal aggregation as a function of temperature and salinity were detected by QELS. The poly(NIPAM) microspheres were highly diluted in aqueous solutions at a constant ionic strength and temperature, and then the colloidal stability was analyzed by monitoring the hydrodynamic size as a function of time.

2.5. Electrokinetic Study.

The electrophoretic mobility (μ_e) of microgel particles was measured as a function of salinity and temperature using a Zetasizer 3000HS from Malvern Instrument (Malvern UK). Due to the surface complexity of these microgels, the μ_e data have not been translated into zeta potential values, as usual when working with hard colloidal spheres.

III. Results and Discussions

Since the main objective of this work is to present the colloidal properties and electrokinetic characterization of the elaborated microgel particles, the polymerization kinetics, conversions and the polymer partition between water phase (water soluble polymer) and particles are not considered in this paper. For more information regarding the polymerization aspects, the readers may consult the references.[14, 26]

3.1. Particle Size Analysis.

Transmission electron micrographs of dried microspheres (Figure 1) showed spherical particles with a similar size. As other authors have noted,[7,10,24] a hexagonal arrangement was observed. The ratio between the particle diameter and the average centre-to-centre distance for neighboring particles allows an estimation of the decrease upon particle collapse during the drying process.[7] This ratio was approximately 2.5 for both of our samples, which was in line with the PCS data presented below. The mean diameter and polydispersity index values for dried particles are given in Table 2. The high monodispersity of the latex pools is reflected in the PDI values, which are very close to unity in both cases. The mean diameter obtained by TEM cannot be compared with those values given by QELS measurements, as particles are hydrated in this last case. Nevertheless, both techniques showed that the anionic particles were much bigger than the cationic ones. The lower size of the positive particles can be justified by the presence of the AEMH co-monomer. During the polymerization reaction, the effect of this charged co-monomer on the nucleation step enhances the colloidal stability of the particles that were formed initially and, consequently, reduces the final particle size (compared to the free co-monomer recipe).

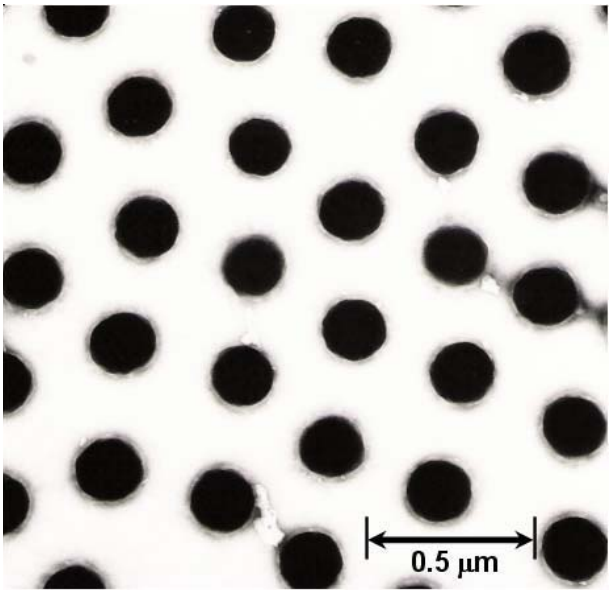

Figure 1. Transmission electron microscopy of cationic poly(NIPAM) microgel particles deposited from water at a temperature below the T_{VPT}.

Table 2. Hydrodynamic particle diameter at 20ŋC and 50ŋC from QELS (D_h); dried particle diameter from TEM (D_{TEM}); swelling ratios (S_W) and polydispersity index (PDI).

	D_h(20 ° C) [nm]	D_h(50 ° C) [nm]	D_{TEM} [nm]	S_w	PDI
Anionic particles	1050	600	780	5.4	1.013
Cationic particles	500	200	230	15.6	1.030

(a) Volume Phase Transitions. The hydrodynamic diameter of the microgel particles was first examined as a function of temperature in a 10^{-3} M NaCl nonbuffered solution. The data are shown in Figure 2. The hydrodynamic particle size for both microspheres decreases with increasing

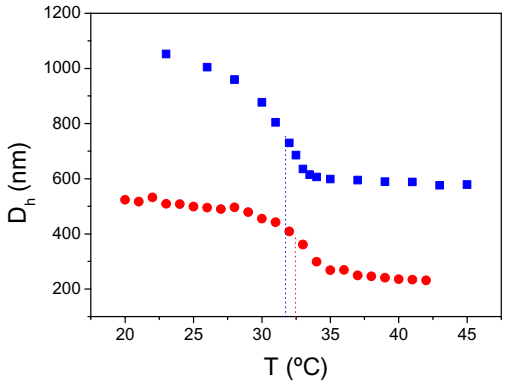

Figure 2. Hydrodynamic particle size of negative (■) and positive (●) microgels as a function of temperature in a 10^{-3} M NaCl solution. Vertical lines have been drawn to guide the eye toward the T_{VPT} values.

temperature (from 20 to 45 °C). Drastic changes in the diameters were observed in the vicinity of the LCST of the pure poly(NIPAM) polymer (32 °C). Therefore, the volume reduction is attributed to the hydrogen bonding disruption between water and the polymer. The temperature that separates the regime wherein water behaves as a good solvent from the other one where it behaves as a poor solvent (T_{VPT}) was calculated from the maximum of the $\delta D_h/\delta T$ curve versus T, using a polynomial fitting. The T_{VPT} values obtained in this way were 31.7 °C and 32.4 °C for the anionic and cationic samples, respectively. This small difference is plausible, and it may be originated by the presence of the water-soluble co-monomer (AEMH) in the cationic particles, which enhanced the hydrophilic character of these particles. This increment in hydrophilicity would make the T_{VPT} shift toward higher values.

The particle swelling ratios (S_W) were calculated from the hydrodynamic volumes at 20 °C (swollen state) and 50 °C (collapsed state), and the data are also shown in table 2. As can be seen, the swelling capacity of the cationic latex is higher than that of the anionic one. Once again, this difference in the swelling behavior may be caused by the effect of the AEMH co-monomer, which, in addition to its tendency to be hydrated, probably alters the internal structure (cross-linking density) during the synthesis of the positive particles.

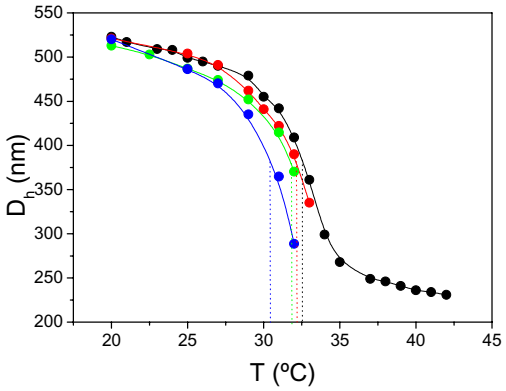

Figure 3. Effect of salt concentration on the volume phase transition of the cationic microgel. 1 mM (●), 10 mM (●), 30 mM (●) and 100 mM (●).

(b) Salt Effect. The effect of salt concentration on the hydrodynamic diameters was studied in two different ways: *i)* on one hand, by studying how the ionic strength shifts the volume phase transition temperature, and *ii)* on the other hand, by observing the effect of salinity on the swelling processes at a fixed temperature.

In the first study, the particles were dissolved in solutions with different NaCl concentrations (from 10^{-3} M to 10^{-1} M). For each salt concentration the diameter evolution versus temperature was registered. Data corresponding to the cationic system are shown in Figure 3. Due to the low colloidal stability of the collapsed particles when increasing both salinity and temperature, it was not possible to determine the particle diameter in some cases. Thus, the curves shown in Figure 3 finished when the aggregation process began. Nevertheless, a clear relationship can be seen between the ionic strength and the volume phase transition temperature: T_{VPT} values decrease when salt concentration is increased. This behavior (which was also observed for the anionic particles) is attributed to the effect of salt on the solubility of poly(NIPAM) chains. The hydration of the ions generates an important competition for the water molecules that hydrate polymer chains. Addition of NaCl to the dispersion produces dehydration of the poly(NIPAM) chains, leading to particle deswelling which becomes more pronounced with increased

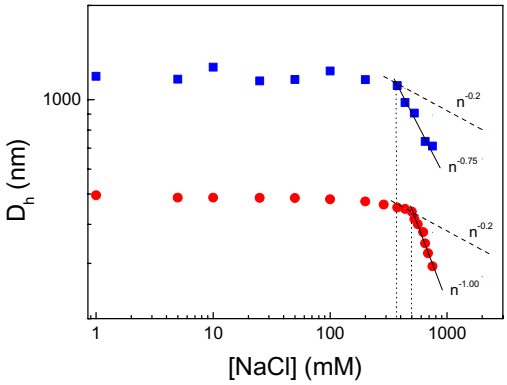

Figure 4. Hydrodynamic particle size of the negative (■) and positive (●) microgels as a function of salt concentration at 25 °C. Dependence on c_s^{-n} has been drawn. Osmotic theory predicts n = 0.2, while the experimental values are higher: n = 1 for the cationic latex and n = 0.75 for the anionic one.

electrolyte concentration.[28] In addition, most recently data suggest that the salting-out of the isopropyl group in NIPAM chains is also due to the increase of the surface tension of the aqueous solution with the addition of salt.[29,30]

Figure 4 shows the second set of experiments, where salinity is increased at constant temperature (25 °C). As can be seen, particle size decreases with an increase in ionic strength, and the shrinkage is more important at high salt concentrations. At low salt concentrations, the hydrodynamic diameter of both microgel particles remains almost unaltered by the medium salinity. However, there is a critical salt concentration from which particle size rapidly diminishes. This concentration is about 330 mM and 480 mM for the anionic and cationic sample, respectively. Once again, this difference is a result of the presence or absence of the hydrophilic AEMH co-monomer in the particles. Competition between ions and polymer chains for hydration becomes more intense if soluble AEMH molecules are interspersed in the poly(NIPAM) skeleton. This is why the salt concentration needed to dehydrate the microgel particles is higher for the positive sample.

Despite the differences, both latex pools present similar behavior that can be justified as follows. (1) The first and most important factor in the decrease in particle size induced by addition of salt is the solubility reduction

of poly(NIPAM) domains. In fact, the LCST of homopoly(NIPAM) is dramatically affected by salinity.[31] As has been discussed above, this is due to the perturbation of the water cage surrounding the isopropyl group caused by the competitive hydration of the added ions. Consequently, poly(NIPAM) chains collapse at lower temperatures in the presence of ions than in free salt solutions.[11, 28, 32](2) In addition, the osmotic pressure of the solution increases for increasing ionic strength. Therefore, water is released from the inside of the microgel by means of an osmotic mechanism, reducing the mean particle diameter.[18, 33] (3) Finally, a hairy particle model also would explain the particle size reduction by salt. If particle surfaces are formed by polyelectrolyte chains, the addition of salt would screen electrostatic repulsion between them, promoting the collapse of the chains.[34]

Although these three mechanisms occur simultaneously, the size variation is mainly given by the first one. At the very least, a simple theoretical treatment can be used to confirm that osmotic pressure increment is not the major driving mechanism. The influence of salt on the osmotic pressure theoretically produces a size decrease with asymptotic behavior:[33,35] $D_h \sim c_s^{-1/5}$, where c_s is the salt concentration, irrespective of the particle network charge. This linear behavior has been also plotted in Figure 4. As shown, the experimental size reduction is much sharper than was theoretically predicted, which demonstrates that a mechanism other than that related to the osmotic pressure must be responsible for the particle deswelling.

3.2. Colloidal Stability as a Function of Salinity and Temperature.

The Hamaker constant of swollen poly(NIPAM) microgels is similar to that of water. Thus, van der Waals attraction forces between these particles embedded in water is almost nonexistent. In addition, polymer tails are extended from the gel structure enhancing steric repulsion which also contributes to the stability of the system. Therefore, colloidal aggregation is possible only for deswollen particles, where the van der Waals attraction becomes significant[28] and the steric barrier disappears. Due to the high sensitivity shown by the volume transition of the poly(NIPAM) particles on both ionic strength and temperature, the colloidal stability was also studied considering these two parameters. In order to elaborate a stability diagram, aggregation was analyzed as described below. Stability was studied at different

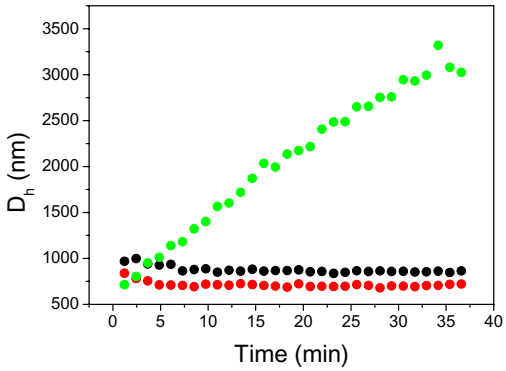

Figure 5. Effect of salt concentration on the hydrodynamic size of the positive particles as a function of temperature, 24ºC (●), 25ºC (●) and 26ºC (●), at constant salt concentration (750 mM NaCl).

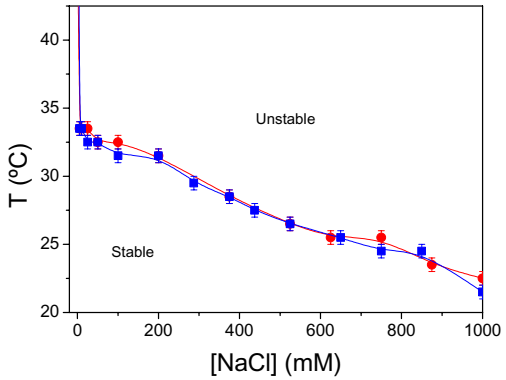

Figure 6. Stability diagram for the negative (■) and positive (●) microgels as a function of salt concentration and temperature.

temperatures keeping the salinity constant. Aggregation was detected by monitoring the temporal evolution of the particles' diameter, as shown in Figure 5. If the system was stable, the particles would continue to be single entities and the hydrodynamic diameter would remain constant. On the contrary, if aggregation took place the average hydrodynamic diameter would increase. So, temperature was carefully changed degree by degree at constant salinity to determine the critical temperature that separated the stable from

the unstable domain. As an example, the positive particles did not aggregate at 25 ˚C in a 750 mM NaCl solution, but they did so at 26 ˚C. This laborious procedure gives the critical flocculation temperature (CFT) and the critical flocculation ionic strength (CFI), which are used to plot the stability diagram shown in Figure 6. It exhibits two domains (stable and unstable). The limit between both domains was found to be similar for the two microgels, indicating that interactions involved in colloidal stability of the two samples are similar. Therefore, aggregation must be governed by the hydration/dehydration characteristic of the poly(NIPAM) chains. At very low salinity concentration, shrunken particles are stable (a potential barrier exists), and aggregation occurs only at high temperature where thermal agitation can make particles overcome the potential barrier. However, at moderate and high salinity, particles aggregate almost at room temperature. A similar study has been recently reported by Daly et al..[28] Although the technique used by these authors to evaluate the stability is different and insufficient data were collected in that case, their results agree with those shown in Figure 6. It is worth highlighting the reversibility of the aggregation process. Aggregates can be completely broken yielding to individual stable particles just by reducing temperature and/or ionic strength. The reversible aggregation of soft particles has also been theoretically justified by means of osmotic and elastic effects.[36] All these results illustrate the complexity of the colloidal stability of poly(NIPAM) particles, where interaction potentials are a combination of van der Waals, electrostatic, steric and hydration contributions.

3.3. Electrokinetic properties as a function of temperature.

The electrophoretic mobility of poly(NIPAM) microgel particles was studied as a function of temperature at a constant salinity (10^{-3} M NaCl) in a non-buffered solution. The data are shown in Figure 7. The positive mobility found for the cationic latex would confirm that the AEMH copolymer was incorporated into the polyNIPAM mesh. Results can be explained taking into account the fact that the motion of microgel particles under an external electric field is the result of a competition between electric and frictional forces.[37] Below 32 ˚C, the electrophoretic mobility of both microgels is found to be around zero, reflecting both the low surface charge density and the high friction coefficient of the swollen particles. However, a dramatic change in the

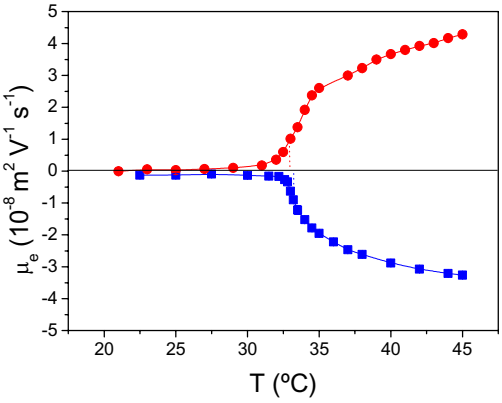

Figure 7. Electrophoretic mobility of the negative (■) and positive (●) microgels as a function of temperature in a 10^{-3} M NaCl solution.

electrophoretic mobility versus temperature was observed above the T_{VPT}. As expected, the absolute values of the electrophoretic mobility increase with an increase in temperature, reflecting the thermal sensitivity of the elaborated particles. This μ_e increment is attributed to three factors: *i)* the increase in the surface charge density due to the reduction in the particle size, *ii)* the enhancement of the local charge concentration on the particles' surface owing to the reorganization of the charged groups, which would tend to be relocated in hydrophilic environments when particles shrink, and *iii)* the frictional coefficient reduction of the particles when they collapse.

A deeper analysis shows that both latexes differ when comparing the hydrodynamic (Figure 2) and the electrophoretic data (Figure 7). The T_{VPT} was defined as the temperature where the $\delta D_h/\delta T$ curve versus T reached a maximum. Daly and Saunders[24] defined an analogous term for the temperature associated to transitions in the electrophoretic mobility, namely, "electrokinetic transition temperature" (T_{ET}). The T_{ET} values obtained from Figure 7 were 33.2 °C and 33.0 °C for the anionic and cationic sample respectively. A difference between the T_{VPT} and T_{ET} values (ΔT) would suggest that the collapse of polyNIPAM microgel particles occurs in different stages.[24] This difference was 1.5 °C and 0.6 °C for the anionic and cationic nanogels respectively. Although the ΔT value for the anionic particles is lower than those reported in refs,[24,38] it triples the value for the cationic sample.

Accordingly to Daly and Saunders,[24] the internal structure of the anionic particles could be heterogeneous, with a core made of high density cross-linked polyNIPAM chains and a lightly cross-linked periphery. This structure would support a volume transition in different stages, which would lead to differences between the T_{VPT} and T_{ET} values. As the ΔT value for the cationic latex is very low, no different transition stages should be expected. Therefore, the cationic nanogel would present a more homogeneous internal structure promoted by the addition of the AEMH copolymer during the particle synthesis. To confirm this statement about hetero or homo-distribution of polymer chains, another simple theoretical treatment can be applied by using both Helmholtz's and Smoluchowski's formula, as reported by Pelton et al.[38] If particles are considered as hard spheres with all the charged groups located at the surface (which is a rather bad approximation for polyNIPAM particles), the electrophoretic mobility can be related to the surface charge density and the hydrodynamic particle radius r_h using the following equation: $\mu_e = -Ne/4\pi\eta\kappa r_h^2$, where κ is the reciprocal Debye length, η the viscosity of the medium, e the elementary charge and N the number of superficial charged groups per particle. The thermal shrinkage of the hydrogel particle leads to an increase in the surface charge density and, subsequently, in the electrophoretic mobility (in absolute value) as experimentally observed. In this way, the electrophoretic mobility was plotted versus r_h^{-2}, and its value was controlled by the incubation temperature, as shown in Figures 8a and 8b. Again, a difference between the anionic and the cationic sample is observed. A single linear dependence is observed for the latter, while a two-step linearity is found for the former. Regions with different linearity represent different stages of collapse. Daly and Saunders[24] found three stages for their anionic polyNIPAM particles. We observe a two stage transition for the anionic sample and only one stage for the cationic one, which must be caused by differences in the internal structure among both samples. The anionic latex must have a heterogeneous distribution, whilst a homogeneous chain distribution would be expected in the cationic sample, as depicted in Figure 9. Finally, the good linearity observed in Figures 8a and 8b allows us to obtain some quantitative information. N can be calculated from the slope of a linear regression. The N value for the cationic latex is 4.6×10^3, whereas that of the anionic particles is equal to 1.0×10^5. A higher N value would be expected for the cationic sample, as it contains charges supplied by the EAMH co-monomer; however, the

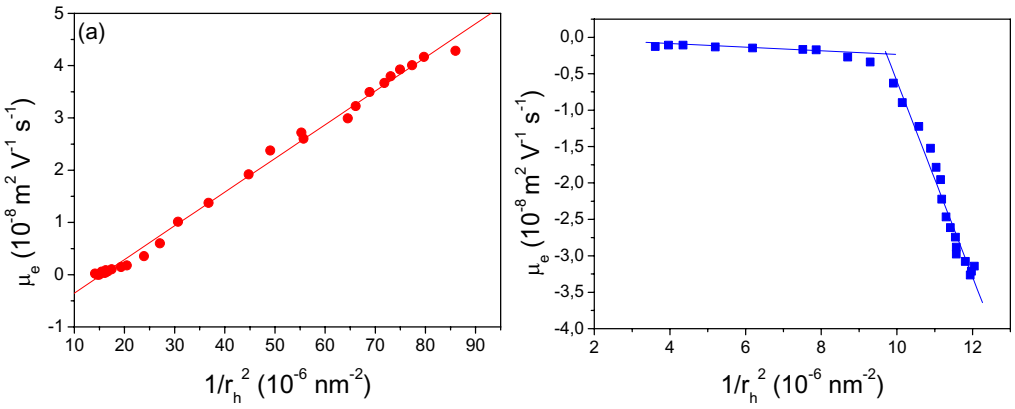

Figure 8. Variation of the electrophoretic mobility of the poly(NIPAM) microgel as a function of r_h^{-2} (r_h is the hydrodynamic particle radius). (a) cationic and (b) anionic latex.

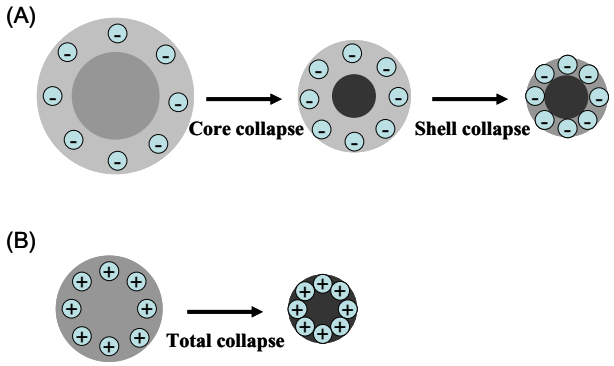

Figure 9. Schematic model for the temperature-dependent deswelling of the (A) anionic and (B) cationic polyNIPAM particles.

results are opposite to those expected. Moreover, these large differences in the number of superficial charged groups can not be justified taking into account the similar values of electrophoretic mobility obtained for both microgels (see Figure 7). Therefore, this theoretical treatment only fits the experimental results qualitatively but not quantitatively.

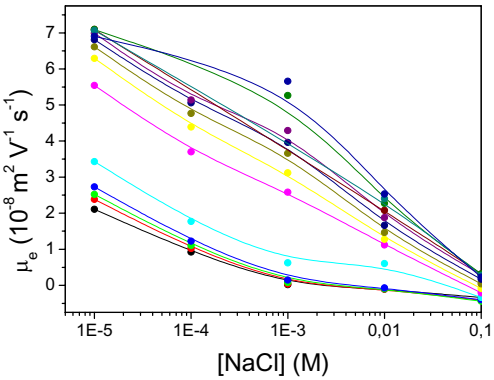

Figure 10. Electrophoretic mobility of the cationic latex as a function of ionic strength. Temperatures were set at the following values: 22.5ºC (●), 25ºC (●), 27.5ºC (●), 30ºC (●), 32.5ºC (●), 35ºC (●), 37.5ºC (●), 40ºC (●), 42.5ºC (●), 45ºC (●), 47.5ºC (●), 50ºC (●), 52.5ºC (●), and 55ºC (●).

3.4. Electrokinetic Properties as a Function of Ionic Strength

The effect of ionic strength on the electrophoretic mobility of the cationic microgel was studied at different temperatures. Data of this positive latex are shown in Figure 10. The mobility exhibited a continuous decrease, irrespective of the temperature value, although different patterns could be observed above and below the T_{VPT}. Below 32 ˚ C the μ_e shows an exponential behavior. The exponential decay disappears as soon as particles begin to collapse. Above the T_{VPT}, there is a linear behavior that changes to a convex curve as temperature increases. The convexity, along with the mobility reduction at high ionic strengths, is a common feature found in hard colloidal particles, which usually show a maximum. This widespread behavior has been often explained by referencing hairy layer models, preferential ion adsorptions or anomalous surface conductances.[39] It should be noted that the convexity becomes more marked at high temperatures where the particle size is reduced to its minimum value, increasing the hardness of the microgel as much as possible.

Nevertheless, a deeper analysis can be made for these soft particles using Ohshima's theory,[40] which is applicable to systems with an

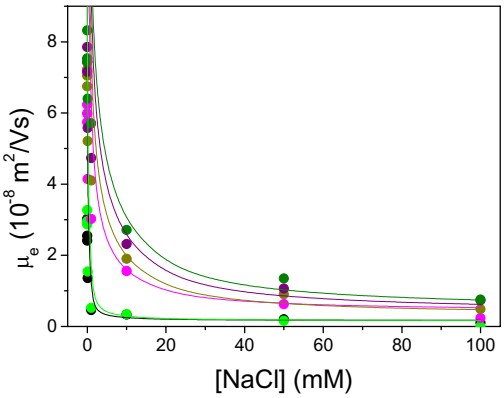

Figure 11. Electrophoretic mobility of the cationic latex as a function of ionic strength. Symbols are experimental data, while lines are theoretical predictions of Ohshima's theory: 22.5°C (●), 27.5°C (●), 35°C (●), 40°C (●), 45°C (●), 50°C (●).

ion-penetrable layer located at the water/particle interface. Ohshima et al.[25,26] successfully applied such a theory for polystyrene particles coated by an adhered polyNIPAM layer. Daly and Saunders[24] also checked the validity of the theory for pure polyNIPAM nanogels. In order to apply this theory to our μ_e data, the logarithmic scale shown in Figure 10 has been converted into a linear scale (see Figure 11). In addition, it must be assumed that the nanoparticles consist of a relatively high cross-linked core and a lightly cross-linked shell that contains most of the charged groups incorporated from the initiator and the water soluble poly(AEMH). The latter is assumed to be equivalent to Ohshima's surface charged layer and has a thickness δ. Provided that δ is larger than the double layer thickness ($1/\kappa$) the following equations can be applied:

$$\mu_e = \frac{\varepsilon_r \varepsilon_0}{\eta} \frac{\Psi_0 / \kappa_m + \Psi_{DON} / \lambda}{1/\kappa_m + 1/\lambda} + \frac{zeN}{\eta \lambda^2}$$

with

$$\Psi_{DON} = \frac{kT}{\upsilon e} \ln \left[\frac{zN}{2\upsilon n} + \left\{ \left(\frac{zN}{2\upsilon n} \right)^2 + 1 \right\}^{1/2} \right]$$

$$\Psi_0 = \frac{kT}{\upsilon e}\left(\ln\left[\frac{zN}{2\upsilon n}+\left\{\left(\frac{zN}{2\upsilon n}\right)^2+1\right\}^{1/2}\right]\right)+\frac{2\upsilon n}{zN}\left[1-\left\{\left(\frac{zN}{2\upsilon n}\right)^2+1\right\}^{1/2}\right]$$

$$\lambda = \left(\frac{\gamma}{\eta}\right)^{1/2}$$

$$\kappa_m = \kappa\left[1+\left(\frac{zN}{2\upsilon n}\right)^2\right]^{1/4}$$

$$\kappa = \left(\frac{2ne^2\upsilon^2}{\varepsilon_r\varepsilon_0 kT}\right)^{1/2}$$

Here, η is the viscosity of the medium, γ is the frictional coefficient of the hydrogel layer, ε_r is the relative permittivity of the solution, ε_0 is the permittivity of a vacuum, e is the electronic charge, Ψ_{DON} is the Donnan potential of the hydrogel layer, and Ψ_0 is the potential at the boundary between the surface layer and the surrounding solution. κ_m is the reciprocal of the double layer thickness within the surface charge layer. N is the density of charged groups of valency z in the surface layer, and n is the density of electrolyte ions of valency υ in the bulk. Thus, zeN represents the density of fixed charges in the hydrogel layer. λ represents the degree of friction experienced by the liquid flowing through the surface layer. $1/\lambda$ is a softness parameter that approaches zero as particle becomes rigid. Finally, k is the Boltzmann constant and T the absolute temperature.

The fitting procedure explained by Daly and Saunders[24] was then used by means of a Mathematica software. Despite having few experimental data in the 10^{-3} M - 10^{-1} M range, where Ohshima's theory works well, the data were properly fitted by the theoretical predictions, as shown in Figure 11. The $1/\lambda$ and N values obtained by the fitting process are plotted as a function of temperature in Figure 12. The softness parameter ($1/\lambda$), which serves as a measure of the flow penetration, decreases with increasing temperature, as

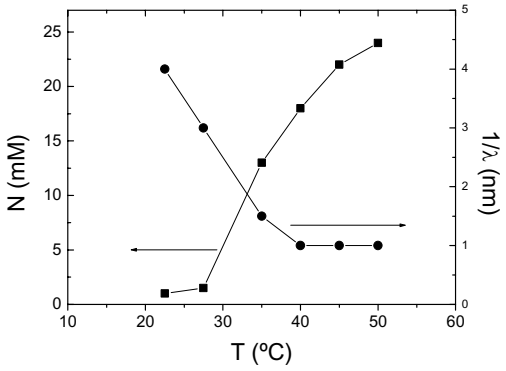

Figure 12. Density of charge groups, N, (■) and softness parameter, 1/λ, (●) of the cationic polyNIPAM sample as a function of temperature.

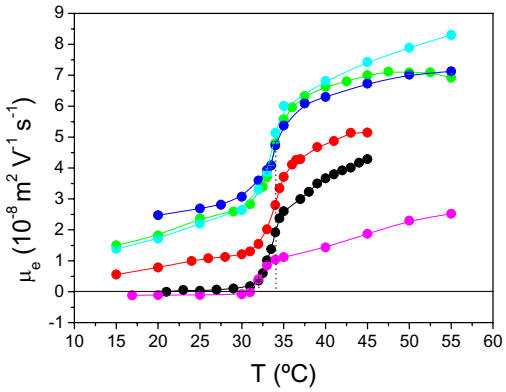

Figure 13. Electrophoretic mobility of the cationic latex as a function of temperature. Vertical lines mark the highest and lowest TVPT. NaCl concentrations were: 10^{-2} M (●), 10^{-3} M (●), 10^{-4} M (●), 10^{-5} M (●), 10^{-6} M (●), and 10^{-7} M (●).

expected. Moreover, the density of charge groups (N) increases with particle collapse, which was also expected. The trends are similar to those obtained by Ohshima et al.[26] and Daly and Saunder.[24] However, our $1/\lambda$ values are lower than those obtained by the last authors working with anionic polyNIPAM microparticles. Therefore, the presence of EAMH co-monomers must originate a special cross-linked structure that gives more rigid nanogels (low $1/\lambda$ values), lower particle size (see Figure 2) and different volume phase transition mechanisms (see Figures 8 and 9) than conventional anionic polyNIPAM formulations.

Finally, mobility versus electrolyte concentration at different temperatures (Figure 10) can be also plotted as μ_e versus temperature varying the ionic strength, as shown in Figure 13. Although both figures (10 and 13) clearly show the mobility diminution for increasing salt concentration, only the latter allow us to observe how the increase in ionic strength makes the T_{ET} shift slightly toward lower values. This feature was already observed with the T_{VPT} (see Figure 3). The drastic relationship between the μ_e and the structure of the particles makes electrophoretic mobility be a powerful tool to evaluate volume transitions of thermal sensitive microgels.

IV. Conclusions

Two highly monodispersed poly(NIPAM) microgel latexes were synthesized via surfactant free polymerization. Swelling/deswelling properties, electrokinetic behavior and colloidal stability have been studied as a function of temperature and NaCl concentration. Cationic particles showed higher T_{VPT} than that of the anionic latex. The presence of a hydrophilic co-monomer (AEMH) in the formulation of the positive microgel produces an increase in the solubility of the thermally sensitive polymer domains. For the same reason, the amount of salt needed to dehydrate the polymer chains, and subsequently shrink the particles, was higher in the cationic sample. The colloidal stability was very sensitive to temperature and ionic strength. A stability diagram with two clearly defined domains (stable and unstable) was obtained. Aggregation was fully reversible and passing from one domain to another was possible simply by controlling the temperature and/or the electrolyte concentration. Finally, electrophoretic mobility measurements have become a useful tool to obtain some information about the structure of anionic and cationic polyNIPAM particles. The former seem to present a heterogenic distribution of polyNIPAM chains with a compact core and a soft external layer, whilst the cationic sample seems to be made of a more rigid and homogeneous mesh.

Acknowledgements

The authors acknowledge the financial support from projects MAT2003-01257 and AGL2004-01531/ALI of the Comisión Interministerial de Ciencia y Tecnología (CICYT), Spain. The authors also thank the bioMérieux Company for research support in the form of chemicals and equipments and Dr. Jhunu Chatterjee for his critical reading of the manuscript and his suggestions.

References and Notes

(1) Peppas, N. A. Curr. Opin. Colloid Interface Sci. 1997, 2, 531.

(2) Kajiwara, K.; Rossmurphy, S. B. Nature 1992, 355, 208.

(3) Quadrat, O.; Snuparek, J. Prog. Org. Coatings 1990, 18, 207.

(4) Sawai, T.; Yamazaki, S.; Ikariyama, Y.; Aizawa, M. J. Electroanal. Chem. 1991, 297, 297.

(5) Morris, G. M.; Vincent, B.; Snowden, M. J. J. Colloid Interface Sci. 1997, 190, 198.

(6) English, A. E.; Tanaka, T.; Edelman, E. R. J. Chem. Phys. 1996, 125, 10606.

(7) Pelton, R.; Chibante, P. Colloid Surf. 1986, 20, 247.

(8) Heskins, M.; Guillet, J. E. J. Macromol. Sci. Chem. 1968, A2, 1441.

(9) Schild, H. G. Prog. Polym. Sci. 1992, 17, 163.

(10) Saunders, B. R.; Vincent, B. Adv. Colloid Interface Sci. 1999, 80, 1.

(11) Pelton, R. Adv. Colloid Interface Sci. 2000, 85, 1.

(12) Hahn, M.; Gornitz, E.; Dautzenberg, H. Macromol. 1998, 31, 5616.

(13) Pinkrah, V. T.; Snowden, M. J.; Mitchell, J. C.; Seidel, J.; Chowdhry, B. Z.; Fern, G. R. Langmuir 2003, 19, 585.

(14) Meunier, F. ; Elaïssari, A.; Pichot, C. Polym. Adv. Technol. 1995, 6, 489.

(15) Nabzar, L.; Duracher, D.; Elaïssari, A.; Chauveteau, G.; Pichot, C. Langmuir 1998, 14, 5062.

(16) Bokias, G.; Hourdet, D. Polymer 2001, 42, 6329.

(17) Charalambopoulou, A. ; Bokias, G.; Staikos, G. Polymer 2002, 43, 2637.

(18) Zha, L.; Hu, J.; Wang, C.; Fu, S.; Luo, M. Colloid Polym. Sci. 2002, 280, 1116.

(19) Sakohara, S.; Nishikawa, K. J. Colloid Interface Sci. 2004, 278, 304.

(20) López-León, T.; Ortega-Vinuesa, J. L.; Bastos-González, D.; Elaïssari, A. J. Phys. Chem.B 2005, submitted.

(21) Collins, K. D.; Washabaugh, M. W. Q. Rev. Biophys. 1985, 18, 323.

(22) Cacace, M. G.; Landau, E. M.; Ramsden, J. J. Q. Rev. Biophys. 1997, 30, 241.

(23) Lyklema, J. Mol. Phys. 2002, 100, 3177.

(24) Daly, E.; Saunders, B. R. Phys. Chem. Chem. Phys. 2000, 2, 3187.

(25) Ohshima, H; Makino, K; Kato, T.; Fujimoto, K.; Kondo, T.; Kawaguchi, H. J. Colloid Interface Sci. 1993, 159, 512.

(26) Makino, K.; Yamamoto, S.; Fujimoto, K.; Kawaguchi, H.; Ohshima, H. J. Colloid Interface Sci. 1994, 166, 251.

(27) Elaïssari, A. In Handbook of Surface and Colloid Chemistry; Birdi, K.S., Ed.; CRC Press: Boca Raton, 2002; Chapter 12.

(28) Daly, E.; Saunders, B. R. Langmuir 2000, 16, 5546.

(29) Boström, M.; Williams, D. R. M.; Ninham, B. W. Langmuir 2001, 17, 4475.

(30) Boström, M.; Kunz, W.; Ninham, B. W. Langmuir 2005, 21, 2619.

(31) Duracher, D. "Elaboration de latex hydrophiles et thermosensibles et leur utilisation comme supports pour l'immobilisation controlée de protéines". Ph.D. Dissertation. Université Claude Bernard-Lyon 1. 1999.

(32) Park, T. G.; Hoffman, A. S. Macromolecules 1993, 26, 5045.

(33) Fernández-Nieves, A.; Fernández-Barbero, A. de las Nieves, F. J. J. Chem. Phys. 2001, 115, 7644.

(34) Seebergh, J. E.; Berg, J. C. Colloid Surf. A 1995, 100, 139.

(35) Pincus, P. Macromolecules 1991, 24, 2912.

(36) Fernández-Nieves, A.; Fernández-Barbero, A.; Vincent, B.; de las Nieves, F. J. Langmuir 2001, 17, 1841.

(37) Fernández-Nieves, A.; Fernández-Barbero, A.; de las Nieves, F. J.; Vincent, B. J. Phys.: Condens. Matter 2000, 12, 3605.

(38) Pelton, R. H.; Pelton, H. M.; Morphesis, A.; Rowell, R. L. Langmuir 1989, 5, 816.

(39) Hidalgo-Álvarez, R.; Martín, A.; Fernández, A.; Bastos, D.; Martínez, F.; de las Nieves, F. J. Adv. Colloid Interface Sci. 1996, 67, 1.

(40) Ohshima, H. Adv. Colloid Interface Sci. 1995, 62, 189.

HOFMEISTER EFFECTS ON PNIPAM MICROGEL PARTICLES: MACROSCOPIC EVIDENCE OF ION ADSORPTION AND CHANGES IN WATER STRUCTURE

T. López-León[a],[b], A. Elaïssari[b], J. L. Ortega-Vinuesa[a] and D. Bastos-González [a]

[a] *Dcolloid and Fuid Pysics Goup, Dpartment of Applied Pysics, Uiversity of Ganada.*

[b] *CNSbioMéieux, MR21, ESN de Lyon, 46allé d'Italie, 0 Lyon Cedex 07, Fance.*

Abstract

The term "Hofmeister effects" is broadly used to refer to ionic specificities in many different physical, chemical and biological phenomena. The origin of this ionic specificity has to be sought in two interdependent microscopic sources: i) the peculiarities of the solvent structure near surfaces and around the ions, and ii) specific ion adsorption-exclusion mechanisms near a surface. In this work, Hofmeister effects on Poly(N-isopropylacrylamide) (poly(NIPAM)) based microgels are examined. Poly(NIPAM) particles are thermally-sensitive microgels exhibiting volume phase transitions with temperature. This temperature sensitive system seems to be suitable to independently observe the two microscopic sources of Hofmeister effects. On the one hand, volume phase transition, evaluated by photon correlation spectroscopy (PCS), gave information about how the presence of ions changes water structure around the poly(NIPAM) chains. On the other hand, electrokinetic studies showed relevant data about ionic adsorption-exclusion phenomena at the polymer surface.

I. Introduction

Hofmeister effects, series, or sequences refer to the relative effectiveness of anions or cations in specifically modifying diverse properties of a wide range of phenomena: cloud points of non-ionic surfactant, critical micellar concentrations (CMC), solubility of salts, surface tensions, pH measurements, zeta-potentials (ζ), molecular forces, colloidal stability, protein solubility, fluid viscosity, etc. Hofmeister effects are truly universal, being present in biological, biochemical, colloidal, and surface sciences. Although they were discovered over a century ago,[1] interest in these specific ionic effects is currently growing, as shown by the numerous papers and reviews published recently[2,3] and even a special issue[4] focusing on these effects.

Despite that Hofmeister phenomena are ubiquitous in physical and biochemical systems, their microscopic origin has not yet been completely understood. In fact, the present theoretical framework that underlies physical chemistry and colloid and surface chemistry is unable to solve the complex Hofmeister puzzle, in which different situations caused by ion-water, surface-water, surface-ion, polyelectrolyte-water, water-water, polyelectrolyte-ion, etc., need to be taken into account. What seems to be generally accepted is that they come from i) changes in water structure (around ions and solvated surfaces), and ii) specific ion adsorption-exclusion mechanisms at interfaces.[5] Both of these are interrelated and seem impossible to disentangle. Despite the inherent complexity of the problem, some researchers have already made major progress in theoretically explaining Hofmeister effects. The most complete and tested current theory has been developed by Ninham et al.[6-14], who argue that when the dispersion forces acting between ions and interfaces are treated on the same level as electrostatics in a non-linear double-layer theory, many of the experimentally observed specificities can be explained. Dispersion forces arise from considering the totality of electrodynamic fluctuation forces (besides no specific electrostatic forces) acting on ions due to the presence of a surface. One of the most determinant parameters associated with these forces is the ion polarizability, which has been correlated with Hofmeister-related quantities. Nevertheless, Hofmeister effects cannot be completely understood exclusively in terms of ion polarizability. Basically, this is because water cannot be treated as an unperturbed medium that simply hosts the dissolved entities. The connection between the Hofmeister series and structural rearrangements in the water network induced by ions near interfaces

has been evidenced by many authors.[1,2,15-17] Traditionally, electrolytes have been classified according to their ability to alter water structure: ions that enhance water hydrogen-bonded structure are known as structure makers or kosmotropics, whereas ions that make this structure looser are called structure breakers or chaotropes. In general, the former are ions of small size and high charge, while the latter present opposite characteristics. The ion specificity is attributed to a nonlocal bulk effect that is determined by processes and energies of ion solvation. Although there is no generally accepted quantitative measure of this quality, the Jones-Dole coefficients are often used as indicative of the structure making/breaking character.[16]

Temperature-sensitive aqueous microgels based on poly(N-isopropylacrylamide) (herein called PNIPAM) form a noteworthy subset of polymer colloids.[18] Below the lowest critical solution temperature (LCST) of the polymer, water behaves as a good solvent for PNIPAM, and the microgel particles are water-swollen. In this state, the system exhibits properties typical of polymers in solution: the microgel behavior is controlled by the solvent-polymer interactions. Above the LCST, water becomes a poor solvent for PNIPAM and particles shrink. In the collapsed state the system displays properties typical of hard-sphere colloidal systems: particle surface properties (in particular, surface charge coming from the initiator used in the synthesis) determine the microgel behavior. This dual character of PNIPAM can be exploited to investigate concomitantly the two mechanisms underlying the Hofmeister effects. Changes in the polymer network configuration - manifested macroscopically by the (de)swelling of the particles - are very sensitive to rearrangements of the water structure caused by ions. Otherwise, interfacial properties such as particle surface potential - reflected in the electrophoretic mobility of the particles - are highly affected by ion accumulation/exclusion mechanisms. Hofmeister effects on poly(NIPAM) particles have been reported in some recent publications.[19-21] However, these works have focused mainly on the swelling and colloidal stability properties of the particles, and nearly no attention has been paid to the electrokinetic behavior of the system. Therefore, differences observed among ions have usually been ascribed to the capability of the electrolytes to interact with water. In this work, we show new experimental evidence of the Hofmeister effects on these thermally-sensitive microgels by means of electrokinetic studies. This property, extremely sensitive to ion effects,[22-24] revealed the existence of specific ion accumulation-exclusion processes at the particle surface. In fact, valuable information concerning the

microscopic origin of the ion specificity was gained from analyzing in parallel the effect of electrolytes on the polymeric structure (microgel swelling) and the particle surface charge (electrophoretic mobility).

II. Experimental section

2.1. Reagents.

NaCl, $NaNO_3$, NaSCN, $Ca(NO_3)_2$, and NH_4NO_3 salts were of analytical grade and purchased from different firms: Merck, Sigma and Scharlau. Water was of Milli-Q quality. N-isopropylacrylamide (NIPAM) from Kodak was recrystallized from toluene/hexane mixture (60/40). N,N-methylenebisacrylamide (MBA) and aminoethyl methacrylate hydrochloride (AEMH) from Sigma and Polyscience, respectively, were used without further purification. 2-2 -Azobis-(amidinopropane) di-chloride (V50) initiator from the Wako Chemical Group (Germany) was recrystallized from a water/acetone mixture. Potassium persulfate initiator (KPS) from Sigma was used as received. Non-buffered solutions were used throughout.

2.2. Poly(NIPAM) microgel particles preparation.

Two pools of poly(NIPAM) particles with different signs of surface charge were used. These latexes were prepared via batch radical polymerization under emulsifier-free conditions. Polymerizations were carried out in a 250 ml thermostated reactor, a round-bottomed four-necked flask, equipped with a glass anchor-shaped stirrer, condenser, thermocouple and nitrogen inlet. Well boiled and deoxygenated water was introduced under a constant stream of nitrogen. Monomers were first dissolved in water and added to the polymerization reactor. The polymerization temperature was set at a constant 70 ºC. After reaching temperature equilibrium, the initiator dissolved in water was introduced. The agitation rate was 200 rpm during all of the polymerization reaction. The duration of the polymerization reaction in both cases was about 4 hours.

Cationic poly(NIPAM) particles were obtained by adding a positive comonomer (AEMH) together with the NIPAM in the polymerization reaction as well as a cationic initiator (V50). As a result, cationic particles have amine and amidine groups on the surface. Conversely, the negative charge of the

anionic poly(NIPAM) particles only comes from the initiator (KPS) which gave rise to sulphate groups on the particle surface. In both cases MBA was used as a cross-linking agent. The characterization of both samples is detailed in greater depth in reference.[27]

2.3. Hydrodynamic particle size analysis.

Particle size was measured by photon correlation spectroscopy (PCS) using the Zetasizer 3000HS from Malvern Instruments (Malvern, UK). The hydrodynamic diameter of a highly diluted latex dispersion was measured as a function of temperature and salt concentration. The samples were prepared using fresh Milli-Q water. The mean hydrodynamic diameter (D_h) was calculated from the diffusion coefficient measurement by using the Stokes-Einstein equation.

$$D = \frac{kT}{3\pi\eta D_h} \tag{1}$$

where D is the diffusion coefficient, k the Boltzmann constant, T absolute temperature, and η the viscosity of the medium.

2.4. Electrokinetic study.

The electrophoretic mobility of microgel particles was measured as a function of salinity, salt nature and temperature using the Zetasizer 3000HS from Malvern Instrument (Malvern UK). Depending on the surface complexity, the measured electrophoretic mobilities (μ_e) cannot be easily converted to ζ-potential as is the case with classic colloids, and thus, μe data but not ζ-potential values are given.

III. Results and discussion

Five different species were chosen for this study: NaCl, NaSCN, $NaNO_3$, $Ca(NO_3)_2$, and NH_4NO_3. As NaCl, NaSCN and $NaNO_3$ are balanced by the same cation (Na^+) these salts allowed us to compare the specific effect of the different anions. Likewise, NaNO3, $Ca(NO_3)_2$, and NH_4NO_3 salts share the same anion (NO_3^-) and thus they were used to compare ion specificities among cations. It has been experimentally shown that the specific effect of any

ion depends on two factors: the sign of charge and the hydrophobic/hydrophilic character of the particle surface.[23] Both aspects can be readily regulated thanks to the versatility of the thermally-sensitive microgels based on PNIPAM formulations. These systems enable us to control the sign of charge of the particles by using different ionic initiators and co-monomers during polymerization,[26,27] and the hydrophilic/hydrophobic character of the polymer just by varying temperature. In this work, a cationic and an anionic PNIPAM microgel have been employed to investigate in parallel the effect of electrolytes acting either as co-ions or counter-ions. Temperature also ranged from 20 ºC to 45 ºC. Four different sets of experiments were performed. First, the effect of temperature was studied in relation to the hydrodynamic diameter of the PNIPAM particles. The experiments were performed at a constant salt concentration (0.01 M) using different electrolytes. In the second set of experiments, electrophoretic mobility was measured under the same conditions. The third and fourth sets were performed at constant temperature but varying the salt concentration: the hydrodynamic diameter versus electrolyte concentration was first studied, and subsequently, the electrophoretic mobility as a function of salinity.

3.1. The effect of temperature on the swelling ability of the microgels.

It is well established that the hydration of PNIPAM results from the formation of water cage-like structures surrounding the hydrophobic groups of the polymer.[28] These structures are stable at room temperature but progressively destabilize as temperature rises. The polymer collapses when, eventually, the thermal energy (entropic contribution) overcomes the favorable enthalpy changes associated with the formation of hydrogen bonds between polymer and solvent. These structural changes are macroscopically manifested through changes in the microgel size. Figure 1 shows the effect of temperature on the hydrodynamic diameter of both the anionic and cationic PNIPAM microgels in the presence of different salts (0.01 M). The typical decrease in hydrodynamic diameter upon raising temperature was observed with both microgels. As expected, the volume phase transition temperature (TVPT) of the microgel particles was found around the LCST of linear poly(NIPAM) chains in water - that is 32 ºC.[25] Nonetheless, the presence of salt induced

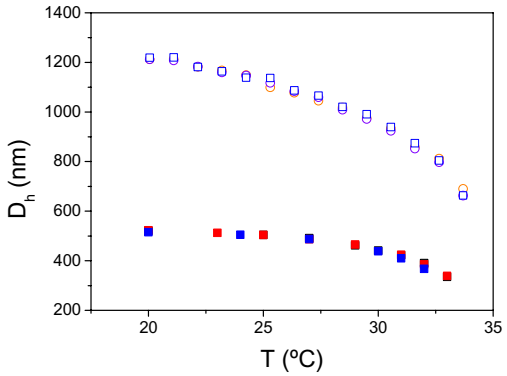

Figure 1. Hydrodynamic particle size as a function of temperature at ionic strength equal to 0.01 M. Cationic microgel (■) NaCl, (■) $NaNO_3$, (■) NaSCN and anionic microgel (□) $NaNO_3$, (○) $Ca(NO_3)_2$, (○) NH_4NO_3.

aggregation as soon as particles collapsed. This is why the D_h data for different ions were found when comparing their respective deswelling curves. This result suggests that, at this low salt concentration, the water cage-like structures responsible for the polymer hydration are not specifically affected by the presence of electrolytes in solution - or at least if structural changes exist they are not substantial enough to be detected by PCS measurements. Analogous experiments were performed by adding $Ca(NO_3)_2$, NH_4NO_3 and $NaNO_3$ to the cationic latex, and NaCl, $NaNO_3$ and NaSCN to the anionic sample. The results (data not shown) showed the same tendency: no significant differences were observed among the various ions at this low ionic strength.

3.2. The effect of temperature on electrokinetic properties.

The electrophoretic mobility (μ_e) of both microgels was measured as a function of temperature for the different electrolytes (0.01 M). The data gathered are shown in Figures 2a-b and 3a-b. Electrophoretic mobility was drastically affected by the medium temperature. Below the TVPT, the particles are in a swollen state, their surface-charge density is very small, frictional forces are high, and consequently μ_e is close to zero. The microgel deswelling caused by the higher temperature leads to an increase in the absolute value of μ_e. The temperature rise causes a progressive size reduction

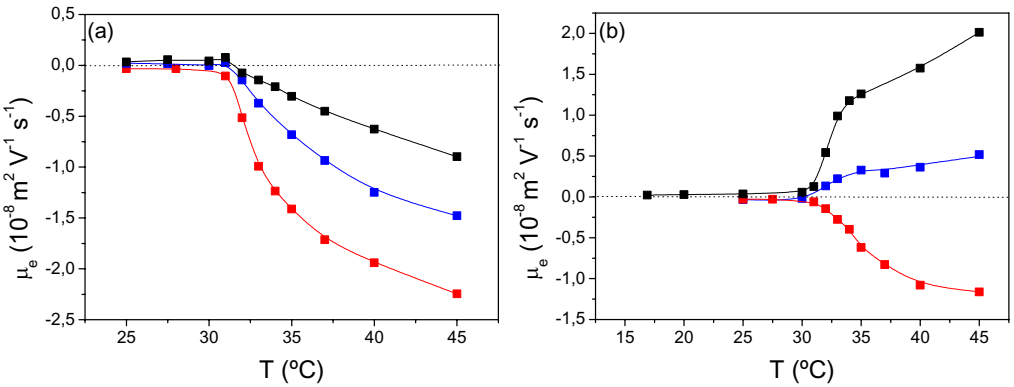

Figure 2. Electrophoretic mobility as a function of temperature at ionic strength equal to 0.01 M. **(a)** anionic microgel **(b)** cationic microgel. (■) NaCl, (■) NaNO3, (■) NaSCN.

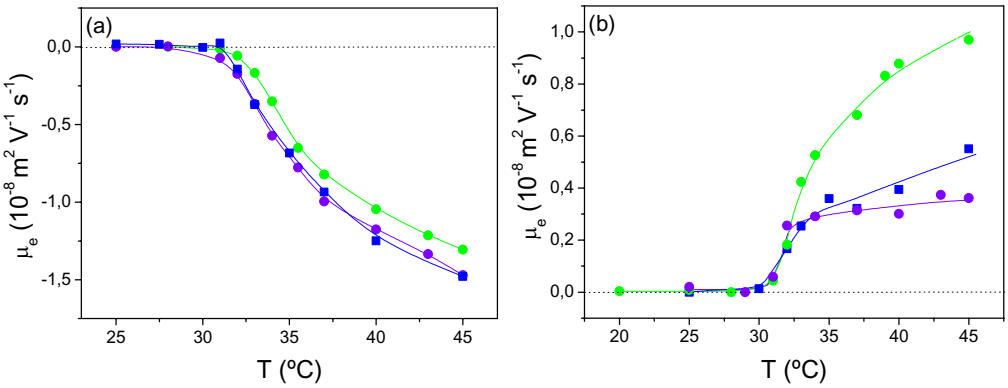

Figure 3. Electrophoretic mobility as a function of temperature at ionic strength equal to 0.01 M. (a) anionic microgel (b) cationic microgel. (■) $NaNO_3$, (●) $Ca(NO_3)_2$, (●) NH_4NO_3.

of the PNIPAM microgel, augmenting the particle surface-charge densities. This greater surface-charge density, together with the reduction of frictional forces, contributes to the increase in particle mobility.[18, 27, 25]

The most striking result, however, is the marked dependence of μ_e on the type of added electrolyte, even working at relatively low ionic strength. This finding contrasts with that shown in the previous section, where no ion specificity regarding particle diameter was detected at the same salt concentration (Fig. 1). Worthwhile observations can be inferred from these results. As mentioned above, the electrophoretic mobility stems from a competition between electrical and frictional forces. Since particle size seems not to be affected by the nature of the salt in this concentration range (Fig. 1), the frictional forces must be constant. Hence, only changes in the electrical state of the particles would be responsible for the differences observed in μe, or equivalently, in ζ-potential. Therefore, electrokinetic results suggest the existence of an ionic accumulation-exclusion mechanism at the particle surface. This argument will be reinforced by later results.

Figure 2a-b shows the effect of anions on both microgels. In the case of the anionic microgel (Fig. 2a) we find that the increase in the μ_e (in absolute value) is higher in the sequence $SCN^- > NO_3^- > Cl^-$. This follows the characteristic relative rank ordering of the Hofmeister series for anions:

$$Citrate^{3-} > SO_4^{2-} > PO_4H^{2-} > F^- > CH_3COO^- > Cl^- > Br^- > I^- > NO_3^- > ClO_4^- > SCN^-$$

where strongly hydrated anions (kosmotropes) are on the left and weakly hydrated anions (chaotropes) are on the right. Accordingly, the more chaotropic the anion, the more negative the values of electrophoretic mobility found, suggesting that chaotropic ions tend to accumulate at the PNIPAM/water interface, making the ζ-potential of the microgel particles more negative. This is consistent with the widely observed ion accumulation on hydrophobic surfaces.[2,22,29] The cationic microgel (Fig. 2b), showed a similar trend. Nevertheless, when the surface was negative the anion accumulation boosted the electrophoretic mobility of the particles, whereas the same phenomenon caused μe to diminish when particles were positive. In this sense, opposite Hofmeister sequences resulted with the cationic and anionic sample. Surprisingly, the accumulation of SCN^- was so strong in the cationic PNIPAM that it even reversed the sign of the mobility, giving negative values

despite the positive surface charge of the particles. Direct and inverse Hofmeister sequences depending on the surface sign of the charge have also been reported in other systems.[5,13,30,22] For example, similar patterns were found in cationic and anionic polystyrene latexes,[22] although in these cases specific ion effects on μ_e were important only in the positive particles. Thus, PNIPAM microgel particles appear to be more sensitive than hard nanospheres with respect to Hofmeister effects induced by anions.

The ion-accumulation phenomena observed in the μ_e-experiments can be interpreted through the theory of Ninham et al.[6-14] This theory takes into account the dispersion forces acting between ions and surfaces, which significantly alter the usual Poisson-Boltzmann ion distribution. The dispersion potential acting on an ion due to an interface depends on both surface and ion characteristics, this being highly specific. Schematically:[7]

$$U_{disp}(x) \approx \frac{\left(n_w^2 - n_s^2\right)}{8x^3}\alpha^*(0)h\nu_i \qquad (2)$$

where n_s and n_w are, respectively, the refractive index of the substrate and water, $\alpha^*(0)$ is the static excess polarizability of the ion in water, and hνi is the ionization energy of the ion in water. Within this theoretical framework, the specific ion accumulation - or exclusion depending on the relative values of n_w and n_s, as well as the plus/minus sign of $h\nu_i$ and $\alpha^*(0)$ - at a given interface can be explained on the basis of the different polarizabilities of the electrolytes. For the species studied and the PNIPAM/water interface, dispersion forces attract (involve ion accumulation) since the refraction index of the PNIPAM is above that of the water and the ionization energy and excess polarizability of the electrolytes are positive. The $\alpha^*(0)$ values corresponding to the anions analyzed are: $\alpha^*(0)_{SCN^-} = 6.61$ Å^3, $\alpha^*(0)_{NO_3^-} = 4.30$ Å^3 , $\alpha^*(0)_{Cl^-} = 3.59$ Å^3.[5] The SCN^- is more polarizable than NO_3^- or Cl^-, and hence, it is more attracted towards the colloidal surface than the other anions, thereby increasing its local concentration more effectively near the interface. This ion accumulation makes μ_e increase for negative particles and decrease for positively charged ones. In conclusion, the specific polarizability values give the sequences observed experimentally. Moreover, this theory is able to explain the reversal of Hofmeister sequences observed for different materials having different charge signs and refractive indexes.[12]

The influence of cations on μ_e was also studied, adding separately $Ca(NO_3)_2$, NH_4NO_3 and $NaNO_3$ at constant ionic strength (0.01 M). The results are shown in Figures 3a and 3b. The first noteworthy result is that the effect of cations was smaller than that of anions. This is a widespread feature observed in Hofmeister phenomena, which are dominated by anion effects.[2,3,5] However, some differences in mobility values were also found among the cations as the temperature rose and particles shrank. For the anionic microgel (Fig. 3a), the μ_e values corresponding to the Na^+ and NH_4^+ ions were almost identical throughout the temperature range studied. The lower mobility detected with the Ca^{2+} could be attributed to its double charge, and hence, to a better ability to screen the particle surface charge –note that the double valency of the Ca^{2+} is especially determinant when it acts as counterion. Regarding the cationic microgel (Fig. 3b) the differences in μ_e originated by the Na^+ and NH_4^+ were not conclusive, either, since the divergence between the respective curves became meaningful only at one point (that corresponding to the highest temperature). By contrast, despite its double valency, the μ_e values found with the Ca^{2+} at T > TVPT were clearly higher to those measured with the other cations, implying the existence of specific adsorption. Generally, dispersion forces felt by cations are much weaker that those felt by anions due to the lower excess polarizability of cations ($\alpha^*(0)_{NH_4^+} = 1.86 Å^3$, $\alpha^*(0)_{Na^+} = 0.15 Å^3, \alpha^*(0)_{Ca^{2+}} = 0.47 Å^3$). [5,31] Because of this feature, together with the low salt concentration employed, dispersion forces were not determinant in these experiments, especially with monovalent cations. This would account for the lack of specificity displayed by Na^+ and NH_4^+. In the case of the Ca^{2+}, ion specificity cannot be ascribed simply to ion polarizability. Certainly, results for double-charged ions must be carefully considered because in most cases the parameters that help to explain the Hofmeister effects can hardly be compared among ions of different valence.[5,32] According to the excess polarizability of the Ca^{2+}, the accumulation of this cation at the PNIPAM/water interface should be comparable to that of the other cations. However, due to its double valence, even weak ion accumulation has a stronger influence on the particle surface potential. This would partially explain the apparent higher adsorption of Ca^{2+}. In addition, calcium might also augment its ability to approach the poly(NIPAM) surface by means of the strong binding affinities of divalent cations for amide groups (similar to those found in peptide bonds or in the poly(NIPAM) backbone).[33] This interaction is attributed to the large dipole moment of the amide group, which promotes a cation binding at or near the

oxygen atom.[34] These two factors are presumably the cause for the mobility data found with Ca^{2+}.

Finally, the extreme sensitivity of μ_e to the nature of salt must be due to the low charge density of the particle surface. The specific ion effects on colloidal systems usually become appreciable at relative high salt concentrations (typically over 0.1 M). In theory, this happens when Coulomb interactions are screened and dispersion forces responsible of ionic accumulation become important.[6] The marked ion specific effects manifested in the electrophoretic mobility of both cationic and anionic particles suggest that even at 0.01 M the electrostatic forces are weakened due to screening. This is consistent with results published previously,[25] where the stability studies and mobility data indicated the low surface-charge density of both systems in deswollen states. Particle aggregation detected at 0.01 M at temperatures higher that 35 ºC also supports this idea. However, as will shown in the next section, salt concentrations higher than 10 mM are necessary to alter polymer solvency.[35]

3.3. The effect of the electrolyte concentration on hydrodynamic diameter.

Another well-known feature of PNIPAM microgels is the deswelling processes that these particles undergo by salt induction. A previous paper[25] provides a detailed discussion concerning the diverse explanations for this phenomenon. The most accepted explanation involves the disruption of the hydrogen-bonded cage responsible for the polymer hydration due to the electrolyte-water interactions. The addition of salt to the dispersion provides competition for the water molecules hydrating the PNIPAM chains. As a result, poly(NIPAM)–H_2O hydrogen bonds decrease, the hydrophobic interactions become notable and the microgel deswells and contracts. In this section, we focus on the different behavior of electrolytes with regard to deswelling processes depending on their Hofmeister nature. Figures 4a and b show the hydrodynamic diameter versus salt concentration at 25 ºC for the anionic and cationic microgels, respectively. The effect of anions will be considered first. At salt concentrations below 0.1 M and 0.2 M for the cationic and the anionic particles, respectively, the average diameter is practically constant. At such concentrations the structural changes provoked by the

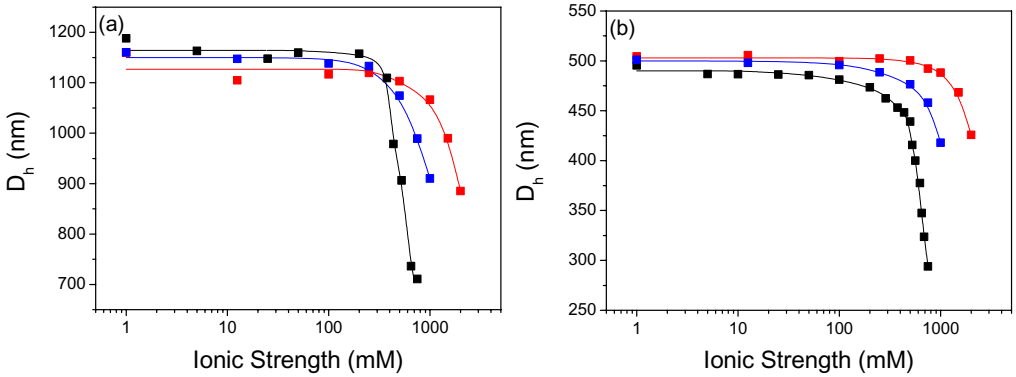

Figure 4. Hydrodynamic particle size as a function of ionic strength at 25 ºC (a) anionic microgel (b) cationic microgel. (■) NaCl, (■) $NaNO_3$, (■) NaSCN.

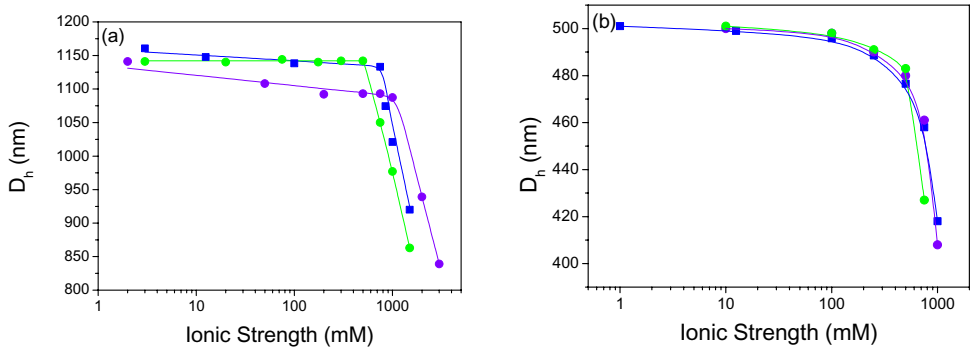

Figure 5. Hydrodynamic particle size as a function of ionic strength at 25 ºC (a) anionic microgel (b) cationic microgel. (■) $NaNO_3$, (●) $Ca(NO_3)_2$, (●) NH_4NO_3.

electrolytes in the cage-like water structure are not substantial enough to be macroscopically observed. However, they become more pronounced with increasing ionic strength. At a certain salt concentration, which is specific for each salt, the hydrodynamic diameter starts to sharply diminish. The minimum salt concentration needed to make the microgel particles collapse follows the sequence $Cl^- < NO_3^- < SCN^-$, for both anionic and cationic particles. In such ranking the chaotropic character increases from left to right, suggesting that the deswelling effect is stronger for the more kosmotropic anions. This finding is consistent with the explanation given above. Since kosmotropic anions interact strongly with water, the relatively strong collapse induced by Cl^- (compared to SCN^-) was probably due to the more effective competition of this ion for the water molecules that hydrate the polymer chains. The same order in the sequence was reported by Zha et al.[20] working with another cationic poly(NIPAM) microgel. Their data showed that the capacity of deswelling the microgel with increasing ionic strength varied in the order $Cit^{3-} > SO_4^{2-} > Cl^- > Br^- > SCN^-$, as in the Hofmeister series. In addition to this, using Cit^{3-}, Cl^- and SCN^- anions and an anionic microgel, Daly and Saunders[19] reached similar conclusions, although they found no differences between Cit^{3-} and Cl^-. In contrast to our results, and those of Zhang, Daly and Saunders also noted an increase in hydrodynamic diameter for the SCN^- anion at high ionic strength, which they explained on the basis that this chaotropic ion promotes hydration and swelling of the microgel.

The effects of cations are shown in Figures 5a and b. Again in this case, differences induced by the cations are not as relevant as those observed with the anions. In general terms, the more kosmotropic the ion, the lower the salt concentration needed to deswell the particles, $Ca^{2+} < Na^+ < NH_4^+$, an idea consistent with the reasoning described above.

The most important points to highlight are: i) first, the effect of the salts on diameter does not depend on the sign of the surface charge of the particles, as opposed to the μ_e results. This means that the capacity to dehydrate the PNIPAM chains depends exclusively on the specific interactions of the ions with the water molecules and with the polymer, regardless of the electrical state of the surface; ii) and second, the effects become significant only at high salts concentrations -that is, when the amount of ions is great enough to compete with the elevated hydrated groups of the surface. These two observations reflect that understandable differences between the mechanism underlying deswelling processes and electrophoretic phenomena

must exist. A comparison of the results found with PNIPAM particles by independently measuring D_h and μ_e reveal that changes in solvent structure and ionic exclusion-accumulation mechanisms simultaneously take part in the these phenomena. Therefore, the combination of both mechanisms at a microscopic level should be considered in the attempts to explain the microscopic origin of the Hofmeister effects.

3.4. The effect of the electrolyte concentration on electrokinetic properties

This last set of experiments was planned to analyze the variation of electrophoretic mobility with electrolyte concentration, while keeping the temperature constant. The measurements were made at moderate salt concentrations, within the 1 mM to 0.1 M range. Two temperatures were chosen for the measurements: 25 ºC, at which the microgels are in an expanded state, and 32 ºC, where particles in a collapsed state predominate. The effect of anions will be discussed first. Figure 6 shows the results for the anionic (Fig. 6a) and cationic (Fig. 6b) system at 25 ºC. Despite that mobility values were close to zero at this temperature, ion-induced differences did exist –especially in the case of the cationic microgel, where anions acted as counterions. The same pattern was found with both cationic and anionic particles. As a general trend, μ_e was nearly zero at low salt concentrations but became progressively more negative as salt concentrations increased. It should be noted that this behavior is contrary to the tendency typically observed in colloidal systems. The effect of the double-layer compression (which commonly occurs in the 1 mM–0.1 M range) is intensified by the ionic strength of the medium, and thus, progressively heavier salt concentrations usually involve the asymptotical approach of μ_e to zero. This tendency, typical of hard-sphere systems, is also predicted by Ohshima's theory[36,37] for soft polyelectrolyte structures. Hence, our experimental results suggest that a non-electrostatic interaction occurs between ions and surfaces. Particularly, this interaction must be such that the electrophoretic mobility becomes higher (in absolute value) when increasing the ionic strength of the medium. The same arguments proposed above to explain the electrokinetic results and supporting a mechanism based on ion accumulation can be here given. In both microgels the anions cause the mobility to acquire more negative values in the order

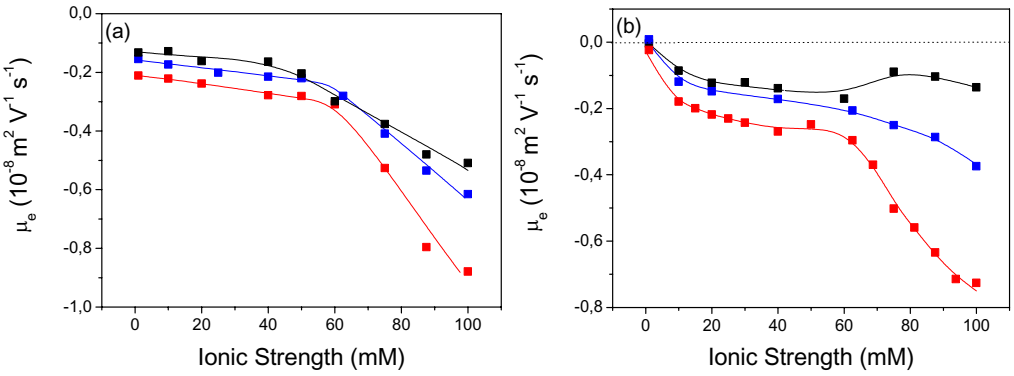

Figure 6. Electrophoretic mobility as a function of ionic strength at 25 ºC (a) anionic microgel (b) cationic microgel (■) NaCl, (■) $NaNO_3$, (■) NaSCN.

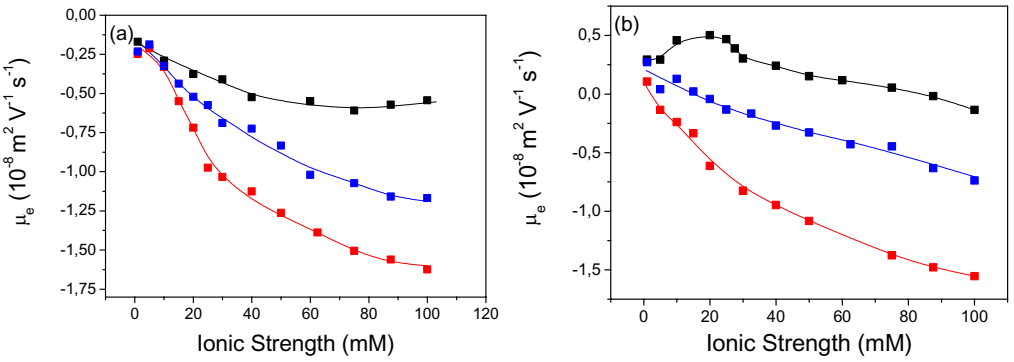

Figure 7. Electrophoretic mobility as a function of ionic strength at 32 ºC (a) anionic microgel (b) cationic microgel. (■) NaCl, (■) $NaNO_3$, (■) NaSCN.

$SCN > NO_3^- > Cl^-$, so that this reduction is more significant for the most chaotropic and polarizable anions. In addition, in this salt-concentration range, no variation in hydrodynamic diameter was detected (see Fig. 4). Therefore, electrokinetic results would again point to an accumulation mechanism governed by dispersion forces. Moreover, such a mechanism appears to be favored by increasing the salt concentration, since differences prompted by the several anions in the μ_e-curves become notable as the salt concentration rises. The data collected at 32 ºC is presented in Figure 7. The trends and specific effects observed at 25 ºC become even clearer at 32 ºC. At this higher temperature, poly(NIPAM) particles partially collapsed are much more sensitive to any change in the surface properties. In addition, it is plausible that dispersion forces are stronger at 32 ºC, since the refractive index of the PNIPAM particles becomes higher as they collapse.[38] Finally, it should be highlighted that the reversed mobility observed in cationic particles at 0.01 M NaSCN (that is, positive particles exhibiting negative μ_e values) intensifies at higher electrolyte concentrations, especially when particles are partially collapsed. In this case, the reversibility was clearly manifested even with the NO_3^-.

The effect of cations on electrophoretic mobility as a function of ionic strength was also analyzed. Inasmuch as the specific effects provoked by cations are usually not very pronounced, measurements were made only at 32 ºC, where ion effects are more notable. The results are plotted in Figure 8. In all cases, mobility tended towards more negative values as the salt concentration increased. This was due to the NO_3^- effect present in these salts, which has been shown to accumulate heavily at interfaces. Nonetheless, this tendency was modulated by the specific effect of cations, especially at high salt concentrations. If cations are ordered according to their ability to make the particle surface potential less negative, the following ranking results: $Ca^{2+} > NH_4^+ > Na^+$. In the same line of argument, this order is related to the capability of the cations to accumulate specifically at the PNIPAM/water interface. Studies performed at constant salt concentrations revealed that no real differences between the monovalent ions exist at 10 mM. This feature was attributed to both the low excess polarizability of cations and the weak salt concentration employed in those experiments. However, the influence of dispersion forces becomes important as the number of ions in solution increases, and differences between NH_4^+ and Na^+ owing to their respective

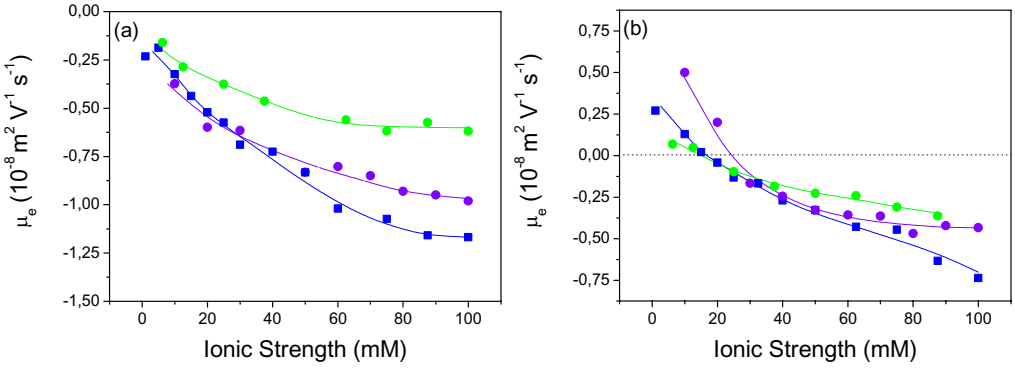

Figure 8. Electrophoretic mobility as a function of ionic strength at 32 ºC (a) anionic microgel (b) cationic microgel. (■) $NaNO_3$, (●) $Ca(NO_3)_2$, (●) NH_4NO_3.

polarizability values ($\alpha^*NH_4^+(0) = 1.86$ Å^3, $\alpha^*Na^+(0) = 0.15$ Å^3) become evident at higher salt concentrations. Ninham's theory can, thus, also account for the specific cation accumulation reported in electrokinetic studies with monovalent ions. Results concerning the Ca^{2+} are consistent with those found at constant salt concentrations. In this case, the cation effect cannot be entirely ascribed to excess calcium polarizability. The double valence of this cation provides a more effective screening of the particle surface charge, reducing the electrophoretic mobility. In addition, its affinity for amide groups augments calcium accumulation at the particle surface. The same tendencies were observed with both cationic (Fig. 8a) and anionic (Fig. 8b) particles, although cation effects are more obviously manifested when the surface is negative and they act as counterions.

IV. Conclusions

This paper shows clear experimental evidence of the two mechanisms underling Hofmeister effects: ion accumulation and water-structure alterations. Although both mechanisms act together, they exert different effects on the properties of the system. Thanks to the extraordinary properties of solvency of PNIPAM (which manifests polymer as well as hard-sphere-particle behavior) it was possible to investigate both mechanisms independently. Hydrodynamic diameter measurements proved to be sensitive to ionic specificities associated

with changes in the structure of water molecules, while electrophoretic mobility studies revealed effects related to ionic accumulation-exclusion processes.

New electrokinetic results concerning specific ion effects on PNIPAM particles have also been provided. This property turned out to be extremely sensitive to the electrolyte nature. For instance, only 0.01 M concentration of NaSCN was sufficient to completely reverse the electrophoretic mobility of the particles. These findings represent the first clear evidence of specific ion accumulation on PNIPAM microgel particles. This phenomenon has been successfully interpreted under the Ninham's approach, which considers dispersion forces acting between ions and surfaces as main driving force of these accumulation mechanisms.

Acknowledgements

The authors wish to thank the financial support granted by "FEDER" and "Comisión Interministerial de Ciencia y Tecnología" (CICYT, Spain), projects MAT2003-01257 and AGL2004-01531/ALI. The authors also wish to thank the bioMérieux Company for research support in terms of chemicals and equipment.

References

[1] F. Hofmeister. Arch. Exp. Pathol. Pharmakol. 1888, 24, 247.

[2] K. D. Collins, M. W. Washabaugh, Q. Rev. Biophys. 1985, 18, 323-422.

[3] M. G. Cacace, E. M. Landau, J. J. Ramsden, Q. Rev. Biophys. 1997, 30, 241-277.

[4] Hofmeister effects special issue: Current Opinion in Colloid Interface Sci. 2004, 9.

[5] W. Kunz, P. Lo Nostro, B. W. Ninham, Current Opinion in Colloid Interface Sci. 2004, 9, 1-18.

[6] B. W. Ninham, V. Yaminsky, Langmuir 1997, 13, 2097-2108.

[7] M. Boström, D. R. M. Williams, B. W. Ninham, Phys. Rev. Letters, 2001, 87, 168103-1-168103-4.

[8] F. W. Tavares, D. Bratko, H. W.Blanch, J. M. Prausnitz, J. Phys.Chem. B, 2004, 108, 9228-9235.

[9] S. A. Edwards, D. R. M. Williams, Current Opinion in Colloid Interface Sci., 2004, 9, 139-144.

[10] W. Kunz, L. Belloni, O. Bernard, B. W. Ninham, J. Phys.Chem. B, 2004,

108, 2398-2404.

[11] M. Boström, W. Kunz, B. W. Ninham, Langmuir, 2005, 21, 2619-2623.

[12] M. Boström, F. W. Tavares, S. Finet, F. Skouri-Panet, A. Tardieu, B. W. Ninham, Biophysical Chem., 2005, 117, 217-224.

[13] M. Boström, B. Lonetti, E. Fratini, P. Baglioni, B. W. Ninham, J. Phys.Chem. B, 2006, 110, 7563-7566.

[14] A. Salis, M. C. Pinna, D. Bilanicová, M. Monduzzi, P. Lo Nostro, B. W.Ninham, J. Phys.Chem. B, 2006, 110, 2949-2956.

[15] R. Leberman, A. K. Soper, Nature(London) 1995, 378, 364-366.

[16] Collins K. D. Methods 2004 34 300-311.

[17] J. Chick, S. Mizzarhi, S. Chi, V. A. Parsegian, D. C. Rau, J. Phys.Chem. B, 2005, 109, 9111-9118.

[18] R. Pelton, Adv. Colloid Interface Sci. 2000, 85, 1-33.

[19] E. Daly, B. R. Saunders, Langmuir 2000, 16, 5546-5552.

[20] L. Zha, J. Hu, C. Wang, S. Fu, M. Luo, Colloid Polym. Sci. 2002, 280, 1116-1121.

[21] Peng Wei Zhu, Donald H. Napper, Colloids Surf. A 1995, 98, 93-106.

[22] T. López-León, A. B. Jódar-Reyes, D. Bastos-González, J. L. Ortega-Vinuesa J., Phys. Chem. B 2003, 107, 5696-5708.

[23] T. López-León, A. B. Jódar-Reyes, J. L. Ortega-Vinuesa, D. Bastos-González, J.Colloid Interface Sci. 2005, 284, 139-148.

[24] T. López-León, P. M. Gea-Jódar, D. Bastos-González, J. L. Ortega-Vinuesa, Langmuir 2005, 21, 87-93.

[25] T. López-León, J. L. Ortega-Vinuesa, D. Bastos-González, A. Elaïssari, J. Phys. Chem. B 2006, 110, 4629-4636.

[26] L. Nabzar, D. Duracher, A. Elaïssari, G. Chauveteau, C. Pichot, Langmuir 1998, 14, 5062-5069.

[27] A. Elaïssari in Handbook of Surface and Colloid Chemistry; (Ed.: K. S. Birdi), CRC Press: Boca Raton, 2002, Chapter 12.

[28] H. G. Schild, Prog. Polym. Sci. 1992, 17, 163-249.

[29] P. M. Wiggins, Physica A 1997, 238, 113-128.

[30] S. Finet, F. Skouri-Panet, M. Casselyn, F. Bonnete, A.Tardieu, Current Opinion in Colloid Interface Sci. 2004, 9, 112-116.

[31] Y. Marcus, Ion Properties, Marcel Dekker, New York, 1997.

[32] W. Wachter, W. Kunz, R. Buchner, G. Hefter J. Phys. Chem. A 2005, 109, 8675-8683.

[33] R. A. Curtis, J. Ulrich, A. Montaser, J. M. Prausnitz, H. W. Blanch, Biotech. and Bioengin. 2002, 79, 367-380.

[34] P. K. Nandi, D. R. Robinson, J. Am. Chem. Soc. 1972, 94, 1299-1308.

[35] Y. Zhang, S. Furyk, D. E. Bergbreiter, P. S. Cremer, J. Am. Chem. Soc. 2005, 127, 14505-14510.

[36] H. Ohshima, K. Makino, T. Kato, K. Fujimoto, T. Kondo, H. Kawaguchi, J. Colloid Interface Sci. 1993, 159, 512-514.

[37] K. Makino, S. Yamamoto, K. Fujimoto, H. Kawaguchi, H. Ohshima, J. Colloid Interface Sci. 1994, 166, 251-258.

[38] S.Tang, Z. Hu, Z. Cheng, J. Wu, Langmuir 2004, 20, 8858-8864.

MACROSCOPICALLY PROBING THE ENTROPIC INFLUENCE OF IONS: DE-SWELLING NEUTRAL MICROGELS WITH SALT

T. López-León[1], A. Fernández-Nieves[2,3]

1Biocolloid and Fluid Physics Group, Department of Applied Physics, University of Granada, Av. Fuentenueva S/N, 18071 Granada , Spain

2 Division of Engineering and Applied Sciences, Harvard University, Cambridge, MA, 02138 (USA)

3Interdisciplinary Network of Emerging Science and Technology (INEST) Group, Research Center, Philip Morris USA, Richmond, VA, 23234 (USA)

Abstract

The Polymeric microgels are very interesting systems to study polymer-solvent interactions since they react to changes in the solvent properties by swelling or de-swelling to reach a final equilibrium state of minimal free energy. Accordingly, factors such as pH, temperature, or salt concentration, can induce size changes. While the volume phase transition undergone by ionic microgels with addition of salt is reasonably well understood in terms of Donnan effects, the origin of these transitions in neutral microgels is devoid from such understanding. In this paper, effects of electrolytes on the swelling behaviour of neutral thermosensitive microgels are interpreted within the Flory-Rehner theory for the swelling of neutral gels, by considering that ionic concentration affects the entropic contribution to the Flory solvency χ-parameter; this manifests macroscopically as particle de-swelling. The entropic changes depend on the ability of the electrolyte to disrupt the neighbouring water structure and result in increasing values of χ with salt concentration. In this sense, we find a clear correlation between the de-swelling ability of the ions and their chaotropic (structure-breaking) or kosmotropic (structure-making) nature as classified in the Hofmeister series.

I. Introduction

Gels are cross-linked polymers immersed in a liquid. Their mesoscopic versions, microgels, exhibit faster kinetics and the inherent richness of colloidal suspensions. Among these, those based on Poly-(N-isopropylacrylamide) (PNIPAM) have received special attention probably because the volume transition is triggered thermally and temperature is easy to tune. The mechanism responsible for the water solubility of these gels is related to the formation of structured water cages around the isopropyl groups of the polymer [1], which are the hydrophobic sites of PNIPAM. Changes in this water structure, as promoted, for example, by molecular agitation or by interaction with electrolytes, induce a hydrophobic attraction among isopropyl groups that results in gel collapse. It is this hydrophobic interaction through the entropic contribution to the free energy of the system that is responsible for de-swelling of PNIPAM gels.

Polymeric macro and microgels are thus very interesting systems to study polymer-solvent interactions, since the system free energy is minimized by dynamically changing the polymer conformation and the surrounding water structure, that in the end determine the final equilibrium size. They can thus be used to access, in a simple way, the effects of a polymer environment change, as induced by changing the solvent itself or by dissolving substances that can potentially change such atmosphere.

The presence of electrolytes in aqueous solutions disrupts the molecular structure of the pure liquid water [2]. The structural modifications induced by different electrolytes are not identical at all; in fact, they can be extremely different depending on the nature of the dissolved salt. Ions that interact with water stronger than water itself are known as structure-makers or kosmotropes, whereas ions having the opposite effect are known as structure breakers or chaotropes [3]. According to this feature, ions are commonly ranked in the so called Lyotropic or Hofmeister series. This ion ranking was first observed in 1888, when Hofmeister studied the effects of different neutral salts on the solubility of proteins [4,5]. Since then, a great number of experiments have revealed the same order when studying systems and properties of very diverse nature [6].

A representative Hofmeister series for anions and cations is given in

Table 1: Hofmeister series & the encountered experimental classification based on the de-swelling capability of the ions.

	Anions	Cations		Anions	Cations
Kosmotropic	SO_4^{2-}				
	PO_4H^{2-}	Mg^{2+}			
	F^-	Ca^{2+}			
.	CH_3COO^-	H^+	**Decreasing de-swelling effect**	Cl^-	Ca^{2+}
.	Cl^-	Na^+		NO_3^-	Na^+
.	Br^-	K^+			
.	I^-	Rb^+	↓	SCN^-	NH_4^+
.	NO_3^-	Cs^+			
	ClO_4^-	NH_4^+			
Chaotropic	SCN^-				

Table 1. Although there is still no general conceptual framework available to provide a compelling explanation for why these effects occur, water structure and how ions modify such structure are key points in understanding Hofmeister effects; this is inferred from a number of experiments with different techniques. Examples include electrochemistry [7,8], quasielastic neutron scattering [9] and neutron diffraction [10], vibrational spectroscopy [11,12] and nuclear magnetic resonance [13].

While the effect of electrolyte concentration over the swelling of ionic macro [14,15,16] and microgels [17] is reasonably well understood, in the case of neutral gels, despite the existence of experimental evidence showing that salt concentration can greatly affect the particle equilibrium size [18, 19, 20, 21], there is little understanding of why this is so. In this paper, we study the equilibrium swelling behavior of PNIPAM microgel particles in the presence of different salts as a function of salt concentration. We find correlation between the de-swelling degree exerted by the different ions and the Hofmeister series and interpret the results by considering that the different ions induce a change in the entropic contribution of the polymer-solvent Flory χ-parameter; for a given salt concentration, χ increases with the kosmotrope character of the ion. Overall, our results indicate that disturbances in the water structure caused by electrolytes affect the swelling behavior of PNIPAM colloidal gels and could in fact be the reason for such observations in other neutral microgel systems.

The rest of the paper is organized as follows. Section II summarizes the thermodynamic background for understanding the swelling behavior of neutral gels. The following section briefly introduces the experimental system and methods. Section IV presents the results. First we describe the temperature volume phase transition of the PNIPAM particles under consideration and theoretically describe the observations with the Flory-Rehner theory for the swelling of neutral gels. This provides information about some of the intervening system parameters, which will we use to estimate entropic changes induced by salt concentration, for different salts. Finally, in section V, we summarize our work and conclude.

II. Swelling thermodynamics

The swelling behavior of PNIPAM microgels is well described by the classic Flory-Rehner theory [22]. At equilibrium, the mixing osmotic pressure (π_m) within the particle is balanced by the elastic osmotic pressure (π_e) of the crosslinked network so that $\pi_{total} = \pi_m + \pi_e = 0$, or equivalently, the free energy of the system is minimal. In this case,

$$\ln(1-\phi) + \phi + \chi\phi^2 + \frac{\phi_0}{N_{gel}}\left[\left(\frac{\phi}{\phi_0}\right)^{1/3} - \frac{\phi}{2\phi_0}\right] = 0 \qquad (1)$$

where ϕ is the polymer volume fraction within the particle, N_{gel} the average number of segments between two neighbouring crosslinking points in the network and χ the Flory polymer-solvent interaction parameter. Equation 1 provides a means to determine ϕ from ϕ_0, N_{gel} and χ. For isotropic swelling, ϕ can be related to the particle diameter d as:

$$\frac{\phi}{\phi_0} = \left(\frac{d_0}{d}\right)^3 \qquad (2)$$

with ϕ_0 and d_0 the polymer volume fraction and particle size in a reference state, typically taken as the shrunken state.

The Flory χ–parameter plays a crucial role in the thermodynamic behavior of the gel. It is defined as the free energy change per solvent molecule (in kBT units) when a solvent-solvent contact is changed into a solvent-polymer contact:

$$\chi = \frac{\Delta G}{k_B T} = \frac{\Delta H - T\Delta S}{k_B T} = \frac{1}{2} - A(1 - \frac{\Theta}{T}) \tag{3}$$

where k_B and T are the Boltzmann constant and temperature, respectively; A and Θ have been defined as:

$$A = \frac{2\Delta S + k_B}{2k_B} \tag{4}$$

$$\Theta = \frac{2\Delta H}{2\Delta S + k_B} \tag{5}$$

As can be seen, A is directly related with entropy changes, whereas Θ depends on both entropic and enthalpic variations. The latter is the so called Θ–temperature and corresponds to the temperature at which the second virial coefficient of the π–series expansion in powers of ϕ vanishes; binary interactions among constituents are then negligible and only excluded volume effects are important. For $T = \Theta$ the Flory χ-parameter equals $\chi = 1/2$. Thereby, the solvent is a good solvent for the polymer when $\chi < 1/2$ and it is a poor solvent when $\chi > 1/2$. The Θ–temperature is analogous to the Boyle temperature of a Van der Waals fluid, where the gas can be taken as ideal. In fact, the volume phase transition of a polymer gel is in some sense analogous to the phase transition of a Van der Waals fluid; swollen and de-swollen gel states would correspond to the gas and liquid phases, respectively [23] (see Fig. 1).

Equation 1 determines the T-ϕ phase diagram for a polymer gel. The temperature dependence is embodied in the Flory χ-parameter, while N_{gel} and ϕ_0 are system properties. Usually, the interactions between polymer and solvent molecules lead to positive values of ΔH and ΔS ($A > 0$). In this case, the system is characterized by an upper-critical-solution-temperature above which the polymer becomes soluble. For PNIPAM, the polymer solvency is governed by order-disorder processes induced by hydrophobic interactions between the polymer and the solvent with possible influences from hydrogen-bonding. As a result ΔH and ΔS are negative ($A < 0$) and the system is characterized by a lower-critical-solution-temperature (LCST). Fig. 2 shows some representative T-d isobars (for different χ-parameters) for a PNIPAM system. These curves have been obtained from equation 1, after considering

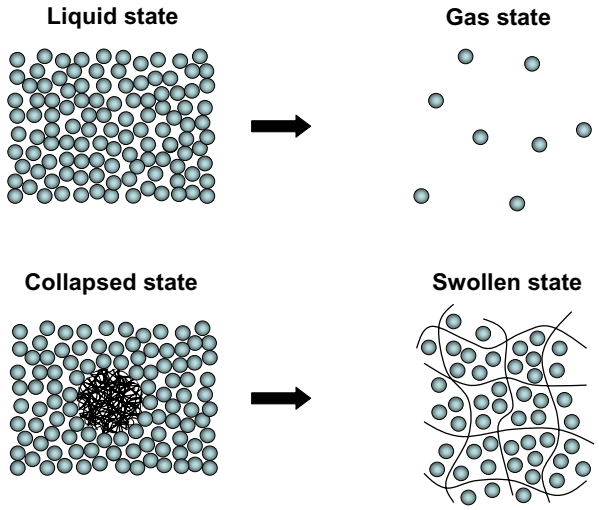

Fig. 1: Analogy between the shrunken-swollen transition in a microgel and the liquid-gas phase transition in a Van der Waals fluid.

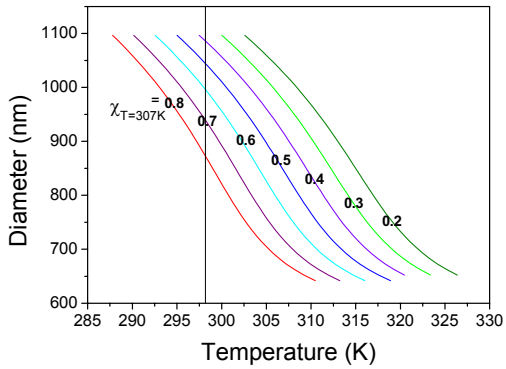

Fig. 2: Size-temperature phase diagram predicted by the Flory-Rehner phenomenological theory for the swelling of neutral microgels. The curves correspond to χ–parameters ranging from $\chi = 0.2$ to $\chi = 0.8$ (at 307 K). Other intervening parameters are taken equal to: $d_0 = 600$ nm, $N_{gel} = 42$ and $\phi_0 = 0.8$; these values are those obtained for the particular PNIPAM system under consideration. The vertical line corresponds to a constant temperature of 25ºC.

isotropic swelling (equation 2) and the χ definition (equation 3). The isobars are plotted using values of N_{gel}, ϕ_0, d_0, and ΔH that characterize our experimental system (see section IV.A). Since the χ-parameter depends on temperature, we provide χ values at 307 K in order to compare the curves. Fig. 2 shows that the particle size decreases with increasing temperature, as one would expect for systems with a LCST. Equivalently, particle de-swelling can be induced by increasing χ, i.e. by making the solvent poorer, as also shown in Fig. 2.

III. Materials and methods

3.1 Experimental system.

PNIPAM particles were prepared via batch radical polymerization under emulsifier-free conditions. The monomers employed were N-isopropylacrylamide (NIPAM) from Kodak and methylenebisacrylamide (MBA) from Sigma. Potassium persufate was used as initiator, leading to sulfate anionic groups at the particles surface. Polymerization was performed in a 250 ml thermostated reactor, round-bottomed four-necked flask, equipped with a glass anchor-shaped stirrer, condenser, thermocouple and nitrogen inlet. The reaction took place in boiled and deoxygenated water, under a constant stream of nitrogen. The polymerization temperature was set constant at 70 ˚ C and the stirring rate was 200 rpm throughout the process. The resulting suspension was cleaned through several centrifugation/re-dispersion cycles (15000 rpm for 30 min at 25 ºC). Further details about particle synthesis and characterization are available in reference [24].

All salts employed, NaCl, $NaNO_3$, NaSCN, $Ca(NO_3)_2$ and NH_4NO_3, are of analytical grade and were purchased from Merck, Sigma or Scharlau. Double-deionized water was used throughout.

3.2 Dynamic light scattering.

Particle sizes were measured by dynamic light scattering (DLS) using a Zetasizer 3000HS (Malvern Instruments, UK). In a typical DLS measurement, the intensity autocorrelation function is determined and used to obtain the mean diffusion coefficient D of the particles. The experiments were performed at a scattering angle $\theta = 90^{o}$ using a He-Ne laser with vacuum wavelength

λ = 633 nm. The mean hydrodynamic diameter is calculated from the diffusion coefficient by using the Stokes-Einstein equation:

$$D = \frac{k_B T}{3\pi\eta d}$$

where η is the medium viscosity. Temperature was controlled with a precision of 0.1 K using a peltier chamber that surrounded the sample cell. The $\eta = \eta(T)$ dependence was obtained from the literature [25].

IV. Results and discussion

4.1 Volume phase transition.

Fig. 3 displays the dependence of the mean hydrodynamic diameter of the PNIPAM particles versus temperature for a salt concentration of 1 mM (NaCl). The particles are de-swollen at high temperatures because thermal agitation is able to break the cage-like water structure surrounding the PNIPAM isopropyl groups. Under these conditions, water is a *poor* solvent for PNIPAM. The volume phase transition temperature T_{VPT}, here considered as the temperature corresponding to the onset of the swelling process, is around 307 K. As in a Van der Waals fluid above the critical temperature, the volume transition of our system is continuous, with no first order discontinuity in the particle size. The swelling process cannot be strictly considered then a phase transition, but nevertheless, for convenience, this term is usually used also when referring to a continuous swelling.

To describe the experimental results with the Flory-Rehner thermodynamic theory presented in section II, it is convenient to rewrite equation 1 in terms of the particle diameter (equation 2), also showing explicitly the temperature dependence (equation 3):

$$T_{\pi=0} = \frac{-A\phi_0^{\,2}\left(\frac{d_0}{d}\right)^6 \Theta}{\ln\left(1-\phi_0\left(\frac{d_0}{d}\right)^3\right)+\phi_0\left(\frac{d_0}{d}\right)^3+\phi_0^{\,2}\left(\frac{d_0}{d}\right)^6\left(\frac{1}{2}-A\right)+\frac{\phi_0}{N_{gel}}\left[\frac{d_0}{d}-\frac{1}{2}\left(\frac{d_0}{d}\right)^3\right]} \quad (6)$$

As can be seen, equation 6 relates T and d by means of A, Θ, ϕ_0, d_0 and N_{gel}.

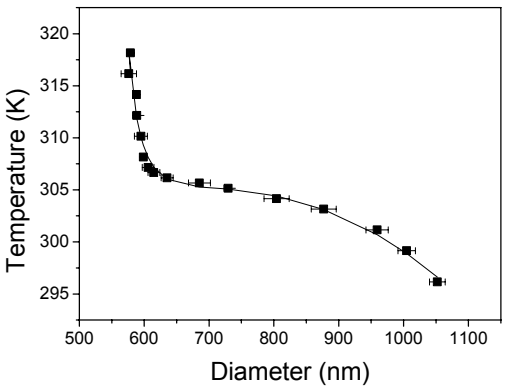

Fig. 3: Experimental mean hydrodynamic diameter versus temperature at 1 mM NaCl. The solid line is the theoretical best least squares fit. Resultant parameter values are: d_0 = 600 nm, A = 11.5, T = 307 K, N_{gel} = 42, χ_2 = 0.19 and χ_3 = 0.81.

We note that in this equation A must be taken negative if the system is characterized by a LCST. Least square fits of the experimental data to this equation leads to physically unrealistic values for the parameters. The reason for this result seems to be related to the volume fraction dependence of χ. This fact has been experimentally observed through solvent activity measurements with a number of different systems revealing a non-linear χ-parameter dependence on the polymer volume fraction [26]. In addition, the inability of the original Flory-Rehner theory to justify the observed discontinuous phase transitions in neutral gels has been interpreted as a need for including the ϕ dependence on the Flory χ-parameter [27]. The microscopic origin of this dependence is one of the current concerns of polymer science. Within the Flory-Rehner phenomenological theory the gel phase transition is understood on the basis of χ, which embodies all the molecular interactions in the system. χ is thus the final cause of such phase transitions and must be determined empirically for every particular case.

The original Flory theory is based on determining the exchange free energy involved in juxtaposing pairs of polymer and solvent segments, and mixed polymer-solvent pairs, in order to obtain the equilibrium polymer configuration. However, in a subsequent work published by Erman and Flory [28], the authors claimed the inadequacy of treating exchange interactions

Table 2: Free parameter values resulting from least squares fit of the d-T experimental data. The bold column corresponds to the best fit.

	$\chi = \chi_1(T)$				$\chi = \chi_1(T) + \chi_2\phi$				$\chi = \chi_1(T) + \chi_2\phi + \chi_3\phi$			
ϕ_0	**0.6**	**0.7**	**0.8**	**0.9**	**0.6**	**0.7**	**0.8**	**0.9**	**0.6**	**0.7**	**0.8**	**0.9**
A	-9.4	-13.6	-20.6	-37.3	-1.6	-3.2	-7.0	-21.0	-0.7	-1.8	**-11.5**	-25.0
Θ(K)	300.0	300.9	301.6	302.9	322.5	319.7	316.2	310.0	299.6	303.0	**307.0**	315.3
N_{gel}	247	131	65	25	245	113	51	19	148	400	**42**	14
χ_2	-	-	-	-	0.70	0.83	1.02	1.16	0.19	0.13	**0.19**	2.58
χ_3	-	-	-	-	-	-	-	-	0.66	0.77	**0.81**	-1.19

merely in terms of contacts between molecules and asserted that interactions of higher order must be considered; they accounted for this by proposing a power series expansion for χ as a function of ϕ:

$$\chi = \chi_1 + \chi_2\phi + \chi_3\phi^2 + \chi_4\phi^3 + \ldots \qquad (7)$$

where χ_1 is the original Flory parameter in equation 3, and χ_2, χ_3... are temperature independent coefficients. If the above series expansion is introduced in equation 1 one obtains an analogous expression to equation 6 with additional terms in χ_2 and χ_3. Better results are then achieved when fitting the diameter-versus-temperature experimental data. Table 2 summarizes the values of the fitting parameters obtained by considering: (i) zero-order $\chi = \chi_1(T)$, (ii) first-order $\chi = \chi_1(T) + \chi_2\phi$ and (iii) second-order $\chi = \chi_1(T) + \chi_2\phi + \chi_3\phi^2$ approximations. Different values of ϕ_0 (0.6, 0.7, 0.8, 0.9) have been tested in the fit. In Fig. 3 the black squares are the experimental points obtained by DLS and the solid line is the theoretical best fit. The latter is selected among all fits with similar statistical χ^2 values (typically around 1.3) based on how realistic the fitting parameters were; these must fulfill three main conditions: (i) the values of A and Θ must be such that $0 < \chi_1 < 1$ within all the temperature range studied, (ii) the Θ-temperature should be close to the experimental volume phase transition temperature $T_{VPT} \approx 307$ K and (iii) the number of segments per chain N_{gel} must reasonably match the value deduced from the cross-linker concentration employed in the microgel synthesis. For a perfect network, where each crosslinking monomer forms two junction points, the number of total chains N_{chains} will be twice the number of

crosslinking molecules. Since the synthesis monomer conversion is close to 100% [29], N_{chains} can be calculated from the mass of MBA to be $N_{chains} = 2.21\ 10^{20}$. By dividing the total number of NIPAM molecules by N_{chains} we get $N_{gel} = 33$.

As can be seen in Table 2, the zero-order and first-order approximations provide low and high values of the Θ, respectively, independent of the chosen ϕ_0. Only the second-order approximation for $\phi_0 = 0.8$ gives a value of Θ in agreement with the experimental phase transition temperature. In this case, reasonable values of A and N_{gel} are also obtained. A further discussion of the resulting parameters is presented below:

i) The value of the Flory Θ–temperature, Θ = (307.0 ± 0.3) K, is very close to the T_{VPT} indicating that the phase transition is related to a change in the solvent quality. The values of A = (-11.5 ± 1.9) and Θ allow determination of the entropy and enthalphy changes when a solvent-solvent contact is replaced by a PNIPAM-solvent contact. From equations 4 and 5:

$$\Delta S = \left(A - \frac{1}{2} \right) k_B = (-1.7 \pm 0.3) \cdot 10^{-22}\, J/K \qquad \Delta H = \theta A k_B = (-4.9 \pm 0.8) \cdot 10^{-20}\, J$$

These quantities agree with the values reported by other authors [30,27,31]. The negative sign of A leads to $\Delta S < 0$ and $\Delta H < 0$, as expected for a system characterized by a LCST.

ii) The polymer volume fraction $\phi_0 = 0.8 \pm 0.1$ implies that around 20% of the particle volume in the reference state is occupied by solvent molecules. This also agrees with previous results on similar systems [32,33,34] and implies that the de-swollen particle size contains water and is not equivalent to the collapsed size that by definition has no solvent molecules.

iii) The average number of segments between two neighbouring crosslinking points, N_{gel} = 42 ± 6, agrees well with the value gauged from the microgel synthesis.

iv) A second-order approximation in $\chi(\phi)$ is required to describe the microgel swelling. The need of introducing $\chi_2 \neq 0$ and $\chi_3 \neq 0$ becomes evident by analyzing the χ=$\chi(T)$ relation. The χ-parameter can be experimentally determined from the d-T data by using equations 1 and 2, provided N_{gel}, ϕ_0 and d_0 are known:

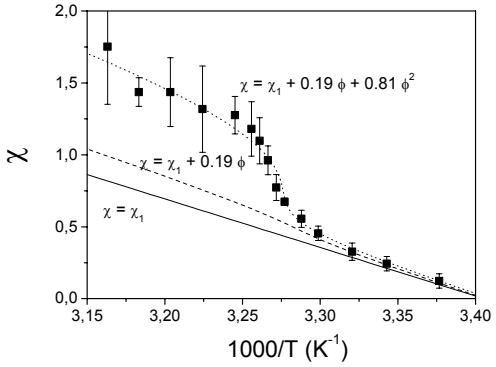

Fig. 4: Flory χ-parameter as a function of the inverse temperature. The points are the experimental χ values obtained from the swelling data. The solid lines correspond to three theoretical approximations within the Flory theory: $\chi = \chi_1$; $\chi = \chi_1 + \chi_2\phi$, with $\chi_2 = 0.6$; $\chi = \chi_1 + \chi_2\phi + \chi_3\phi^2$, with $\chi_2 = 0.19$ & $\chi_3 = 0.81$.

$$\chi = \frac{-1}{\phi_0}\left[\frac{1}{N_{gel}}\left(\left(\frac{d}{d_0}\right)^5 - \frac{1}{2}\left(\frac{d}{d_0}\right)^3\right) + \left(\frac{d}{d_0}\right)^3 + \frac{1}{\phi_0}\left(\frac{d}{d_0}\right)^6 \ln\left(1 - \phi_0\left(\frac{d_0}{d}\right)^3\right)\right] \quad (8)$$

The χ–parameter calculated in this way is plotted as a function of T^{-1} in Fig.4. When $\phi \to 0$, the ϕ-dependent terms in equation 7 can be neglected and $\chi = \chi_1$, which according to equation 3 should be proportional to T^{-1}. This linear dependence between χ and T^{-1} is indeed experimentally observed at high T^{-1} (low temperatures), where the particles are swollen and ϕ is low. Furthermore, as shown in Fig. 4, for high T^{-1} ($\phi \to 0$) the experimental points are well described with the theoretical solid line corresponding to the $\chi_1(T)$ obtained using the A and Θ values that resulted from the d-T fit. Note also that $\chi < 1/2$ in this region, as expected for a polymer in a *good* solvent.

The linear χ–T^{-1} dependence disappears when T^{-1} decreases below ~$1/T_{VPT}$. The system is rather de-swollen in this temperature range and χ exhibits a more pronounced temperature dependence. This behaviour can only be justified if a dependence on ϕ is introduced in χ. Hirotsu interpreted the d-T curve of a neutral PNIPAM gel undergoing a discontinuous phase transition by introducing a linear ϕ correction in the χ–parameter [30]. This author found that $\chi_2 \approx 0.6$; a value that is higher than that theoretically

predicted by Erman and Flory for a discontinuous transition in a gel of infinitely long chains, χ_2=1/3. This suggests that a more important dependence on ϕ is required when dealing with real gels. The dashed line in Fig. 4 corresponds to Hirotsu's results, which clearly cannot account for our experimental data. In our particular case there is no value of χ_2 able to reproduce, within a linear χ–ϕ dependence, the experimental results, and a second-order ϕ dependence needs to be included. The dotted line is the theoretical prediction corresponding to $\chi_2 = 0.19$ and $\chi_3 = 0.81$, the values obtained in the d-T fit (Table 2). With these last values, the experimentally obtained Flory parameters are then rather well reproduced.

A microscopic understanding of this second-order dependence is not evident. The χ–ϕ relation given in equation 7 must be taken as an empirical series expansion that aims to account for various many-body molecular interactions but that lacks a clear physical meaning. According to Erman and Flory [28], the χ_i coefficients are related in some way to the equation of state of the individual components (polymer and solvent) and their mixture. However, these coefficients are not directly related to any specific interaction. First and second order χ–ϕ dependences have been deduced from experiments with systems based on PNIPAM [27, 30, 35]. Typically, the second order dependences on ϕ are associated to discontinuous phase transitions, which are not observed in our case. However, not every set of (χ_1, χ_2, χ_3) values implies coexistence of swollen/de-swollen phases [28] and thus there are values of this triad giving rise to continuous changes in the gel size. In addition, the continuous or discontinuous character of the phase transition depends not only on the interaction coefficients, but also on the structural parameters contained in the Flory-Rehner theory, and on more subtle variables not contemplated in this theory. In fact, Hirotsu observed differences in the character of the phase transition of two PNIPAM gels synthesized under the same conditions and with identical nominal compositions [27]. The only difference was the initiator employed: While sodium bisulfite (BS) led to continuous transitions, N, N, N´, N´-tetramethylethylenediamine (TEMED) led to discontinuous ones. This qualitatively different behaviour was attributed to some imperfections of the network, which were believed to play a decisive role in the phase behavior. Nonetheless, the concrete effect of these imperfections is not well-known yet. In our case, potassium persulfate is employed as initiator, which is certainly more similar to the BS molecule than to the TEMED molecule. The particular χ–ϕ dependence thus seems to delicately depend on

the particularities of the experimental system. The synthesis method and the initiator employed are variables not accounted for in any theory but that seem to affect the system phase behavior; it is the complexity of the many-body interactions that has prevented a microscopic understanding of these effects.

We, in any case, conclude that the Flory-Rehner theory captures the essential physics of the phase transition of neutral PNIPAM microgels, since it reasonably describes the observed swelling curves using reasonable values of the parameters involved. We will use the values of these intervening parameters to interpret the effects of salt on the system swelling behavior at a fixed temperature.

4.2 Salt induced de-swelling.

We study the effects of six electrolytes on the swelling behavior of neutral PNIPAM microgels. We chose the following salts: (i) NaCl, $NaNO_3$ and NaSCN, all with the same cation, and (ii) $Ca(NO_3)_2$, $NaNO_3$ and NH_4NO_3, that share the anion. This selection allows the effects of different anions and cations to be analyzed independently.

Figs. 5a and 5b show the PNIPAM particles diameter against salt concentration n, for anions and cations, respectively. The measurements are made at T = 25ºC $< T_{VPT}$ and thus the particles are swollen. The following conclusions can be extracted from these curves:

i) At low salt concentrations, the particles are swollen. No great differences among the ions can be detected. It is only when $n \approx 300$ mM, that particle diameters decrease and important differences among ions are evidenced. This characteristic is typical of Hofmeister effects – which usually appear from moderate to high ionic concentrations [3].

ii) Although all the ions cause deswelling at roughly the same concentration, the d-n slope is different among these; the salt concentration required to reach a given swelling ratio ϕ_o/ϕ depends strongly on the particular ion. For example, the salt concentration needed to attain a swelling ratio of 1.5 is about 500 mM in the case of NaCl, 1000 mM for $NaNO_3$ and 2000 mM for NaSCN.

iii) Differences among anions (Fig. 5a) are more pronounced than among cations (Fig. 5b). This is also a general feature of all Hofmeister phenomena - which are frequently dominated by anion effects [3].

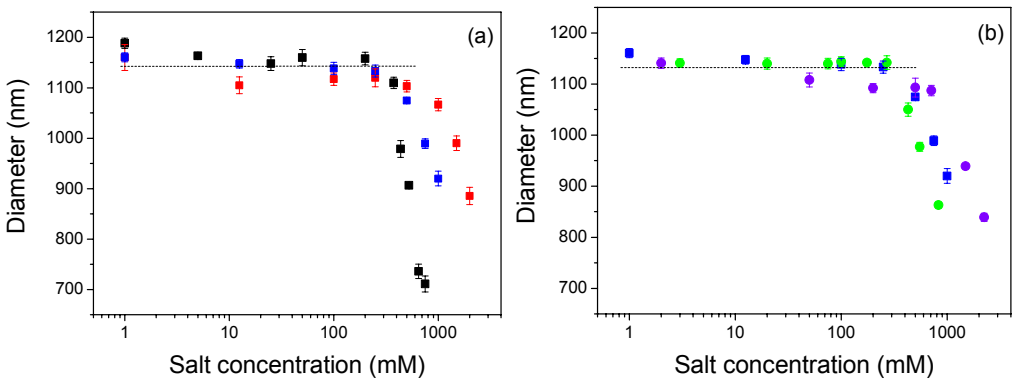

Fig. 5: Hydrodynamic particle size as a function of salt concentration at T = 25ºC (a) Effect of anions: (■) NaCl, (■) $NaNO_3$, (■) NaSCN. (b) Effect of cations: (■) $NaNO_3$, (●) $Ca(NO_3)_2$, (●) NH_4NO_3.

The results can be summarized by classifying the ions in terms of their de-swelling capacity, which we can quantify through the d-n slope for n > 300 mM (Table 1). The obtained series exactly agrees with the Hofmeister series: the more kosmotropic or structure-maker anions have the stronger de-swelling effect, whereas chaotropic ions seem to attenuate this process.

As mentioned before, de-swelling processes promoted by electrolytes have commonly been discussed in terms of a Donnan equilibrium for ions inside and outside the gel. This explanation, plausible for ionic microgels, cannot justify our results because there is no reason to think that a Donnan potential is established in a non-ionic microgel. On the other hand, although the molecular origin of the Hofmeister series is not completely understood, it is well known that they emerge from a combination of effects in which water structure is the cornerstone of the problem. Therefore, it is reasonable to think that the presence of ions above certain concentration modify the entropic contribution to the Flory solubility χ-parameter. Fig. 5 will thus be analyzed by means of the Flory-Rehner theory under the assumption that ions modify the entropic component ΔS of the χ-parameter.

We then calculate ΔS from the experimental (d,n) pairs in Fig. 5, using equations 1 and 3. In this case, χ has been replaced by the experimentally

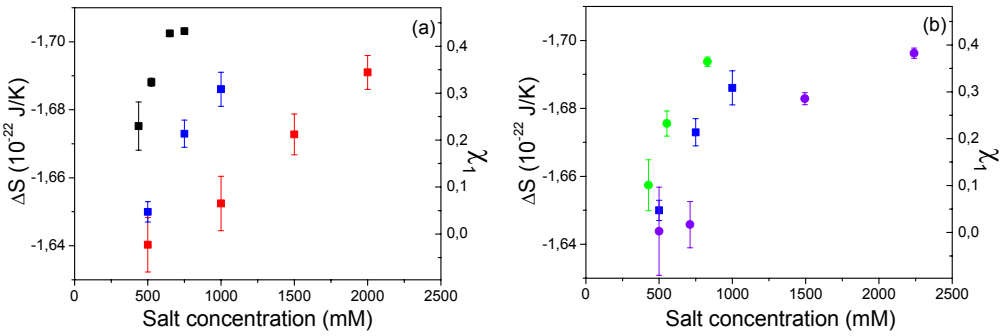

Fig. 6: Experimental changes in the entropy and Flory χ–parameter with electrolyte concentration. (a) Effect of anions: (■) NaCl, (■) $NaNO_3$, (■) NaSCN. (b) Effect of cations: (■) $NaNO_3$, (●) $Ca(NO_3)_2$, (●) NH_4NO_3

found series expansion in ϕ, with χ_1 written in terms of ΔH and ΔS. We also assume that only ΔS changes are responsible for the observed de-swelling. For the rest of parameters, values resulting from the d-T fit are employed. Results are presented in Figs. 6(a) for anions and 6(b) for cations. In the same figures we also plot χ_1. Inasmuch as differences among ions are important beyond 300 mM, only results corresponding to this concentration range are displayed.

To understand the entropic change ΔS, recall that $\Delta S = S_{sp} - S_{ss}$, with S_{sp} and S_{ss} representing the entropies due to solvent-polymer and solvent-solvent contacts, respectively. The fact that $\Delta S < 0$ implies, from an entropic point of view, that the latter are favoured over the polymer-solvent contacts, resulting in the macroscopic de-swelling of the particles. This is why increasing T results in a size reduction. According to Fig. 6, there are two factors that promote the increase in $|\Delta S|$: (i) salt concentration and (ii) the kosmotropic character of the ion. The results can thus be interpreted based on the competition between the polymer and the electrolyte for the water molecules. The highly kosmotropic ions tend to strongly interact with water molecules. As a result, they are able to seriously disturb the water cage responsible for the PNIPAM hydration, thus reducing the polymer-solvent contacts and leading to the polymer collapse. This effect becomes more pronounced as the number of ions in solution increases. Conversely, chaotropic ions, which interact only slightly with water, have a far more attenuated effect. Fig. 6 shows that in these cases high salt concentrations are necessary

to get a considerable increase in $|\Delta S|$. Although anions and cations exhibit the same trend, the entropic changes induced by the former are in general more significant than those provoked by the latter, in agreement with what is typically encountered for Hofmeister effects [3]. Finally, the values for ΔS at low salt concentration are consistent with the value provided by the *d-T* fit, as expected.

Perhaps it is more intuitive to describe the ion effects in terms of χ_1 rather than through entropy changes. As can be seen in Fig. 6, $\chi_1 < 1/2$ as expected for swollen phases. It also increases with salt concentration. Furthermore, for a given n the value of the Flory parameter increases with the kosmotropic character of the ion. This feature can be qualitatively understood from Fig. 2. This diagram displays the microgel phase transition curves for different values of the Flory parameter. The vertical solid line corresponds to a temperature of 25ºC, at which all *d-n* curves were measured. According to this figure, the increase in the Flory parameter implies a reduction in the particle diameter; this is consistent with the experiment and equivalent to increasing temperature. The equivalent effects of temperature and salt concentration can be further emphasized. For example, the change in the Flory parameter caused by adding 750 mM of the most kosmotropic anion Cl^- is analogous to the change provoked by increasing the temperature by $\Delta T = 7.0$ K. Accordingly, 750 mM of NO_3^-, a moderately kosmotropic anion, is equivalent to a temperature change $\Delta T = 1.4$ K, while the same concentration of the less structure-maker anion SCN^- would not have any appreciable effect. Regarding cations, a $\Delta T = 4.3$ K is obtained with Ca_2^+, whereas concentrations above 750 mM are necessary to observe any effect arising from NH_4^+, that is far less kosmotropic than Ca_2^+. This *equivalent increment of temperature* can be used, then, as an estimation of the chaotropic/kosmotropic character of the ion.

V. Conclusions

In this work, we provide a plausible explanation for understanding volume changes induced by salt in neutral microgels. The increase in ionic concentration above ≈ 300 mM induces de-swelling of the particles; the amount is highly dependent on the electrolyte nature, with a clear correlation between de-swelling ability and ion position in the Hofmeister series. These findings emphasize the entropic influence of the ions over the polymer-solvent interactions that control the microgel size. We thus interpret the phase

transitions induced by salt as changes in the entropic contribution to the Flory χ-parameter within the phenomenological Flory-Rehner theory for the swelling of neutral gels. As salt concentration increases the entropy gain due to solvent-solvent contacts raises, implying χ also grows, and the particles de-swell; similar trends are found when the kosmotropic character of the ions in solution is increased. To obtain the entropy changes, knowledge of some important system parameters is necessary. A detail analysis of the particle size temperature dependence provided this information.

Acknowledgements

T. Lopez-León acknowledges financial support from Comisión Interministerial de Ciencia y Tecnología (CICYT, Spain) under project MAT2003-01257. A. Fernández-Nieves is grateful to Ministerio de Ciencia y Tecnologia (MAT2004-03581) and to the University of Almeria (leave of absence). INEST Group is sponsored by PMUSA. The authors would also like to thank J. L. Ortega-Vinuesa and D. Bastos-González for reading the manuscript.

References

[1] H. G. Schild, Prog. Polym. Sci. 17, 163 (1992).

[2] M. G. Cacace, E. M. Landau and J. J. Ramsden, Q. Rev. Biophys. 30, 241 (1997).

[3] K. D. Collins and M. W. Washabaugh, Q. Rev. Biophys. 18, 323 (1985).

[4] S. Lewith, Arch. Exp. Pathol. Pharmakol. 24, 1 (1888).

[5] F. Hofmeister, Arch. Exp. Pathol. Pharmakol. 24, 247 (1888).

[6] W. Kunz, P. Lo Nostro and B.W. Ninham, Curr. Opin. Colloid Interface Sci. 9, 1 (2004).

[7] R. W. Gurney, *Ionic Processes in Solution* (New York, McGraw-Hill)

[8] J. P. Chatterjee and I. N. Basumallick, J. chem. Soc. Faraday Trans. 86, 3107 (1990).

[9] R. Jimenez, G. R. Fleming, P. V. Kumar and M. Maroncelli, Nature (London) 369, 471 (1994).

[10] R. Leberman and A. K. Soper, Nature (London) 378, 364 (1995).

[11] S. E. Jackson and M. C. R. Symons, Chem. Phys. Lett. 37, 551 (1976).

[12] N. G. M. Pay and M. C. R. Symons, J. chem. Soc. Faraday Trans. 89, 2417 (1993).

[13] J. Davies, S. Ormondroyd, and M. C. R. Symons, Trans. Faraday Soc. 67, 3465 (1971).

[14] I. Ohmine and T. Tanaka, J. Chem. Phys. 77, 5725 (1982).

[15] J. Ricka and T. Tanaka, Macromolecules 17, 2916 (1984).

[16] R. A. Siegel and B. A. Firestone, Macromolecules 21, 3254 (1988).

[17] A. Fernández-Nieves, A. Fernández-Barbero and F. J. de las Nieves, J.Chem. Phys. 115, 7644 (2001).

[18] T.G. Park and A.S. Hoffman, Macromolecules 26, 5045 (1993).

[19] K. Suwa, K. Yamamoto, M. Akashi, K. Takano, N. Tanaka, and S. Kunugi, Colloid Polym. Sci. 276, 529 (1998).

[20] E. Daly and B. R. Saunders, Langmuir 16, 5546 (2000).

[21] T. López-León, J. L. Ortega-Vinuesa, D. Bastos-González, and A. Elaïssari (submitted).

[22] P. J. Flory, *Principles of Polymer Chemistry* (Cornell University Press, Ithaca, NY, 1953), Chaps. 12, 13.

[23] M. Shibayama and T. Tanaka, *Volume phase transition and related phenomena in polymer gels*, in *Responsive gels I*, edited by K. Dusek (Springer, Germany, 1993).

[24] T. López-León, J. L. Ortega-Vinuesa, D. Bastos-González, and A. Elaïssari, J. Phys. Chem. B 110, 4629 (2006).

[25] *Handbook of Chemistry and Physics 68th ed.* (CRC press, Boca Raton, FL, 1987-1988).

[26] V.A. Baulin and A. Halperin, Macromolecules 35, 6432 (2002).

[27] H. Hirotsu, Phase Transitions 47, 183 (1994).

[28] B. Erman and P.J. Flory, Macromolecules 19, 2342 (1986).

[29] A. Elaissari, *Handbook of Surface and Colloid Chemistry 2nd ed* (CRC press, 2003), Chap. 12.

[30] A. Fernández-Barbero, A. Fernández-Nieves, I. Grillo, and E. López-Cabarcos, Phys. Rev. E 66, 051803 (2002).

[31] S. Hirotsu, Y. Hirokawa, and T. Tanaka, J. Chem. Phys. 87, 1392 (1987).

[32] W. McPhee, K. C. Tam, and R. Pelton, J. Colloid Interf. Sci. 24, 156 (1993).

[33] X. Wu, R. H. Pelton, A. E. Hamielec, D. R. Woods, and W. McPhee, Colloid Polym. Sci. 272, 467 (1994).

[34] L. C. Dong and A. S. Hoffman, Scientific American 86 (1993).

[35] R. Moerkerke, R. Koningsveld, H. Berghmans, K. Dusek, and K. Solc, Macromolecules, 28, 1103 (1995).

SALT INTERFERENCE IN CO-NONSOLVENCY OF POLY(N-ISOPROPYLACRYLAMIDE) MICROGEL PARTICLES IN MIXED ETHANOL-WATER SOLUTIONS

T. López-León[1,2] , D. Bastos-González[1] J.L. Ortega-Vinuesa[1] and A. Elaïssari[2]

[1] *Biocolloid and Fluid Physics Group, Department of Applied Physics, University of Granada, Av. Fuentenueva S/N, 18071 Granada , Spain.*

[2] *CNRS bioMérieux, UMR 5305, ESCPE Lyon, 43 bld du 11 novembre 1918, 69616 Villeurbanne Cedex, France.*

Abstract

Poly(N-isopropylacrylamide) (PNIPAM) is well known to exhibit reentrant behavior or co-nonsolvency in response to the composition of a mixed solvent consisting of water and a low-chain alcohol. Although some models have been proposed to explain this phenomenon, the origin of the co-nonsolvency is currently uncertain. The present work examines the way that the presence of salt can modify the reentrant-phase diagram displayed by a cationic PNIPAM microgel in the mixed ethanol/water solvent. The effects of four Hofmeister anions - SO_4^{2-}, Cl^-, NO^{3-} and SCN^- - with different abilities to modify the solvent structure were analyzed. The species with kosmotropic or structure-making character - SO_4^{2-}, Cl^- and NO^{3-} - showed a clear competition with ethanol for the water molecules, intensifying the nonsolvency of the PNIPAM with the EtOH volume fraction (ϕ_e). However, striking results were found with the most chaotropic or structure-breaking anion, SCN^-. In contrast to what happens in water-rich solutions, the presence of SCN^- in alcohol-rich solvents enhances the solubility of the polymer, which macroscopically results in the microgel swelling. Moreover, this ion displays great stabilizing properties when $\phi_e > 0.2$. Three differentiated domains can be distinguished in the stability diagram of the SCN^-, which coincides exactly with the different regions of the co-nonsolvency curve. Valuable information on the physical interactions involved in the co-nonsolvency phenomenon can be gained from analyzing these parallels. The conclusions emerging from our results favor a model based on the EtOH/water complexation.

I. Introduction

The solubility of PNIPAM in alcoholic mixtures has attracted much attention in recent decades due to its theoretic interest as well as practical applications. At room temperature, PNIPAM is soluble in both water and alcohols with low molecular weight but tends to become insoluble in mixtures of the two solvents. This phenomenon is termed "co-nonsolvency" and gives rise to a reentrant-phase diagram. PNIPAM co-nonsolvency in water/alcohol mixtures has been extensively studied both in cross-linked gels[1-4] and polymer solutions.[5-7] Despite the number of works published on this subject, its molecular origin is still controversial. Currently, there are three explanations for the PNIPAM co-nonsolvency in alcohol/water mixtures: i) The earliest and most widespread interpretation involves complexation between the two solvents. Calculations based on the Flory-Huggins thermodynamic theory suggest that the reentrant behavior results from the perturbation of the alcohol-water interaction parameter (χ_{12}) in the presence of PNIPAM. Accordingly, the formation of alcohol-water complexes would be dominant over the hydrogen bonds between PNIPAM and water.[1,2,8] However, this model has problems explaining why co-nonsolvency is also observed in highly diluted PNIPAM solutions, where the effect of the polymer on the solution properties should be negligible. ii) Schild et al.[5] suggested, then, that any mechanism to explain the reentrant transition must involve local solvent-polymer interactions. Such a collapse transition mechanism based on local concentration fluctuations was previously proposed by de Gennes[9,10] and would require the preferential adsorption of alcohol on PNIPAM. Nevertheless, the validity of the theory for these phenomena remains to be experimentally proven. iii) From experimental evidence gathered by different spectroscopic techniques, Winnik et al.[6,12] proposed a third mechanism involving both preferential adsorption and ternary complexation among PNIPAM, water, and alcohol. However, their results contrast with recent experimental findings that argue for a swelling-to-collapse-to-swelling transition fully controlled by the water/alcohol binary complexation.[7,13] The exact nature of the PNIPAM reentrant phenomenon in alcoholic solutions thus remains an open question.

In general, the presence of any co-solute in aqueous solution disrupts water structure. Species interacting with water stronger than water with itself are termed structure-makers or kosmotropes, whereas species having the opposite effect are known as structure breakers or chaotropes.[14] A number of

experimental works report evidence for a correlation between the ability of the ions to modify the water structure, on the one hand, and the Hofmeister ranking, on the other.[15] The typical order of the anion series is:

$$CO_3^{2-} > SO_4^{2-} > PO_4H^{2-} > F^- > CH_3COO^- > Cl^- > Br^- > I^- > NO_3^- > ClO_4^- > SCN^-$$

where species on the left are typically kosmotropes whereas the chaotropic character arises on moving to the right. The effect of salt on PNIPAM/water binary systems has received special attention in recent years. Many studies reveal how the presence of electrolytes can dramatically influence the solubility of the polymer. Particularly, in PNIPAM microgels this feature is manifested by the deswelling of the particles when the salt concentration increases sufficiently. In addition, the ion character according to the Hofmeister series has been shown to be determinant in these processes.[16-20] Valuable information concerning the mechanisms governing PNIPAM hydration has been drawn from these investigations. However, despite its great interest, no comprehensive studies are available on the salt effects on PNIPAM/water/alcohol ternary systems. If the reentrant behavior exhibited by the PNIPAM is in any way related to the solvent structure, it should then be highly affected by the presence of electrolytes capable of significantly modifying such a structure. Therefore, insights into the mechanisms underlying the co-nonsolvency phenomenon can be gained by investigating the Hofmeister effects in these processes. On the other hand, the study of the salt effect in PNIPAM/ethanol/water ternary systems also bears practical interest, since co-nonsolvency has been recently exploited in the controlled release of alcohol-soluble drugs.[21,22] According to the foregoing arguments, the presence of salt would be expected to modify the drug encapsulation efficiency by changing the solubility properties of the components involved in the process. Furthermore, it has been demonstrated that the encapsulation efficiency of certain systems depends on the Hofmeister character of the salt used.[23]

In the present paper, a cationic PNIPAM microgel was used to test the effect of four different Hofmeister anions - SO_4^{2-}, Cl^-, NO_3^- and SCN^- - in the reentrant-phase transition displayed by the system when embedded in a mixed ethanol/water solvent. First, co-nonsolvency was studied in the absence of salt. Based on the different trends observed, the phase diagram was divided in three independent regions: a water-rich one, an EtOH-rich one, and a transition region. The effect of the electrolytes was analyzed separately in each of these regions. Two basic features were investigated: the stability and the extent of

swelling of the microgel particles as a function of the salt concentration. Useful conclusions about the solvent structure can be drawn from the overall comparison of the experimental results. Thus, for sake of clarity, the experimental data will first be presented in Section III and, subsequently, a general discussion will be provided in Section IV.

II. Experimental

2.1 Experimental system.

The PNIPAM microgel was prepared via batch radical polymerization. Reactions were performed under emulsifier-free conditions and were carried out in a 250 ml thermostated reactor, round-bottomed four-necked flask, equipped with a glass anchor-shaped stirrer, condenser, thermocouple and nitrogen inlet. The polymerization was conducted under anaerobic conditions by using well boiled and deoxygenated water under a constant stream of nitrogen. Monomers were first dissolved in water and subsequent introduced in the polymerization reactor. A cationic comonomer (AEMH, aminoethyl methacrylate hydrochloride, from Polyscience) was added together with NIPAM (from Kodak) in order to increase the surface charge of the particles. MBA (N,N-methylenebisacrylamide, from Sigma) was used as crosslinking agent. The polymerization temperature was set constant at 70 ºC and the stirring rate was 200 rpm throughout the process. After thermal stabilization, the cationic initiator V50 (2-2'-azobis-(amidinopropane) di-hydrochloride, from Wako Chemical Group) dissolved in water was introduced. The total monomer conversion was achieved after 4 hours of polymerization. The resulting suspension was cleaned through several centrifugation/re-dispersion cycles (15000 rpm for 30 min at 25 ºC). Further details about particles synthesis and characterization are available in reference.[24]

All salts employed, i.e., Na_2SO_4, NaCl, $NaNO_3$ and NaSCN, were of analytical grade and were purchased from Merck, Sigma or Scharlau. Ethanol was also of analytical grade and purchase from Merck. Water was Milli-Q grade.

2.2 Dynamic light scattering.

The hydrodynamic diameter of the particles was measured by using dynamic light scattering (DLS). A Zetasizer 3000HS from Malvern Instruments, UK, was employed as experimental device. The experiments were performed at a scattering angle $\theta = 90^{\circ}$ using a He-Ne laser with vacuum wavelength $\lambda = 633$ nm. A Peltier chamber surrounding the sample cell enabled to control the temperature with a precision of 0.1 ºC. Temperature was kept constant at 20 ºC. As typically in DLS measurements, the hydrodynamic diameter was obtained from the intensity autocorrelation function, which is connected with the mean diffusion coefficient D of the particles. The mean hydrodynamic diameter (d) is calculated from D by using the Stokes-Einstein equation: $D = k_B T / 3\pi\eta d$, where η is the viscosity of the medium and the rest of the constants have their usual meaning. The values of η (together with the refraction index of the medium which was also required) corresponding to the different mixtures EtOH/water at 20 ºC were obtained from the literature.[25]

III. Results

Figure 1 displays the co-nonsolvency curve drawn for the cationic microgel by monitoring particle size as a function of the volume fraction of EtOH (ϕ_e) in the absence of salt. In this curve, three regions can be clearly distinguished: i) at ϕ_e values lower than 0.2 the particle diameter decreases on increasing the volume fraction of ethanol; then, ii) it reaches a minimum within the $0.2 < \phi_e < 0.5$ range; afterwards iii) a reentrant swelling occurs, when ϕ_e exceeds 0.5. The volume fraction of alcohol required to produce the minimum deswelling ratio and the trends in the data are comparable to others reported for related systems. [26-28]

Prior to an analysis of the effect of salt on the PNIPAM co-nonsolvency curve, it is important to determine the conditions under which the colloidal particles remain stable. In many cases, the presence of electrolytes or alcohol molecules in solution triggers aggregation. Such aggregation was detected by monitoring the temporal evolution of the particle diameter. When the system is stable, particles remain single entities with a constant hydrodynamic diameter. On the contrary, with aggregation, the average hydrodynamic diameter expands with time. This criterion quite accurately

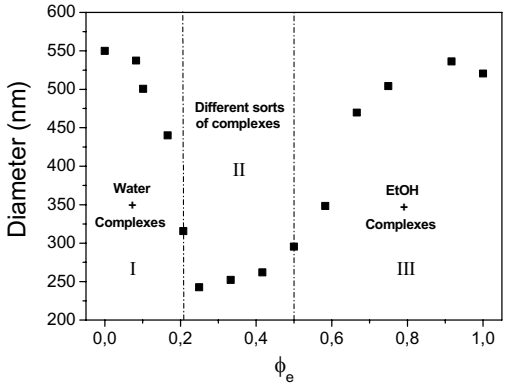

Figure 1. Particle diameter as a function of the alcohol volume fraction in the water/EtOH mixed solvent (cononsolvency curve). Vertical lines delimit the three different tendencies observed, attributed to changes in the solvent structure.

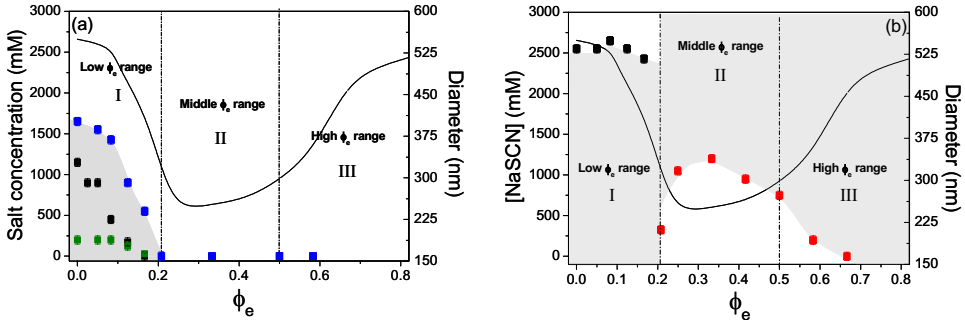

Figures 2. Stability diagrams for the PNIPAM microgel particles in the ternary water/EtOH/salt solvent. Figure 2a corresponds to the most kosmotropic electrolytes: (■) $NaNO_3$, (■) NaCl, (■) Na_2SO_4, and Figure 2b to the most chaotropic one: (■) NaSCN. Symbols refer to the critical salt concentrations separating the stable (grey areas) from the instable regions (white areas). The solid line refers to the cononsolvency curve (Figure 1) which divides the diagram in three regions separated by vertical lines.

distinguishes the stable from the unstable samples. Diameter-versus-time curves were drawn for each ϕ_e at different salt concentrations c varying from 0 to 3000 mM in 100-mM increments (figures not shown). The critical value c^* separating the stable from the unstable domains was so determined for each

volume fraction of EtOH. Due to salt solubility, only regions with $\phi_e < 0.7$ were examined. The ϕ_e-c stability diagrams corresponding to the different salts are presented in Figures 2a (for Na_2SO_4, NaCl and $NaNO_3$) and 2b (for NaSCN). In these figures symbols represent the experimental c^* values, the gray regions correspond to stable systems, and the white areas indicate aggregation. For easy location of the stability domains, the co-nonsolvency curve (Figure 1) is also displayed in these graphs (solid line).

At low EtOH concentrations, region I, all the species followed the same trend. Particles were stable below a critical salt concentration, above which the system destabilized. This is the classical behavior observed with PNIPAM microgels in pure-water solutions. The effect of adding EtOH results in a decrease of c^*, which shifts towards lower salt concentrations as ϕ_e increases. Hence, in this region, the addition of both salt and ethanol promotes aggregation. This feature was observed with all the salts except for NaSCN, registered almost the same c^* throughout this ethanol range ($\phi_e < 0.2$). In addition, the stability domains measured in the presence of the different electrolytes varied greatly according to the nature of the ion. While only 200 mM of Na_2SO_4 led to the total destabilization of the system, around 2500 mM of NaSCN was necessary for the same result at region I. Based on the ability of the ion to destabilize the PNIPAM particles, the different species were classified as follows:

More destabilizing → $SO_4^{2-} > Cl^- > NO_3^- > SCN^-$ ← Less destabilizing

(Kosmotropic character) (Chaotropic character)

This provided a ranking that exactly coincides with the Hofmeister series. From these results, it can be concluded that the most kosmotropic ions give rise to less extensive stability regions.

Two opposite patterns were observed on increasing the EtOH concentration. In the most cases - NaCl, $NaNO_3$ and Na_2SO_4 - when $\phi_e > 0.2$ the system became completely unstable under nearly any salt concentration (see Figure 2a). This trend fits well with that observed at lower ϕ_e values. By contrast, the behavior exhibited by the NaSCN at $\phi_e > 0.2$ completely diverges from that observed with the other salts (see Figure 2b). In this case, an abrupt change in the stability diagram was detected - that is, contrary to what happens when $\phi_e < 0.2$, particles aggregated at low salt concentrations while

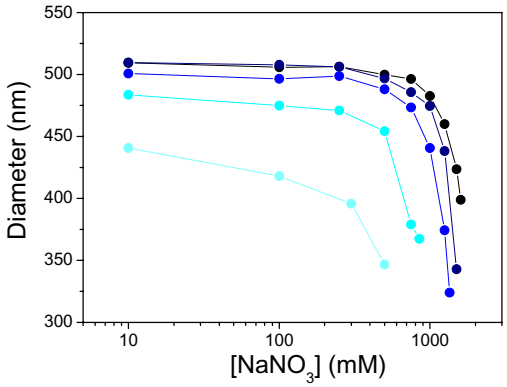

Figure 3. Particle diameter plotted versus the concentration of $NaNO_3$ for different ϕ_e values within the region I: (●) 0.00, (●) 0.05, (●) 0.08, (●) 0.12 and (●) 0.17. Similar figures were obtained with the other salts.

they stabilized above the c^*. This stabilization of PNIPAM via salt addition has not been found in pure-water solutions. Moreover, the stability curve of the NaSCN presents an asymmetric Gaussian shape which is characterized by an initial increasing slope (c^* increases with ϕ_e) that changes into a decreasing one (c^* decreases with ϕ_e) after surpassing a maximum. It is also worth noting that the turning point between the two regimes (Gaussian maximum) coincides with the minimum of the co-nonsolvency curve. In the end, the system was fully stable at any NaSCN concentration beyond $\phi_e = 0.67$.

The three regions distinguished in the co-nonsolvency curve and glimpsed in the stability diagrams become clear when the microgel swelling is investigated. The impact of salt on the PNIPAM particle size was analyzed within the stability domains of the system. For every volume fraction of EtOH the hydrodynamic diameter was measured by progressively increasing the ionic strength of the medium. Figure 3 shows the curves corresponding to $NaNO_3$ within region I ($\phi_e < 0.2$). As a general trend, the particle diameter remained nearly constant until the salt concentration reached a critical value, whereupon particles began to drastically de-swell. Such critical concentration depends on ϕ_e, shifting towards lower values as ϕ_e increases. The same trends have been observed with the other salts (curves not shown). However, although the different electrolytes reveal the same qualitative behavior,

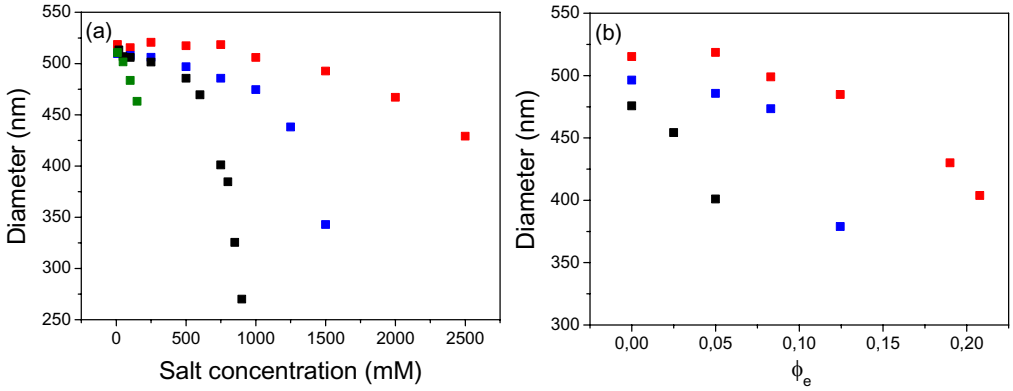

Figures 4. Comparison of the deswelling induced by the different electrolytes in region I: (■) NaSCN, (■) $NaNO_3$, (■) NaCl, and (■) Na_2SO_4. Figure 4a exhibits curves measured at a fixed EtOH concentration ($\phi_e = 0.05$) and Figure 4b at a fixed salt concentration ($c = 750$ mM).

important quantitative differences arise when they are compared. Figure 4a contrasts the ability of the NaSCN, $NaNO_3$, NaCl and Na_2SO_4 to de-swell the microgel at a fixed EtOH volume fraction ($\phi_e = 0.05$). As a counterpoint, the salt concentration required for a 10 % reduction of the microgel diameter is in each case approximately 150 mM Na_2SO_4, 600 mM NaCl, 1000 mM $NaNO_3$, and 2000 mM NaSCN. Again, if ions are now ranked according to these values, the result is a sequence which exactly coincides with the Hofmeister series. Differences among the salts become more striking when the volume fraction of EtOH increases, as shown in Figure 4b. In this case, the hydrodynamic diameter is plotted against ϕ_e at a constant salt concentration (750 mM). The curve corresponding to the Na_2SO_4 does not appear in Figure 4b because at this salt concentration the system was not stable.

Regions II and III were then analyzed. As shown, at these ϕ_e values the particles were completely unstable upon salt addition, except in the case of the NaSCN. This is why the study of the salt effect in these regions was narrowed down to the NaSCN. The evolution of the particle size with the NaSCN concentration is plotted in Figures 5a and 5b, which refer to region II ($0.17 < \phi_e < 0.5$) and region III ($0.5 < \phi_e < 0.7$), respectively. Figure 5b, which corresponds to alcohol-rich solutions, reveals that an increasing salt

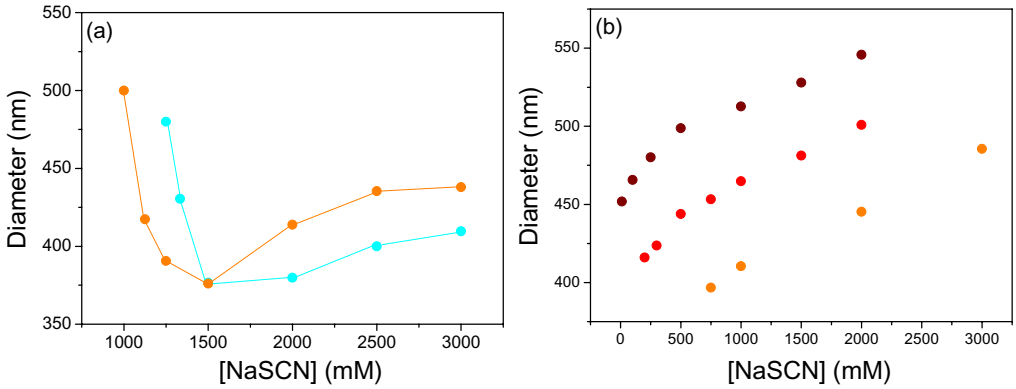

Figure 5a and 5b Particle diameter plotted versus the concentration of NaSCN. Figure 2a refers to the region II: (●) $\phi_e = 0.33$ and (●) $\phi_e = 0.42$; and Figure 2b displays curves in the region III: (●) $\phi_e = 0.50$, (●) $\phi_e = 0.58$ and (●) $\phi_e = 0.67$.

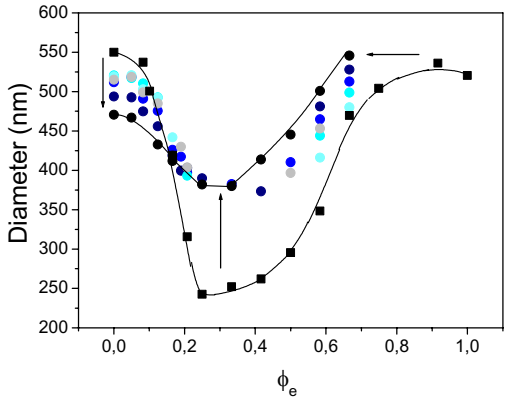

Figure 6 Particle diameter versus the EtOH volume fraction for several concentrations of NaSCN: (■) 0 mM, (●) 200 mM, (●) 500 mM, (●) 750 mM, (●) 1000 mM, (●) 1500 mM and (●) 2000 mM. Arrows indicate the effect of the increasing salt concentration on the shape of the cononsolvency curve.

concentration involves the swelling of the particles. This behavior is completely opposite to that commonly observed in pure-water solutions. It has been widely reported in the literature that salt can deswell PNIPAM particles; however, no work is available on salt-induced swelling, especially at these high

ionic strengths. The pattern observed in region II is not less surprising, Figure 5a. In this case, an initial reduction in the particle diameter followed by a reentrant swelling was detected upon progressive salt addition. These shapes appear to arise only from the superposition of the trends observed in the low(Figure 2) and the high (Figure 5b) ϕ_e ranges.

To provide a general vision of the effect of the NaSCN on the co-nonsolvency phenomenon, the swelling curves have been replotted as a function of ϕ_e in Figure 6.For stability reasons, some of the curves have not been plotted in certain concentration ranges. These data offer evidence suggesting that the addition of NaSCN strongly alters the shape of the co-nonsolvency curve. The most striking result is that increasing salt concentrations generated curves with less pronounced minima (upward-pointing arrow). In other words, the solvent content of the collapsed state increases with the NaSCN concentration. In addition, at low ϕ_e values, the slopes of the curves became less steep with the increasing ionic strength of the medium (downward-pointing arrow), whereas at concentrations rich in EtOH the points shifted toward the center of the phase diagram (left-pointing arrow).

IV. Discussion

A consistent interpretation of the experimental results can be given with reference to a model involving alcohol-water complexation. It is thought that in a water-ethanol-PNIPAM ternary system, water molecules can readily form complexes with EtOH molecules, since the hydrogen bonding between them is stronger than that between water and PNIPAM.[1,29,30] As a result, the complexation reduces the hydrogen-bonding sites in the water-ethanol mixture responsible for the PNIPAM hydration, which involves the microgel deswelling. Moreover, the decrease in hydrogen-bonding sites also restricts the solvent molecules from forming a microscopically continuous phase, and the incomplete mixing at the molecular level further promotes the desolvation.

The co-nonsolvency curve appearing in Figure 1 can be interpreted in these terms. The stepwise collapse observed in the region I may be explained by means of the increase in the number of complexes formed upon EtOH addition, which reduces the number of water molecules available for hydrating PNIPAM. Accordingly, region II is reached when the EtOH concentration is

such that the hydrogen bonding between the mixture and PNIPAM is overwhelmed by the polymer-polymer hydrophobic interaction. At this point the complexation between water and ethanol is saturated so that further addition of EtOH can only result in free alcohol molecules, which are responsible of the microgel reentrant swelling observed in region III. In conclusion, in the low and high ϕ_e range, the mixture could be regarded, respectively, as a binary mixture of "water and the complexes" and "ethanol and the complexes", while in the middle range, different sorts of water/ethanol complexes coexist.[31] Below, an analysis is made of the way in which electrolytes alter this picture. For sake of clarity, results concerning each region will be discussed separately.

4.1 Region I: Low ethanol concentrations.

The solubility of PNIPAM in alcohol-poor solutions can be understood in parallel with the polymer hydration in pure-water solutions. The rare properties of solvency exhibited by PNIPAM in water can be ascribed to the presence of both polar (amide) and apolar (isopropyl) groups in its polymeric structure. This feature prompts the formation of cage–like water structures around the hydrophobic isopropyl groups concomitantly with the establishment of hydrogen bonds between the water molecules and the amide groups at room temperature. Any factor disturbing this water structure – such as rising temperature, salt addition, etc. – enhances hydrophobic interactions and induces the polymer collapse. Particularly, the addition of co-solvents or co-solutes with tendency to interact strongly with water results in competition with the polymer for the water molecules. In a PNIPAM/water/ethanol/salt quaternary system, both ethanol and salt are agents that effectively compete with PNIPAM for hydration. In the case of ethanol, it is the removal of water molecules solvating the PNIPAM chains to form the water-EtOH complexes that causes the microgel deswelling. Likewise, the effect of salt is attributed to the self-hydration power of the ions. This is reflected in Figure 3 with a sharp deswelling of the particles when the salt concentration is high enough to cause the disruption of the water cages surrounding the isopropyl groups. This effect is stressed when ethanol is added, evidencing the competition mechanism just described. In addition, the different nature of the electrolytes can notably influence this tendency, as shown in Figures 4a and 4b. The correlation found between the electrolyte capability to promote particle collapse and the

Hofmeister series manifests a direct connection between this series and the strength of the water-electrolyte interaction. Accordingly, the electrolytes that more strongly interact with water, i.e. the most kosmotropic ions, provoke a stronger disruption of the cage-like water structure that hydrates PNIPAM and, hence, promote further deswelling in the microgel particles. This is clearly the case of the SO_4^{2-}, which has the most kosmotropic character of the ions studied. Conversely, the water structure surrounding the isopropyl group is hardly altered by the presence of highly chaotropic anions such as the SCN^-, which has a weak tendency to interact with water. Thus, in these cases, great amounts of salt are required to produce some meaningful deswelling effect.

Analogously, the colloidal stability of the system can be explained simply by considering the ability of the ethanol molecules and electrolytes to cause deswelling. When the microgel is fully swollen the system is intrinsically stable inasmuch as: i) the attractive Van der Waals forces among the particles are negligible since the effective Hamaker constant for the swollen particles is similar to the Hamaker constant for the solvent, and ii) the repulsive forces coming from the overlapping among the hairy surface layers of the polymeric particles are present. The electrostatic repulsive contribution that exists in charged microgels is insignificant when the particles are swollen due to the low surface-charge density that they present. When the system collapses, the attractive Van der Waals forces increase and the steric repulsion caused by the hairy layers disappears. Hence, the electrostatic repulsive forces remain the only stabilizing mechanism. Considering a constant number of charged groups at the particle surface, the reduction of the interfacial area through the microgel collapse implies an increase in the surface-charge density of the particles. However, in most cases this charge is not very high and can be screened by salt addition. As a result, the presence of salt once particles collapse triggers aggregation.

Curves delimiting the stable and unstable domains in region I (Figures 2a and 2b) can be explained in these terms. The progressive increase in salt concentration first induces the microgel deswelling and eventually system destabilization. This feature is evidenced in Figure 3, in which the D-c curves stop being plotted after the sharp drop of the particle size, indicating the onset of the aggregation process. Since the addition of EtOH favors the collapse of the particles, the critical concentration c^* at which the system destabilizes lowers as ϕ_e rises. This is why the stability curves in the c-ϕ_e representation (Figure 2a and 2b) show generally declining slopes. The area

delimited by these curves is strongly determined by the character of the salt used. The connection between the position of the anion in the Hofmeister series and its destabilizing power is consistent with the assumptions of the present work: the most kosmotropic ions provoke a more efficient deswelling in the microgel, which also results in a stronger destabilizing effect.

The foregoing discussion is common to all the species studied, although certain characteristics specific to some anions should be emphasized. Regarding the electrolyte charge, all the ions used were monovalent apart from the SO_4^{2-}, which was divalent. Consequently, the strong destabilization induced by the kosmotropic character of the SO_4^{2-} is also reinforced by its double valence, which causes a more efficient screening of the particle surface charge. On the other hand, contrary to that observed with the other ions, the weak destabilizing effect of the SCN^- seems not to be significantly affected by the EtOH concentration within this ϕ_e range. In general, both salt and ethanol effectively compete with PNIPAM for the water molecules so that the two factors join and simultaneously cause de-swelling. However, the domination of one factor over the other gives rise to the following two extreme situations. In the case of the SO_4^{2-}, which strongly interacts with water, the stability of the system is salt-controlled throughout most of the region I. This is why a rather elevated ϕ_e value (regarding region I) is necessary to observe some ϕ_e-effect. The opposite limit is found with the SCN^-, the presence of which hardly affects the hydration of PNIPAM. In this case it is plausible that the stability of the microgel is governed mainly by the EtOH capability of de-swelling, or, what is the same, by the EtOH-water complexation. Hence, since the collapse provoked by EtOH in absence of salt is not very significant within the $0 < \phi_e < 0.16$ range (see Figure 1) the stability curve corresponding to the NaSCN is expected not to change severely with ϕ_e at this range, as was experimentally found. This fact also implies that at $\phi_e = 0.2$ the system remains very stable in presence of NaSCN, in contrast to what happens with the other species. At $\phi_e > 0.2$ the dehydration provoked by Na_2SO_4, $NaNO_3$, and NaCl is heightened by the EtOH insofar as insignificant salt concentrations give rise to the total destabilization of the microgel.

4.2 Region III: High ethanol concentrations.

The assumption that the state of swelling of PNIPAM in ethanol/water/NaSCN solutions is governed by the formation of EtOH-water

complexes rather than by electrolyte-water interactions becomes evident when the stability of the system is investigated over the entire ϕ_e range. It was found that the whole stability diagram corresponding to the NaSCN (Figure 2b) presents three differenced parts which exactly coincide with the regions identified in the co-nonsolvency curve. Since the existence of these regions has been attributed to EtOH-water complexation, then it follows that the solvent structure also determines the stability of the system in ethanol/water/NaSCN solutions. In this sense, the way in which the SCN^- interferes with such structure is essential to an understanding of the rare stabilizing properties displayed by this ion. In region III, the solvation of the PNIPAM particles is subordinated to the existence of free EtOH molecules capable of interacting with the polymer. Therefore, the swelling induced by the addition of NaSCN (Figure 5b) can be explained only if free EtOH molecules are released due to the influence of salt. Thus, there is evidence to suggest that the SCN^- is in some way able to disrupt the clathrate structures formed between water and EtOH, thereby boosting the number of hydrogen-bond sites of the solvent. This assumption is consistent with the structure-breaking character that the SCN^- displays in water, which has been experimentally detected using a number of different techniques – including electrochemistry,[32,33] quasi-elastic neutron scattering,[34] neutron diffraction,[35] vibrational spectroscopy,[36,37] and nuclear magnetic resonance.[38] Thus, since the SCN^- is able to disrupt the hydrogen-bonding structure of water, it might similarly be expected that it is also capable of altering the water-alcohol interactions which are thought to be hydrogen-bonding, too.[13]

The striking effects of the SCN^- on the microgel swelling are readily explained in this context. Changes provoked by the SCN^- in the solvent structure are expected to become more significant the higher the number of ions in solution. Thus, the progressive addition of NaSCN implies the growing release of free EtOH molecules able to interact with the PNIPAM: as a result, the microgel swells. This would explain the positive slope of the curves plotted in Figure 5b. In addition, the salt effect appears to be invariant to the EtOH concentration, since curves corresponding to different ϕ_e values are parallel differences are due only to the initial (without salt) particle diameter. This fact emphasizes the saturated character of the EtOH-water complexation in region III. Another important inference from these experimental results is that the EtOH-PNIPAM interaction appears not to be affected by the presence of NaSCN in the medium, contrary to what happens in water rich solutions.

Comparing results obtained in regions I and III, it can be stated that the SCN^- turns the water-rich solutions and the alcohol-rich solutions, respectively, into "poorer" and "better" solvents for the PNIPAM. In terms of the Flory's solvency parameter χ for the PNIPAM-solvent interaction, the SCN^- causes χ to increase in water-rich solutions and decrease in alcohol-rich solutions. Although the mechanism responsible for the PNIPAM hydration is well known, the origin of the polymer solvency in alcohol is still not clear. What seems evident from our results is that, whatever the mechanism, it is not affected by the ionic strength of the medium. This finding is consistent with other studies which reveal that such a mechanism is not affected by temperature, either.[2] Since both salt and temperature, have analogous effects in water pure-solutions – i.e., disrupting the cage-like water structure surrounding the isopropyl groups of PNIPAM – these results suggest that the nature of the solvation driven by alcohol is completely different from that driven by water.

Under the above considerations, the origin of the Gaussian-shaped stability curve becomes obvious (Figure 2b). Although only the right side of this curve refers to region 3, for sake of clarity the general explanation of the whole curve will be displayed here. Features distinguishing region II from region III will be presented in the next section. As discussed, the stability of the system is readily connected with the state of swelling of the PNIPAM particles. Basically, aggregation occurs once the microgel has collapsed; in this situation, the repulsive steric forces are not present and the electrostatic ones can be screened by only small quantities of salt. Consequently, the addition of NaSCN to the medium has two simultaneous and opposite effects: on the one hand, it screens the particle-surface charge favoring aggregation but, on the other hand, it also promotes the disruption of the alcohol-water clathrate structures, thereby encouraging the microgel swelling. In the range $0.2 < \phi_e < 0.7$, in which the PNIPAM particles are in general slightly swollen, the stability of the system is controlled mainly by electrostatic repulsion. Hence, small concentrations of NaSCN only trigger aggregation. However, the microgel swelling becomes more and more important as the ionic strength of the medium increases. At the critical concentration c^*, the microgel is sufficiently swollen for the steric repulsion to become important. As a result, the system re-stabilizes. Clearly, this critical concentration depends on the initial state of swelling of the microgel in the absence of salt. The most collapsed particles require greater SCN^- concentrations to reach the "stable

swollen state". In this sense, the stability diagram should reflect the inverse outline of the swelling curve. In fact, this is exactly what was experimentally found, since the Gaussian-like shape of the stability diagram results directly from inverting the co-nonsolvency curve.

4.3 Region II: Moderate ethanol concentrations

Up to now, the effect of NaSCN it has been investigated in solutions where one solvent predominates over the other, and opposite effects have been found when water or EtOH acts as the main component. Region II can, then, be considered as a region of transition between the two extreme regimes. In this middle ϕ_e range, the free solvent molecules scarcely exist and the EtOH-water complexes appear as the main component of the solution. This makes region II of special interest, since all the interactions involved in the PNIPAM solvency are manifestly present. Accordingly, such "critical" solutions allow a comparison, at the same time, of the PNIPAM-EtOH and PNIPAM-water interactions. In particular, it can be established when one dominates the other and the way in which they are differently affected by the ionic strength of the medium. All this information is reflected in the swelling curves plotted in Figure 5a. Firstly, the stepwise collapse of the microgel with the NaSCN concentration suggests a solvation mechanism controlled by the PNIPAM-water interactions. Otherwise, the reentrant swelling at high salt concentrations reveals a solvation process governed by the EtOH-PNIPAM interactions. The abrupt change of sign exhibited by the slope of these curves at a given NaSCN concentration establishes the limit between the two regimes.

From a molecular standpoint, the two scenarios envisaged respectively for regions I and III converge perfectly to explain region II. In the middle ϕ_e range, even in the absence of any salt, particles are strongly collapsed and, in general, rather high concentrations of NaSCN are necessary to attain the stable swollen state (see Figure 2b). This effect, observed previously in alcohol-rich solutions, has been attributed to the capacity of SCN^- to release free solvent molecules by disrupting the clathrate structures formed between the EtOH and water. However, in contrast to region III, in the middle ϕ_e range an increase in free water molecules first makes the polymer swell, as discussed above. This finding has an important implication: the interaction between the SCN^- and the complexes must be such that both water and EtOH molecules are simultaneously released. Since this region is poor in free solvent molecules,

almost all the species participating in the polymer solvency come from the disruption of the complexes. Thus, the water-induced swelling observed upon salt addition is due to the fact that water is the main component of the clathrate structures in region II.

Accordingly, parallel to the scenario in region III, the raising of the salt concentration to values higher than c^* would be expected to result in the polymer swelling, simply, because the number of water molecules released would also rise. However, the hydration mechanism of the PNIPAM is very sensitive to the ionic strength of the medium. Even in pure-water solutions, salt concentrations of the order of c^* are sufficient to destabilize the cage-like structures responsible for polymer hydration. This is why SCN^- concentrations higher than c^* prompt microgel deswelling. The solvation mechanism associated with the EtOH, however, has been demonstrated not to be affected by the ionic strength of the medium. Consequently, PNIPAM-ethanol interactions become important at high salt concentrations where the number of EtOH molecules begins to be significant and the interactions PNIPAM-water are weak. The result is a reentrant behavior following a pattern analogous to that observed in region III.

Finally, the foregoing discussion sheds light on the microscopic origin of the Gaussian-shaped stability diagram (Figure 2b). If the limits left and right of the stability curve are first considered, both are found to be situated in regions where the complexes coexist with free water molecules ($\phi_e = 0.2$) and free EtOH molecules ($\phi_e = 0.7$), respectively. Microgel is, then, partially swollen, and only moderate concentrations of NaSCN are necessary to reach the stable swollen state. On approaching the center of the Gaussian – which coincides with the minimum of the co-nonsolvency curve – the EtOH-water complexation becomes stronger and stronger while the number of free solvent molecules gradually decreases. As a result, steadily higher NaSCN concentrations become necessary to release the amount of water (in region II) or EtOH (in region III) required to attain the stable swollen state. The highest critical concentration c^* is found just at the minimum of the co-nonsolvency curve.

V. Conclusions

The study of the salt effect on the PNIPAM co-nonsolvency in mixed water/EtOH solutions has proved to be a useful tool to investigate the interactions governing these phenomena. In water-rich solutions ($\phi_e < 0.2$) the addition of salt induces particles to collapse, promoting system destabilization. This result has been attributed to the capability of the ions to interact with the water molecules responsible for the PNIPAM solvation. A correlation was found between the Hofmeister series and the effectiveness of the electrolytes to deswell the microgel: the ion ability to disrupt the water structure determines the macroscopic swelling state of the particles. This feature evidences the structural nature of the PNIPAM hydration. Due to the deswelling provoked by the co-nonsolvency phenomenon, most of the electrolytes drove the system to complete destabilization when $\phi_e > 0.2$, even at very low salt concentrations. However, noteworthy results were found with the NaSCN. In alcohol-rich solutions ($\phi_e > 0.5$) – where the polymer solvation is probably driven by EtOH molecules –completely different trends from those observed in water-rich solutions were found. First, the PNIPAM-EtOH interactions appeared not to be affected by the presence of NaSCN, even when values were raised to around 2 or 3 M. Moreover, the increasing concentration of NaSCN involved microgel swelling and bolstered system stability. A consistent explanation of these results can be derived from considering a microscopic model based on the complexation between the EtOH and water. The striking properties of the NaSCN can, then, be ascribed to the structure-breaking character of this ion, which might be able to disrupt the EtOH-water complexes, thereby favoring the solvency of the polymer. The two opposite effects displayed by the NaSCN in water and EtOH-rich solutions, enabled the macroscopic detection of whether the polymer solvation was driven by water or by EtOH molecules, respectively. Accordingly, the present study concludes that in the intermediate ϕ_e region the PNIPAM solvation was firstly controlled by polymer-water interactions and secondly by polymer-EtOH interactions as the concentration of NaSCN increased. These findings reflect a scenario in which the PNIPAM solvency is controlled by the formation/disruption of the EtOH-water complexes.

Acknowledgements

The authors would like to thank the financial support granted by "FEDER" and "Comisión Interministerial de Ciencia y Tecnología" (CICYT, Spain), projects MAT2003-01257 and AGL2004-01531/ALI. They also gratefully acknowledge the bioMérieux company for the support provided in terms of chemicals and equipment.

References

(1) Amiya, T.; Hirokawa, Y.; Hirose, Y.; Li, Y.; Tanaka, T. *J. Chem. Phys.* **1987**, *86*, 2375.

(2) Hirotsu, S. *J. Chem. Phys.* **1988**, *88*, 427.

(3) Mukae, K.; Sakurai, M.; Sawamura, S.; Makino, K.; Kim, S. W.; Ueda, I.; Shirahama, K. *J. Phys. Chem.* **1993**, *97*, 737.

(4) Asano, M.;. Winnik, F. M; Yamashita, T.; Horie, K. *Macromolecules* **1995**, *28*, 5861.

(5) Schild, H. G.; Muthukumar, M.; Tirrell, D. A. *Macromolecules* **1991**, *24*, 948.

(6) Winnik, F. M.; Ottaviani, M. F.; Bossmann, S. H.; Garcia-Garibay, M.; Turro, N. J. *Macromolecules* **1992**, *25*, 6007.

(7) Zhang, G.; Wu, C. *Phys. Rev. Lett.* **2001**, *86*, 822.

(8) Katayama, S.; Hirokawa, Y.; Tanaka, T. *Macromolecules* **1984**, *17*, 2641.

(9) De Gennes, P.G. *J.Phys.Lett* **1976**, *37*, L-59.

(10) Brochard, F. ; de Gennes, P.G. *Ferroelectrics* **1980**, *39*, 33.

(11) Heskins, M. ; Guillet, J. E. *J. Macromolec. Sci. Chem.* **1969**, *2*, 1441.

(12) Winnik, F. M.; Ottiviani, M. F.; Bossmann, S. H.; Pan, W.; Garcia-Garibay, M.; Turro, N. J. *Macromolecules* **1993**, *26*, 4577.

(13) Liu, G.; Zhang, G. *Langmuir* **2005**, *21*, 2086.

(14) Collins, K. D.; Washabaugh, M. W. *Q. Rev. Biophys.* **1985**, *18*, 323.

(15) Cacace, M. G.; Landau, E. M.; Ramsden, J. J. *Q. Rev. Biophys.* **1997**, *30*, 241.

(16) Schild, H. G.; Tirrell, D. A. *J. Phys. Chem.* **1990**, *94*, 4352.

(17) Zhang, Y.; Furyk, S.; Bergbreiter, D. E.; Cremer, P. S. *J. Am Chem. Soc* **2005**, *127*, 14505.

(18) Daly, E.; Saunders, B. R. *Langmuir* **2000**, *16*, 5546.

(19) Lopez-Leon, T.; Ortega-Vinuesa, J. L.; Bastos-Gonzalez, D.; Elaissari, A. (submitted to Chem. Phys. Chem.).

(29) Lopez-Leon, T.; Fernandez-Nieves, A. (submitted to Phys. Rev. E).

(21) Mukae, K.; Bae, Y. H.; Okano, T.; Kim, S. W. *Polym. J.* **1990**, *22*, 250.

(22) Bae, Y. H.; Okano, T.; Kim, S. W. *Pharmacol. Res* **1991**, *8*, 624.

(23) Al-Maaieh, A.; Flanagan, D. R. *J. Controlled Release* **2001**, *70*, 169.

(24) López-León, T.; Ortega-Vinuesa, J. L.; Bastos-González, D.; Elaïssari, A. *J. Phys. Chem. B* **2006**, *110*, 4629.

(25) *Handbook of Chemistry and Physics 68th ed.* (CRC press, Boca Raton, FL, 1987-1988).

(26) McPhee, W.; Tam, K. C.; Pelton, R. *J. Colloid Interface Sci.* **1993**, *156*, 24.

(27) Saunders, B. R.; Crowther, H. M.; Vincent, B. *Macromolecules* **1997**, *30*, 482.

(28) Crowther, H. M.; Vincent, B. *Colloid Polym. Sci.* **1998**, *276*, 46.

(29) Winnik, F. M.; Ringsdorf, H.; Venzmer, J. *Macromolecules* **1990**, *23*, 2415.

(30) Zhu, P. W.; Napper, D. H. *J. Colloid Interface Sci.* **1996**, *177*, 343.

(31) Noskov, S. Y.; Lamoureux, G.; Roux, B. *J. Phys. Chem. B* **2005**, *109*, 6705.

(32) Gurney, R. W. *Ionic Processes in Solution*; McGraw-Hill: New York.

(33) Chatterjee, J. P.; Basumallick, I. N. *J. chem. Soc. Faraday Trans.* **1990**, *86*, 3107.

(34) Jimenez, R.; Fleming, G. R.; Kumar, P. V.; Maroncelli, M. *Nature (London)* **1994**, *369*, 471.

(35) Leberman R.; Soper, A. K. *Nature (London)* **1995**, *378*, 364.

(36) Jackson, S. E.; Symons, M. C. R. *Chem. Phys. Lett.* **1976**, *37*, 551.

(37) Pay, N. G. M.; Symons, M. C. R. *J. chem. Soc. Faraday Trans.* **1993**, *89*, 2417.

(38) Davies, J.; Ormondroyd, S.; Symons, M. C. R. *Trans. Faraday Soc.* **1971**, *67*, 3465.

THERMOSENSITIVE REVERSIBLE NANOPARTICLES FORMED BY SELF-ASSEMBLY OF POLY(N-ISOPROPYLACRYLAMIDE) CHARGED CHAINS: TESTING HOFMEISTER EFFECTS.

Teresa López-León[1], Juan L. Ortega-Vinuesa[1], Delfi Bastos-González[1] and Abdelhamid Elaïssari[2]

[1] *Colloid and Fluid Physics Group, Department of Applied Physics, University of Granada, Av. Fuentenueva S/N, 18071 Granada , Spain*

[2] *CNRS bioMérieux, UMR 5305, ESCPE de Lyon, 43 boulevard du 11 novembre 1918, 69616 Villeurbanne Cedex, France*

Abstract

Traditionally PNIPAM has been synthesized by using nonionic initiators. This implies that the increase of temperature above the LCST triggers polymer aggregation and consequently leads to the water-polymer phase separation. However, the use of PNIPAM charged chains has allowed us to generate stable colloidal particles as reported in this work. The stability of the particles formed by inter-chain aggregation stem from the charged chemical groups attached on the PNIPAM macromolecules. The particle formation was fully reversible, that is, it was possible to change from stable polymer solutions to stable colloidal dispersions and vice versa just by varying the temperature. In addition, we have also proved that the polymer LCST, the final particle size and the electrokinetic behavior of the formed particles were highly dependent on the electrolyte nature and the salt concentration. The particular characteristics of this novel PNIPAM based system were exploted to analyze the effects produced by the electrolyte nature, that is, those effects associated with the Hofmeister series. It is currently accepted that Hofmeister effects come from i) changes in water structure (around ions and solvated surfaces), and ii) specific ion adsorption - exclusion mechanisms at interfaces. The first one, related to the ion hydration, was clearly observed when changes in the LCST were studied. The second one, connected with ion accumulation, made more evident when electrokinetic properties were analyzed. Finally, the results concerning to the ion accumulation mechanisms have been theoretically treated by the Ninham's theory.

I. Introduction

Poly(N-isopropylacrilamide) (PNIPAM) has been extensively studied in the last two decades. The great interest in this polymer is due to its extraordinary properties of solvency, highly dependent on the solvent characteristics, such as salt concentration, pH and, especially, the temperature. It is well known that single polymer chains of PNIPAM dissolved in water undergo a sharp collapse transition from expanded coil to compact globule as temperature is raised [1-4]. This peculiar behavior is due to the presence of hydrophilic (amide groups) and hydrophobic (isopropyl groups) moieties in the NIPAM molecule. The collapse of individual polymer chains from a highly hydrated extended coil into a globule happens when the temperature is increased above 31-34 ºC [5], which is close to the Flory θ-temperature separating the good solvent from the poor solvent regions. Water behaves as a good solvent through hydrogen bonding with the amide groups at room temperature. This hydrogen bonding with water is increasingly disrupted on heating, causing water to act as a poorer solvent. When increasing temperature, the monomer-monomer interactions become stronger than the monomer–solvent interactions, what leads to the polymer chain contraction since the number of monomer–monomer contacts increases. This process involves an important loss of entropy in the PNIPAM chains due to factors related to excluded volume and conformational freedom. The general coil to globule phase transition has been widely investigated from a theoretical point of view [1-3,6,7]. Grosberg and Kuznetsov established a kinetic phase diagram of a polymer solution [7] by calculating the characteristic relaxation times of the processes involved in the phase transition. They proposed four hypothetical kinetic stages: In the single-chain regime they predicted (i) an initial crumpling process, whereby a polymer chain contracts towards its centre followed by (ii) the knotting of the crumpled polymer chain. The first theoretical stage has been experimentally observed by Wu et al. recently [8], while the second one has been observed by Zhu and Napper [9] . The third and fourth stages give phase separation, which would be triggered by (iii) polymer aggregation followed by (iv) the mutual entanglement of aggregated chains. The relaxation times associated to the previous processes (τ_{crumb}, τ_{eq}, τ_{collis}, τ_{ent}, respectively) determine the final state of the polymer solution. The regions of fast coil aggregation and phase separation, which occur when $\tau_{collis} < \tau_{crumb} < \tau_{eq}$, have been experimentally observed by numerous authors when working with uncharged PNIPAM chains. However, the aggregation

process could be stopped before starting the phase separation if any stabilizing mechanism appears. In this work, we propose a stabilization mechanism based on electrostatic repulsion. The chosen strategy was to employ PNIPAM chains synthesized by using an ionic initiator, so that polymer chains had certain amphiphilic character. In this case, the aggregation process gives rise to multichain particles formed by PNIPAM self-association with charged groups attached at the extreme of the chains. This generates a surface charge density that would be able to stabilize the growing particles and subsequently prevent the phase separation. Thus, just by varying the temperature, it would be possible to change from a stable polymeric solution to a stable colloidal suspension and vice versa. We report here the preparation and properties of these "reversible" particles and how they are affected by ions of different nature.

It is widely known that different ions are able to specifically modify a broad range of phenomena: solubility of salts, surface tensions, zeta potentials, cloud points of non-ionic surfactants, critical micelle concentrations, microemulsion microstructures, transport across membranes, gel swelling, colloid stability and so forth [10-12]. These ionic specificities are commonly known as Hofmeister effects. They are universal phenomena present in biology, biochemistry, chemistry and chemical engineering, colloid and surface science, and, even though they were observed for the first time in 1888, their origin is still a matter of debate [12]. Recently, great efforts have been made to theoretically justify these effects. Ninham and co-workers [13-20] have developed a model which predicts specific ion adsorption by considering an ionic dispersion potential that acts between an ion and an interface. The universal attractive dispersion force between any ion and any interface depends, among other things, on the ion polarizability. Hence, ions with different polarizabilities would experiment specific attractive forces when approaching a surface. This theory, although is able to explain many Hofmeister phenomena, fails when water structure effects appear. Hofmeister effects also seem to be associated with how solutes modify the water structure. It has been proved that there exist a certain correlation between Hofmeister effects and thermodynamic parameters such as entropy of hydration of ions. It evidences that the hydration properties, seen as local distributions and binding energies of water molecules in the hydration shell of ions are central to this problem [10,11,21]. The twin properties, ion adsorption at interfaces and changes in water structure, are related and seem impossible to disentangle.

In this work, the two mechanisms underlying the Hofmeister effects are observed by using temperature sensitive colloidal particles generated by self assembly of PNIPAM charged chains. The paper has been divided into two parts. The first one deals with the solubility – insolubility of the PNIPAM chains as a function of temperature in presence of different salts (Na_2SO_4, NaCl, $NaNO_3$ and NaSCN). As will be shown, the experiments developed in this part reflect the water structure origin of the Hofmeister effects. The second part of the paper is aimed to study the properties of the stable colloidal particles that appear when PNIPAM chains collapse and aggregate. Average size, colloidal stability and electrophoretic mobility data have been analyzed; the results corroborate the ion accumulation mechanism as responsible for the observed Hofmeister effects. Therefore, this PNIPAM chain – colloidal particle "reversible" system has allowed us to confirm that Hofmeister effects come from hybrid mechanisms where ion accumulation processes originated by high-frequecy dispersion forces and changes in the water structure induced by the presence of the ions coexist and act simultaneously.

II. Experimental Section

2.1. Electrolytes.

Na_2SO_4, NaCl, $NaNO_3$, and NaSCN salts were of analytical grade and purchased from different firms: Sigma, Panreac and Scharlau. Water of Milli-Q quality was used throughout.

2.2. Sample preparation.

Anionic and cationic Poly(NIPAM) polymers were prepared by batch radical polymerization using N-isopropylacrylamide (NIPAM, 1.38 g) as monomer and potassium persulfate (KPS, 33 mg) and 2,2'-azobis(2-amidinopropane) dihydrochloride (V50, 33 mg) as anionic and cationic initiators, respectively. NIPAM (from Kodak) was purified by recrystallization from a (60/40) (v/v) toluene/pentane mixture, V50 (from Wako) was recrystallized from 50/50 (v/v), acetone/water mixture and KPS (reagent grade from Prolabo) were used as received. Polymerizations were performed in 50 ml of dionized water contained in a 100 ml volume capacity reactor during 12 hours at 70 $^{\circ}$C under a constant stir (200 rpm) and nitrogen stream. The

obtained polymers were used as such after dilution in dionized water. All the experiments were performed at constant polymer concentration of 0.05 mg/ml.

2.3. Lower critical solubility temperature (LCST).

The LCST of the polymer solutions was determined by using an UnikonxL spectrophotometer equipped with Thermosystem (from Serbolabo Technologies, France). Solubility was evaluated by monitoring changes in sample optical density (O.D.). The LCST values were taken as the initial break points of the O.D. versus temperature curves.

2.4. Diameter and electrophoretic mobility.

Particle size and electrophoretic mobility were measured with a Zetasizer 3000HS from Malvern Instruments (Malvern UK). The particle size was determined by dynamic light scattering: the cumulant analysis of the measured intensity-intensity time correlation function resulted in the translational diffusion coefficient distribution G(D), from which the hydrodynamic size distribution f(R_h) can be calculated by using the Stokes-Einstein equation, $D = k_B T/(6\pi\eta R_h)$ with k_B, η and T the Boltzmann constant, the solution viscosity and the absolute temperature, respectively.

III. Results and Discussions

Four anions with different Hofmeister character were chosen for this study, namely sulfate, chloride, nitrate, and thiocyanate. Their relative positions in the Hofmeister series are:

$$CO_3^{2-} > \mathbf{SO_4^{2-}} > PO_4H^{2-} > F^- > CH_3COO^- > \mathbf{Cl^-} > Br^- > I^- > \mathbf{NO_3^-} > ClO_4^- > \mathbf{SCN^-}$$

The species on the left are referred to as *kosmotropes / structure-makers / strongly hydrated / salting-out* ions while those on the right are called *chaotropes / structure-breakers / weakly hydrated / salting-in* ions. The Cl^- and the Na^+ ions are considered as indifferent species [10,11]. This is why, to compare the effect exerted by the different anions, four sodium salts were used (NaSCN, $NaNO_3$, NaCl, Na_2SO_4). As all of them share the same cation, the specific effects observed in our experiments must be attributed to the anions.

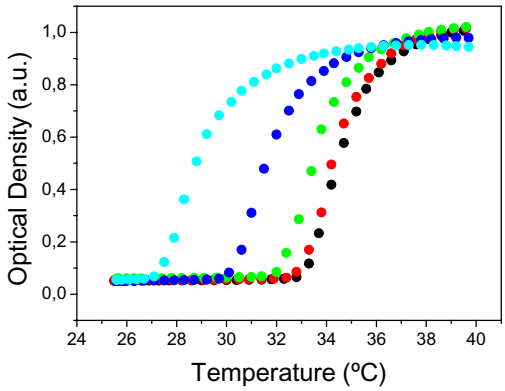

Figure 1. Optical density of cationic PNIPAM solutions as a function of temperature in presence of different NaCl concentrations. (●) 10 mM; (●) 50 mM; (●) 100 mM; (●) 250 mM; and (●) 500 mM.

Moreover, as the study has been developed working in parallel with positive and negative PNIPAM, it has been feasible to analyze differences when the anions acted either as counter or co-ions.

3.1. Charged-PNIPAM polymer solutions

The first part of the present work deals with polymeric solutions. Attention will be specially paid on how the electrolytes modify the solvency properties of PNIPAM in aqueous solutions. In this case, polymer-polymer, polymer-water, polymer-ion, and water-ion interactions must be considered. Although the temperature is the major factor that governs the solubility of PNIPAM, the presence of salts also affects it. Figure 1 shows the phase transition undergone by PNIPAM with temperature at different NaCl concentrations. The presence of salt shifts the LCST to lower values, becoming this effect more pronounced as the ionic strength increases. This feature, common for all the electrolytes studied, has been ascribed to the ability of ions to disrupt polymer-water hydrogen bonds [22-24]. Similar patterns were also observed with the anionic sample (figure not shown). It should be noted, however, that in pure water cationic and anionic pools show a slight divergence in the LCST values, 33ºC and 34ºC respectively, which may

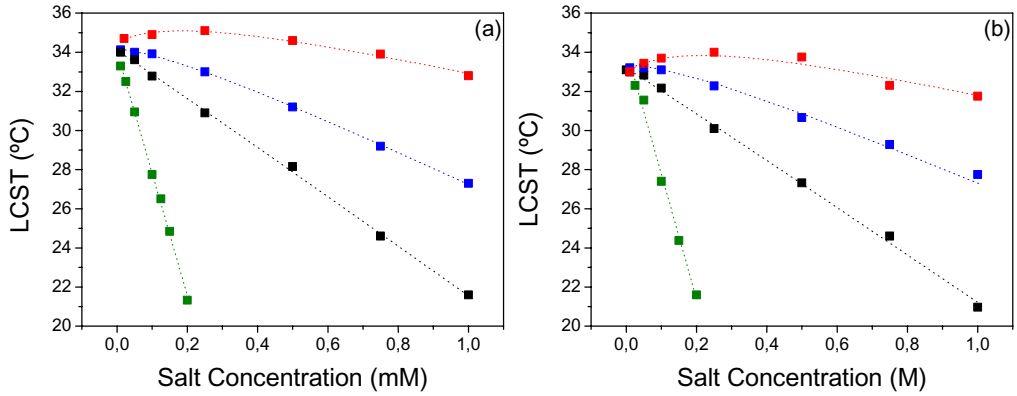

Figure 2. LCST of the **(a)** anionic and **(b)** cationic PNIPAM solutions in presence of different salt concentrations. (■) NaSCN; (■) $NaNO_3$; (■) NaCl; and (■) Na_2SO_4.

probably come from differences in the initiators used. The KPS employed in the synthesis of the anionic pool gives rise to sulfate groups, more hydrophilic than those resulting from the cationic initiator (AEMH), which holds apolar sites as well as ionic groups. Therefore KPS enhances the global hydrophilic character of PNIPAM and shift the LCST to a little higher temperature than AEMH [25]. Nevertheless, as can be seen afterwards, this difference vanishes as salt effect becomes important.

The specific effects of anions were then analyzed. The LCST of PNIPAM aqueous solutions as a function of salt concentration and anion type are plotted in Figure 2a for the anionic pool, and 2b for the cationic one. Great differences among the anionic species were observed. For a given salt concentration (i.e. 0.2 M), the LCST values order the anions according to the Hofmeister series, $SCN^- > NO_3^- > Cl^- > SO_4^{2-}$, so that species with more accentuated kosmotropic nature provide lower LCST values. In other words, the destabilizing effect of the salt increases with the kosmotropic character of the anion employed. These results can be explained according to a microscopic mechanism based on ion-induced changes in water structure. Hydration of electrolytes in solution induces PNIPAM–H_2O hydrogen bonding disruption, and consequently, to the desolvation of the carbonyl and amide groups of the polymer. As a result, the dehydrated chains collapse and aggregate through intra and interchain hydrophobic interactions, which become dominant above

the LCST. This effect is more pronounced for kosmotropic than for chaotropic ions. It is widely recognized that kosmotropes interact more strongly with water than chaotropes, and thus, they are expected to cause a more effective disruption of the amide-water hydrogen bonds [22-24]. Therefore, the competition for the water molecules hydrating PNIPAM would be more effective for the former than for the latter, resulting in a more destabilizing effect. It is interesting to note that similar results were found with both cationic and anionic PNIPAM samples, indicating that no specific interaction of ions with the charged groups of the polymer exists. Our results are consistent with those obtained by other authors working with PNIPAM microgels, or neutral PNIPAM macromolecules [26-28].

The mechanism concerning water-structure modifications has been commonly referred to explain Hofmeister effects in PNIPAM based systems. However, recent studies on electrophoretic behavior of PNIPAM nanoparticles have also evidenced the existence of specific ion accumulation phenomena [24]. Both mechanisms seem to be interconnected and represent a suitable framework to fully understand the Hofmeister effects. In order to afford quantitative information about these phenomena, a model proposed by Zhang at al. [28] involving specific ion accumulation has been contrasted with our experimental results. Furthermore, recent works underline that dispersion forces are a key point in the research of a general explanation of the specific ion (Hofmeister) effects that are ubiquitously observed in many experiments [13-20]. Inclusion of dispersion forces in theories concerning interfaces results in ion accumulation/exclusion depending on the adjoining media. In the present paper, Zhang's model has been re-interpreted by incorporating some concepts related to ion polarizability; specifically, the universal dispersion forces contemplated in Ninham's theory will be considered.

Figures 2a and 2b shows a linear dependence of the PNIPAM LCST on salt concentration. The linearity is extremely high for the kosmotropic anion (sulfate) and progressively disappears as ion nature becomes more chaotropic. Zhang et al. [28], working with a non-ionic PNIPAM system, modelled the changes in the LCST (ΔT) caused by adding salt proposing the following equation:

$$\Delta T = c[M] + \frac{B_{\max} k[M]}{1 + k[M]} = \Delta T_{linear} + \Delta T_{Langmuir\ isotherm} \qquad (1)$$

Table 1. Fitted values for c, B_{max} and k from the LCST data corresponding to the anionic and cationic samples.

Anion	c (ºC/mol)		B_{max} (ºC)		k (M^{-1})	
	$P_{anionic}$	$P_{cationic}$	$P_{anionic}$	$P_{cationic}$	$P_{anionic}$	$P_{cationic}$
SO_4^{2-}	-62.4	-63.8	-	-	-	-
Cl^-	-12.8	-12.3	0.6	0.5	1.1	1.3
NO_3^-	-8.6	-7.8	2.3	2.3	3.0	3.2
SCN^-	-4.0	-4.1	3.0	3.6	4.2	4.3

The equation includes a linear term and a Langmuir isotherm contribution. In this expression $[M]$ is the molar concentration of salt. The Langmuir term contains two constants: Bmax is the increase in the LCST due to direct ion binding at saturation, while k is the binding constant of the anion to the polymer. The constant c appearing in the linear term has different interpretations depending on the kosmotropic/chaotropic character of the ion. According to Zhang's work [28], c is directly related to the hydration entropy of the ion for kosmotropic ions, while it is related to changes in the surface tension ($\Delta\gamma$) at the water/hydrophobic interface for chaotropes. The dashed lines in Figures 2a and 2b result from fitting Equation 1 to the experimental data, using c, Bmax and k as fitting parameters. Table 1 summarizes the values of the parameters obtained from this fitting. As can be seen, the linear term is dominant for kosmotropic anions whereas the non-linear term becomes important for the more chaotropic anions.

In our case, all the electrolytes analyzed, except the SO_4^{2-}, are chaotropes. Therefore, the lineal term ($c[M]$) would be related to changes in the surface tension at the PNIPAM/water interface, while the Langmuir isotherm would be the result of specific ion binding to the amide group of PNIPAM. Both terms have, then, opposite effects. An increase in the surface tension ($\Delta\gamma$) entails a lower solubility of the polymer that will tend to reduce its interfacial area by collapsing. On the contrary, ion adsorption will promote polymer expansion due to electrostatic repulsions. This explains the opposite sign of the fitting parameters shown in Table 1. The relation proposed by Zhang et al. between the c parameter and changes in surface tension is direct:

$$\Delta T_{linear} = c[M] \qquad (2)$$

Table 2. Literature values of surface tension increment (σ), ions excess polarizability (α), and B parameter for the ions analyzed.

Ions	σ (μNm²/mol)	α (Å³)	B (10^{-49} Jm³)
Cl^-	2.74	3.59	-1.61
NO_3^-	1.55	4.30	-1.89
SCN^-	0.89	6.61	-2.96
SO_4^{2-}	0.54	6.66	5.35
Na^+	-	0.15	-0.40

Since at a hydrophobic/water interface the surface tension increases proportionally to the salt concentration [10]:

$$\Delta\gamma = \sigma[M] \tag{3}$$

Consequently, the c parameter and the σ one ($\sigma = d\Delta\gamma/d[M]$) might be related. In fact, Zhang et al. do find a direct proportionality between them when working with chaotropic ions. The same linear correlation was revealed when plotting the c values obtained from our experimental data versus the corresponding σ values acquired from literature (see Table 2), as shown in Figure 3a. It is worthwhile to recall that this interpretation for the lineal term only works for chaotropic and null ions, but not for kosmotropes (i.e. SO_4^{2-}). Hence, although only three experimental points are available with each sample (those corresponding to SCN^-, NO_3^- and Cl^-), they suggest the linear dependence observed by Zhang et al. with non-charged PNIPAM.

On the other hand, Ninham et al. explained changes in surface tensions recurring to an ionic accumulation mechanism governed by high frequency dispersion forces, where the ion polarizability (α) is the key point. As the c parameter is related to σ [28], and σ could be related to α [14,17], we propose to relate c with the ion polarizability, that is, connect Zhang's model with Ninham's theory. According to Ninham et al. the specific ion effects on surface tension are dominated (at high salt concentrations) by dispersion forces, and the change in surface tension obeys the equation shown below [14,17]:

$$\Delta\gamma(M) = 2.7\, k_B T(\beta B)^{1/3}[M] \tag{4}$$

where B is approximately $B \approx \left(n_w^2 - n_{air}^2\right)\alpha^*(0)\hbar\omega_i/8$ and $\beta = 1/k_B T$.

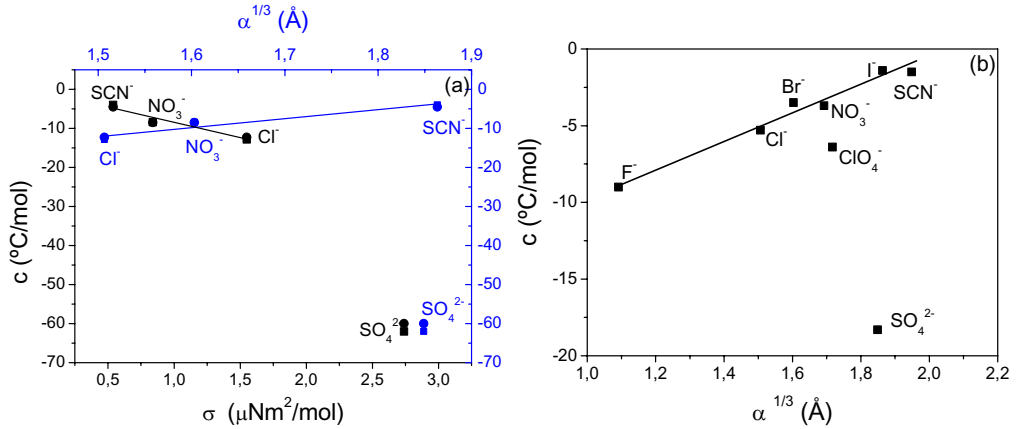

Figure 3. c parameter of eq. 1 (and/or 2) versus: **(a)** σ parameter of eq. 3 (black symbols) and versus the ion static excess polarizability to the cubic root (blue symbols) for anionic (squares) and cationic PNIPAM (circles). **(b)** c parameter of eq. 1 (and/or 2) versus the ion static excess polarizability to the cubic root (open symbols) for a non-charged PNIPAM. Data extracted from reference [25].

Here, n is the refractive index (corresponding to water, nw, and air, nair), $\hbar\omega_i$ is the electron affinity of the ion, $\alpha^*(0)$ is the static excess polarizability of an ion in water, k_B is the Boltzmann constant and T is the temperature. In our case n_{air} should be substituted by n_{PNIPAM}. As Equation 4 predicts for $\Delta\gamma$ a linear dependence on salt concentration, thus:

$$\sigma = \frac{\partial \Delta\gamma}{\partial [M]} = 2.7\, k_B T (\beta B)^{1/3} \tag{5}$$

According to B definition, the ion specificity arises from the different values of $\alpha^*(0)$ and $\hbar\omega_i$ associated to the diverse species. However, monovalent ions usually have similar electron affinities, what makes that in practice differences among ions could be entirely ascribed to their different ion excess polarizability. That is, for the different electrolytes, σ should depend on $\alpha^*(0)^{1/3}$. If the c parameter of the Zhang's model depends linearly on σ, then, a $c \propto \alpha^*(0)^{1/3}$ relation might be expected. This hypothesis was experimentally corroborated, as shown in Figure 3a, where such linearity is clearly manifested by the chaotropic ions. However, the number of experimental points is not sufficient to establish any definitive conclusion. In order to confirm this c

versus $\alpha^*(0)^{1/3}$ linearity with more ions, we have performed the same analysis with c data provided by Zhang et al. for a number of chaotropic anions [28]. The results are shown in Figure 3b. The linear dependence is clearly confirmed, excepting SO_4^{2-}. In addition, the results do not depend on the PNIPAM charge, since no real differences were detected between anionic and cationic samples (see Fig. 3a) – the analysis is also successful for uncharged chains (Fig. 3b) – suggesting that charged groups are not involved in the PNIPAM solubility changes when salt is added. Therefore, the Zhang´s model that accounts for the ion specificity in charged or uncharged PNIPAM chains can be successfully related with the Ninham´s theory based on dispersion forces. It should be noted that this relation has only be confirmed for the linear contribution in Equation 1 (and for chaotropic ions). However, it is reasonable to think that the Langmuir isotherm contribution be the most sensitive term to ion accumulation mechanisms. Thus, it is more than likely that the k parameter (in Eq. 1) can be related somehow to ion polarizability, although this relation might not be simple and more experimental data would be necessary for an accurate interpretation. Results pointing in that sense have been observed in caliexarene monolayers, where differences in the Langmuir isotherms due to the presence of different anions in the subphase are justified on the basis of dispersion forces [29].

Summarizing, the solubility of PNIPAM chains is strongly affected by the nature of the dissolved ions. The tested anions changed the LCST values according to usual Hofmeister series. Results are independent on the PNIPAM sign of charge, that is, they do not depend on whether anions act as co-ions or counter ions. Results can be well explained if the water structure mechanism underlying Hofmeister effects is considered. In addition, ion accumulation phenomena driven by dispersion forces have been proved to be also present. To take them into account, a semiempirical model proposed by Zhang et al. has been correlated with the Ninham's theory. Changes in surface tension have become the bridge to link the model and the theory. Nevertheless, the explanation based on ion polarizability only works for chaotropic species, but it fails for the most kosmotropic ion, SO_4^{2-}, albeit it possesses a high polarizability. The high destabilizing effect of SO_4^{2-} must be seen in the strong capability of this ion to interact with water. Zhang et al. found, as a matter of fact, a clear correlation between the parameter c and the hydration entropy of the ions. Hence, although dispersion forces are always present, they become non-meaningful when changes in water structure are dominant.

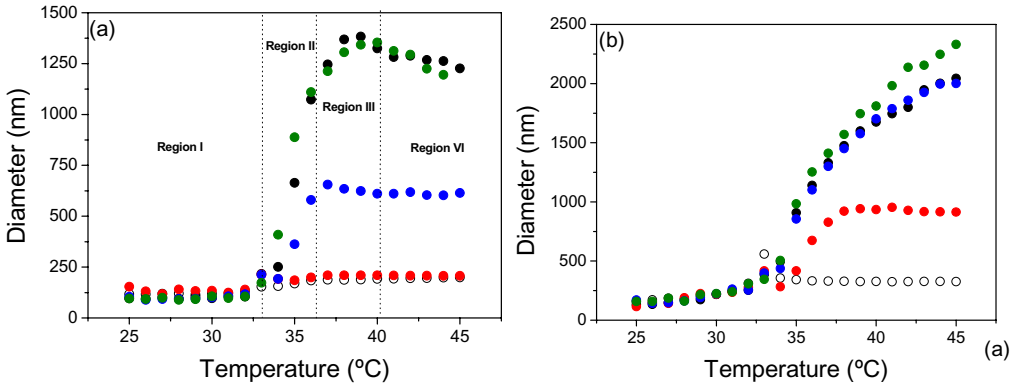

Figure 4. Diameter of **(a)** anionic and **(b)** cationic PNIPAM particles formed by increasing the temperature in: (○) a free salt, (●) 10 mM NaSCN, (●)10 mM $NaNO_3$, (●)10 mM NaCl, and (●)10 mM Na_2SO_4 solutions. A vertical line locates the temperature where any curve shows its corresponding maximum.

3.2. Nanoparticles formed by self-assembly of PNIPAM..

Solvency properties of charged-PNIPAM macromolecules have allowed us to compare with previous works related with noncharged-PNIPAM macromolecules. However, the interest in working with charged polymers is fundamentally due to their ability to form stable colloidal systems above the LCST. These particles may allow us to analyze ion effects from another point of view.

Particle formation

The particles formation resulting from increasing temperature was analyzed by monitoring the hydrodynamic diameter (D_h) evolution. Measurements were made heating progressively the sample in presence of a constant salt concentration (10 mM). Figures 4a and 4b show these data for the anionic and cationic PNIPAM, respectively. Anionic particles will be first analyzed. Curves shown in Figure 4a exhibit all them the same trend: at low temperatures the average hydrodynamic diameter keeps constant until the phase transition temperature is reached (33-34 ºC), then the average diameter begins to increase, achieves a maximum and finally stabilizes. This behaviour

can be explained considering a succession of different states/regimes the system passes through:

i) Region of thermodynamic stability: At temperatures below the LCST no changes in the average diameter were observed. The low light intensity scattered by the system reflects the existence of single PNIPAM macromolecules: water behaves as a good solvent and polymer presents a well hydrated coil configuration within all this temperature range. It is worth to note that, in this case, diameter values must be considered just as indicative, since this region deals only with non-spherical coil-conformations.

ii) Region of thermodynamic instability: The sudden increase of D_h as soon as temperature rises above the LCST is caused by the fast aggregation of PNIPAM chains and the consequent formation self-assembly structures. Although measurements do not allow us to distinguish if the initial aggregation deals with coils, crumpled coils or globules, it is plausible to think that it is a fast coil aggregation ($\tau_{collis} < \tau_{crumb} < \tau_{eq}$), due to the high polymer concentration and the polydispersity of the polymers employed [1]. This regimen prevails only during the first instants of the process: as the aggregation process progresses, the new clusters formed are also implicated in the growing of the particles. Hence, there are two factors favouring the particles growing: temperature and time. This would explain the steepness of the increasing slopes observed in Figure 4a.

iii) Region of kinetic stability by electrostatic repulsion. Figure 4a shows that D_h stops growing at certain temperature at which clusters achieve their maximum size, which is about 200 nm in a salt free solution. The stabilization of the system at high temperatures has its origin in the repulsive electrostatic forces. The PNIPAM chains have charged groups coming from the initiator used in the synthesis. As a result, the macromolecules possess certain amphiphilic character. Thus, during the interchain collapse, these charged groups are expected to stay at the water/polymer interface assembling a cage in which the polymer hydrophobic backbones are enclosed. Hence, the resulting precursor particles have certain surface charge which is enhanced as the interchain association occurs. It is just such charge what prevents further interaggregate association. As a result, monodisperse kinetically stable colloidal particles are obtained instead of a complete phase separation at high temperatures.

iv) Region of polymer relaxation. Once D_h attains its maximum it declines toward a plateau. From this moment no further evolution of hydrodynamic diameter was observed with temperature. This decrease in particles size could be due to the relaxation process predicted by Grosberg and Kuznetsov in which the mutual entanglement of aggregated chains occurs. This phenomenon has been experimentally observed in PNIPAM chains grafted to polystyrene particles [9].

Although all the curves appearing in Figure 4a show the same trend, clear differences among the different electrolytes are observed. Even working at relatively low salt concentrations (10 mM), ion specificity leads to large quantitative differences, especially regarding the final particle size. If ions are ranked according with the D_h values obtained once particles reach kinetic stability, the following series is obtained:

$$SCN^- < NO_3^- < Cl^- \leq SO_4^{-2}$$

which exactly coincides with the Hofmeister series. It is worth remarking that the hydrodynamic diameter obtained in salt free solutions is always lower than in presence of any salt. In extremely low ionic strength solutions, the repulsive electric potential is important even at low surface charge densities. As a result, the aggregation process rapidly stops and stable nanospheres with small diameters are obtained. The presence of salt in solution reduces this repulsive electric barrier, basically because of the screening provoked by counterions on the particle surface charge density. Hence, particles continue growing until they reach a stable configuration where the potential barrier is high enough to prevent aggregation. Differences observed with the diverse salts can be explained considering specific ion accumulation mechanisms. In fact, the screening caused by the counterions (Na^+ ions for the anionic system) can be partially balanced if any specific adsorption of anions occurs. Thereby, particles with different diameter would be obtained owing to the different nature of the ions employed (even if all of them have the same valence). Particularly, it would be expected the final particle size to be inversely proportional to the anion accumulation effectiveness. Ninham's theory, employed in the previous section to interpret the LCST values, can satisfactorily account for the ion specificities regarding the particle formation. According to Ninham's theory, the concentration of any ion at the proximities of a surface depends (among other energetic terms) on the dispersion forces acting between ions and surfaces [13-20]. Although a deeper description of this

theory will be presented later, it is worthwhile mentioning that such dispersion potential is controlled by the *B*-parameter defined in Equation 4. The *B* values corresponding to the different species are also listed in Table 2. In the case of monovalent anions $B < 0$, and thus, dispersion forces involve ion accumulation. The attractive force felt by an anion toward the particle surface will be progressively more intense as the ion polarizability increases (*B* also increases). That would explain why the most polarizable anions like SCN- tend to accumulate more effectively at the water/PNIPAM interface, enhancing the local charge density and subsequently stabilizing the growing particles at lower sizes, as experimentally observed. In the case of SO_4^{2-}, $B > 0$, and then, dispersion forces have the opposite effect: they make the ion move away from the particle surface. The exclusion of SO_4^{2-} from the interface, enhance the counterion screening and gives rise to lower repulsive interparticle potentials. This fact, together with the double valence of the ion, would explain why bigger particles are formed in the presence of SO_4^{2-}.

Another interpretation of these results is also plausible. There are some authors [21,30] that state that the ionic accumulation or exclusion mechanism usually associated to the Hofmeister effects has an entropic origin. It is a well known fact that water structure around hydrophilic and hydrophobic surfaces completely differs. In terms of hydration entropies the "*like likes like*" rule can be phenomenologically rationalized as preferring the partner that produces similar entropy changes. Accordingly, kosmotropic ions would tend to locate near hydrophilic surfaces and would be rejected from hydrophobic ones. Chaotropes would exhibit the opposite tendency. It should be noted that above the LCST, water is a *poor* solvent for the polymer, that is, PNIPAM behaves as a hydrophobic material. This would explain (independently on dispersion forces) that the most chaotropic ion (SCN^-) would accumulate more effectively at the hydrophobic PNIPAM surface while the most kosmotropic one (SO_4^{2-}) would be excluded from it. Therefore, the structure breaking/making character that orders the ions in the Hofmeister series could also explain our experimental results.

Once the formation of anionic particles is analyzed in depth, the patterns corresponding to the cationic particles can be readily understood. The positive sample (Fig. 4b) showed similar trends than the anionic one, with the difference that colloidal stable systems were only found with the SCN^- or salt free solutions. For the other ionic species, diameter increased without reaching a *plateau* over all the temperature range studied. In addition, bigger diameters

were obtained when the cationic PNIPAM was employed. This finding is consistent with the specific-ion-accumulation mechanism above described. The asymmetric behaviour found with the anionic and cationic PNIPAM can be ascribed to differences in anion and cation excess polarizabilities. When the surface is positive, the specific accumulation of Hofmeister anions, which now act as counter-ions, intensifies the screening of the particle surface charge, and thus, has a destabilizing effect. Such an effect is scarcely counterbalanced by sodium ions, which experiment weak attractive dispersion forces due to their low excess polarizability (see Table 2). This is the reason why stable particles have not been obtained with NO_3^- or Cl^- ions. The destabilizing effect of SO_4^{2-}, however, is mainly due to its double valence (in this case, SO_4^{2-} acts as counterion and the electrical interactions dominate over dispersion forces). Finally, the formation of stable particles in the presence of SCN^- can be explained considering the great tendency of this ion to accumulate at the particle surface. If this accumulation is important enough, it could provoke an inversion in the particle surface potential, which is able to stabilize the system. This possibility will be confirmed with electrophoretic measurements.

Electrophoretic mobility

Valuable insights into the mechanisms responsible for particle formation can be gained from electrophoretic mobility (μ_e) measurements. Particularly, phenomena involving ion accumulation, since μ_e is an indirect measure of the charge state nearby the particle surface. The influence of the ionic strength on μ_e was first studied. For this task, NaCl, frequently considered as a reference salt, was chosen. Figure 5 displays the temperature dependence of μ_e (for both anionic and cationic PNIPAM pools) at two NaCl concentrations. Some relevant comments concerning these results are listed below.

1. Although curves present a shape similar to that typically obtained with PNIPAM microgels [25,31,32], their origin is completely different. Regarding microgels, electrophoretic mobility raises with temperature due to an increase in surface charge density and a reduction in friction forces when particles shrink. The case of PNIPAM polymer solutions is more complex. At temperatures below the LCST, μ_e is around zero essentially because there are no particles in solution but slightly charged polymers with a random coil configuration. Beyond the LCST, rather spherical aggregates start to form.

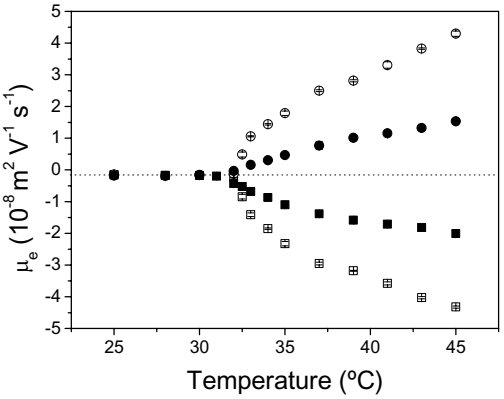

Figure 5. Electrophoretoc mobility versus temperature for the anionic (squares) and cationic (circles) PNIPAM. Open symbols: 1 mM NaCl. Solid symbols: 10 mM NaCl.

This self-assembly structures present a non-negligible surface charge which heightens as particles grow, which is reflected in the increase of electrophoretic mobility with temperature.

2. As commonly observed in colloidal systems, higher salt concentrations imply lower values of μ_e due to the compression of the electrical double layer [33]. Note that only increasing salt concentration from 1 mM to 10 mM makes μ_e reduce to the half. This fact reflects the low charge density of these particles.

3. Another interesting point is the surprising symmetry between the curves corresponding to the anionic and cationic pools at 1mM, when salt effects are negligible. This feature suggests similar surface charge densities for both pools. However, symmetry partially disappears when the ionic strength becomes more important: the effect of 10 mM of NaCl on the reduction of the μ_e values is more pronounced in the case of the cationic pool. This is consistent with diameter results, which also reveal less stable particles in such a case (Fig. 4b). Hence, although sodium and chloride are both monovalent ions, the effect of the anion on PNIPAM surface charge appears to be stronger, suggesting a more effective ion accumulation. This feature has been attributed to the high excess polarizability of Cl^- with respect to that of Na^+.

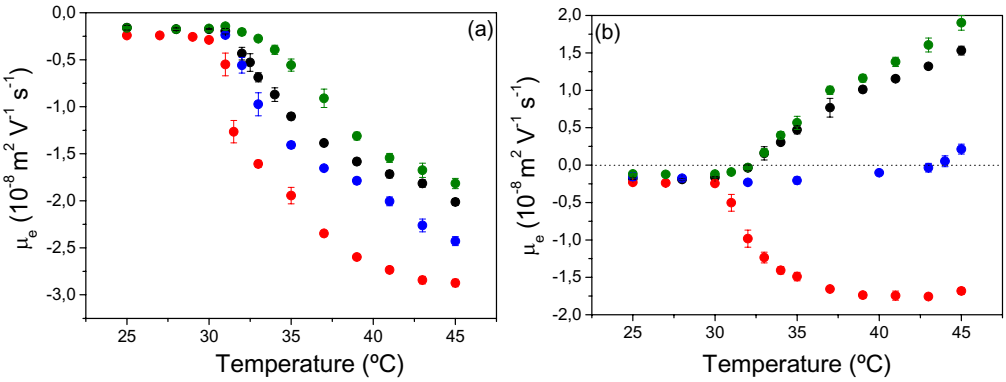

Figure 6. Electrophoretic mobility (symbols) and ζ-potential (dotted lines) of **(a)** anionic and **(b)** cationic PNIPAM particles as a function of temperature in saline solutions (10 mM). (●) NaSCN, (●) $NaNO_3$, (●) NaCl, and (●) Na_2SO_4 solutions. ζ-potential values were obtained from the μ_e data applying the O'Brian & White theory.

However, the ion specificity emerges when the other ionic species are considered. Figures 6a (anionic pool) and 6b (cationic pool) compare the curves corresponding to the different salts at 10 mM concentration. These results manifestly evidence the ion accumulation mechanism proposed to explain differences in particle size with different salts. Regarding the anionic sample, all the species make increase the negative electrophoretic mobility of the nanospheres (with respect to Cl^-) evidencing anion accumulation. The increment induced by the different anions in μ_e provides information about the effectiveness of the accumulation process in each case. These results confirm that anion accumulation becomes more important in the sequence SCN^- > NO_3^- > Cl^- > SO_4^{2-}, as proposed to explain size results. The same conclusion can be drawn from curves corresponding to the positive sample. In this case, however, the accumulation of anions at the particle surface involves a reduction in the ζ-potential, and consequently, in the electrophoretic mobility of the particles. Although μ_e values different from zero were found with Cl^- and SO_4^{2-} ions, they were not high enough to stabilize the aggregates. Note that in the case of SO_4^{2-}, despite it possesses double valence and acts as counterion, μ_e values are similar to those obtained with Cl^-. This feature manifests the exclusion of the SO_4^{2-} ions from the particle surface due to

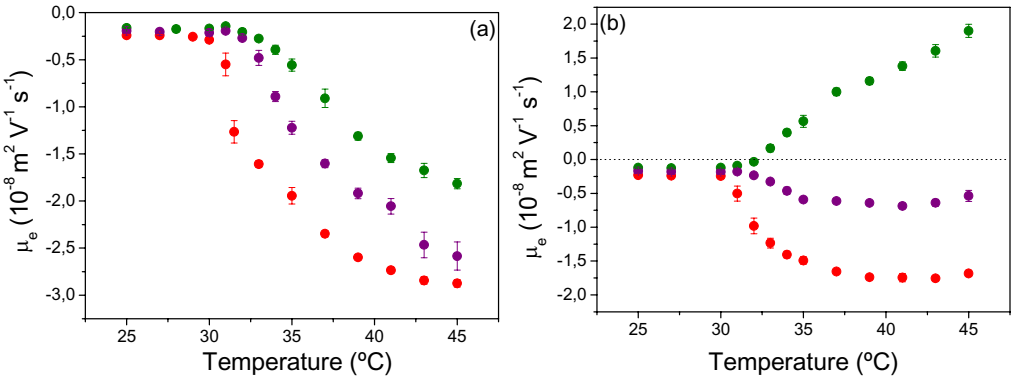

Figure 7. Electrophoretic mobility versus temperature at 10 mM of Na_2SO_4 (●); 10 mM of NaSCN (●); 5 mM of NaSO4 + 5 mM NaSCN (●). **(a)** Anionic sample. **(b)** Cationic Sample.

dispersion forces. The charge inversion proposed to explain the existence of stable nanospheres in the presence of SCN^- was also confirmed by electrophoretic mobility measurements. The accumulation of SCN^- is so important in the cationic sample (in which dispersion forces and electrostatic interactions both promote accumulation) that particles even exhibited μ_e values similar to those obtained with an anionic system and the same concentration of an indifferent ion.

Finally, it is customarily accepted that the Hofmeister effects are approximately additive over all species in solution [10]. This feature can be readily tested with this PNIPAM based system by measuring electrophoretic mobility. Figures 7a (anionic sample) and 7b (cationic sample) compare the μ_e-versus-T curves corresponding to a 10 mM concentration of SCN^-, SO_4^{2-} and $SCN^- + SO_4^{2-}$ (5mM SCN^-, 5mM SO_4^{2-}) independently. These two ions, exhibiting opposite tendencies when they are alone, have an intermediate effect when they act together. Nonetheless, the curves obtained are not rigorously additive, especially in the case of cationic particles.

Theoretical approach (Ninham's model)

In order to get a deeper insight into the accumulation processes experimentally observed, some calculations were done to estimate the ion

concentration profiles next to the PNIPAM surface when dispersion forces are taken into account [13-20].

The ionic distribution near an interface is given by a Boltzmann distribution:

$$c_{\pm}(x) = c_b \exp\left(-\beta U_T^{\pm}(x)\right); \quad \beta = k_B T \tag{6}$$

where c_b is the bulk concentration, and $U_T^{\pm}(x)$ is the total potential energy of the electrolytes at a certain normal distance x from the particle-water interface to the ion – note that particle surface can be considered as flat with respect to ions. The plus/minus sign distinguish cations from anions respectively. According to Ninham's theory, when ions in aqueous solutions are located at the proximity of a charged dielectric material (i.e. charged PNIPAM particles) three major contributions to the $U_T^{\pm}(x)$ energy appear:

i) An electrostatic term $U_{elec}(x)$ coming from electrical interactions between the charged surface and the ion:

$$U_{elect}^{\pm}(x) = \pm z\, e\, \Psi(x) \tag{7}$$

where z is the ion valency, e the elementary charge and $\Psi(x)$ a self consistent electrostatic potential set up by the surface charge and the ions themselves, resulting from solving the generalized Poisson-Boltzmann differential equation:

$$\frac{d^2\Psi(x)}{dx^2} = -\frac{(c(x)_+ - c(x)_-)}{\varepsilon_0 \varepsilon_w} \tag{8}$$

with ε_0 the electric permittivity of a vacuum and ε_w the relative permittivity of the electrolyte solution (which has been assumed equal to that of pure water: 78.5)

ii) An image term $U_{image}(x)$ arising from the image force between the ion and the dielectric material. The $U_{image}(x)$ expression derived from the original Onsager-Samaris' theory [34] and adapted for a PNIPAM-water interface is:

$$U_{image}(x) \approx \frac{1}{4\pi\varepsilon_0\varepsilon_w}\frac{e^2}{4x}\Delta \exp(-2\kappa x) \tag{9}$$

Here, κ is the well-known Debye-Hückel parameter and $\Delta = (\varepsilon_w - \varepsilon_p)/(\varepsilon_w + \varepsilon_p)$ with ε_p the relative permittivity of PNIPAM. Since $\varepsilon_p << \varepsilon_w$, then, $\Delta \approx 1$.

iii) A dispersion term $U_{disp}(x)$ whose origin lies in the dispersion forces between ions and interfaces:

$$U_{disp}^{\pm}(x) \approx \frac{\left(n_w^2 - n_p^2\right)}{8x^3}\alpha^*(0)^{\pm}\hbar\omega_i^{\pm} = \frac{B^{\pm}}{x^3} \tag{10}$$

the B parameter appearing in this equation have already been defined (see Eq. 4). The B values are listed in Table 2.

If these terms are assumed additive, then:

$$c^{\pm}(x) = c_b \exp\left(-\beta\left[U_{elect}^{\pm}(x) + U_{image}^{\pm}(x) + U_{disp}^{\pm}(x)\right]\right) \tag{11}$$

In the above equation all the contributions to the total potential are explicitly known excepting $\Psi(x)$. To obtain the self-consistent electrostatic potential $\Psi(x)$, it is necessary to solve the nonlinear Poisson-Boltzmann equation (Eq. 8). This has to be done numerically; we have used the method of relaxation assuming the boundary conditions $\Psi(a) = cte$ ("a" is a cutoff distance defined below) and $\Psi(L) = 0$. The second condition does not pose any problem, at a distance L far enough from the interface the electric potential should vanish. The first one is a constant surface potential condition. However, with the most of ions (when $B < 0$) the dispersion potential makes that the exponential function appearing in the second term of the Poisson-Boltzmann equation diverge at $x = 0$, so that no boundary condition can be established at particle surface. Besides this mathematical restriction there is a physical one, that is, ions cannot approximate to the particle surface further than a distance equal to their radius. To solve this problem it has been used a cutoff radius of $a = 2$Å in calculations. The ζ-potential of the particles in a 1mM solution of NaCl at 45 ºC has been considered as an estimation of the electric potential at this distance. This value is around 8 mV and -8 mV for the cationic and anionic samples respectively (μ_e was converted into ζ-potential by using the O'Bryan & White theory [35]).

The ion concentration profiles obtained from these calculations are displayed in Figures 8a (anionic sample) and 8b (cationic sample). These curves correspond to a situation in which the salt concentration is 10 mM and temperature is 45 ºC. The tendencies observed with the different ions perfectly match the experimental results. Specific ion accumulation is observed with

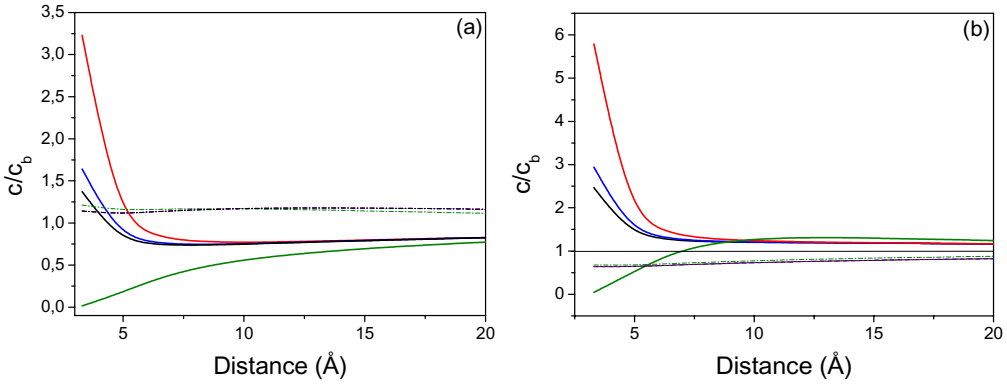

Figure 8. Ion specific self-consistent relative concentration profiles as a function of distance to the PNIPAM-water interface **(a)** Anionic sample **(b)** Cationic sample. Solid lines are for anions and dashed lines for cations : NaSCN (red), $NaNO_3$ (blue), NaCl (black), Na_2SO_4 (green).

SCN^- and NO_3^- ions. In addition, the concentration of SCN^- ions next to the PNIPAM/water interface doubles that of NO_3^- ions. The most outstanding SCN^- accumulation is found with the positive surface, in which charge inversion is experimentally observed. In this situation the SCN^- concentration is eight-fold higher than the bulk concentration. On the other hand, these theoretical results also reveal the exclusion of SO_4^{2-} ions from the PNIPAM surface. It can be concluded, hence, that Ninham's theory can account for our experimental results.

IV. Conclusions

The synthesis and properties of a new system based in the self-association of PNIPAM charged chains have been reported. These PNIPAM particles have the advantage of being highly versatile: it is possible to turn a polymer solution into a colloidal particle dispersion just by tuning the temperature, being this process reversible. In addition, the characteristic of the final particles can be controlled by salt addition. It is worth stressing that final particle diameters varying within a range between about 200 nm and 1200 nm were obtained just embedding the PNIPAM chains in a 10 mM solution of the

proper salt. The high responsiveness of this system to the salt effects makes it an interesting test-ground for investigating Hofmeister effects.

In the first part of this paper, specific ion effects on the solubility of charged PNIPAM macromolecules were investigated. It was concluded that the changes in the LCST induced by the different electrolytes are not dependent on the positive or negative charge of the polymer. The empirical model proposed by Zhang et al. for neutral PNIPAM macromolecules fits well our experimental results. This model (particularly the lineal term) has been reinterpreted by using Ninham's theory which attributes ion specificity to dispersion forces between ions and surfaces. A correlation between ion excess polarizability and changes in the LCST has been found with the chaotropic anions. Nonetheless, mechanisms involving the rearrangements in water structure induced by ions must be also invoked to give a complete explanation of these phenomena.

The second part of the paper concerns particle formation processes. Four different stages are successively reached upon increasing temperature: i) thermodynamic stability of PNIPAM macromolecules at $T <$ LCST, ii) PNIPAM interchain aggregation at $T >$ LCST, iii) kinetic stability by electrostatic repulsion and iv) polymer relaxation. The final particle size is highly dependent on the ion specific nature. These results, supported by electrophoretic measurements, reveal the existence of specific ion accumulation processes at the PNIPAM/water interface. This accumulation is more important in the sequence: $SCN^- > NO_3^- > Cl^- > SO_4^{2-}$. This order can be explained considering both dispersion forces and the capability of ions to disrupt water structure. The Ninham's model was employed to calculate the ion profiles next to the surface with the different salts. The theoretical predictions fit perfectly well with the experiments.

Acknowledgements

The authors would like to thank the financial support granted by "FEDER" and "Comisión Interministerial de Ciencia y Tecnología" (CICYT, Spain), projects MAT2003-01257 and AGL2004-01531/ALI, and from the "Consejería de Innovación, Ciencia y Tecnología de la Junta de Andalucía" Project FQM 392. They also gratefully acknowledge the bioMérieux company for the support provided in terms of chemicals and equipment.

References and Notes

[1] Flory P. J. *Principles of Polymer Chemistry*, Cornell University Press: Ithaca, NY,**1953**.

[2] Stockmayer W. H. *Makromol. Chem.* **1960**, *35*, 54. [3] Wang X.; Qiu X.; Wu C. *Macromolecules* **1998**, *31*, 2972.

[3] Shibayama M.; Tanaka T. *Adv.in Polym. Sci.* **1993**, 109,1.

[4] Wang X.; Qiu X.; Wu C. *Macromolecules* **1998**, *31*, 2972.

[5] Schild H. G. *Prog. Polym. Sci.* **1992**, *17*, 163.

[6] Yamakawa H Modern Theory of Polymer Solutions; Harper & Row: New York, 1971.

[7] Grosberg A. Y.; Kuznetsov D. V. *Macromolecules* **1992**, *25*, 1970, 1980, 1991, and 1996, a series of four papers.

[8] Wu C.; Zhou S. *Macromolecules* **1995**, *28*, 5388.

[9] Zhu W. Z.; Napper D. H. *J. Colloid Interface Sci.* **1994**, *168*, 380.

[10] Collins K. D.; Washabaugh, M. W. *Q. Rev. Biophys.* **1985**, *18*, 323.

[11] Cacace, M. G.; Landau, E. M.; Ramsden, J. J. *Q. Rev. Biophys.* **1997**, *30*, 241.

[12] Hofmeister effects special issue: *Current Opinion in Colloid Interface Sci.* **2004**, *9*.

[13] Ninham B. W.; Yaminsky V. *Langmuir* **1997**, *13*, 2097.

[14] Böstrom M.; Williams D. R.; Ninham B. W. *Langmuir* **2001**, *17*, 4475.

[15] Böstrom M.; Williams D. R.; Ninham B. W. *Langmuir* **2002**, *18*, 6010.

[16] Kunz W.; Lo Nostro P.; Ninham B. W. *Current Opinion Colloid Interface Sci.* **2004**, *9*, 1.

[17] Böstrom M.; Kunz W.; Ninham B. W. *Langmuir* **2005**, *21*, 2619.

[18] Böstrom M.; Williams D. R.; Ninham B. W. *J Phys Chem B* **2002**, *106*, 7908.

[19] Böstrom M.; Williams D. R; Steward P. R.; Ninham B. W. *Phys Rev E* **2003**, *68*, 0419021.

[20] Kunz W.; Belloni L.; Bernard O.; Ninham B. W. *J Phys Chem B* **2004**, *108*, 2398.

[21] Wiggins P. M. *Physica A* **1997**, *238*, 113.

[22] Daly E.; Saunders B. R. *Langmuir* **2000**, *16*, 5546.

[23] Zha L.; Hu J.; Wang C.; Fu S.; Luo M. *Colloid Polym. Sci.* 2002, 280, 1116.

[24] López-León T.; Elaïssari A.; Ortega-Vinuesa J. L.; Bastos-González D. (*ChemPhysChem*, in press).

[25] López-León T.; Ortega-Vinuesa J. L.; Bastos-González D.; Elaïssari A. *J Phys. Chem. B* **2006**, *110*, 4629.

[26] Freitag R.; Garret-Flaudy F. *Langmuir* **2002**, 18, 3434.

[27] Suwa K.;Yamamoto K.; Akashi M.; Takano K.; Tanaka N.; Kunugi S. *Colloid Polym. Sci.* **1998**, *276*, 529.

[28] Zhang Y.; Furyk S.; Bergbreiter D. E.; Cremer P. S. *J. Am. Chem. Soc.* **2005**, 127, 14505.

[29] Lonetti B.; Lo Nostro P.; Ninham B. W.; Baglioni P. *Langmuir* **2005**, *21*, 2242.

[30] Lyklema J. *Mol. Phys.* **2002**, *100*, 3177.

[31] Saunders B. R.; Vincent B. *Adv. Colloid Interface Sci.* **1999**, *80*, 1.

[32] Pelton R. *Adv. Colloid Interface Sci.* **2000**, *85*, 1.

[34] Onsager, L.; Samaris, N.T. *J. Chem Phys.* **1934**, *2*, 528.